STUDIES TOWARDS THE DESIGN AND DEVELOPMENT OF PHOTOACTIVE SUPERMOLECULES FOR SIGNALING TRANSITION METAL IONS

A thesis

Submitted for the degree of

DOCTOR OF PHILOSOPHY

by

Sandip Banthia

School of Chemistry
University of Hyderabad
Hyderabad 500 046
INDIA

June 2005

To my

Family members

Contents

Contents

Contents

STATEMENT

I hereby declare that the matter embodied in the thesis entitled *"Studies towards the design and development of photoactive supermolecules for signaling transition metal ions"* is the result of investigations carried out by me in the School of Chemistry, University of Hyderabad, Hyderabad, India under the supervision of **Prof. Anunay Samanta**.

In keeping with the general practice of reporting scientific investigations, due acknowledgements have been made wherever the work described is based on the findings of other investigators. Any omission or error that might have crept in is regretted.

June 2005 **Sandip Banthia**

SCHOOL OF CHEMISTRY
UNIVERSITY OF HYDERABAD
HYDERABAD-500 046, INDIA

Phone: +91-40-2301 1594 (O)
+91-40-2301 0715 (R)
Fax: +91-40-2301 2460
Email: assc@uohyd.ernet.in
anunay_s@yahoo.com

Anunay Samanta, F.A.Sc.
Professor

20th June 2005

CERTIFICATE

Certified that the work embodied in the thesis entitled ***"Studies towards the design and development of photoactive supermolecules for signaling transition metal ions"*** has been carried out by **Mr. Sandip Banthia** under my supervision and that the same has not been submitted elsewhere for any degree.

Anunay Samanta
(Thesis Supervisor)

Dean
School of Chemistry
University of Hyderabad

Acknowledgement

I express my sincere gratitude to Prof. Anunay Samanta, my research supervisor, for his constant encouragement, cooperation and kind guidance. He has been quite helpful to me in both academic and personal fronts.

I am thankful to Prof. Samudranil Pal for all his help and cooperation. Without his ready solutions, X-ray crystallography would not have been that easy.

I would like to thank the former and present Dean, School of Chemistry, for their constant inspiration and for the available facilities. I am extremely thankful individually to all the faculty members of the school for their help, cooperation and encouragement at various stages of my stay in the campus.

I value my association with Satyen, Sankaran and Rana from whom I have learned many unwritten aspects of research. I acknowledge my junior friends, Tamal, Prasun, Moloy, Aniruddha and Bhaswati for maintaining the friendly and cooperative atmosphere in the lab. I also thank Tin for his company during working at late hours.

I thank all the non-teaching staff of the school for their time to time cooperation. They had all been quite helpful, Raghavaiah in particular.

Financial assistance from CSIR, New Delhi is greatly acknowledged.

Friends are a hearty lot and it is indeed a difficult task to mention them all here. I acknowledge whole-heartedly the contributions of each and every one of them. I thank Satyenda for being a Big B with a friendly attitude. My association with Pankaz, Hari, Charan, Sahoo, Anoop and FTP are unforgettable. Cherry Nisha Pari, sounds like poetry; I can never imagine myself here without them. I also take pleasure in each and every moment spent with Raghu, Annu, Ranjeeth, Hari and Avanthi. Old friends depart in search of a new life and I miss them all.

Rocks are rocking and so would have been the life in the campus without the VC-rock, Heaven & Earth and the Mushroom rock. I treasure each and every night spent on them. From these very rocks I pitch high to thank my "Bindaas" gang that include Abhik, Baba, Suni, Subhash, Dinu, Jethu, Bishu, Archan, Ullas, Prashant, Binoy, Saikat, Manab, Abhijeet and many more to add on.

Sandip

List of Publications

1. Photophysical and transition metal ion signaling behavior of a three-component system comprising a cryptand moiety as the receptor. **S. Banthia** and A. Samanta. *J. Phys. Chem. B*, **2002**, *106*, 5572.

2. Fluorescence signaling of the transition metal ions: A new approach. N. B. Sankaran, **S. Banthia**, A. Das and A. Samanta. *New J. Chem.*, **2002**, *26*, 1529.

3. Fluorescence signaling of the transition metal ions: Design strategy based on the choice of the fluorophore component. N. B. Sankaran, **S. Banthia** and A. Samanta. *Proc. Ind. Acad. Sci. (Chem. Sci.)*, **2002**, *114*, 539.

4. N-(4-Amino-2-methylphenyl)-4-chlorophthalimide. **S. Banthia** and A. Samanta. Acta *Cryst. E.*, **2004**, *60*, o740.

5. In situ reduction of copper(II) forming an unusually air stable linear complex of copper(I) with a fluorescent tag. **S. Banthia** and A. Samanta. *Inorg. Chem.*, **2004**, *43*, 6890.

6. Photophysical and transition metal ion signaling properties of some 4-amino-1,8-naphthalimide derivatives. **S. Banthia**, M. Sarkar and A. Samanta. *Res. Chem. Intermed.*, **2005**, *31*, 25.

7. Calix[4]azacrown and 4-aminophthalimide-appended calix[4]azacrown: synthesis, structure, complexation and fluorescence signaling behavior. **S. Banthia** and A. Samanta. *Org. Biomol. Chem.*, **2005**, *3*, 1428.

8. Influence of structure on the unusual spectral behavior of 4-dialkylamino-1,8-naphthalimide. **S. Banthia** and A. Samanta. *Chem. Lett.*, **2005**, *34*, 722.

9. Two-dimensional chromogenic sensor as well as fluorescence inverter: selective detection of copper(II) in aqueous medium. **S. Banthia** and A. Samanta. *New J. Chem.* (in press).

10. Multiple logical access with a single fluorophore-spacer-receptor system: realization of inhibit (INH) logic function. **S. Banthia** and A. Samanta (submitted).

11. Linear complexes of copper(I) based on 4-aminophthalimide platform: synthesis, structure and unusual stability. **S. Banthia** and A. Samanta (submitted).

12. A new tiling pattern, long and short brick, comprising three-connecting nodes. **S. Banthia** and A. Samanta (submitted).

13. Ratiometric fluorescent sensor for transition metal ions: A dual fluorophore approach. **S. Banthia** and A. Samanta (in preparation).

Conference presentations

1. Fluorescence response of some 4-amino-1,8-naphthalimide derivatives in the absence and in the presence of various metal ions. **S. Banthia**, and A. Samanta. National Symposium on Radiation and Photochemistry, at Indian Institute of Technology, Kanpur, India, Feb. 2003 (Poster presentation).

2. Fluorescent buckets for the recognition of transition metal ions. **S. Banthia** and A. Samanta. 3rd Trivandrum International Symposium on Recent Trends in Photochemical Sciences, at Regional Research Laboratory, CSIR, Trivandrum, India, Jan. 2004 (Poster presentation).

3. Photophysical and transition metal ion signaling behavior of a three-component system comprising a cryptand moiety as the receptor. **S. Banthia** and A. Samanta. K. V. R. Scientific Society, India, March 2004 (Oral presentation).

4. Molecular sensors and switches based on fluorescence signaling toward protons and transition metal ions. **S. Banthia**, M. Sarkar and A. Samanta. ChemFest – 2005, 2nd annual in-house symposium of the School of Chemistry, University of Hyderabad, Hyderabad, India, Feb. 2005 (Oral presentation).

Thesis Layout

The thesis has been divided into eight chapters. ***Chapter 1*** provides a brief introduction to molecular photonics and fluorescence signaling with focus on systems based on photoinduced electron transfer (PET) mechanism. ***Chapter 2*** provides details of the methodologies studies undertaken. The instrumental details are also presented in this chapter. ***Chapter 3*** deals with multi-component systems comprising macrocyclic cryptand and calix[4]azacrown moieties as receptors and a 4-aminophthalimide moiety as the fluorophore component. ***Chapter 4*** describes a simple fluorescent signaling system involving 4-aminophthalimide fluorophore and di-(2-picolyl)amine receptor that mimics several logic functions. ***Chapter 5*** presents interesting structural features of two-coordinated linear complexes of copper(I) based on 4-aminophthalimide platform that are unusually inert towards oxidation. ***Chapter 6*** provides the results of the investigation on a simple molecular system constructed of 4-amino-7-nitrobenzoxa[1,3]diazole chromophore and di-(2-picolyl)amine ionophore. This system acts as a chromogenic sensor as well as a fluorescence inverter for selective detection of cupric ions at physiological pH. ***Chapter 7*** focuses on the photophysical and ratiometric signaling behavior of a dual-fluorophore system based on anthracene and 4-amino-7-nitrobenzoxa[1,3]diazole chromophores. ***Chapter 8*** summarizes the findings of this investigation touching upon the achievements and looking into the scope of further work and upcoming challenges.

Chapter 1

Introduction

This chapter provides an overview of the fundamentals of sensing via molecular recognition, leading to molecular photonics and electronics, with emphasis on fluorescent signaling systems. The common analytes of interest and various mechanisms employed in fluorescence signaling of these species are touched upon. Photoinduced electron transfer (PET), the mechanism that is primarily employed in the present study for signaling of transition metal ions is discussed in detail. Several PET sensors developed in the recent past for various analytes and continued dearth of practical sensor systems for transition metal ions have been our primary motivation. A brief introduction of the systems designed and developed in the present investigation concludes the chapter.

1. 1. Molecular recognition

The process of binding of the analyte to a molecular fragment called receptor is defined as recognition.[1-3] Efficient binding of the substrate by the receptor can be achieved by employing a large number of binding sites. Molecular recognition thus refers to recognition of the substrate by the receptor leading to strong and specific complexation. Sensing typically refers to the monitoring of a chemical species (the analyte) in a given matrix (air, blood, a tissue, waste effluents, drinking water, a glass vessel in the lab etc.). However, sensing is not simply recognition, but requires that the recognition event to be signaled by the drastic change of a given property, which should be visually and/or instrumentally detectable. The recognition process has to be fast, guest selective and reversible for better efficiency and potential for reutilization of a sensor system. These features are typical of the metal – ligand interaction and it is not by chance that majority of sensors operate through a mechanism that involves coordinative binding.[4] Molecular recognition has become important because of its significance and diverse applications in physical, chemical as well as biological sciences.[5-7]

1. 1. 1. Molecular photonics and electronics

Molecular recognition events between the host and the guest are intrinsic part of the operation of a supramolecular device, which is designed to bind and then signal the presence of a guest. Among the various possible approaches to constructing a supramolecular device, the use of a photoactive component is considered to be a versatile one.[5] The role of light in photosynthesis, its importance in inducing events such as charge separation and catalysis, its use in sensing applications and its ability to travel through a variety of media have contributed to the development of photoactive supramolecular devices. In addition, useful processes such as energy migration, perturbations of optical transitions and polarizabilities, modification of ground and excited state redox potentials, photoregulation of binding properties and selective photochemical reactivity can be achieved by incorporating a photoactive component while constructing a multi-component system.

The need in the advancement of computing, engineering and medicine is gathering great interest as classical electronics approaches its size limit and the public clamors for even faster, cheaper and more efficient devices. The relatively recent development of supramolecular chemistry along with technologies such as scanning probe microscopies[8] and surface spectroscopic techniques,[9] which allow the design, characterization and manipulation of new devices, has stimulated interest in the construction of simple electronics or photonics driven systems and networks that function as molecular-level devices.[10-12] Examples include simple host–guest complexes as well as more advanced molecular wires,[13] gates,[14] brakes,[15] ratchets,[16] rectifiers,[17] gears,[18] switches,[19] shuttles[20] etc. These developments build further hopes among the scientists, as high as to realize “molecular robotics or “molecular computer”, a next generation artificial intelligence.[21]

Arithmetic and logic operations are the twin pillars on which the entire information technology has been built. Molecular-level devices that perform elementary arithmetic and logic operations are thus gaining increasing importance and are being taken up as a challenge of today. Mimicking the functions of semiconductor logic gates used in modern computing is of particular interest.[22] The relationship between the input and the output may be described by truth tables, where “1” represents an active input/output and “0”

represents an inactive one.[23,24] For a two-input system there are 16 different logic gate functions.[24]† Some of these functions such as the OR,[25] NOR,[26] AND,[27] XOR[28] and INH[29] functions have recently been demonstrated where ions and molecules are used as inputs and changes in the optical properties of the system are used as outputs. In this context, molecules are used to yield the active and passive components of electronic or integrated circuits. Arithmetic operations are currently implemented in semiconductor technology by combining AND and XOR logic gates in parallel. Therefore, logical combinations of available molecular systems that act as AND and XOR logic gates would result into elementary arithmetic operations at the far smaller molecular-scale.[30] The AND and XOR logic gates employed for the purpose should be fully compatible with each other in terms of chemical inputs, optical outputs and power supplies. For certain applications, such as molecular-based memory or logic circuitry, the devices are simply molecular-based analogues of devices with more conventional silicon-based circuitry. In those cases, molecular-electronics components may have the advantages of less manufacturing complexity, lower power consumption, and easier scaling. The field of molecular electronics is evolving rapidly, and even though there are no commercial applications as yet, the science coming out of this research is spectacular.

1. 1. 2. Fluorescence sensors

The importance of sensing and reporting of specific ions or neutral molecules is mainly due to their biological and environmental significance in our day-to-day life. Among the cations, the interest has been primarily focused on protons and the s-block metal ions viz. Na^+, K^+, Mg^{2+} and Ca^{2+} owing to their importance in biology.[31] Heavy and transition metal (HTM) ions, though important in biology and environment, the sensing of these metal ions has been taken up actively only in the recent years.[32-34] The toxicity of Cd^{2+}, Hg^{2+} and Pb^{2+} are growing concern among environmentalists and

† The ONE and ZERO functions are trivial, the output being a 1 or 0 respectively, regardless of the input. Four functions depend on a single input, namely both ID (or YES) and both INV (or NOT) functions. The remaining ten are functions of two inputs, and of these AND, OR, XOR, NAND, NOR and EQU (or XNOR) satisfy commutation. The last four functions corresponding to INH and IMP gates do not satisfy commutation.

priority is being attached to developing sensors for these metal ions specifically. Among the neutral molecules, sensing of saccharides,[35] peptides,[36] carbon monoxide,[37] alcohols[38] etc. have been taken up recently. Anions also play a fundamental role in a wide range of biological and chemical processes. Thus, anion sensing is also emerging as a hot field of research.[39-41]

Molecular sensors that employ variation of fluorescence for signal transduction are referred to as fluorosensors. As a technique, fluorescence is quite advantageous and superior to other techniques such as the shift of an NMR line, the displacement of a polarographic/voltammetric wave, the appearance-disappearance of an absorption band in the UV-vis region etc. due to very high sensitivity, resolution, multi-dimensionality and remote sensing capability. Furthermore, real-time sensing is possible employing luminescence techniques.[42] In fact, a large number of luminescent sensors have been developed during the last decade for a variety of applications, which include cell biology investigations, medical diagnosis, environmental analysis, food quality control and so on.[43]

Sensing of analytes using fluorescence is monitored by changes in various fluorescence parameters. For example, a shift in the emission band occurs if the charge transfer nature of the sensor molecule gets altered upon binding of the analyte. The emission intensity may also get quenched or enhanced depending on the nature of the interaction between the various components of the sensor system. An enhancement in the intensity of the emission upon guest binding is represented as “on” state of the fluorescence relative to an initially weakly fluorescent “Off” state. A reverse of this case, in which the initial system is highly fluorescent (“On” state) and the bound system is weakly fluorescent (“Off” state), is also possible. These types of sensors are called fluorescence “Off-On” or “On-Off” sensors.[44] In the case of wavelength-ratiometric probes, the analyte concentration can be determined independently of the probe concentration by the ratio of intensities at two emission wavelengths. Changes in fluorescence lifetime on binding of the analyte can also be used for sensing applications.[43] In fact, the difficulties of intensity-based measurements (discussed later) and the scarcity of the wavelength-ratiometric probes may be circumvented by the use of time-resolved or lifetime-based sensing.

1. 2. Fluorescence signaling strategies

Several mechanisms are being employed for fluorescence signaling of various analytes.[44] These include monitoring of the nπ*,[45,46] ππ*,[47] metal-centered (MC),[48] intramolecular charge transfer (ICT),[49-51] metal to ligand charge transfer (MLCT),[52] twisted intramolecular charge transfer (TICT)[53] and triplet[54-56] excited states. Fluorescence sensing by monitoring the monomer-excimer emission bands is also an established technique for quite some time.[57-60] In fact, such ratiometric probes are superior to the conventional intensity based probes. Electronic energy transfer (EET)[61] and fluorescence resonance energy transfer (FRET)[62] are also common mechanisms employed in fluorescence signaling of the analytes. However, despite the availability of various mechanisms pointed out above, the most commonly employed mechanism for fluorescence signaling of various guest species is based on photoinduced electron transfer (PET) process.[63] In the following sub-sections, representative fluorosensors based on some of these phenomena are discussed with special emphasis on the design principles for fluorosensors based on PET mechanism.

1. 2. 1. $n\pi^* - \pi\pi^*$ excited state inversion

Molecules with lowest excited singlet states of the $n\pi^*$ type are usually non-emissive in fluid solution.[64-67] The fluorescence of these systems can be switched "on" if the $n\pi^*$ state is perturbed such that the lowest energy singlet excited state is of the $\pi\pi^*$ type. For example, the hydrogen bond-donating solvent methanol increases the energy of the $n\pi^*$ excited state of **1** to such an extent that the fluorescence quantum yield increases over a 100-fold compared to the apolar (and aprotic) solvent hexane.[45] $n\pi^*$–$\pi\pi^*$ state inversions are easier to arrange if stronger forces can be brought into play. 2,2′-bipyridyl-based macrocycle **2** demonstrate this by 1000-fold increase in its fluorescence intensity when it engages in Lewis base-acid interaction with Li^+.[46]

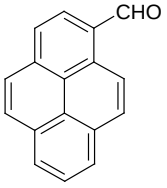

1

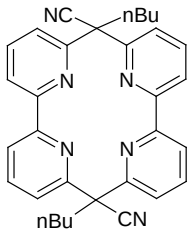

2

1. 2. 2. $\pi\pi^*$ excited state fluorophores

Conjugated alkenes with flexible structures are generally non-emissive in fluid media. Internal twisting (torsion) is primarily responsible for the rapid non-radiative decay of the excited molecules.[64-67] However, when incorporated into structures with rigid configuration like membranes, cyclodextrins, etc., the barrier to internal twisting is increased resulting in an enhancement of the fluorescence efficiency of the systems.[68,69] Compound **3** is perhaps one of the classic systems that display significant fluorescence only in semi-rigid membrane environments where the double-bond torsion in the excited state is obstructed.[70-72] Compound **4** is an elegant example of this class that employs covalent but reversible interactions.[73] The fluorescence of this system switches "On" upon rigidification via macrocyclization with disaccharide guests.

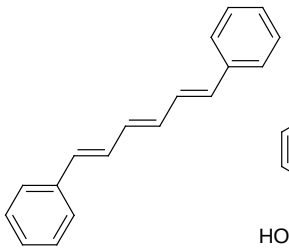

3

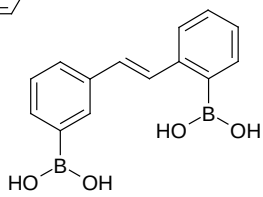

4

1. 2. 3. Metal-centered (MC) excited states and energy transfer

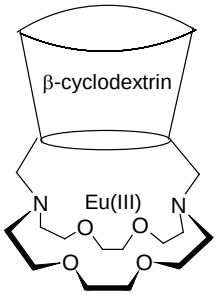

5

The huge influence of emissive MC excited states on photophysics and assay procedures is largely due to two species Eu(III) and Tb(III). Since f-f electronic transitions are intrinsically forbidden, lanthanide(III) ions are poor absorbers. In order to populate the excited states of such metal ions, special techniques like laser pumping is used.[74] The use of a photon antenna is an alternative way to overcome this difficulty.[75-77] The basic principle is that an intrinsically strong photon absorber with a relatively high excited-state energy will transfer the photonic energy to populate a MC excited-state held nearby. Thus, sensors with lanthanide complexes can be designed on this basis for photon absorbing aromatic compounds. Sensor **5**, for example, is one of the systems belonging to this class in which an enhancement of Eu(III) emission is observed in the presence of benzene as the guest molecule.[78] Energy transfer from

cyclodextrin-encapsulated benzene to azacrown-bound Eu^{3+} is believed to be responsible for the observed fluorescence enhancement.[78]

1. 2. 4. Charge transfer (CT) excited states

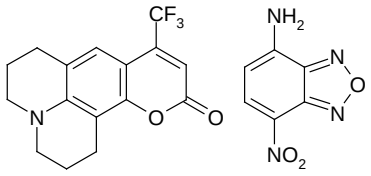

6 **7**

The lowest singlet excited state of the electron donor-acceptor (EDA) molecules is most often charge transfer (CT) in nature.[42] Electronic excitation of the EDA molecules is associated with significant changes in the dipole moment. The excited state dipole moment of a majority of the EDA compounds is higher than that in the ground state, although, the opposite is true for a few systems such as betaines.[79] Because of their significant dipole moments, these systems are highly solvated in polar media. Moreover, since electronic excitation is accompanied by a change in the dipole moment of the system, the extent of stabilization due to solvation is different for the ground and excited states. As a result of this, a shift in the wavelength corresponding to the ICT emission maximum on change of the polarity of the media is observable. In addition, a change in the polarity of the medium is also associated with changes in the fluorescence quantum yield and lifetime of the systems. Thus, π-electron systems with push–pull substituent pairs show Stokes shift of the fluorescence maximum on increase in the polarity of the medium due to increase in the dipole moment of the systems. Compounds **6**[80] and **7**[81] fall in this category.

Ions can exert strong electric field on the ICT states of the EDA molecules because of their uncompensated charge. However, the effect of the ions, usually present in low concentration, is masked by the influence of large number of solvent molecules around the fluorophore. Therefore, effective molarity of the ions needs to be increased in the vicinity of the fluorophore, usually by trapping the ion using a suitably built-in receptor. Systems **8** and **9** are typical examples of ion-responsive ICT fluorosensors.[82,83] In **8**, the receptor moiety is connected to the electron-deficient acceptor end of the molecule. This type of systems display a cation-induced red-shift of the fluorescence maxima[82] as the charge separation between the donor and acceptor moieties increases in the presence of the cationic guest. The effect will be relatively larger for the excited state that has a

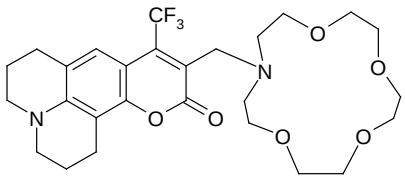

8

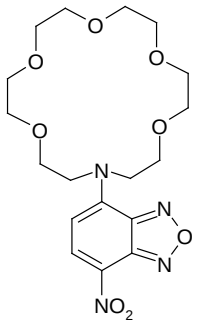

9

higher dipole moment. On the other hand, systems in which the receptor is connected to the electron-rich donor moiety, as in **9**, display a blue-shift of the emission maxima.[83] In this case, guest binding results in a decrease of the separation of charge between the donor and the acceptor moieties leading to a reduction in the dipole moment of the ground and excited states. This results into a blue-shift of the spectral maxima.

1. 2. 5. Twisted intramolecular charge transfer state (TICT)

Complete charge separation in EDA systems can be achieved by decoupling of the HOMO of the donor and the LUMO of the acceptor by twisting the donor and the acceptor moieties through 90° with respect to each other. This phenomenon is commonly known as twisted intramolecular charge transfer (TICT) process.[84] The enhanced separation of charge makes the fluorescent TICT state highly sensitive to the polarity of the environment. 4-N,N-dimethylaminobenzonitrile (DMABN) is the most extensively

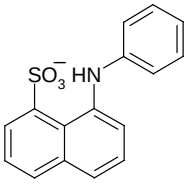

10

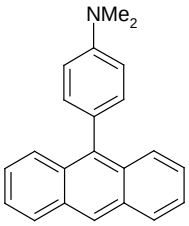

11

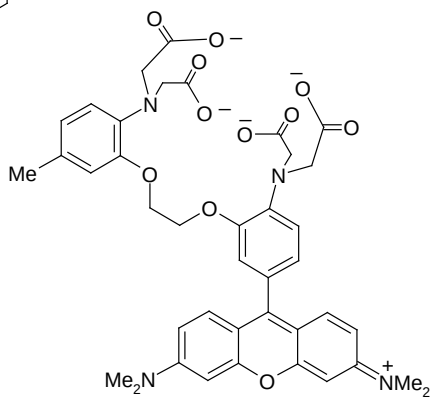

12

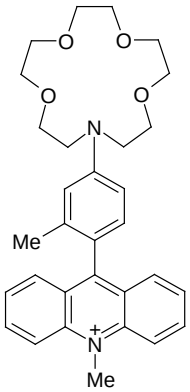

13

studied molecule of this class.[84-89] Compound **10**[90,91] and its relatives[92] are another set of molecules of this class that are being used as polarity sensors in biochemical research for over five decades. Compounds **11**,[93] **12**[94] and **13**[95] belong to this class of ion-responsive fluorosensors for H^+, Ca^{2+} and Ag^+ ions, respectively.

1. 2. 6. PET mechanism

1. 2. 6. 1. Design principle

A guest responsive fluorescent sensor must necessarily possess a guest-binding site (receptor) and a photon-interaction site (fluorophore). The most commonly employed design for "Off-On" fluorescence signaling of a guest is based on multi-component molecular system with a *fluorophore-spacer-receptor* architecture (Scheme 1.1).[44]‡

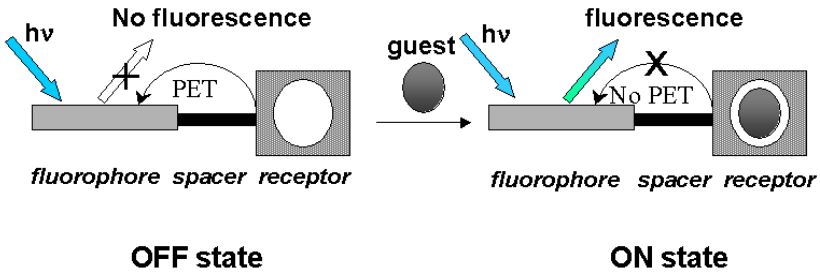

Scheme 1.1 The assembly of functional components in a fluorescent "Off-On" sensor based on PET mechanism.

In this design the fluorophore and the receptor sites are separately identifiable within a structure because of an intervening spacer unit. This means that the separate sets of guest-binding and photophysical properties of the terminal modules serve as quantitative predictors for the sensory properties of the three-module supermolecule. Sensing implies that the act of guest binding at the receptor site is communicated across the spacer to cause a change in the photophysical properties of the fluorophore moiety. For a typical

‡ The symbolism for the receptor module does not necessarily imply a macrocycle. It is taken to be a generic representation for binding sites of various forms.

"Off-On" fluorescence sensor, the fluorescence of the system is quenched due to the communication between the receptor and the fluorophore moieties. In the presence of a guest, the communication between the terminal moieties gets cut-off leading to the recovery of the fluorescence. Thus, a sensor can be designed such that communication between the receptor and the photo-excited fluorophore leads to fluorescence quenching of the system ("Off" state) in the absence of any guest. In the presence of a guest, the guest-receptor interaction should lead to a disruption of the communication between the receptor and the fluorophore thereby "switching on" the fluorescence. Since photoinduced electron transfer (PET) is the most common mechanism of communication between the fluorophore and the receptor, sensors based on this mechanism are termed as PET sensors.[44,63] PET is sufficiently long-range interaction that leads to the sensory behavior, by entering into competition with fluorescence for the deactivation of the excited fluorophore module. The chosen fluorophore should have high fluorescence efficiency. The chosen receptor should bind the guest tightly and should be optically transparent at the absorbing wavelength of the fluorophore. Finally, the fluorophore and the receptor should be linked through a spacer such that PET is maximized in the *fluorophore-spacer-receptor* system. In general, a short and flexible spacer unit is better than long and rigid ones for an efficient PET in the system.

If PET between the fluorophore and receptor modules is to control the sensory action of the supermolecule, the photo energy contained within the electronically excited fluorophore must be thermodynamically allowed to drive the electron transfer process.[96] This can be schematized with a frontier orbital energy diagram for the PET pair as shown in Scheme 1.2. The thermodynamic driving force for PET can be calculated from the knowledge of the redox potentials of the fluorophore and the receptor and the singlet energy of the fluorophore using the following equation.[96,97]

$$\Delta G^{*} = [E_{ox}\,(\text{receptor}) - E_{red}\,(\text{fluorophore})] - E_{0,0} \qquad (1.1)$$

where ΔG^{*} is the free energy of the photoinduced electron transfer process, E_{ox} (receptor) is the oxidation potential of the receptor, E_{red} (fluorophore) is the reduction potential of the fluorophore and $E_{0,0}$ is the singlet energy of the fluorophore.

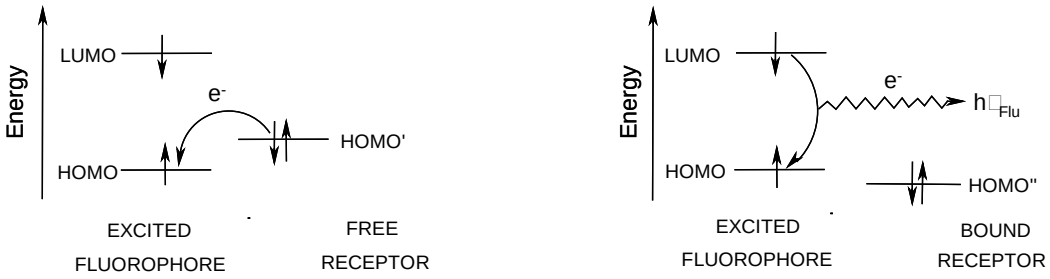

Scheme 1.2 Frontier orbital energy diagram for a fluorophore-receptor pair (a) where PET is feasible, (b) when the receptor is occupied by a cation.

The exothermicity ($\Delta G^* < 0$) is the primary requirement for an efficient electron transfer process. Small exergonic driving force is preferred over a large exergonicity so that it can be easily switched over to an endergonic condition by a suitable charge perturbation. Such a perturbation can occur when a guest lodges in the receptor unit, which should cause an increase in the oxidation potential of the guest bound receptor. A frontier orbital energy diagram for a guest-bound situation is shown in Scheme 1.2.

The receptors commonly employed in the design of PET fluorosensors contain amine functionalities as they are generally efficient quenchers of the fluorescence and are also good ligands for various guests. The popularity of the fluorescence PET signaling mechanism lies in the fact that the receptor systems can vary from very simple amines to very complex functionalities. A sensor can be made for various guest molecules by varying the receptor moieties satisfying the redox conditions. The discovery of crown ethers by Pederson has drastically changed the scenario of coordination chemistry.[98] Over the years, this branch of science has produced uncountable number of receptors suitable for specific binding and recognition of any kind of substrate, either ionic or neutral. Our job now is to link them to a light-emitting fragment to realize the luminescent sensor for a given molecule or ion of prominent interest in environmental chemistry, biology, medical analysis and diagnostics.

1. 2. 6. 2. Some examples

A breakthrough in fluorescence sensing was achieved when Tsien reported a system for real-time and real-space determination of the activity of Ca^{2+} within living cell by fluorescence microscopy.[99] From thereon, we have come a long way in the development of fluorescent PET sensors. Major contributions to the development of this class of fluorosensors have come from the research groups of Lehn, de Silva, Czarnik, Balzani, Fabbrizzi, Shinkai and Valeur. Some representative examples of PET sensors developed for various cations have been highlighted here.

Compound **14** is an early example of a fluorescent pH sensor.[100] Several systems based on anthracene chromophore followed with improved binding properties of the receptor units. Compound **15** exhibits pH dependent fluorescence in acetonitrile/water solutions.[101] The fluorescence is particularly quenched above pH 4.0 when the amino groups are proton free. With Cu^{2+} and Ni^{2+}, quenching of fluorescence is observed, while Zn^{2+} induces fluorescence enhancement.[101] Compound **16** behaves as more sophisticated "Off-On-Off" switch for protons.[102] This system also exhibits "Off-On" signaling behavior with Zn^{2+}.

The higher ligand field stabilization energies of Ni^{2+} and Cu^{2+} have been employed in designing selective fluorosensor **17** for these metal ions by using a dioxo-tetramine ligand.[103] The complexation mechanism involves abstraction of the amide protons. This can take place only with metal ions that profit by a large ligand field stabilization.[104] The difference in ligand field stabilization energy between Cu^{2+} and Ni^{2+} allows their distinction too. **18** is a cyclic analogue of **17** wherein the macrocyclic effect in binding the cations, Cu^{2+} and Ni^{2+}, results disadvantageously in narrowing the pH window available for selective titration.[101]

Compound **19** employs two PET active receptors. A degree of length recognition is achieved with this system and excellent switching "On" of fluorescence was found with α,ω-alkanediammonium ions.[105]

Compound **20** is capable of mimicking the switching phenomena based on molecular logic devices.[106] This system acts as an AND logic gate when H^+ and Na^+ are considered as the two ionic inputs, fluorescence as the output and exciting light as the power supply.

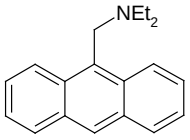

14

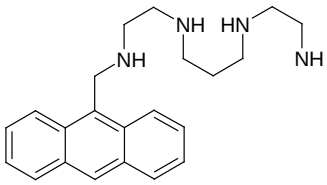

15

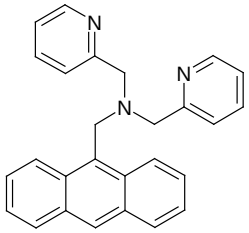

16

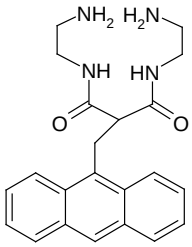

17

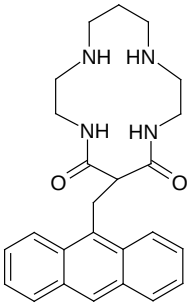

18

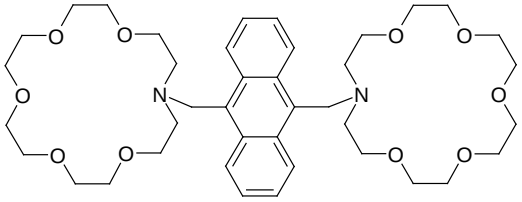

19

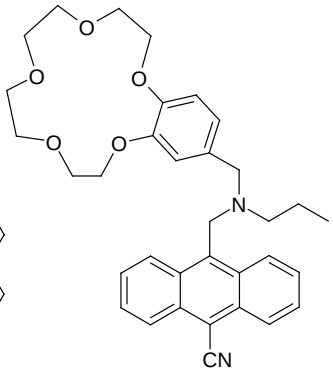

20

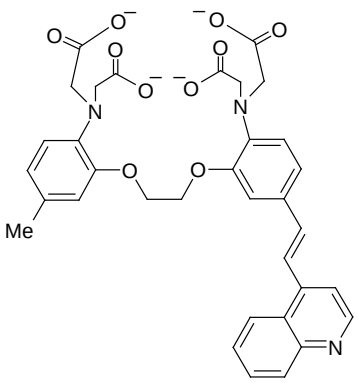

21

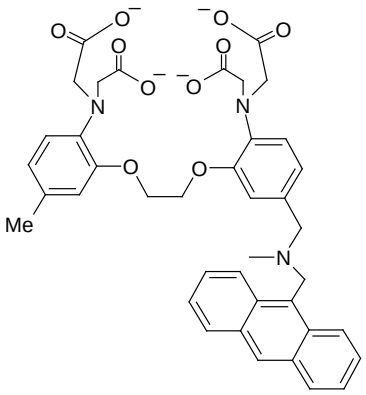

22

Compound **21** mimics the function of XOR logic gate induced by H^+ and Ca^{2+} ions.[30] Based on the design principle of **20**, molecule **22** was constructed that also responds to H^+ and Ca^{2+}, showing AND logic.[30] Operation of XOR gate **21** and AND gate **22** in parallel results into molecular-scale binary addition. Thus, elementary arithmetic operations with designed molecules using chemical inputs and optical outputs have been demonstrated.[30]

Compound **23** is reported to be the first system that is useful for the ratiometric determination of Zn^{2+} in aqueous medium.[107] The free molecule shows excimer emission in the 450-600 nm region. Addition of Zn^{2+} increases the excimer emission intensity. This behavior serves for a direct concentration measurement by following the monomer/excimer emission intensity ratio. Compounds **24** and **25** also represent fluorescent PET sensors in which the monomer-excimer emission intensity ratio serves as the tool to study the sensing behavior towards cations.[108,109] **24** gives larger stability constants with K^+ and Ba^{2+}. In **25**, the monomer like emission enhances in intensity and the excimer emission vanishes on binding $H_3N^+(CH_2)_7N^+H_32Cl^-$.

Compound **26** provides the first example of a metal-triggered metal-centered emission.[110] It contains a terpyridyl diester that can strongly bind Eu^{3+} and a crown to potentially bind K^+. PET from the azacrown moiety quenches the fluorescence of Eu^{3+} bound to the terpyridyl diester site. Binding of K^+ results in an enhancement in the fluorescence intensity of the system.

A cryptand based receptor has been employed in system **27**.[111] The cavity of the cryptand receptor is suitable for K^+. This system has been used quite successfully in monitoring the level of K^+ in blood and across biological membranes.

In **28**, the luminescence of dansyl chromophore and the high affinity of the tetra-azacrown are combined for signaling Zn^{2+} ions.[112] The system is found to bind Zn^{2+} with very high affinity at physiological pH. Compound **29**[113] is one of the several fluorescein-based fluorescent probes developed by Lippard and co-workers in recent years. These systems are developed for selective detection of Zn^{2+} ions at physiological conditions and are shown to be the promising candidates for application in neurosciences.

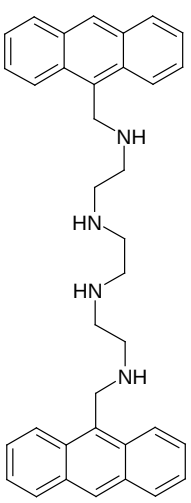

23

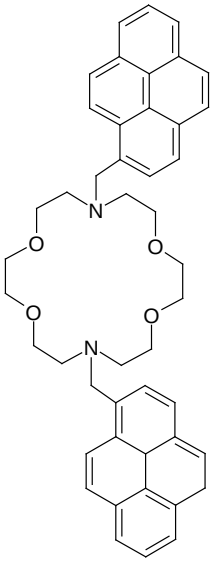

24

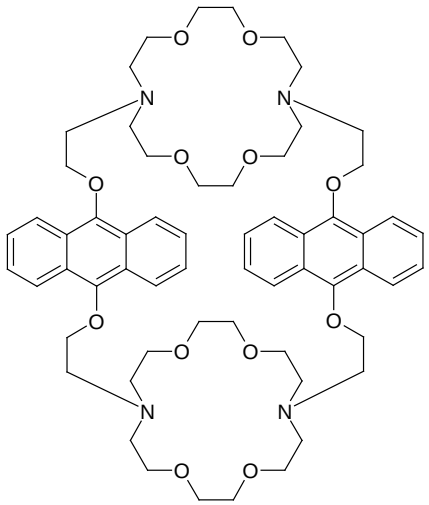

25

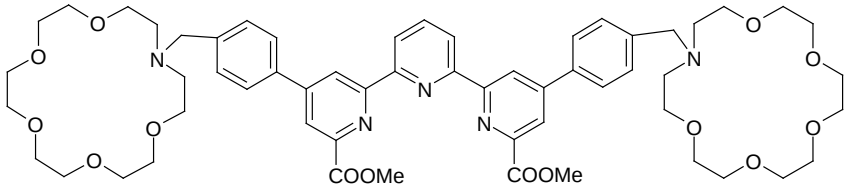

26

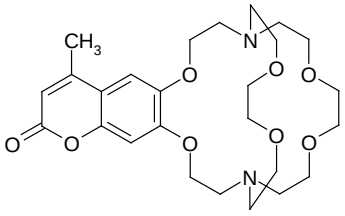

27

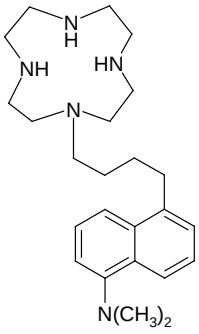

28

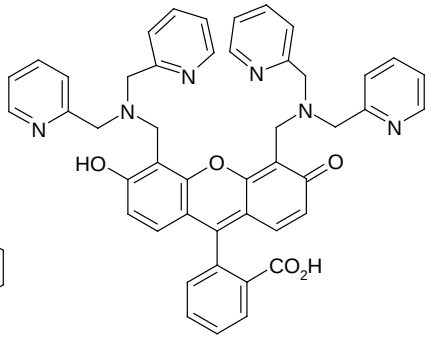

29

Macrocycles based on calix[4]arene[114] framework are also highly specific ligands[115-117] and their potential applications as hosts and sensing agents for various analytes have received increasing interest.[118] One representative example is compound **30** in which a pyrene fluorophore is attached to the calix[4]azacrown ether with a methylene spacer to prepare a calix[4]azacrown based fluoroionophore.[119] In the presence of metal ions, PET between the nitrogen atom of the azacrown moiety and the pyrene fluorophore is blocked and chelation enhanced fluorescence (CHEF) is observed. However, since the azacrown loop in this compound comprised ether units, it shows CHEF even in the presence of alkali and alkaline earth metal cations making the system non-selective.[119]

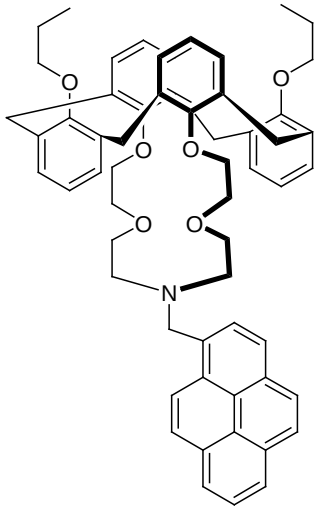

30

As evident from the above discussion, considerable work has been done on fluorescence signaling of the cations of s-block elements and d^{10} metal ions such as Zn^{2+}. What eluded the literature till recently were the "Off-On" fluorescence signaling systems for some of the heavy and transition metal (HTM) ions, though, as stated previously, these are metal ions of increasing importance in biology and environment. This is believed to be due to the fact that the transition metal ions are notorious quenchers of fluorescence.[120,121]

In order to develop efficient "Off-On" signaling systems for the transition metal ions, Bharadwaj and coworkers utilized a tripodal cryptand receptor to develop **31** that not only binds the metal ions tightly but also insulates them from the fluorophore moiety thereby preventing the quenching interaction between the metal ions and the fluorophore.[122] This system is reported to be the first fluorosensor for transition metal ions that are notorious for their quenching abilities.

On the other hand, Ramachandram and Samanta used a different strategy for the development of the "Off-On" sensor systems for the quenching metal ions.[123] Considering the redox nature of the interaction between the fluorophore and the transition metal ions, electronically deficient 4-aminophthalimide fluorophore has been employed

in the *fluorophore-spacer-receptor* system, **32**. This largely nullifies the quenching interaction of transition metal ions and significant fluorescence enhancement is observed.[123] Following these simultaneous breakthroughs, several systems are designed by employing variety of new strategies.[33,34]

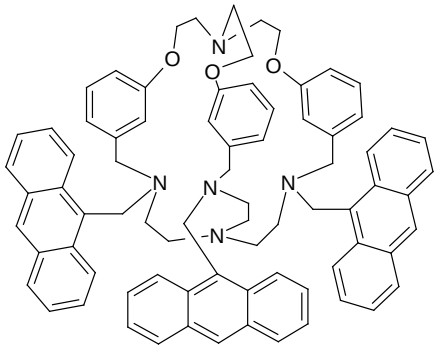

31

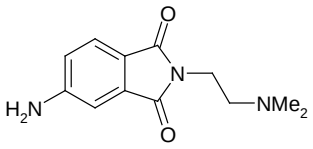

32

1. 3. Motivation behind the thesis

A large number of PET sensor molecules for alkali and alkaline earth metal ions are available in the literature.[31,32,44] Several fluorescent probes for the d^{10} metal ion Zn^{2+}, based on polypeptide,[124-126] protein,[127] macrocyclic[128-130] and acyclic receptors,[131] have also been designed in the recent years. Detection of heavy and transition metal (HTM) ions at the molecular level is also crucial as these metal ions represent an environmental concern when present in uncontrollable amounts and at the same time some of them such as iron, zinc, copper and cobalt are present as essential elements in biological systems. However, development of efficient "Off-On" fluorescence signaling systems for selective detection of HTM ions still remains a challenge[132] because of the inherent fluorescence quenching nature of these species. This prompted us to design and develop several photoactive molecular systems for the recognition and signaling of HTM ions. Also, considering the growing interest in molecules capable of performing logic and arithmetic operations, the sensory actions of our supermolecules are therefore logically interpreted. Even though more advanced practical integration of such molecular level logic gates into circuits is somewhat beyond the horizon, progress depends on the

generation of all fundamental logic operations and, our goal is to look into the potential of these systems in functioning of various logic operations. Moreover, in order to establish this and also to understand the factors leading to these operations, we have carried out single crystal X-ray structure analyses on most of the systems. Knowledge of structural assembly of molecules leading to specific network architecture and design is important for the construction of supramolecular machines or motors. In addition, although several multi-component systems have been designed and developed in our laboratory,[133,134] attempts have never been made to explore the coordination properties of the metal ions with these systems. This is primarily because of the lack of definite structural information on these systems. Because of these, special emphasis has been given to the solid-state structural analyses of the multi-component systems as well as their complexes with transition metal ions.

A significant disadvantage of intensity-based sensing is the problem of referencing the intensity measurements. The efficiency of light transmission and collection can vary from one instrument to another, and a constant intensity reference is frequently unavailable. The fluorescence intensity can also vary due to light scattering and/or absorption characteristics of the sample. Moreover, most fluorophores photobleach rapidly, which further complicates the ability to quantitatively use the intensity measurements. These effects require frequent recalibration and other corrections. As a result of these difficulties, alternative fluorescent probes and sensing methods are highly sought. Therefore, alternative strategies such as chromogenic and ratiometric sensing of HTM ions have also been explored.

In this context, several new systems, with a *fluorophore-spacer-receptor* architecture, have been developed and their fluorescence (“Off-On”) and optical signaling ability toward protons and HTM ions has been explored. Some of these systems are found to be highly selective for the recognition of metal ions and may have potential analytical applications. Systems that are found to be essentially non-selective have been used in the design of molecular switches for the operation of OR, NOR and INH logic gates. The strong and interesting binding properties of structurally well-developed cryptand or calix[4]azacrown macrocycles toward the transition metal ions have motivated us to design and develop the first set of compounds (**APL1** and **APL2**, Chapter 3).[135-137] The

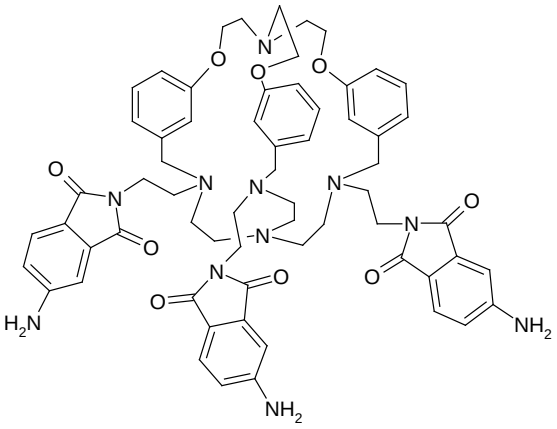

APL1

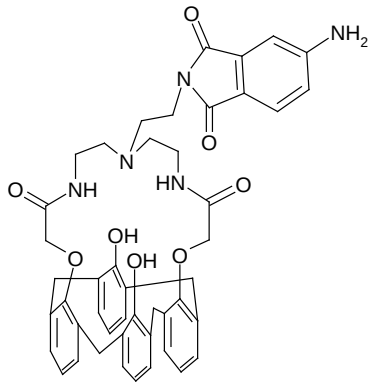

APL2

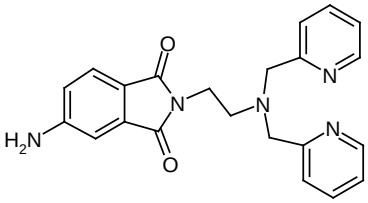

APDPA

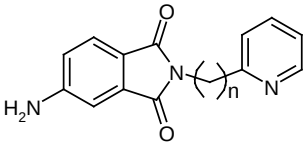

n = 1; APMPY
2; APEPY

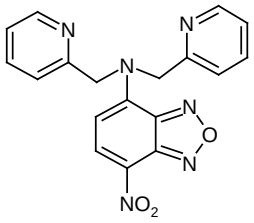

NBDDPA

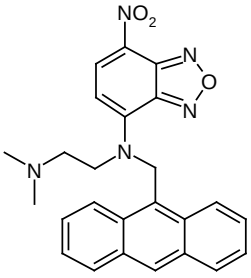

AMNEA

second and third sets of compounds constitute structurally simple molecular systems based on 4-aminophthalimide, which is a fluorophore of choice for designing fluorescent sensor systems for transition metal ions[123] (**APDPA**, Chapter 4; **APMPY** and **APEPY**, Chapter 5). PET is not observable in systems **APMPY** and **APEPY** and therefore they are not good candidates for signaling purposes. However, they serve as judicious candidates for the stabilization of Cu^{+} ions. Subsequently, we have developed a

chromogenic sensor based on 4-amino-7-nitrobenzoxa[1,3]diazole as an alternative approach for selective recognition of Cu^{2+} ions (**NBDDPA**, Chapter 6). A dual-fluorophore system has been designed with a view to providing a new approach to the ratiometric fluorescence signaling of HTM ions (**AMNEA**, Chapter 7).

References

1 Vögtle, F. *Supramolecular Chemistry*; John Wiley & Sons: Chichester, 1991.
2 Lehn, J.-M. *Supramolecular Chemistry*; VCH, Weinheim, 1995.
3 Steed, J. W.; Atwood, J. L. *Supramolecular Chemistry*; John Wiley & Sons: New York, 2000.
4 *Chemosensors of Ion and Molecular Recognition*; Desvergene, J. P.; Czarnik, A. W., Eds.; Kluwer Academic: Dordrecht, 1997; Vol. C492.
5 *Supramolecular Photochemistry*; Balzani, V., Ed.; Reidel Publishing Company.: Dordrecht., 1987.
6 Lehn, J.-M. *Angew. Chem., Int. Ed.* **1990**, *29*, 1304.
7 Spichiger-Keller, U. S. *Chemical Sensors and Biosensors for Medical and Biological Applications*; Wiley-VCH: Weinheim, 1998.
8 McCarty, G. S.; Weiss, P. S. *Chem. Rev.* **1999**, *99*, 1983.
9 Janshoff, A.; Nietzert, M.; Oberdorfer, Y.; Fuchs, H. *Angew. Chem., Int. Ed.* **2000**, *39*, 3213.
10 *Molecular Electronic Devices*; Carter, F. L.; Siatkowski, R. E.; Wohltjen, H., Eds.; Elsevier: Amsterdam, 1988.
11 de Silva, A. P.; McClenaghan, N. D.; McCoy, C. P. *Molecular Switches*; Wiley-VCH: Weinheim, 2000.
12 Balzani, V.; Venturi, M.; Credi, A. *Molecular Devices and Machines*; Wiley-VCH: Weinheim, 2003.
13 Bumm, L. A.; Arnold, J. J.; Cygan, M. T.; Dunbar, T. D.; Burgin, T. P.; Jones II, L.; Allara, D. L.; Tour, J. M.; Weiss, P. S. *Science* **1996**, *271*, 1705.
14 Wagner, R. W.; Lindsey, J. S.; Seth, J.; Palaniappan, V.; Bocian, D. F. *J. Am. Chem. Soc.* **1996**, *118*, 3996.
15 Kelly, T. R.; Bowyer, M. C.; Bhaskar, K. V.; Bebbington, D.; Garcia, A.; Lang, F.; Kim, M. H.; Jette, M. P. *J. Am. Chem. Soc.* **1994**, *116*, 3657.
16 Kelly, T. R.; Tellitu, I.; Sestelo, J. P. *Angew. Chem., Int. Ed.* **1997**, *36*, 1866.
17 Martin, A. S.; Sambles, J. R. *Adv. Mater.* **1993**, *5*, 580.
18 Clayden, J.; Pink, J. H. *Angew. Chem., Int. Ed.* **1998**, *37*, 1937.
19 Raymo, F. M.; Giordani, S. *J. Am. Chem. Soc.* **2001**, *123*, 4651.
20 Bissel, R. A.; Cordova, E.; Kaifer, A. E.; Stoddart, J. F. *Nature* **1994**, *369*, 133.
21 Ball, P. *New Scientist* **1997**, *155*, 32.
22 de Silva, A. P.; McClenaghan, N. D. *Chem. Eur. J.* **2004**, *10*, 574.
23 Katz, R. H. *Contemporary Logic Design*; Benjamin Cummings: CA, 1994.
24 Burger, P. *Digital Design: A Practical Course*; Wiley: New York, 1988.
25 de Silva, A. P.; Gunaratne, H. Q. N.; Maguire, G. E. M. *Chem. Commun.* **1994**, 1213.
26 de Silva, A. P.; Dixon, I. M.; Gunaratne, H. Q. N.; Gunnlaugsson, T.; Maxwell, P. R. S.; Rice, T. E. *J. Am. Chem. Soc.* **1999**, *121*, 1393.

27 de Silva, A. P.; Gunaratne, H. Q. N.; McCoy, C. P. *J. Am. Chem. Soc.* **1997**, *119*, 7891.
28 Credi, A.; Balzani, V.; Langford, S. J.; Stoddart, J. F. *J. Am. Chem. Soc.* **1997**, *119*, 2679.
29 Gunnlaugsson, T.; Mac Donail, D. A.; Parker, D. *Chem. Commun.* **2000**, 93.
30 de Silva, A. P.; McClenaghan, N. D. *J. Am. Chem. Soc.* **2000**, *122*, 3965.
31 de Silva, A. P.; Fox, D. B.; Huxley, A. J. M.; Moody, T. S. *Coord. Chem. Rev.* **2000**, *205*, 41.
32 Valeur, B.; Leray, I. *Coord. Chem. Rev.* **2000**, *205*, 3.
33 Prodi, L.; Bolletta, F.; Montalti, M.; Zaccheroni, N. *Coord. Chem. Rev.* **2000**, *205*, 59.
34 Rurack, K. *Spectrochim. Acta, Part A.* **2001**, *57*, 2161.
35 James, T. D.; Shinmori, H.; Shinkai, S. *Chem. Commun.* **1997**, 71.
36 Mandl, C. P.; Konig, B. *J. Org. Chem.* **2005**, *70*, 670.
37 Orellana, G.; Moreno-Bondi, M. C.; Segovia, E.; Marazuela, M. D. *Anal. Chem.* **1992**, *64*, 2210.
38 Pinalli, R.; Nachtigall, F. F.; Ugozzoli, F.; Dalcanale, E. *Angew. Chem., Int. Ed.* **1999**, *38*, 2377.
39 Fabbrizzi, L.; Lichelli, M.; Rabaioli, G.; Taglietti, A. *Coord. Chem. Rev.* **2000**, *205*, 85.
40 Parker, D. *Coord. Chem. Rev.* **2000**, *205*, 109.
41 Beer, P. D.; Cadman, J. *Coord. Chem. Rev.* **2000**, *205*, 131.
42 Lakowicz, J. R. *Principles of Fluorescence Spectroscopy*; Second ed.; Kluwer Academic/Plenum Publishers: New York, 1999.
43 *Topics in Fluorescence Spectroscopy*; Lakowicz, J. R., Ed.; Plenum Press: New York, 1994; Vol. 4.
44 de Silva, A. P.; Gunaratne, H. Q. N.; Gunnlaugsson, T.; Huxley, A. J. M.; McCoy, C. P.; Rademacher, J. T.; Rice, T. E. *Chem. Rev.* **1997**, *97*, 1515.
45 Kalyanasundaram, K.; Thomas, J. K. *J. Phys. Chem.* **1977**, *81*, 2176.
46 Ogawa, S.; Tsuchiya, S. *Chem. Lett.* **1996**, 709.
47 Nagasaki, T.; Tajirl, Y.; Shinkai, S. *Rec. Trav. Chim. Pays Bas* **1993**, *112*, 407.
48 Bunzli, J.-C. G. In *Lanthanide Probes in Life, Chemical and Earth Sciences*; Bunzli, J.-C. G., Choppin, G. R., Eds.; Elsevier: Amsterdam, 1989.
49 Martin, M. M.; Plaza, P.; Meyer, Y. H.; Badaoui, F.; Bourson, J.; Lefebvre, J. P.; Valeur, B. *J. Phys. Chem.* **1996**, *100*, 6879.
50 Létard, J.-F.; Lapouyade, R.; Rettig, W. *Pure Appl. Chem.* **1993**, *65*, 1705.
51 Mathevet, R.; Jonasauskas, G.; Rullière, C.; Létard, J.-F.; Lapouyade, R. *J. Phys. Chem.* **1995**, *99*, 15709.
52 Demas, J. N.; DeGraff, B. A. In *Topics in Fluorescence Spectroscopy*; Lakowicz, J. R., Ed.; Plenum Press: New York, 1994; Vol. 4.
53 Rettig, W.; Lapouyade, R. In *Topics in Fluorescence Spectroscopy*; Lakowicz, J. R., Ed.; Plenum Press: New York, 1994; Vol. 4.
54 Sousa, L. R.; Larson, J. M. *J. Am. Chem. Soc.* **1977**, *99*, 307.
55 Larson, J. M.; Sousa, L. R. *J. Am. Chem. Soc.* **1978**, *100*, 1943.
56 Shirai, M.; Tanaka, M. *Chem. Commun.* **1988**, 381.
57 Nishizawa, N.; Watanabe, M.; Uchida, T.; Terame, N. *J. Chem. Soc. Perkin Trans. 2* **1999**, 141.
58 Marquis, D.; Desvergne, J.-P.; Bouas-Laurent, H. *J. Org. Chem.* **1995**, *60*, 1784.
59 Kubo, K.; Sakurai, T. *Chem. Lett.* **1996**, 959.
60 Strauss, J.; Daub, J. *Org. Lett.* **2002**, *4*, 683.
61 Harriman, A.; Sauvage, J.-P. *Chem. Soc. Rev.* **1996**, *25*, 41.

62 Szmacinski, H.; Lakowicz, J. R. In *Topics in Fluorescence Spectroscopy*; Lakowicz, J. R., Ed.; Plenum Press: New York, 1994; Vol. 4.
63 Bissel, R. A.; de Silva, A. P.; Gunaratne, H. Q. N.; Lynch, P. L. M.; Maguire, G. E. M.; McCoy, C. P.; Sandanayake, K. R. A. S. *Top. Curr. Chem.* **1993**, *168*, 223.
64 Barltrop, J. A.; Coyle, J. D. *Excited States in Organic Chemistry*; Wiley: London, 1975.
65 Turro, N. J. *Modern Molecular Photochemistry*; University Science Books: Mill Valley, CA, 1991.
66 Wayne, R. P. *Principles and Applications of Photochemistry*; Oxford University Press: Oxford, 1988.
67 Kopecky, J. *Photochemistry: A Visual Approach*; VCH: New York, 1992.
68 Kalyanasundaram, K. *Photochemistry in Microheterogeneous Systems*; Academic Press: New York, 1983.
69 *Photochemistry in Organised and Constrained Media*; Ramamurthy, V., Ed.; VCH: New York, 1991.
70 Bisby, R. H.; Cundall, R. B.; Davenport, L.; Johnson, I. D.; Thomas, E. W. In *Fluorescent Probes*; Beddard, G. S., West, M. A., Eds.; Academic Press: London, 1981.
71 Waldeck, D. H. *Chem. Rev.* **1991**, *91*, 415.
72 Whitten, D. G. *Acc. Chem. Res.* **1993**, *26*, 502.
73 Sandanayake, K. R. A. S.; Nakashima, K.; Shinkai, S. *Chem. Commun.* **1994**, 1621.
74 Horrocks, W. D.; Sudnick, D. R. *Acc. Chem. Res.* **1981**, *14*, 384.
75 Richardson, F. H. *Chem. Rev.* **1982**, *82*, 541.
76 Balzani, V.; Sabbatini, N.; Scandola, F. *Chem. Rev.* **1986**, *86*, 319.
77 Sabbatini, N.; Guardigli, M.; Lehn, J.-M. *Coord. Chem. Rev.* **1993**, *123*, 201.
78 Pikramenou, Z.; Johnson, K. M.; Nocera, D. G. *Tetrahedron Lett.* **1993**, *34*, 3581.
79 Reichardt, C. *Chem. Rev.* **1994**, *94*, 2319.
80 Jones, G.; Jackson, W. R.; Kanoktanaporn, S.; Bergmark, W. R. *Photochem. Photobiol.* **1985**, *42*, 477.
81 Saha, S.; Samanta, A. *J. Phys. Chem. A* **1998**, *102*, 7903.
82 Bourson, J.; Borrel, M. N.; Valeur, B. *Anal. Chim. Acta* **1992**, *257*, 189.
83 Street, K. W.; Krause, S. A. *Anal. Lett.* **1986**, *19*, 735.
84 Grabowski, Z. R.; Dobokowski, J. *Pure Appl. Chem.* **1983**, *55*, 245.
85 Rettig, W. *Angew. Chem., Int. Ed. Engl.* **1986**, *25*, 971.
86 Kosower, E. M.; Huppert, D. *Ann. Rev. Phys. Chem.* **1986**, *37*, 127.
87 Grabowski, Z. R. *Pure Appl. Chem.* **1992**, *64*, 1249.
88 Bhattacharya, K.; Chowdhury, M. *Chem. Rev.* **1993**, *93*, 507.
89 Rettig, W. *Top. Curr. Chem.* **1994**, *169*, 253.
90 Weber, G.; Laurence, D. J. R. *Biochem. J.* **1954**, *31*, 56.
91 Kosower, E. M. *Acc. Chem. Res.* **1982**, *15*, 266.
92 Cowley, D. J. *Nature* **1986**, *319*, 14.
93 Shizuka, H.; Ogiwara, T.; Kimura, E. *J. Phys. Chem.* **1985**, *89*, 4302.
94 Minta, A.; Kao, J. P. Y.; Tsien, R. Y. *J. Biol. Chem.* **1989**, *164*, 8171.
95 Jonker, S. A.; Verhoeven, J. W.; Reiss, C. A.; Goubitz, K.; Heijdenrijk, D. *Rec. Trav. Chem. Pays Bas* **1990**, *109*, 154.
96 Rehm, D.; Weller, A. *Isr. J. Chem.* **1970**, *8*, 259.
97 Weller, A. *Pure Appl. Chem.* **1968**, *16*, 115.
98 Pedersen, C. J. *J. Am. Chem. Soc.* **1967**, *89*, 7017.

99 Grynkiewicz, G.; Poenie, M.; Tsien, R. Y. *J. Biol. Chem.* **1985**, *260*, 3440.
100 de Silva, A. P.; Rupasinghe, R. A. D. *Chem. Commun.* **1985**, 1669.
101 Fabbrizzi, L.; Lichelli, M.; Pallavicini, P.; Perotti, A.; Taglietti, A.; Sacchi, D. *Chem. Eur. J.* **1996**, *2*, 75.
102 de Silva, S. A.; Zaveleta, A.; Baron, D. E.; Allam, O.; Isidor, E. V.; Kashimura, N.; Percarpio, J. M. *Tetrahedron Lett.* **1997**, *38*, 2237.
103 Fabbrizzi, L.; Licchelli, M.; Pallavicini, P.; Perroti, A.; Sacchi, D. *Angew. Chem., Int. Ed.* **1994**, *33*, 1975.
104 Cotton, F. A.; Wilkinson, G. *Advanced Inorganic Chemistry*; Third ed.; Wiley Eastern Limited: New Delhi, 1976.
105 de Silva, A. P.; Sandanayake, K. R. A. S. *Angew. Chem., Int. Ed.* **1990**, *29*, 1173.
106 de Silva, A. P.; Gunaratne, H. Q. N.; McCoy, C. P. *Nature* **1993**, *364*, 42.
107 Scalfani, J. A.; Maranto, M. T.; Sisk, T. M.; Van Arman, S. A. *Tetrahedron Lett.* **1996**, *37*, 2193.
108 Kubo, K.; Kato, N.; Sakurai, T. *Bull. Chem. Soc. Jpn.* **1997**, *70*, 3041.
109 Fages, F.; Desvergne, J.-P.; Kampke, K.; Bouas-Laurent, H.; Lehn, J.-M.; Meyer, M.; Albrecht-Gary, A.-M. *J. Am. Chem. Soc.* **1993**, *115*, 3658.
110 de Silva, A. P.; Gunaratne, H. Q. N.; Rice, T. E.; Stewart, S. *Chem. Commun.* **1997**, 1891.
111 Golchini, K.; Mackovic-Basic, M.; Gharib, S. A.; Masilamani, D.; Lucas, M. E.; Kurtz, I. *J. Physiol.* **1990**, *258*, F438.
112 Kimura, E.; Koike, T. *Chem. Soc. Rev.* **1998**, *27*, 179.
113 Walkup, G. K.; Burdette, S. C.; Lippard, S. J.; Tsien, R. Y. *J. Am. Chem. Soc.* **2000**, *122*, 5644.
114 Gutsche, C. D. *Calixarenes*; Royal Society of Chemistry: Cambridge, 1989.
115 Bohmer, V. *Angew. Chem. Int. Ed. Engl.* **1995**, *34*, 713.
116 Ikeda, A.; Shinkai, S. *Chem. Rev.* **1997**, *97*, 1713.
117 Halouani, H.; Dumazet-Bonnamour, I.; Perrin, M.; Lamartine, R. *J. Org. Chem.* **2004**, *69*, 6521.
118 Diamond, D.; McKervey, M. A. *Chem. Soc. Rev.* **1996**, *25*, 15.
119 Kim, J. S.; Shon, O. J.; Rim, J. A.; Kim, S. K.; Yoon, J. *J. Org. Chem.* **2002**, *67*, 2348.
120 Varnes, A. W.; Dodson, R. B.; Wehry, E. L. *J. Am. Chem. Soc.* **1972**, *94*, 946.
121 Kemlo, J. A.; Shepherd, T. M. *Chem. Phys. Lett.* **1977**, *47*, 158.
122 Ghosh, P.; Bharadwaj, P. K.; Roy, J.; Ghosh, S. *J. Am. Chem. Soc.* **1997**, *119*, 11903.
123 Ramachandram, B.; Samanta, A. *Chem. Commun.* **1997**, 1037.
124 Godwin, H. A.; Berg, J. M. *J. Am. Chem. Soc.* **1996**, *118*, 6514.
125 Walkup, G. K.; Imperiali, B. *J. Am. Chem. Soc.* **1997**, *119*, 3443.
126 Walkup, G. K.; Imperiali, B. *J. Org. Chem.* **1998**, *63*, 6727.
127 Thompson, R. B.; Maliwal, B. P.; Fierke, C. A. *Anal. Chem.* **1998**, *70*, 1749.
128 Czarnik, A. W. *Acc. Chem. Res.* **1994**, *27*, 302.
129 Koike, T.; Watanabe, T.; Aoki, S.; Kimura, E.; Shiro, M. *J. Am. Chem. Soc.* **1996**, *118*, 12696.
130 Hirano, T.; Kikuchi, K.; Urano, Y.; Higuchi, T.; Nagano, T. *Angew. Chem., Int. Ed. Engl.* **2000**, *39*, 1052.
131 Burdette, S. C.; Frederickson, C. J.; Bu, W.; Lippard, S. J. *J. Am. Chem. Soc.* **2003**, *125*, 1778.
132 Royzen, M.; Dai, Z.; Canary, J. W. *J. Am. Chem. Soc.* **2005**, *127*, 1612.
133 Ramachandram, B. Ph.D. Thesis, University of Hyderabad, Hyderabad, India, 2000.

134 Sankaran, N. B. Ph.D. Thesis, University of Hyderabad, Hyderabad, India, 2003.
135 Chand, D. K.; Bharadwaj, P. K. *Inorg. Chem.* **1996**, *35*, 3380.
136 Oueslati, I.; Abidi, R.; Thuery, P.; Nierlich, M.; Asfari, Z.; Harrowfield, J.; Vicens, J. *Tetrahedron Lett.* **2000**, *41*, 8263.
137 Abidi, R.; Oueslati, I.; Amri, H.; Thuery, P.; Nierlich, M.; Asfari, Z.; Vicens, J. *Tetrahedron. Lett.* **2001**, *42*, 1685.

Chapter 2

Materials, Methods and Instrumentation

This chapter lists the materials used in this study that were procured from various commercial sources, describes the methods of solvent purification, various methodologies employed in the present investigation such as fluorescence quantum yield measurements, estimation of fluorescence enhancement upon guest binding and estimation of binding constant values. Methods for theoretical calculations, details concerning the instruments used and X-ray structure determinations are also presented. The standard error limits of various parameters conclude this chapter.

2. 1. Materials

4-Aminophthalimide (AP) and anthracene were obtained from TCI (Japan) and Sisco Chem. Industries, respectively. AP was recrystallized twice from ethanol/water mixture prior to photophysical experiments but used as received for synthesis. Anthracene was recrystallized from methanol. 4-Chloro-7-nitrobenzoxadiazole, methylbromoacetate, 1,2-dibromoethane, tris-(2-aminoethyl)amine, diethylenetriamine, aminomethylpyridine, aminoethylpyridine and N,N-dimethylethylenediamine used for synthesis were obtained from Lancaster. Di-2-picolylamine was obtained from TCI (Japan). Triethanolamine, thionyl chloride, 3-hydroxybenzaldehyde, p-t-butylphenol, phenol and 37% formaldehyde solution were obtained either from Merck (India) or Sisco Chem. Industries. Common chemicals such as sodium hydride, sodium hydroxide, sodium borohydride, potassium hydroxide, potassium carbonate, potassium permanganate, potassium iodide, iodine, aluminium chloride and benzophenone were obtained either from Rankem or Loba. Silica gel and neutral alumina, used for thin-layer and column chromatography, were purchased from Acme Scientifics (India). HEPES and PIPES buffer salts were obtained from Lancaster. The various drying agents used such as sodium sulphate, calcium oxide, magnesium turnings, sodium metal etc. and synthesis grade solvents were procured from local companies. Calcium hydride was obtained from

Spectrochem (India). GR grade solvents were obtained from Merck (India) for spectroscopic purposes and were dry-distilled before use. Deuteriated solvents, chloroform-d, methanol-d_4, acetonitrile-d_3, dimethylsulphoxide (DMSO)-d_6 and D_2O used for NMR spectral measurements were obtained either from Aldrich or from Merck (India). All the metal salts described in the investigation were hydrated perchlorate salts and were obtained either from Aldrich or Acros Organics.

2. 2. Purification of solvents

The solvents used at various stages of the study were purified using the general procedures available in the literature.[1] We adopted the following procedures for the purification of various solvents. The purified solvents were optically transparent in the spectral region of interest.

Toluene, 1,4-dioxane and tetrahydrofuran: The solvent was refluxed over metallic sodium for 3-4 h and added benzophenone. The dark blue solution was refluxed for a further one hour and collected under dry conditions.

Acetonitrile: Acetonitrile was stirred with calcium hydride for 5-6 h and then distilled. The distilled solvent was collected and stored under dry conditions.

Methanol: After the initial drying over CaH_2 by keeping overnight, 50-75 mL of methanol was added to clean dry magnesium turnings (5 g) and iodine (0.5 g) and warmed until all magnesium was converted into magnesium methoxide. About 1 L of methanol was added to this, refluxed for 2-3 h and distilled out.

Ethanol: Ethanol was refluxed with stirring over anhydrous calcium oxide for 6 h. The solution was left at room temperature overnight. This was then distilled and further dried over magnesium and iodine and collected under dry atmosphere.

N,N-dimethylformamide: The solvent was stirred with calcium hydride for 5-6 h and distilled under vacuum at 80°C. Precautions were taken to store the solvent under dry conditions.

Water: Water was initially distilled using potassium permanganate and potassium hydroxide. This was subsequently distilled twice before taken to study.

2. 3. Sample preparation for spectral measurements

The solutions of the sensor systems were prepared such that the absorbance of the solution (1 cm path length) at the excitation wavelength is between 0.1 and 0.2. The actual concentrations of the sensor systems varied depending on the extinction coefficients of the systems. The concentration for all the systems corresponding to an absorbance value of 0.2 was in the range of 1×10^{-6} – 1×10^{-4} M. A concentrated stock solution of the metal salt was prepared in a given solvent. The concentration of this solution was then adjusted such that not more than 150 μL were added (using a microlitre syringe) during the titration experiment with 3 mL solution of the sensor molecule, taken in a quartz cuvette.

2. 4. Measurement of the fluorescence quantum yield

Fluorescence quantum yield was calculated by measuring the integrated area under the emission curves and by using the following equation.[2]

$$\Phi_{\text{sample}} = \frac{I_{\text{sample}} \times OD_{\text{standard}} \times \eta^2_{\text{sample}}}{I_{\text{standard}} \times OD_{\text{sample}} \times \eta^2_{\text{standard}}} \times \Phi_{\text{standard}} \qquad (2.1)$$

where Φ is the quantum yield, I is the integrated intensity, OD is the optical density, and η is the refractive index. The subscript ‘sample’ or ‘standard’ refers to the fluorophore of unknown quantum yield or the reference fluorophore of known quantum yield, respectively.

For quantum yield measurements, optically matched solutions of the sample and the standard at a given absorbing wavelength were prepared. Fluorescence quantum yield of AP-substituted compounds was measured with reference to that of **AP** (ϕ_f in acetonitrile is 0.63).[3] In the case of **NBDDPA**, the fluorescence quantum yield was determined with reference to that of 4-amino-7-nitrobenzoxadiazole (**ANBD**) fluorophore (ϕ_f in acetonitrile is 0.70).[4] For the dual emissive compound **AMNEA**, the fluorescence quantum yield was determined with reference to anthracene (ϕ_f in THF is 0.297)[5] and **ANBD**.

2. 5. Estimation of fluorescence enhancement

The magnitude of the maximum fluorescence enhancement was calculated from the following equation, using the integrated area of the fluorescence curves.

$$FE = I_F\,(max)/I_F\,(zero) \tag{2.2}$$

where, FE is the fluorescence enhancement, I_F (max) is the integrated area of the fluorescence curve obtained on adding the maximum required amount of the guest species and I_F (zero) is the corresponding area at zero concentration of the guest. Both I_F (max) and I_F (zero) were measured under identical experimental conditions.

2. 6. Estimation of binding constant[6]

2. 6. 1. Using absorption data

Binding affinity of a sensor system for transition metal ions was investigated from the changes in their absorption spectrum in the presence of these metal ions. A Job's plot experiment was performed to estimate the stoichiometry of the complex formed.

1:1 complex formation between the fluorosensor (*F*) and the metal salt (*M*) can be represented as

$$F + M = C \tag{2.3}$$

where *C* stands for the complex.

The association constant (*K*) was evaluated from the absorption data by the following method.

At equilibrium, the equilibrium constant

$$K = \frac{[C]}{([F]_0 - [C])([M]_0 - [C])} \tag{2.4}$$

where $[C]$ is the equilibrium concentration of the complex, $[F]_0$ is the initial concentration of the fluorosensor, and $[M]_0$ is the initial concentration of the metal salt.

By substituting the term $\Delta A/\Delta\varepsilon$ for [*C*] (for a path length of 1 cm) the following equation can be derived,

$$\frac{[F]_0[M]_0}{\Delta A} = \left([F]_0 + [M]_0 - \frac{\Delta A}{\Delta \varepsilon}\right)\frac{1}{\Delta \varepsilon} + \frac{1}{K\Delta \varepsilon} \qquad (2.5)$$

where, ΔA is the change in absorbance due to the addition of metal salts, and $\Delta \varepsilon$ is the difference between the molar extinction coefficient of the complex and the fluorosensor.

A plot of $\frac{[F]_0[M]_0}{\Delta A}$ vs. $\left([F]_0 + [M]_0 - \frac{\Delta A}{\Delta \varepsilon}\right)$ would yield a straight line with slope $1/\Delta \varepsilon$ and intercept $1/K\Delta \varepsilon$.

However, knowledge of the unknown quantity $\Delta \varepsilon$ was needed to make this plot. Consequently, a tentative value of $\Delta \varepsilon$ was determined by using data from two solutions and solving equation (2.5) simultaneously for $\Delta \varepsilon$ and K. Using this value of $\Delta \varepsilon$ a plot was made, employing data from a series of solutions, and a new value of $\Delta \varepsilon$ was determined along with a new value of K. This procedure was repeated until a consistent set of values for both $\Delta \varepsilon$ and K were obtained from two successive plots.

2. 6. 2. Using Fluorescence data

Since metal ion-induced changes of the fluorescence spectra are more pronounced than those of the absorption spectra, the K values, in a certain case, were evaluated from the fluorescence data. The method based on which the K values were estimated is given below.

The association constant (K) for 1:1 complexation is given by,

$$K = \frac{[C]}{([F]_0 - [C])([M]_0 - [C])} \qquad (2.6)$$

where $[C]$ is the equilibrium concentration of the complex, $[F]_0$ is the initial concentration of the fluorosensor, and $[M]_0$ is the initial concentration of the metal salt. Because the measurements were performed with $[F]_0 >> [M]_0$, $([F]_0 - [C]) \approx [F]_0$. Hence,

$$K = \frac{[C]}{[F]_0([M]_0 - [C])} \qquad (2.7)$$

By rearranging, we obtain

$$\frac{[C]}{[F]_0} = \frac{K[M]_0}{1+K[F]_0} \tag{2.8}$$

The total fluorescence yield, ϕ, is

$$\phi = \frac{\phi_F I_F + \phi_C I_C}{I_F + I_C} \tag{2.9}$$

where ϕ_F and ϕ_C represent the fluorescence yield of the fluorophore and the complex, respectively and I_F and I_C stand for the number of photons absorbed per unit volume per unit time by the fluorophore and the complex, respectively.
Therefore, we can write

$$\phi = \frac{\phi_F + \phi_C I_C / I_F}{1+ I_C / I_F} \tag{2.10}$$

Also, $I_F/I_C = \varepsilon_F [F]_0 / \varepsilon_C [C]$ where ε_F and ε_C are the molar extinction coefficients of the fluorophore and the complex, respectively, at the exciting wavelength.
Hence,

$$\frac{[C]}{[F]_0} = \frac{\varepsilon_F I_C}{\varepsilon_C I_F} \tag{2.11}$$

By combining eqs 2.8 and 2.11 and using $\varepsilon_F = \varepsilon_C$, we get

$$\frac{I_C}{I_F} = \frac{K[M]_0}{1+K[F]_0} \tag{2.12}$$

By substituting eq 2.12 into eq 2.10, we obtain

$$\phi = \frac{\phi_F + \phi_C K[M]_0 /(1+K[F]_0)}{1+K[M]_0 /(1+K[F]_0)} \tag{2.13}$$

After rearranging, we get

$$\frac{1}{\phi - \phi_F} = \frac{(1 + K[F]_0)/K(\phi_C - \phi_F)}{[M]_0} + \frac{1}{(\phi_C - \phi_F)} \qquad (2.14)$$

Hence, a plot of $(\phi - \phi_F)^{-1}$ against $[M]_0^{-1}$ should yield a straight line whose slope (m) and intercept (c) are given by $m = (1 + K[F]_0)/K(\phi_C - \phi_F)$ and $c = 1/(\phi_C - \phi_F)$. Therefore, the complexation constant

$$K = (m/c - [F]_0)^{-1} \qquad (2.15)$$

2. 7. Theoretical calculations

The structural parameters of the molecules in gas phase and their ground-state dipole moments were calculated using quantum mechanical calculation based on semi-empirical PM3 or AM1 (Austin Model 1) method.[7,8] PM3 is a reparameterization of the AM1 method. The calculations were performed using HyperChem package (Release 5.0) for Windows obtained from Hypercube, Inc. Unrestricted geometry optimization of the molecular structure was done at the semi-empirical level using conjugate gradient (Polak-Ribiere) type of algorithm with root-mean-square (rms) gradient as the convergence criterion. The rms gradient was kept below 0.001 kcal/(Åmol) in all the cases. The ground state dipole moment and the structural parameters were determined from single point calculation on the optimized geometry.

2. 8. Instrumentation

IR spectra were recorded either on a Jasco FT-IR/5300 spectrometer or on a Shimadzu spectrometer. NMR spectra were recorded either on a Brucker ACF 200 MHz or Brucker AVANCE 400 MHz spectrometer at ambient temperature and were referenced to the internal ^{1}H and ^{13}C solvent peaks.

Fast atom bombardment (FAB) mass spectrometry was performed at Central Drug Research Institute (CDRI) and Indian Institute of Chemical technology (IICT). The spectra were recorded at room temperature on a JEOL SX 102/DA-6000 Mass

spectrometer using argon/xenon (6kV, 10mA) as the FAB gas. The accelerating voltage was 10 kV. m-Nitrobenzyl alcohol was used as the matrix.

The UV-vis absorption spectral measurements were carried out on a Shimadzu UV-3101PC spectrophotometer. The fluorescence spectra were recorded either on a Spex FluoroMax-3 or Spex FluoroLog-3 spectrofluorimeter.

The fluorescence lifetimes were measured using the IBH-5000 single photon counting spectrofluorimeter.[9] A hydrogen flash lamp of pulse width 1.2 ns with a repetition rate of 40 kHz was employed as the excitation source for all measurements described in chapter 3. For measurements described in chapter 7, diode lasers (FWHM 75 – 100 ps) as the excitation source and an MCP photomultiplier (rise time of 60 ps) as the detector were used. After deconvolution, the time resolution of the setup was around 40 ps. A small fraction of the excitation pulse was detected by a photomultiplier tube (IP28) and the photomultiplier signal was fed into a constant fraction discriminator (CFD) to discriminate the background noise and to generate a precise timing pulse. The output of CFD served as the START pulse of the time to amplitude converter (TAC). A fluorescence photon recorded by the emission photomultiplier (Hamamatsu 3235), as determined by the discriminator, generated a pulse, which served as the STOP signal for TAC. The TAC signal produced was proportional to the time taken from the excitation event to the first photon recorded. The signal from TAC was digitized by the analog to digital converter (A/D converter) and sent to the appropriate channel, depending on the digitized value of the TAC voltage of a multi-channel analyzer (MCA). The whole process was repeated so that the MCA counts represented the number of photon events as a function of time. After many excitation pulses, the MCA memory contents represented a histogram of the emission decay i.e. time profile of the fluorescence intensity. For recording the lamp profile, a scatterer (dilute solution of Ludox in water) was placed in the place of the sample.

Data Analysis: The program used for the estimation of fluorescence lifetimes from the fluorescence decay curves was based on reconvolution least squares method.[10] When the decay time is long compared to the decay time of the excitation pulse, the excitation may be described as a δ-function. However, when the lifetime is short, distortion of the experimental data occurs by the finite decay time of the lamp pulse and response time of

the photomultiplier and associated electronics. Since the measured decay function is convolution of the true fluorescence decay, it is necessary to analyze the data by deconvolution in order to get the fluorescence lifetime. The mathematical statement of the problem is given by the following equation:

$$D(t) = \int_0^t P(t')G(t-t')dt' \qquad (2.16)$$

where, D(t) is the fluorescence intensity at time t, P(t') is the intensity of the exciting light at time t' and G(t-t') is the response function of the experimental system. The experimental data D(t) and P(t') from the MCA were fed into a personal computer (PC) to determine the lifetime. We used the IBH program to analyze the multi-exponential decays. An excitation pulse profile was recorded and then deconvolution started with mixing of the excitation pulse and a projected decay to form a new reconvoluted set. The data was compared with the experimental set and the difference between the data points summed, generating χ^2 function for the fit. The deconvolution proceeded through a series of such iterations until an insignificant change of χ^2 occurred between iterations. The inspection of reduced χ^2, a plot of weighted residuals and autocorrelation function of the residuals, assessed the quality of the fit.

2. 9. X-ray crystallography

Single crystals for all the compounds, suitable for X-ray diffraction studies, were grown from the slow evaporation of their dilute solutions. The raw data were collected either on Enraf-Nonius Mach-3 four circle CAD-4 diffractometer or Bruker CCD X-ray diffractometer. The details of the collection and reduction of data for various compounds are given below.

Collection and reduction of X-ray data from CAD-4 diffractometer: A tiny single crystal was mounted on the tip of glass fiber and then mounted on the goniometer. The X-ray data were collected on an Enraf-Nonius Mach-3 four circle CAD-4 diffractometer employing graphite monochromatized Mo Kα radiation (λ = 0.71073 Å) by ω-scan method. Unit cell parameters were determined by least squares fit to 25 reflections within a narrow θ range. The data were collected at room temperature using CAD4 software.

Intensities of three check reflections were measured after every 1.5 h during the data collection to monitor the stability of the crystals. Intensity decay was not observed for any of the crystals. XCAD4 was employed for the data reduction.[11] Wherever required, absorption corrections were applied using psi-scan absorption correction method.

Collection and reduction of X-ray data from CCD diffractometer: A tiny single crystal was mounted on the tip of glass fiber and transferred to a Bruker CCD X-ray diffraction system with a graphite-monochromatized Mo Kα radiation (λ = 0.71073 Å) controlled by a Pentium-based PC running the SMART software package.[12] Data were collected either at room temperature or at 100 K and the raw data frames were integrated by the SAINTPLUS program package.[13] Empirical absorption corrections were applied with the SADABS program[14] and the space group was determined by examining systematic absences and confirmed by the successful solution and refinement of the structure.

The structures were solved by direct methods and refined by full matrix least-squares and difference Fourier techniques with SHELXS-97 and SHELXL-97 programs[15] respectively or with SHELXTL program package.[16] In one particular case, the structure was solved by patterson method where direct method solution failed.[17] All non-hydrogen atoms were refined anisotropically. Hydrogen atoms attached to amine nitrogen atoms and water molecules were introduced as found on the Fourier difference maps and refined with restraint N–H = 0.87 Å and O–H = 0.82 Å, respectively, with displacement parameter equal to 1.5 times that of the parent atom. All other hydrogen atoms were introduced geometrically and refined using a riding model with a displacement parameter equal to 1.2 (amide NH, CH, CH_2) or 1.5 (OH, CH_3) times that of the parent atom. Multipurpose crystallographic tools, PLATON,[18] ORTEP-3[19] and MERCURY,[20] were used for molecular graphics. Relevant crystallographic parameters and the thermal ellipsoid plot for various compounds are presented in their respective chapters. Detailed information for all the structures have been provided as appendix.

2. 10. Standard error limits

Standard error limits involved in the measurements are:

λ_{max} (abs./fluo.)	± 2 nm	
ϕ_f	± 10%	
FE	± 10%	
τ_f (> 1 ns)	± 5%	(Applicable to the fluorescence lifetime data
τ_f (< 1 ns)	± 15%	presented in chapter 3)
τ_f (> 40 ps)	± 5%	(Applicable to the fluorescence lifetime data presented in chapter 7)

References

1 Perrin, D. D.; Armerego, W. L. F.; Perrin, D. R. *Purification of Laboratory Chemicals*; Pergamon Press: New York, 1980.
2 Austin, E.; Gouterman, M. *Bioinor. Chem.* **1978**, *9*, 281.
3 Soujanya, T.; Fessenden, R. W.; Samanta, A. *J. Phys. Chem.* **1996**, *100*, 3507.
4 Ramachandram, B.; Samanta, A. *J. Phys. Chem. A* **1998**, *102*, 10579.
5 Ghosh, P.; Bharadwaj, P. K.; Mandal, S.; Ghosh, S. *J. Am. Chem. Soc.* **1996**, *118*, 1553.
6 Connors, K. A. *Binding Constants*; Wiley: New York, 1987.
7 Dewar, M. J. S.; Zoebisch, E. G.; Healy, E. F.; Stewart, J. J. P. *J. Am. Chem. Soc.* **1985**, *107*, 3902.
8 Dewar, M. J. S.; Dieter, K. M. *J. Am. Chem. Soc.* **1986**, *108*, 8075.
9 O'Connor, D. V.; Phillips, D. *Time-Correlated Single Photon Counting*; Academic Press: London, 1984.
10 Bevington, P. R. *Data Reduction and Error Analysis for the Physical Sciences*; McGraw-Hill: New York, 1969.
11 Harms, K.; Wocadlo, S. ; University of Marburg: Germany, 1995.
12 *SMART*; 5.629 ed.; Bruker AXS, Inc.: Madison, WI, 2003.
13 *SAINTPLUS*; 6.45 ed.; Bruker AXS, Inc.: Madison, WI, 2003.
14 *SADABS*; 2.10 ed.; Bruker AXS, Inc.: Madison, WI, 2003.
15 Sheldrick, G. M. *SHELXS-97 and SHELXL-97, Program for the Solution and Refinement of Crystal Structures*; Universität of Göttingen: Göttingen, Germany, 1997.
16 *SHELXTL*; 6.14 ed.; Bruker AXS, Inc.: Madison, WI, 2003.
17 Sheldrick, G. M. *Acta Cryst.* **1990**, *A46*, 467.
18 Spek, A. L. ; Utrecht University: Utrecht, The Netherlands, 1998.
19 Farrugia, L. J. *J. Appl. Cryst.* **1997**, *30*, 565.
20 *MERCURY*; 1.2.1 ed.; CCDC: UK, 2004.

Chapter 3

4-Aminophthalimide appended cryptand and calix[4]azacrown

This chapter discusses the synthesis, characterization, photophysical properties and transition metal ion signaling behavior of two three-component systems, comprising cryptand and calix[4]azacrown moieties as the receptor components. Both the systems have been developed employing a 4-aminophthalimide moiety as the fluorophore and a dimethylene moiety as the spacer components. These systems, based on *fluorophore-spacer-receptor* architecture, were targeted at efficient sensing of the transition metal ions by exploiting the strong coordination properties of the macrocyclic cryptand and the calix[4]azacrown ligands.

3. 1. Introduction

As stated earlier, development of practical "Off-On" fluorescence sensors for transition metal ions still remains a challenge because of their fluorescence quenching nature. The quenching interaction between these metal ions and the fluorophore can be suppressed by employing a structurally well-developed receptor unit in the fluoroionophore system.[1] Therefore, macrocyclic cryptand (**L1**) and calix[4]azacrown (**L2**) have been chosen as a receptor unit to design multi-component systems for efficient chelation enhanced fluorescence sensing of the transition metal ions. An electron-deficient 4-aminophthalimide (**AP**) moiety is chosen as the fluorophore component so that the metal-fluorophore quenching interaction is minimized.[2] The fluorophore and the receptor have been linked through a dimethylene spacer unit to develop fluorescence PET sensors, **APL1** and **APL2**, with a *fluorophore-spacer-receptor* framework.

APL1 is found to be non-selective in its response towards various transition metal ions because of poor chemoselectivity of the receptor part moiety. Thus, **APL1** represents a molecular photonic OR logic gate with the transition metal ions functioning as logic inputs. On the other hand, **APL2** exhibits certain degree of selectivity for Fe^{3+} and Cu^{2+}

ions over other transition metal ions. Both **APL1** and **APL2** are inactive in their response towards alkali and alkaline earth metal ions. The complexation properties of both the systems are discussed in detail. The association constants calculated from either absorption or fluorescence spectral data suggest that these systems bind strongly with transition metal ions. Single crystal structure analyses of the ligand **L2** and its complex with perchloric acid (**L2-HClO$_4$**) provided a tentative explanation for the interesting complexation feature of calix[4]azacrown on the basis of intra- and intermolecular hydrogen bonding investigated in the structure.

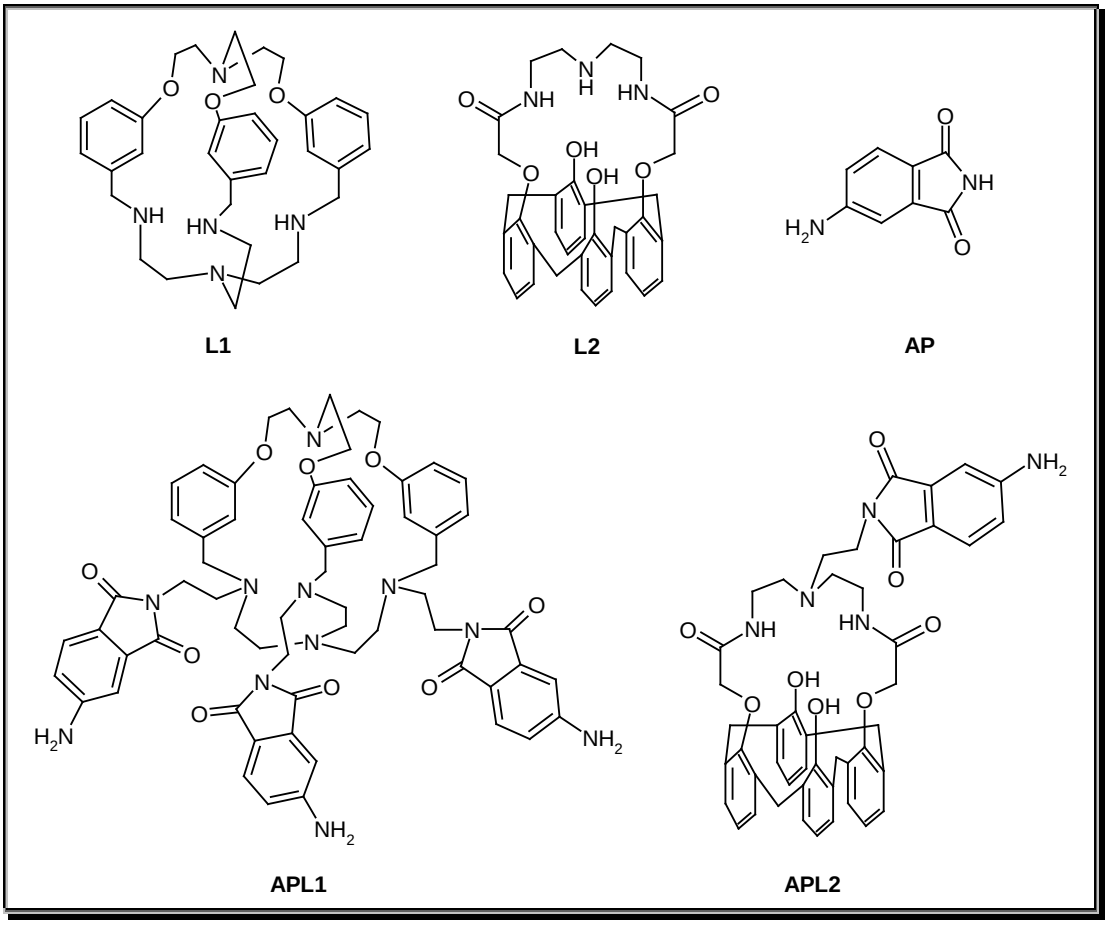

3. 2. Synthesis

3. 2. 1. Synthesis of APL1

The cryptand derivative of **AP** was synthesized following a multi-step synthetic procedure (Scheme 3.1).

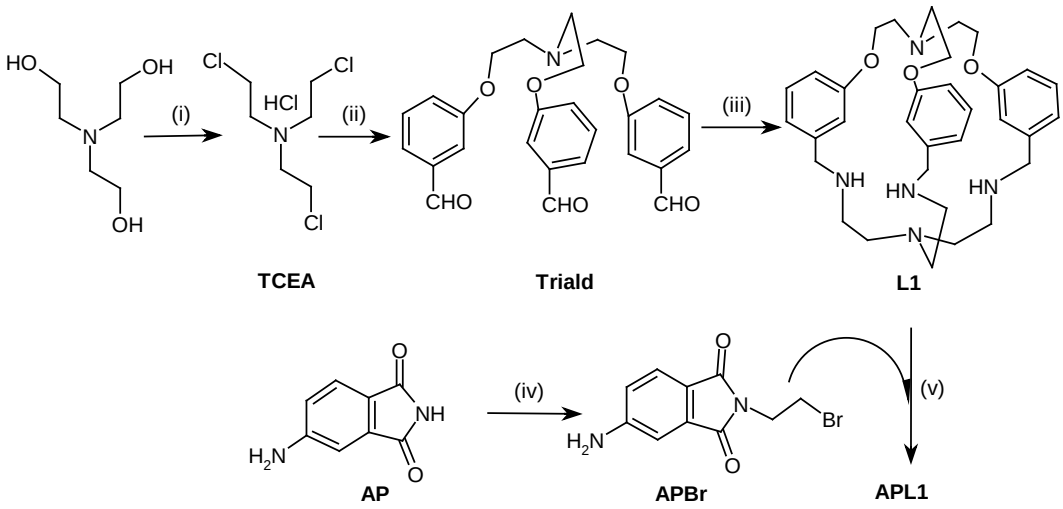

Scheme 3.1 Synthetic routes for the fluorescent sensor **APL1**. Conditions: (i) $SOCl_2$, $CHCl_3$; (ii) 3-hydroxybenzadehyde, NaOH, propanol, reflux, 4 h; (iii) tris(2-aminoethyl)amine, dry MeOH–THF, 5°C; $NaBH_4$, reflux, 4 h; (iv) NaH, dry DMF, 1,2-dibromoethane, room temperature, 24 h; (v) K_2CO_3, KI, MeCN, reflux, 36 h.

The cryptand (**L1**) was prepared in three steps starting from triethanolamine, according to the published procedure.[3,4] The fourth step consisted of the preparation of N-bromoethyl-4-aminophthalimide (**APBr**). The final step involved the reaction between **APBr** and **L1** to obtain the sensor system, **APL1**. All the products were purified by recrystallization and/or column chromatography and were characterized by conventional methods.

Step 1: Tris-2-chloroethylamine hydrochloride (TCEA). Triethanolamine (41 mL, 0.3 mol) was dissolved in $CHCl_3$ (40 mL) and added drop by drop, with stirring, to a solution of thionylchloride (90 mL, 1.2 mol, 33% excess) in $CHCl_3$ (60 mL). When all the amine had been added, the volatile products were distilled off and the remaining crystalline mass was recrystallized from acetone.[3]‡

Step 2: Tris{[2-(3-(oxomethyl)phenyl)oxy]ethyl}amine (Triald). To a solution of 3-hydroxybenzaldehyde (7.33g, 60 mmol) in propanol (200 mL) was added crushed NaOH (3.2 g, 80 mmol) and stirred at 30°C for 30 min. To the resulting brown solution, **TCEA** (4.8 g, 20 mmol) was added at once, and the mixture was heated under reflux for 4 h. After this period, the brown solution was allowed to cool to room temperature, and poured into 200 mL of cold water. The product was extracted from this mixture with $CHCl_3$ (3 × 50 mL). The organic layer was washed several times with water, then dried over anhydrous Na_2SO_4 and finally treated with activated charcoal. The tripodal trialdehyde was obtained by evaporating the organic layer as a pale yellow semisolid in 72% yield (lit. 80%).[4]

Step 3: Cryptand (L1). **Triald** (3.68 g, 8 mmol) dissolved in a mixture of dry MeOH (500 mL) and dry THF (50 mL) was cooled to 5°C. To this was added a solution of tris(2-aminoethyl)amine (1.17 g, 8 mmol) in MeOH (300 mL) over a period of 12 h with constant stirring while maintaining the temperature at 5°C. After the addition was complete the light yellow solution was allowed to warm to room temperature and kept for another 12 h. The Schiff base formed was not isolated but immediately treated with an excess of solid $NaBH_4$ (~1.6 g) and refluxed for 4 h. The white solid left after complete removal of the solvent was shaken with water (40 ml) and the desired cryptand was extracted with $CHCl_3$ (4 × 50 mL). The organic layer after drying over anhydrous Na_2SO_4 was completely evaporated to obtain a pale yellow solid that was washed with acetonitrile (50 mL) to afford the desired cryptand. Yield 25% (lit. 39%).[4]

‡ Caution! The product as well as the free base have a marked vesicant action. After few hours of it had been handled, irritation between the fingers started and the next morning large red welts and blisters had formed at several places on the hands, arms, etc.

Step 4: N-Bromoethyl-4-aminophthalimide (APBr). 4-Aminophthalimide (0.81 g, 5 mmol) was treated with previously washed NaH (0.6 g, 25 mmol) in dry DMF (10 mL) at room temperature with constant stirring for 1 h. Subsequently, 1,2-dibromoethane (0.87 mL, 10 mmol) was added to the reaction mixture and stirred for 24 h at room temperature. The excess NaH present in the reaction mixture was destroyed with water (5–15 mL), and the product was extracted with chloroform (3 × 20 mL). The chloroform extract was dried over anhydrous Na_2SO_4 and evaporated under vacuum. The resulting solid was purified by column chromatography (neutral alumina, 1:1 hexane/ethylacetate). Yield 60%. The purified compound was characterized by the following ^{1}H NMR spectral data.

^{1}H NMR ($CDCl_3$): δ (ppm) 3.58 (t, 2H), 4.05 (t, 2H), 4.45 (bs, 2H), 6.82 (dd, 1H), 7.05 (d, 1H), 7.7 (dd, 1H).

Step 5: Tris(4-aminophthalimido)cryptand (APL1). The cryptand **L1** (0.56 g, 1 mmol) was taken in dry acetonitrile (40 mL) and heated to 60–65°C for 30 min to dissolve it completely. To this solution were added **APBr** (1.35 g, 5 mmol), K_2CO_3 (0.69 g, 5 mmol), and catalytic amount of KI. The mixture was allowed to reflux under nitrogen atmosphere for 36 h with constant stirring. Subsequently, the solvent was evaporated, and the solid residue was extracted with chloroform (3 × 40 mL). The chloroform extract was dried over anhydrous Na_2SO_4 and evaporated to obtain a pale yellow solid that was purified by column chromatography (neutral alumina, 98:2 $CHCl_3$/MeOH). Yield 30%. The desired product was characterized by the following analytical results.

CHN analysis calculated for $C_{63}H_{69}N_{11}O_9$: C, 67.31; H, 6.14; N, 13.71. Found: C, 66.12; H, 6.26; N, 12.79.

FAB-MS *m*/*z*(%): 1125 (100) $[M + 1]^+$.

^{1}H NMR ($CDCl_3$): δ (ppm) 2.3 (s, 12H), 2.5 (t, 6H), 2.9 (t, 6H), 3.4 (s, 6H), 3.6 (t, 6H), 3.8 (t, 6H), 4.4 (s, 6H), 6.5-7.5 (m, 21H).

^{13}C NMR ($CDCl_3$): δ (ppm) 35.9, 51.3, 52.2, 53.3, 56.8, 58.8, 68.5, 108.5, 114.1, 114.2, 117.7, 120.6. 121.1, 124.8, 128.7, 135.0, 141.2, 152.4, 158.9, 168.4, 168.5.

3. 2. 2. Synthesis of APL2

The calix[4]azacrown derivative of **AP** was also prepared by following a multi-step synthetic procedure (Scheme 3.2). The calix[4]azacrown (**L2**) was prepared in four steps starting from *p-tert*-butylphenol.[5-8] The fifth step consisted of the preparation of **APBr**. The final step involved the reaction between **APBr** and **L2** to obtain the sensor system, **APL2**.

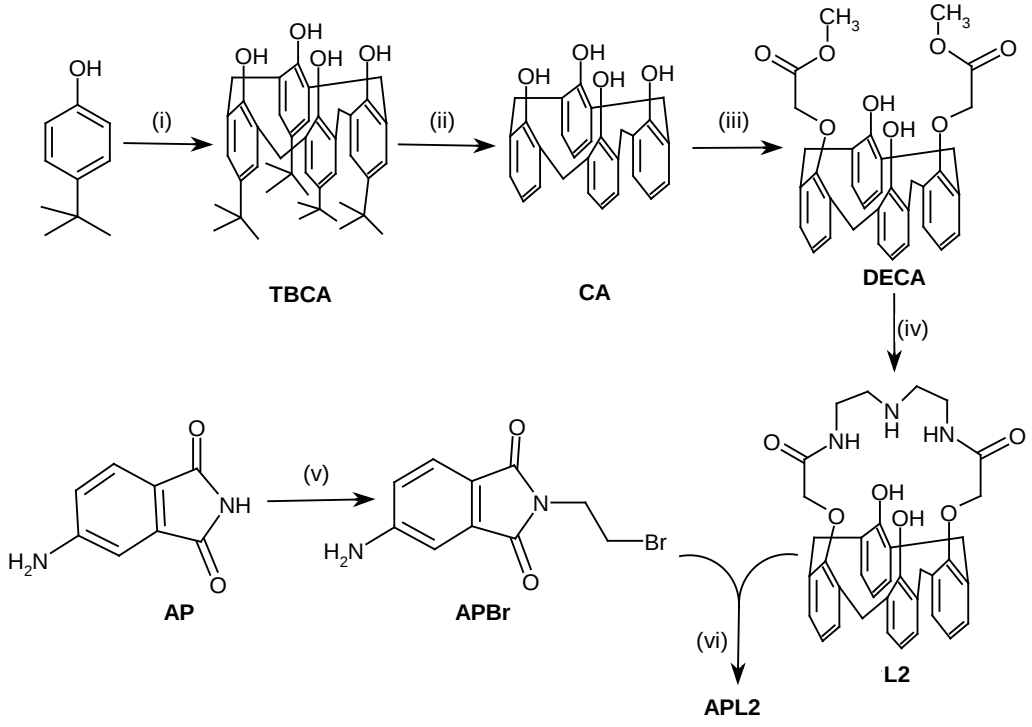

Scheme 3.2 Synthetic routes for the fluorescent sensor **APL2**. Conditions: (i) HCHO, NaOH, diphenylether; (ii) $AlCl_3$, phenol, toluene; (iii) K_2CO_3, methylbromoacetate, acetone, reflux, 24 h; (iv) diethylenetriamine, MeOH–toluene, reflux, 24 h (v) NaH, dry DMF, 1,2-dibromoethane, room temperature, 24 h; (vi) K_2CO_3, KI, MeCN, reflux, 36 h.

Step 1: p-tert-Butylcalix[4]arene (TBCA). *p-tert*-butylphenol (50 g, 0.33 mol), 37% formalin (31.2 mL, 0.42 mol of HCHO), and NaOH (0.6 g, 15 mmol) dissolved in minimum amount of water were heated for 1.5–2 h, maintaining the temperature at 110–120°C. During this period the reaction mixture, which was clear in the beginning, became viscous and turned orange at first and then changed to a thick yellow mass. After cooling to room temperature, the contents (precursor) were removed and broken into small pieces. The precursor was then suspended in diphenylether (500 mL) in 1L three-necked flask and heated with stirring in a silicone-oil bath. During the first phase of the reaction, as the yellow precursor went into solution, nitrogen was blown rapidly over the reaction mixture to facilitate the removal of water that evolved. When the water evolution subsided and when a precipitate started to form, prior to attaining the reflux temperature, a condenser was placed and the contents of the flask were refluxed for 1.5–2 h. During this phase of the reaction, the initial precipitate disappeared to give a clear solution. The reaction mixture was then cooled to room temperature, treated with 500 mL of ethylacetate, stirred for 15–30 min, and allowed to stand for 30 min. Filtration yielded material which was washed with ethylacetate (2 × 50 mL) and then with acetic acid (100 mL) to obtain the crude product. Recrystallization from toluene gave the desired product as glistening white plates. Yield 48%, m.p. 342°C (lit. yield 50%, m.p. 342–344°C).[5]

Step 2: Calix[4]arene (CA). A slurry of **TBCA** (13.3 g, 20 mmol), phenol (9.02 g, 96 mmol) and $AlCl_3$ (14 g, 105 mmol) was stirred in toluene (125 mL) at room temperature for 1 h under nitrogen atmosphere. The mixture was poured into 0.2 N HCl (250 mL), the organic phase was separated, and the toluene was evaporated. Addition of MeOH led to the formation of a precipitate that was filtered and recrystallized from MeOH–$CHCl_3$ to afford colorless crystals. Yield 75%, m.p. 312°C (lit. yield 78 %, m.p. 313–315°C).[6]

Step 3: 25,27-di(phenoxy-acetic acid methyl ester)calix[4]arene (DECA). **CA** (12.72 g, 30 mmol), K_2CO_3 (4.45 g, 32 mmol) and methylbromoacetate (9.64 g, 63 mmol) taken in acetone (600 mL) were refluxed for 24 h. The residue obtained after evaporating the solvent to dryness was treated with MeOH to yield a white solid that was filtered and recrystallized from MeOH–$CHCl_3$ to afford colorless crystals. Yield 75% (lit. 80%).[7]

Step 4: 25,27-(diamidomonoazacrown-5)-calix[4]arene (L2). **DECA** (0.233 g, 0.41 mmol) and diethylenetriamine (0.0824 g, 0.8 mmol) in 1:1 MeOH/toluene (20 ml) were refluxed for 24 h. After removal of the solvents, the crude mixture was precipitated with MeOH to give the desired product as a white solid. Yield 80%. The product was confirmed by the following analytical data.[8]

IR (KBr pellet, cm^{-1}): 3381 (OH), 1670 (C=O).

^1H NMR ($CDCl_3$): δ (ppm) 2.98 (t, 4H), 3.46 (d, 4H), 3.55 (t, 4H), 4.21 (d, 4H), 4.52 (s, 4H), 6.73-6.84 (m, 8H), 7.15 (d, 4H), 8.30 (t, 2H).

^{13}C NMR ($CDCl_3$): δ (ppm) 168.23, 152.42, 151.32, 132.15, 129.44, 129.03, 128.02, 126.09, 120.29, 74.91, 49.02, 40.22, 31.14.

The purified compound adopts a *cone* conformation, which is evident from the presence of an AB system in ^1H NMR at 3.46 ppm and 4.21 ppm (J = 13.5 Hz) characteristic of methylene bridge protons (ArCH_2Ar) and the position of the carbon atoms of the methylene bridges in the ^{13}C NMR at 31.14 ppm.[9].

Step 5: N-Bromoethyl-4-aminophthalimide (APBr). As described in ***Step 4***, section 3. 2. 1.

Step 6: N-(4-aminophthalimidoethyl)-25,27-(diamidomonoazacrown-5)-calix[4]arene (APL2). To a solution of **L2** (0.0607 g, 0.1 mmol) in dry acetonitrile (25 mL) were added **APBr** (0.242 g, 0.9 mmol), K_2CO_3 (0.124 g, 0.9 mmol), and catalytic amount of KI. The mixture was allowed to reflux under a nitrogen atmosphere for 36 h with constant stirring. Subsequently, the solvent was evaporated, and the solid residue was purified by column chromatography (neutral alumina, ethylacetate/hexane). Yield 25%. The desired product was characterized by the following analytical results.

CHN Analysis Calculated for $C_{46}H_{45}N_5O_8$: C, 69.43; H, 5.66; N, 8.81. Found: C, 69.21; H, 5.59; N, 8.98.

FAB-MS, m/z: 797 $(M+2H)^+$.

IR (KBr pellet, cm^{-1}): 3362 (OH), 1703 (imide C=O), 1664 (amide C=O).

^1H NMR ($CDCl_3$): δ (ppm) 2.81 (t, 2H), 2.91 (t, 4H), 3.43 (d, 4H), 3.55 (t, 4H), 3.75 (t, 2H), 4.22 (d, 4H), 4.53 (s, 4H), 6.78-6.85 (m, 9H), 7.08-7.11 (m, 5H), 7.51 (d, 1H), 8.30 (t, 2H).

^{13}C NMR ($CDCl_3$): δ (ppm) 168.29, 167.99, 152.53, 151.31, 151.25, 146.26, 132.31, 129.45, 128.90, 128.09, 126.62, 124.85, 120.47, 117.68, 110.50, 74.81, 55.60, 55.20, 39.22, 38.92, 31.24.

The persistence of the *cone* conformation is confirmed by the presence of an AB system in ^{1}H NMR at 3.43 ppm and 4.22 ppm (J = 13.5 Hz) for ArCH_2Ar protons and by the position of the carbon atoms of the methylene bridges in the ^{13}C NMR at 31.24 ppm.

3. 3. Spectral Features

3. 3. 1. Electronic Absorption Behavior

The absorption behavior of the systems has been studied in tetrahydrofuran (THF) and acetonitrile (AN). Both the compounds show broad bands with maximum between 345 and 366 nm typical of the parent fluorophore, **AP**. Representative absorption spectra of these systems are shown in Figure 3.1. This band arises due to the intramolecular charge transfer (ICT) transition between the electron-donating amino group and the electron-withdrawing carbonyl group of the fluorophore.

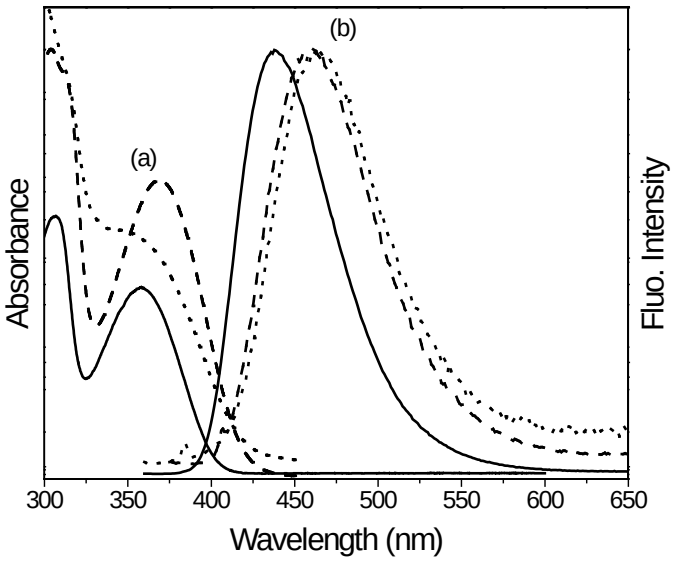

Figure 3.1 Absorption (a) and fluorescence (b) spectra of **AP** (——), **APL1** (----) and **APL2** (····) in THF. Fluorescence spectra were normalized at the respective wavelength maxima.

Table 3.1 Absorption and fluorescence properties of **AP**, **APL1** and **APL2** in tetrahydrofuran (THF) and acetonitrile (AN).

	THF			AN		
Compound	λ_{max}^{abs} /nm	λ_{max}^{flu} /nm	ϕ_f	λ_{max}^{abs} /nm	λ_{max}^{flu} /nm	ϕ_f
AP[a]	357	445	0.70	357	458	0.63
APL1	366	460	0.028	366	480	0.025
APL2	345	464	0.05	348	477	0.04

[a] These data have been collected from ref. 10.

The charge-transfer within the fluorophore moiety is significantly affected upon linking the spacer and the receptor moieties to it. This is evident from the different position of the ICT absorption maxima of **APL1** and **APL2** as compared to **AP**. The spectral data for both the compounds and that of the parent fluorophore in THF and AN are listed in Table 3.1.

3. 3. 2. Fluorescence Behavior

The fluorescence behavior of these systems has been studied in THF and AN. The fluorescence spectra of these systems are also characterized by broad structureless band typical of the transition to the intramolecular charge-transfer state of the fluorophore moiety. Contrary to the absorption spectra, the location of the fluorescence maxima is determined by the polarity of the media (Table 3.1). This behavior is consistent with a higher dipole moment of the excited state of the fluorophore.[10] Apart from a shift of the wavelength maxima, the spectral shape of these systems is remarkably similar to that of **AP** (Figure 3.1). However, although **AP** is highly fluorescent (Φ_f = 0.70 in THF),[10] the fluorescence quantum yield of both the systems is measured to be significantly low (Table 3.1). A lower fluorescence quantum yield is due to the intramolecular PET between the receptor and the fluorophore moieties. The fluorescence quantum yield of **APL1** and **APL2** is lower than that of the bare fluorophore by a factor of ~25 and ~14, respectively. The magnitude of reduction of the fluorescence quantum yield of a given system compared to the parent fluorophore is an indication of the maximum fluorescence

enhancement (FE) can be expected in the presence of the guest, assuming complete recovery of fluorescence. Therefore, these systems are expected to show reasonably good signaling efficiency.

3. 3. 3. Fluorescence Decay Behavior

The time-profile of the fluorescence of **APL1** and **APL2** is characterized by a tri-exponential decay (Figure 3.2) with the lifetime of the major component of the decay is measured to be much shorter than that of **AP** (Table 3.2).

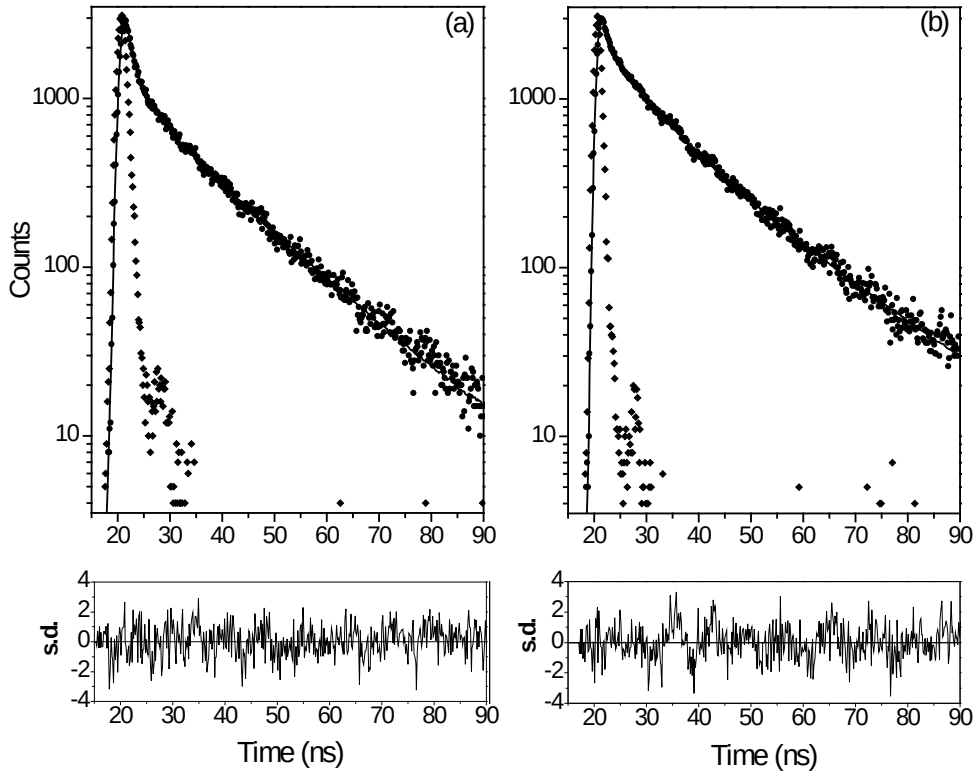

Figure 3.2 Fluorescence decay behavior of (a) **APL1** and (b) **APL2** in THF. The solutions were excited and monitored respectively at 366 nm and 460 nm for **APL1**, and at 360 nm and 470 nm for **APL2**.

Table 3.2 Fluorescence decay parameters[a] for **AP**, **APL1** and **APL2** in THF and AN.

	THF				AN			
Compound	$\tau_1(\alpha_1)$	$\tau_2(\alpha_2)$	$\tau_3(\alpha_3)$	τ_{av}	$\tau_1(\alpha_1)$	$\tau_2(\alpha_2)$	$\tau_3(\alpha_3)$	τ_{av}
AP[b]	12.4	-	-	12.4	14.0	-	-	14.0
APL1	0.2(92)	3.0(4)	15.5(4)	0.9	0.9(65)	6.3(27.5)	19.6(7.5)	3.8
APL2	0.6(66)	5.8(17)	17.3(17)	4.3	1.1(62)	6.1(21)	18.2(17)	5.1

[a] τ values are in ns, and α represents relative % of each component. [b] These data have been collected from ref. 10.

The lifetime of the minor long-lived component is comparable to that of the free fluorophore, **AP**.[10] The molecular flexibility afforded by the dimethylene spacer and the presence of several hetero atoms that can be involved in PET, it is not surprising that these systems exhibit multi-exponential decay behavior. This particular trend of the decay behavior in these systems is suggestive of the *through-space* nature of the PET process with more than one dominant configuration of the systems. The short-lived species arises from those molecules in which the spatial disposition of the terminal moieties, which are involved in the electron transfer process, is favorable for PET. On the other hand, the long-lived species, which represents a small percentage of the molecules, arises from those molecules where the spatial disposition of the terminal moieties is not favorable for PET.

3. 4. Metal ion signaling behavior

3. 4. 1. Changes in the absorption spectra

Typical changes in the absorption spectrum of **APL1** in the presence of the transition metal ions are depicted in Figure 3.3. Addition of the metal salts leads to a bathochromic shift of the absorption maximum, with the shift ranging between 4 and 10 nm depending on the metal ion. An isosbestic point (at around 358 nm in AN and 363 nm in THF) could be observed with most of the metal salts over a certain concentration range, suggesting 1:1 complexation between **APL1** and the metal ions. However, in the case of Cr^{3+} (and Fe^{3+}), as seen from Figure 3.3 (b), a continuous shift of the spectral maximum could be observed in the concentration range employed in the measurement.

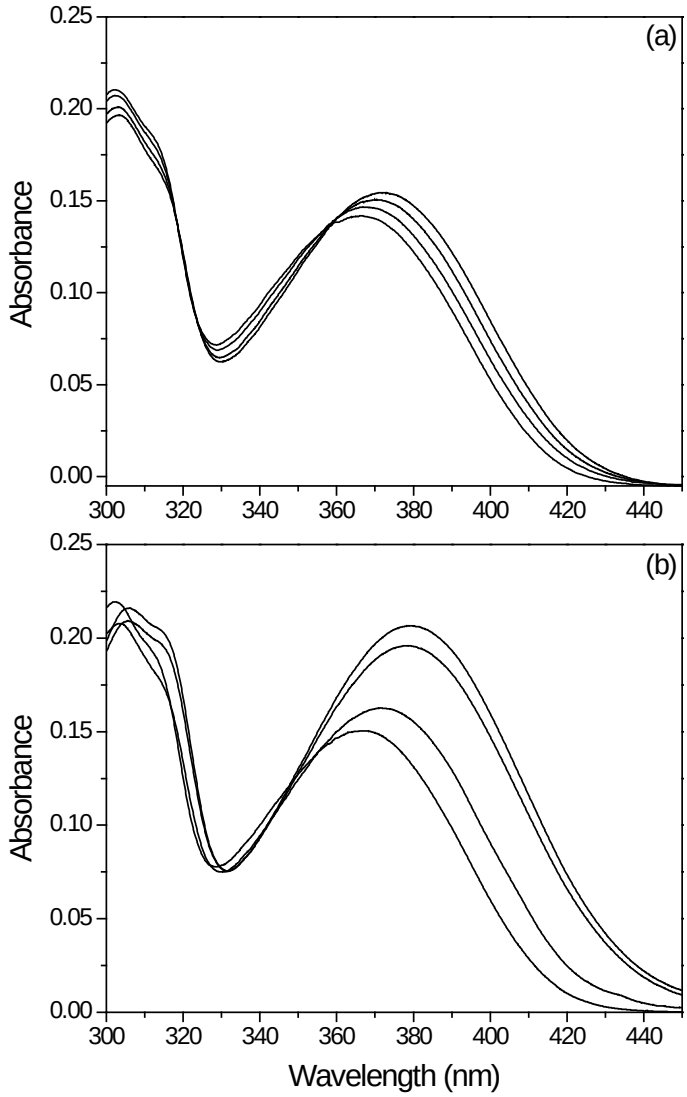

Figure 3.3 Effect of (a) Ni^{2+} and (b) Cr^{3+} ions on the absorption spectrum of **APL1** (2×10^{-5} M) in AN. The various concentrations of Ni^{2+} in increasing order of absorbance at 400 nm are 0, 4.5×10^{-5}, 10.5×10^{-5} and 24×10^{-5} M. The concentrations of Cr^{3+} are 0, 6×10^{-5}, 12×10^{-5} and 24×10^{-5} M.

Addition of the metal salts to **APL2** also leads to changes in the absorption spectrum though the changes are not very prominent. The absorption spectra of **APL2** in THF in the presence of the Cu^{2+} and Zn^{2+} ions are shown in Figure 3.4. An isosbestic point over a certain concentration range could be observed. Among the metal ions studied, Cr^{3+} and Mn^{2+} do not show any changes in the absorption spectrum of **APL2**. In the presence of Ni^{2+}, the absorption spectrum of **APL2** is affected in a similar manner. However, the changes occurred at much higher concentration than that of Fe^{3+} and Cu^{2+}.

The different effect for different metal ions is expected considering the varied coordination chemistry of these metal ions and the difference in the stability of the complexes formed.[11] The detailed complexation properties and the measurement of binding constants are discussed in the following sections.

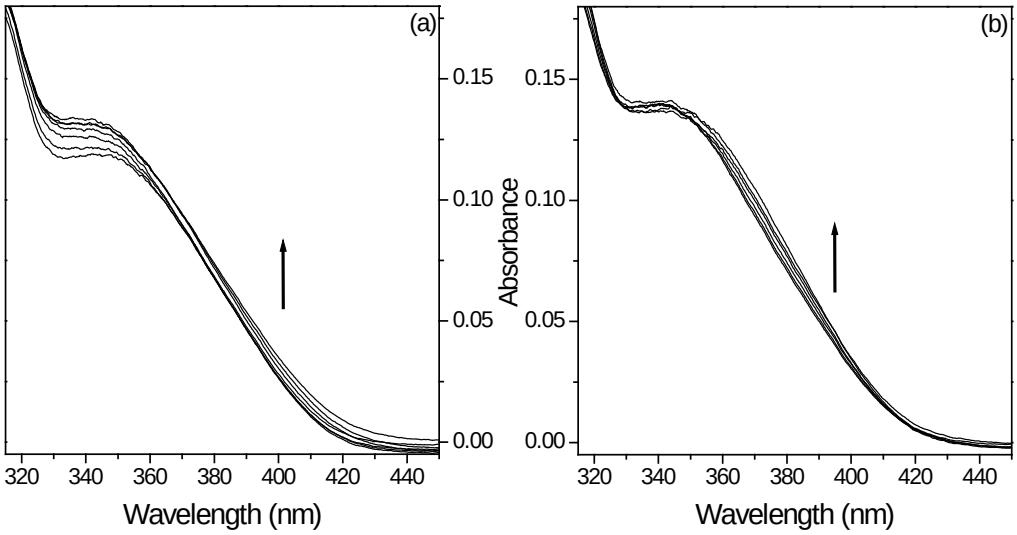

Figure 3.4 Effect of (a) Cu^{2+} and (b) Zn^{2+} ions on the absorption spectrum of **APL2** (20 μM) in THF. The various concentrations of Cu^{2+} in increasing order of absorbance at 400 nm are 0, 3, 6, 9, 18, 27 and 39 μM. The concentrations of Zn^{2+} are 0, 12, 20, 37, 61 and 86 μM.

3. 4. 2. Changes in the fluorescence spectra

Addition of the metal salts to **APL1** and **APL2** leads to a Stokes shift of the fluorescence maximum and is associated with an enhancement of the fluorescence intensity of the system (Figure 3.5). The fluorescence parameters of both the systems in the presence of the metal ions are tabulated in Table 3.3. Upon complexation, the PET quenching communication between the receptor and the fluorophore moieties cuts "Off" leading to the recovery of fluorescence. The magnitude of the fluorescence enhancement (FE), which is a measure of the signaling efficiency of the systems, is found to vary between 6 and 14 for **APL1** and between 2.4 and 2.8 for **APL2**. The highest enhancement is observed in the presence of Zn^{2+}, a metal ion that has a d^{10} electronic configuration and is well known for its non-quenching nature. Interestingly, FE in the presence of Fe^{3+}, a metal ion that has a d^5 electronic configuration and is known to be one of the most efficient fluorescence quenchers among the transition metal ions, is also observed.

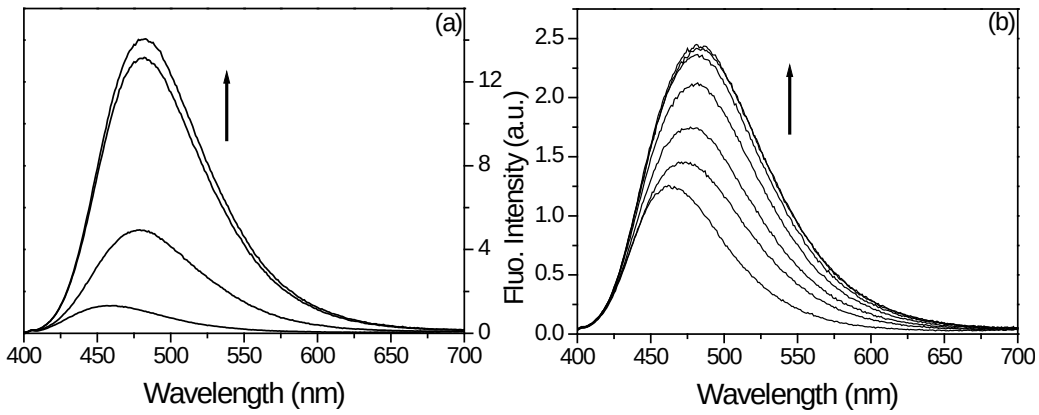

Figure 3.5 Fluorescence spectra of (a) **APL1** and (b) **APL2** in THF in the presence of Ni^{2+} ions. The concentrations of the metal salt in increasing order of the fluorescence intensity are 0, 2.8, 14 and 28 μM for **APL1**, and 0, 1.1×10^{-4}, 2.1×10^{-4}, 3.4×10^{-4}, 4.7×10^{-4}, 6.6×10^{-4} and 7.2×10^{-4} M for **APL2**.

Table 3.3 Fluorescence response of **APL1**, **APL2** and **APDEA** in the presence of different transition metal salts.[a]

	APL1						**APL2**			**APDEA**[b]	
	in THF			in AN			in THF			in AN	
Metal ion[c]	[M][d]	λ_{max}^{flu} [e]	FE	[M][d]	λ_{max}^{flu} [e]	FE	[M][d]	λ_{max}^{flu} [e]	FE	[M][d]	FE
None	-	460	1	-	480	1	-	464	1	-	1
Cr^{3+}	3.2	484	13	6.2	486	6	-[f]	-[f]	-[f]	12.0	39
Mn^{2+}	2.7	483	12	5.7	487	6	-[f]	-[f]	-[f]	17.0	32
Fe^{3+}	3.0	482	13	3.8	485	6	2.0	482	2.5	10.0	34
Ni^{2+}	2.8	483	13	5.9	485	7	66.0	483	2.4	30.0	37
Cu^{2+}	2.1	484	12	2.5	486	6	3.9	487	2.8	19.0	38
Zn^{2+}	2.6	482	14	4.0	483	8	8.6	482	2.7	39.0	55

[a] Concentration of **APL1** and **APL2** was maintained around 2×10^{-5} M. Samples were excited at the isosbestic point. [b] From ref. 2 and ref. 13. [c] Hydrated metal perchlorate salts were used. [d] Represents the concentration of the metal salt in units of 10^{-5} M for which the maximum fluorescence enhancement (FE) was observed. [e] Values in nm. [f] Not observed.

The fluorescence response of all the first-row transition metal ions towards **APL1** is quite similar. The metal ion concentrations required for the maximum FE are also not very different. The near-identical response for similar input levels makes this system essentially non-selective. Thus, **APL1** can act as a photonic OR logic system.[12] However, these metal ions respond very differently with **APL2**. For instance, no enhancement in the fluorescence of **APL2** was observed in the presence of Cr^{3+} and Mn^{2+} ions indicating their inability to form complex with this system. Moreover, even though the magnitude of FE observed in the presence of Ni^{2+} and Zn^{2+} ions is similar to that observed for Cu^{2+} and Fe^{3+} ions, the sensitivity and selectivity in the ion recognition by **APL2** can be determined by observing the changes in the emission intensity as a function of the metal ion concentration. Both Ni^{2+} and Zn^{2+} modulate the fluorescence spectra in a similar fashion. However, the desired changes occur at a much higher concentration than that of Cu^{2+} and Fe^{3+} (Table 3.3). Thus, the modulation of the fluorescence spectra of

APL2 in the presence of transition metal ions is in correlation with the selectivity trend observed from the UV-vis study.

It should be noted here that even though the observed FE values are sufficiently high for **APL1** and reasonably good for **APL2** thus pointing to the potential utility of these systems in sensing applications, it is interesting that the FE values for these systems in the presence of the metal ions are significantly lower than those observed for **APDEA** (*vide* last column of Table 3.3), a quite similar multi-component system containing the same fluorophore and the same spacer but with a much simpler receptor moiety.[2,13] Thus, even though a tighter binding by the macrocyclic cryptand or calix[4]azacrown receptor allows for the detection of the metal ions in trace quantity, as is evident from the data provided in Table 3.3, this alone cannot ensure a higher degree of fluorescence enhancement. The fluorescence yields of **APL1**, **APL2** and **APDEA** are 0.025, 0.04 and 0.013,[2] respectively. These values suggest that PET between the receptor and the fluorophore is more efficient in **APDEA** than in **APL1** or **APL2**. Thus, even though **APDEA** contains a receptor that is not as good for complexation with metal ions, a more efficient PET in this system gives rise to a higher FE value in the presence of transition metal ions. Therefore, while designing a fluorosensor for the metal ions, the various components for the *fluorophore-spacer-receptor* system should be selected such that PET in the system and binding of the guests are optimized.

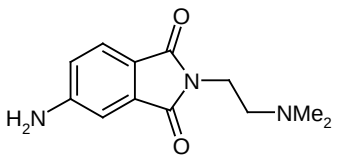

APDEA

3. 4. 3. Effect on the fluorescence decay behavior

The effect of the transition metal salts on the fluorescence decay behavior of **APL1** and **APL2** has also been examined. The amplitude associated with the sub-nanosecond component of the fluorescence decay decreases substantially and a significant increase in the amplitude of the long component is observed on progressive addition of the metal salts. For instance, the decay parameters for **APL1** observed in the presence of Zn^{2+} (2.6-4.0 × 10^{-5} M) are 4.4 (77%) and 13.4 ns (23%) in AN and 4.5 (47%) and 15.3 ns (53%) in THF. The lifetime of the long component that is observed in the presence of the metal ions is, as expected, very similar to that of the bare fluorophore, **AP** (12.4 ns in THF). An

increase in the lifetime of these systems in the presence of the metal ions is in accordance with metal ion-induced suppression of PET in these systems. Interestingly, in the case of **APL2**, the amount of metal ion required to effect these changes depends on the association constants (*vide* section 3.4) of various complexes. Higher the association constant, lesser is the amount of metal ion required. Thus, the selectivity among the metal ions for **APL2** is also observed by the change in the fluorescence lifetime values in the presence of metal ions.

3. 4. 4. Interference of protons

Since the hydrated metal perchlorate salts used in this study are Lewis acids, the possibility that the fluorescence response could be due to the protonation of the amine nitrogen atom next to the fluorophore needs to be taken into account. Addition of hydrated perchlorate salts of sodium does not result into any spectral change of these systems. This rules out the possibility of coordinated water molecules being responsible for the observed fluorescence response in the presence hydrated transition metal salts. Moreover, the very fact that no change in the fluorescence of **APL2** was observed in the presence of some of the acidic hydrated metal salts such as Cr^{3+} and Mn^{2+} salts also ensures that proton is not the culprit. This is further supported by the large difference in the binding constant values (section 3.5.2) of **APL2** for Fe^{3+} or Cu^{2+} ions (~10^5 M^{-1}) as compared to that observed for Ni^{2+} (~10^3 M^{-1}).

3. 4. 5. Studies in aqueous medium

The fluorescence signaling studies are also carried out in pH-buffered water to investigate the effect of solvent and the utility of these systems in aqueous medium. The fluorescence spectrum of both **APL1** and **APL2** in water at pH 7 is not much altered in the presence of metal ions. That the lack of metal ion-induced FE in aqueous solution is due inefficient PET is evident from the similar fluorescence quantum yield of these systems as compared and the parent fluorophore, **AP**. The inefficient PET in aqueous environment could be due to the specific hydrogen bond interaction of the fluorophore moiety with solvent water molecules. At higher pH values, where the contribution of

protons is negligible, the compound dissociates and becomes non-fluorescent. This could be due to base-induced imide ring-opening of the fluorophore moiety in these systems.

3. 5. Complexation properties

3. 5. 1. APL1

The cryptand receptor, which consists of two different tripodal binding sites separated by the aromatic rings, is believed to form complexes with transition metal ions through the tripodal N_4 moiety.[4] Because 1:1 complexation between **APL1** and the metal ions is evident in many cases from the absorption spectral data, the complexation constants (*K*) can be evaluated from the absorption and fluorescence spectral data. In this particular system, the *K* values were evaluated from the fluorescence data because metal ion-induced changes of the fluorescence spectra are more pronounced than those of the absorption spectra. The method for the estimation of *K* values is described in chapter 2, section 2.7.2.

A typical plot from which the binding constants have been evaluated is shown in Figure 3.6. The binding constants (*K*) of the metal ions with **APL1**, which were estimated from the fluorescence data by assuming the formation of 1:1 complex, lie between 1×10^5 and 7×10^5 M^{-1} in THF and between 6×10^3 and 1×10^4 M^{-1} in AN for various metal ions (Table 3.4). These data suggest that **APL1** forms tight complexes with transition metal ions. A comparatively lower magnitude of the *K* values in AN accounts for the lower FE values observed in this medium (Table 3.3). The *K* values for the various complexes involving the cryptand ligand, as estimated from the potentiometric titration in aqueous solution, lie between $10^{3.25}$ and $10^{15.22}$ M^{-1}.[14] A comparison of these values with the ones we have estimated may not be relevant because the media of the complexation and hence the actual complexes in the two cases are quite different. Moreover, although the *K* values reported in aqueous media are for the cryptand devoid of any fluorophore, the *K* values estimated by us are for the cryptand moiety that is covalently linked to three **AP** moieties.

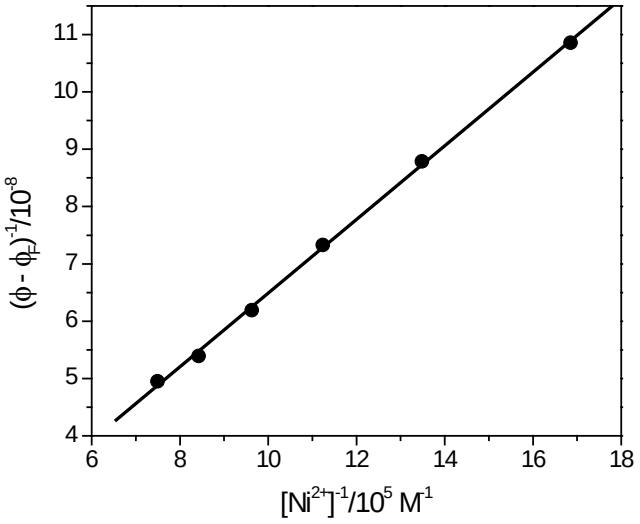

Figure 3.6 Typical plot from which the binding constant was estimated. The data shown in the plot are for Ni^{2+} with **APL1** in acetonitrile.

Table 3.4 Binding constant (K)[a] of metal ions with **APL1** (estimated from fluorescence spectral data) and **APL2** (estimated from absorption spectral data).

	K/M^{-1}		
	APL1		**APL2**
metal ion	in THF	in AN	in THF
Mn^{2+}	2.5×10^5	6.7×10^3	-[a]
Fe^{3+}	-[a]	-[a]	2.3×10^5
Ni^{2+}	6.4×10^5	1.0×10^4	1.7×10^3
Cu^{2+}	1.0×10^5	6.0×10^3	1.6×10^5
Zn^{2+}	2.5×10^5	6.7×10^3	2.5×10^4

[a] Estimated only in those cases where 1:1 complexation was clearly evident.

3. 5. 2. APL2

Binding affinity of **APL2** for transition metal ions in THF was investigated from the changes in the absorption spectrum of **APL2** in the presence of these metal ions. Since the 1:1 complexation was not very convincing from the absorption titration, a Job's plot experiment was performed to estimate the stoichiometry of the complex. Figure 3.7 illustrates that **APL2** – M^{n+} complex concentration approaches maximum when the molar fraction of $[M^{n+}]/([M^{n+}] + [\mathbf{APL2}])$ is 0.5, suggesting that **APL2** forms 1:1 complex with these metal ions. Obviously, **APL2** has various binding sites even though it forms 1:1 complex because an electrostatic repulsion between the two metal ions in the case of 1:2 complex in solution is highly possible.

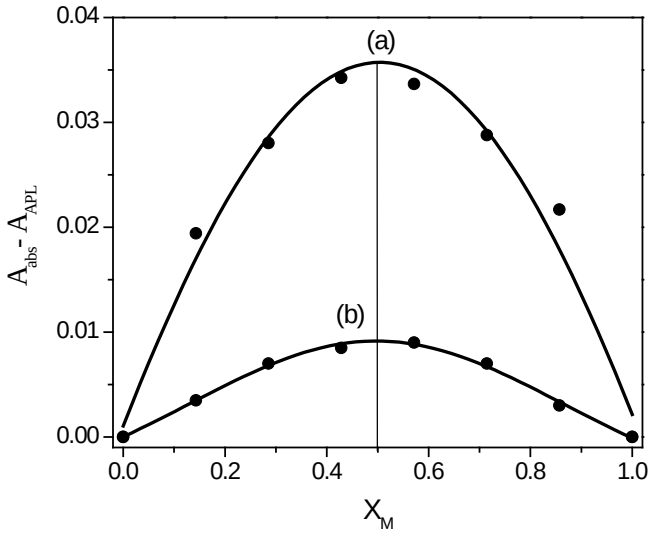

Figure 3.7 Job plot of **APL2** with (a) Cu^{2+} and (b) Ni^{2+} ions in THF. The variation of the absorption at 380 nm was measured as a function of the molar ratio $[M^{n+}]/([M^{n+}] + [\mathbf{APL2}])$.

The association constant (*K*) of the complex can be evaluated from the absorption data by the method described in chapter 2, section 2.7.1. A Typical plot from which the association constants have been evaluated is shown in Figure 3.8. The linearity of the plot further supports the formation of 1:1 complex and also suggests that the experimentally determined values of *K* are not uncertain. The association constant, which is found to vary from 1.7×10^3 M^{-1} for Ni^{2+} to 2.3×10^5 M^{-1} for Fe^{3+} in THF, clearly indicates the selectivity of the present system towards binding with various transition metal ions (Table 3.4). A very high value of *K* for Fe^{3+} and Cu^{2+} compared to that for Ni^{2+} and Zn^{2+} ions implies that **APL2** is essentially sensitive and selective for Fe^{3+} and Cu^{2+} ions.

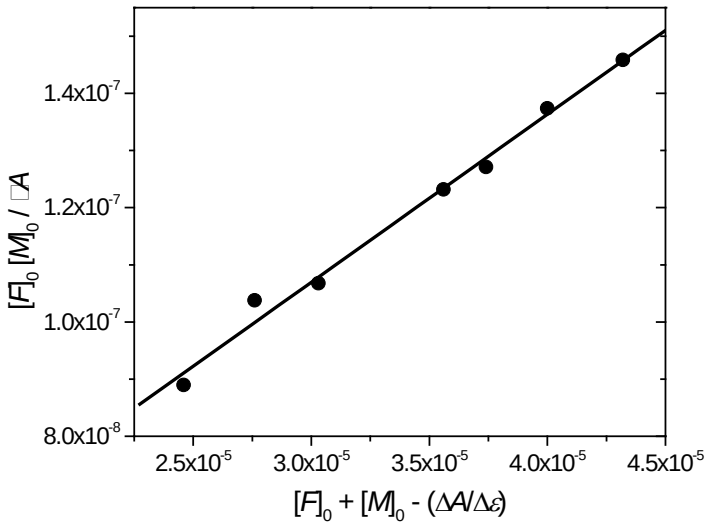

Figure 3.8 Typical plot from which the association constant was estimated. The data shown in the plot are for Cu^{2+} with **APL2** in THF. The change in absorption is monitored at 380 nm. $[F]_o$ and $[M]_o$ are the initial concentrations of **APL2** and metal salt respectively. ΔA is the change in absorbance due to the addition of metal salts, and $\Delta\varepsilon$ is the difference between the molar extinction coefficient values of the complex and **APL2**.

3. 6. X-ray crystallographic measurements

3. 6. 1. Structure of L2

Single crystal structure analyses were carried out to probe the solid-state conformation of **L2**. A single crystal obtained by slow evaporation of the MeOH/$CHCl_3$ solution crystallizes in the monoclinic space group $P2_1/n$. The ORTEP diagram of the X-ray structure is shown in Figure 3.9 and the relevant crystallographic data are presented in Table 3.5 while atomic coordinates and details of other parameters are tabulated in Appendix I.

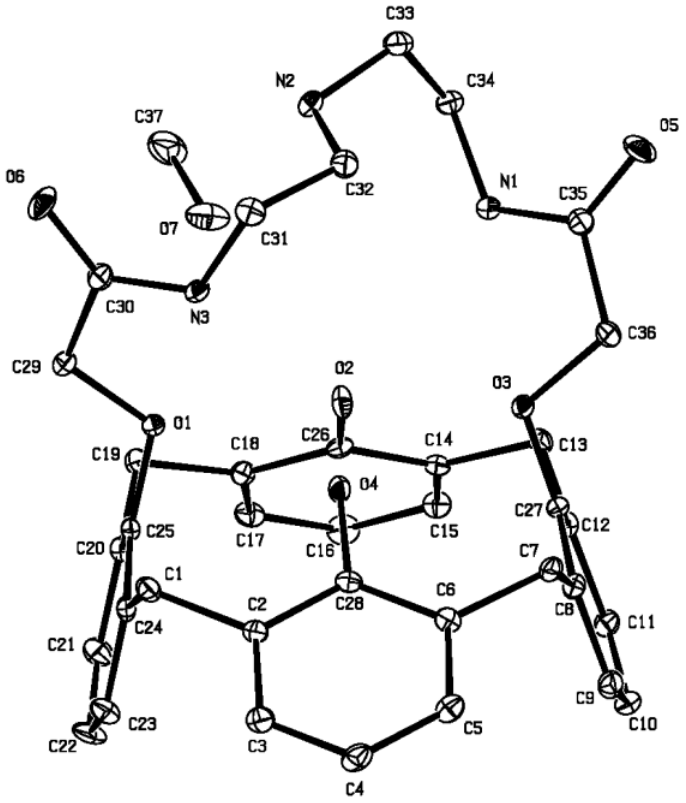

Figure 3.9 Ortep view of the molecular structure of **L2·CH_3OH**, with displacement ellipsoids shown at 10% probability level. Hydrogen atoms are omitted for clarity.

Table 3.5 Crystallographic parameters for Calix[4]azacrown (**L2·CH_3OH**)

Formula	$C_{36}H_{37}N_3O_6 \cdot CH_4O$
Formula wt	639.73
Crystal system	Monoclinic
Space group	$P2_1/n$
a (Å)	12.470(8)
b (Å)	15.549(8)
c (Å)	16.864(3)
β (°)	98.63(4)
V (Å^3)	3233(3)
Z	4
F(000)	1360
ρ_{calcd} (g cm^{-3})	1.314
Radiation (Å) (Mo-Kα)	0.71073
No. of reflections for measd	25
θ_{range} □(°)	5.41-10.17
μ (mm^{-1})	0.091
Temperature (K)	293(2)
Crystal size	0.48 × 0.40 × 0.32
Color	Colorless
Diffractometer	Enraf-Nonius Mach3 four circle (CAD-4)
Data collection method	ω scans
Absorption correction	None
Total no. of reflections	5676
No. of unique reflections	5676
No. of observed reflections [I > 2σI)]	1765
θ_{max} (°)	24.98
hkl range	0 → 14; 0 → 18; -20 → 19
No. of parameters	429
R1 [$F^2 > 2\sigma(F^2)$], wR1 (F^2)	0.0654, 0.1298
GOF	0.96
$(\Delta/\sigma)_{max}$	0.002
$\Delta\rho_{max}$, $\Delta\rho_{min}$ (e/Å^3)	0.216, -0.239

The asymmetric unit is composed of one calix[4]azacrown molecule in *cone* conformation and a methanol molecule. This combination gives strong hydrogen-bond donors and acceptors, which is reflected in the hydrogen-bonding network consisting of both intra- and intermolecular hydrogen bonds (Table 3.6).

Table 3.6 Hydrogen-bonding geometry (Å, °) in the crystal structure of **L2·CH$_3$OH**.

D–H···A	D–H	H···A	D···A	< D–H···A
O4–H4···O3	0.82	2.07	2.846(5)	157.8
O2–H2···O1	0.82	2.12	2.878(5)	154.0
O2–H2···O7	0.82	2.42	2.891(6)	117.7
N3–H3···O4	0.86	2.25	3.100(5)	170.3
N3–H3···O1	0.86	2.18	2.578(5)	108.1
N1–H1···O2	0.86	2.34	3.200(5)	174.1
N1–H1···O3	0.86	2.23	2.638(5)	108.8
O7–H7···N2	0.82	2.02	2.823(7)	164.3
N2–H2A···O6^{i}	0.92(4)	2.14(4)	2.909(6)	140(4)

^{i}Symmetry code: 2-x, -y, -z

The dihedral angles between the aromatic rings of the calix[4]arene and the mean plane defined by the four methylene bridges are 35.18(17)°, 73.86(12)°, 40.21(14)° and 75.95(12)°. The aromatic rings are tilted away from the calixarene cavity, the inter-planar angle between the two opposite rings are 75.39(17)° and 30.20(18)°. This conformation leads to O···O separations of 4.654(4) Å between O(1) and O(3) and 3.202(5) Å between O(2) and O(4). The average O···O distance between adjacent oxygen atoms is 2.85 Å. The strong hydrogen-bonding network is the main conformation-determining feature of this molecule. While one phenolic proton is bound to an ether oxygen atom, the second one shows a bifurcated intramolecular hydrogen bond with a neighboring ether oxygen atom of the calixarene and an intermolecular hydrogen bond with the oxygen atom of a methanol molecule. Two intramolecular hydrogen bonds due to the amide protons are also bifurcated between the amide protons and the oxygen atoms bound to the calixarene.

The proton of the amine function is bound to the amide oxygen atom of a neighboring molecule leading to a supramolecular cyclic dimer in the solid state that is 'capped' at both ends by an association to the methanol molecule (Figure 3.10).

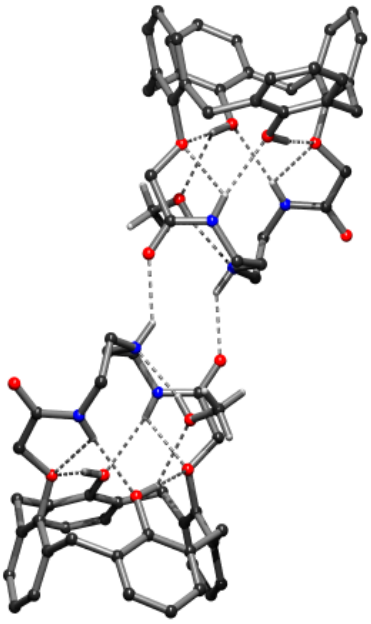

Figure 3.10 View of the dimeric superstructure of **L2** 'capped' with a methanol molecule illustrating the intra- and intermolecular hydrogen bonding, shown as dashed lines. Hydrogen atoms of **L2** except those involved in H-bonding are omitted for clarity.

3. 6. 2. Structure of L2-perchloric acid complex

There exists considerable doubt on the metal extraction ability of a related *p-tert*-butylcalix[4]azacrown molecule.[15] Moreover, while *p-tert*-butylcalix[4]azacrown does not extract transition metal ions, the corresponding 1,3-dimethoxy-*p-tert*-butylcalix[4]azacrown extract Cu^{2+} ions selectively with respect to Co^{2+} and Ni^{2+} ions.[15,16] The N-methyl-1,3-dimethoxy-*p-tert*-butylcalix[4]azacrown, however, showed changes in its NMR spectrum in the presence of all of these three metal ions. Thus, a

simple substitution by methyl groups leads to dramatic changes in the complexation properties of these systems. Therefore, we carried out the reaction between **L2** and copper(II)perchlorate in methanol at room temperature.† As expected, **L2** did not form complex with Cu^{2+} instead it extracted perchloric acid. Subsequent storage of the reaction mixture for slow evaporation yielded crystals, suitable for X-ray diffraction studies, of the calix[4]azacrown-perchloric acid complex (**L2-HClO$_4$**). It crystallizes in the triclinic space group *P*-1. The ORTEP diagram of the X-ray structure is shown in Figure 3.11 and the relevant crystallographic data are presented in Table 3.7 while atomic coordinates and details of other parameters are tabulated in Appendix I.

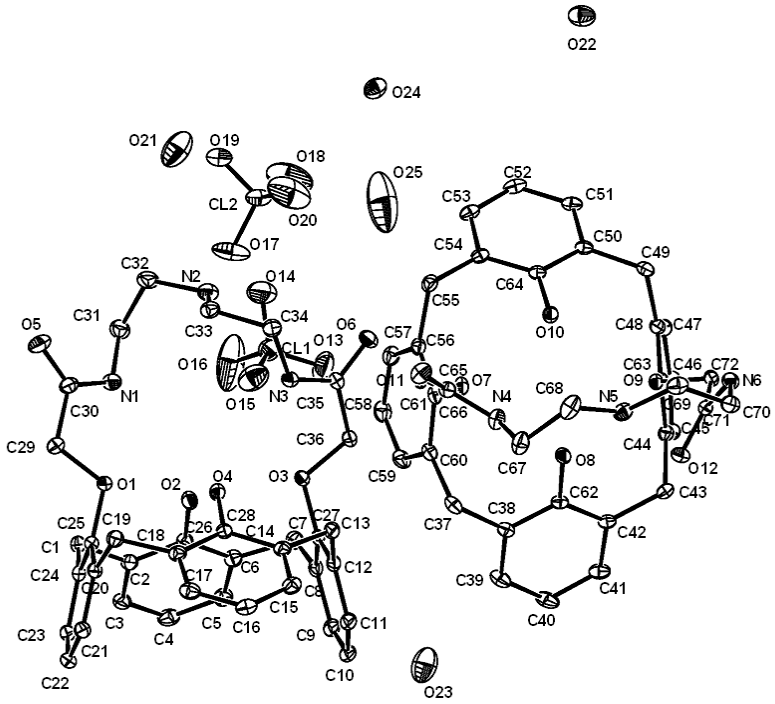

Figure 3.11 Ortep view of the molecular structure of **L2-HClO$_4$·2.5H$_2$O**, showing displacement ellipsoids at 10% probability level and the atom labeling. Hydrogen atoms are omitted for clarity.

† Caution! Care should be taken while treating organic compounds with metal perchlorates as potentially explosive mixtures may be formed.

Table 3.7 Crystallographic parameters for **2(L2-$HClO_4$)·$5H_2O$**

Formula	$2(C_{36}H_{38}N_3O_6).2(ClO_4).5(H_2O)$
Formula wt	1506.37
Crystal system, Space group	Triclinic, *P*-1
a (Å)	12.7722(18)
b (Å)	15.865(2)
c (Å)	20.138(3)
α (°)	78.132(2)
β (°)	71.638(2)
γ (°)	69.810(2)
V (Å^3)	3613.3(9)
Z	2
F(000)	1588
ρ_{calcd} (g cm^{-3})	1.385
Radiation (Å) (Mo-Kα)	0.71073
No. of reflections for measd	6704
θ_{range} □(°)	2.29-21.98
μ (mm^{-1})	0.175
Temperature (K)	293(2)
Crystal size	0.29 × 0.12 × 0.04
Color	Yellow
Diffractometer	CCD area detector diffractometer
Data collection method	Φ and ω scans
Absorption correction	Multi-scan (SADABS)
T_{min}, T_{max}	0.864, 0.993
Total no. of reflections	42510
No. of unique reflections	16948
No. of observed reflections [I > 2σI)]	7827
θ_{max} (°)	28.32
No. of parameters	970
R1 [$F^2 > 2\sigma(F^2)$], wR1 (F^2)	0.0910, 0.3236
GOF	1.031
$\Delta\rho_{max}$, $\Delta\rho_{min}$ (e/Å^3)	0.802, -0.510

The asymmetric unit is composed of two independent calix[4]azacrown-perchloric acid and five disordered water molecules. The perchlorate motifs are also highly disordered. Thus, it proves that compound **L2** exhibits poor complexation ability towards the transition metal ions.

Thus, we have seen that while calix[4]azacrown (**L2**) does not extract transition metal ions, N-(4-aminophthalimidoethyl)calix[4]azacrown (**APL2**) has the ability to bind with transition metal ions with certain amount of selectivity. Previous studies on the *p-tert*-butylcalix[4]azacrown have revealed that metal complexation property can be varied upon substitution on phenolic OH group or both phenolic OH and amine NH groups.[15] While compounds with labile-protons are found to extract picric acid, O-methylated and N-methylated *p-tert*-butylcalix[4]azacrown are shown to complex transition metal ions as their picrates, suggesting that the complexation ability of such calix[4]azacrown systems is enhanced significantly upon substitution of the proton-ionizable atoms.[15,16] Here, we find that substitution on only amine NH group can also make the system capable of binding with transition metal ions. The possible explanation for this observation can be offered on the basis of the hydrogen-bonding pattern found in this system. These systems, possessing donor and acceptor sites for hydrogen bonding can behave as polydentate ligands capable of complexation with neutral molecules containing OH or NH groups. As can be seen from the structure of **L2**, a CH_3OH molecule is encapsulated upon hydrogen bonding with the phenolic proton and amine nitrogen, which in turn is hydrogen-bonded to the neighboring molecule to give a dimeric structure (Figure 3.8). As most of the metal salts are hydrated, it is highly possible that formation of a hydrogen-bonded complex with the neutral molecules such as water is favored more than the metal ion complexation. However, upon substitution on phenolic OH and amine NH, complexation with the metal ions predominates due to the decrease in the number of donor sites for hydrogen bonding thereby making the azacrown loop more flexible and available for the metal cations.

3. 7. Conclusions

In conclusion, we have synthesized two photoactive supermolecules (**APL1** and **APL2**), comprising macrocyclic cryptand and calix[4]azacrown moieties as receptor

components. The photophysical and transition metal ion signaling studies were carried out in detail. Results indicate that while **APL1** is non-selective in its response towards various transition metal ions, **APL2** exhibits certain degree of selectivity towards Fe^{3+} and Cu^{2+} ions. This suggests that macrocycles based on calixarene platform may act as versatile ligands for selective recognition of metal ions. Complete study on calix[4]azacrown system, including the X-ray structure analyses, reveal that the poor complexation properties of this type of calix[4]azacrown systems could be due to the highly ordered hydrogen-bonding pattern leading to a supramolecular dimeric structure. However, a slight modification on this type of calix[4]azacrown framework may result into potential hosts for the selective recognition of transition metal ions. Another important lesson that we learnt from this study is that the molecular components of a sensor system have to be chosen such that optimized conditions for PET and guest-binding are attained.

References

1 Ghosh, P.; Bharadwaj, P. K.; Mandal, S.; Ghosh, S. *J. Am. Chem. Soc.* **1996**, *118*, 1553.
2 Ramachandram, B.; Samanta, A. *Chem. Commun.* **1997**, 1037.
3 Ward, K., Jr. *J. Am. Chem. Soc.* **1935**, *57*, 914.
4 Chand, D. K.; Bharadwaj, P. K. *Inorg. Chem.* **1996**, *35*, 3380.
5 Gutsche, C. D.; Iqbal, M.; Stewart, D. *J. Org. Chem.* **1986**, *51*, 742.
6 Gutsche, C. D.; Lin, L.-G. *Tetrahedron* **1986**, *42*, 1633.
7 Unob, F.; Asfari, Z.; Vicens, J. *Tetrahedron Lett.* **1998**, *39*, 2951.
8 No, K.; Lee, H. J.; Park, K. M.; Lee, S. S.; Noh, K. H.; Kim, S. K.; Lee, J. Y.; Kim, J. S. *J. Heterocyclic Chem.* **2004**, *41*, 211.
9 Jaime, C.; de Mendoza, J.; Prados, P.; Nieto, P. M.; Sanchez, C. *J. Org. Chem.* **1991**, *56*, 3372.
10 Soujanya, T.; Fessenden, R. W.; Samanta, A. *J. Phys. Chem.* **1996**, *100*, 3507.
11 Cotton, F. A.; Wilkinson, G. *Advanced Inorganic Chemistry*; Third ed.; Wiley Eastern Limited: New Delhi, 1976.
12 Ghosh, P.; Bharadwaj, P. K.; Roy, J.; Ghosh, S. *J. Am. Chem. Soc.* **1997**, *119*, 11903.
13 Ramachandram, B. Ph.D. Thesis, University of Hyderabad, Hyderabad, India, 2000.
14 Bazzicalupi, C.; Bandyopadhyay, P.; Bencini, A.; Bianchi, A.; Giorgi, C.; Valtancoli, B.; Bharadwaj, D.; Bharadwaj, P. K.; Butcher, R. J. *Eur. J. Inorg. Chem.* **2000**, 2111.
15 Oueslati, I.; Abidi, R.; Thuery, P.; Nierlich, M.; Asfari, Z.; Harrowfield, J.; Vicens, J. *Tetrahedron Lett.* **2000**, *41*, 8263.
16 Abidi, R.; Oueslati, I.; Amri, H.; Thuery, P.; Nierlich, M.; Asfari, Z.; Vicens, J. *Tetrahedron. Lett.* **2001**, *42*, 1685.

Chapter 4

4-Amino-(N-(di-(2-picolyl)amino)ethyl)phthalimide

This chapter deals with the synthesis, complexation and signaling behavior of the title compound comprising 4-aminophthalimide and di-(2-picolyl)amine as the fluorophore and the receptor components, respectively. This simple multi-component system with a *fluorophore-spacer-receptor* backbone mimics the function of a number of logic gates and switches, which can be accessed by modulating the combination and levels of ionic inputs. Complexation with specific metal ions inhibits the PET quenching pathway leading to the enhancement of fluorescence. This is also evident from the single crystal X-ray structure data of this system and its Zn^{2+} complex.

4. 1. Introduction

In the preceding chapter we have learnt that the molecular components of a sensor system based on a *fluorophore-spacer-receptor* design have to be chosen such that PET in the system and binding of the guests are optimized. There, we have observed that systems employing rigid macrocyclic ligands such as a cryptand and a calix[4]azacrown although form strong complexes with transition metal ions, PET is more efficient in systems that comprise a much simpler and flexible ligands like dimethylamine. Therefore, in our design of a multi-component fluorosensor, we have chosen an acyclic di-(2-picolyl)amine (DPA) as a receptor component to develop **APDPA**. The tridentate DPA ligand is known for its strong complexation behavior with transition metal ions.[1] In fact, systems based on anthracene or fluorescein fluorophores employing DPA as a receptor unit have been developed for the detection metal ions.[2,3] However, unlike the macrocyclic cryptand or calix[4]azacrown receptors, DPA is very much flexible. Thus, optimized conditions for PET and guest-binding is expected in **APDPA**.

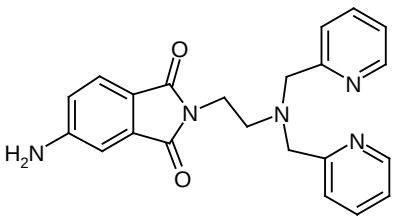

APDPA

The fluorescence of **APDPA** switches "On" with a blue-to-green color change in the presence of Zn^{2+}, Cd^{2+} or Pb^{2+} (OR logic). This system also acts as an "Off-On-Off" switch stimulated by protons. The H^{+}-driven "Off-On-Off" switch can be integrated with Zn^{2+}, Cd^{2+} or Pb^{2+}-induced OR logic gate to construct an Inhibit (INH) logic gate employing these ionic inputs. Thus, **APDPA** is a versatile system that not only acts as a chelation-enhanced fluorescent sensor for Zn^{2+}, Cd^{2+} or Pb^{2+} ions but, more importantly, can be switched to OR, "Off-On-Off" and INH logic behavior by varying the combination and levels of ionic inputs. While photonic OR logic function is easy to achieve and therefore well-documented,[4,5] molecules behaving as an "Off-On-Off" switch are very rare.[2,6,7] The inhibit function is even more scarce[8-10] and no molecular system acting as an INH logic gate employing transition/heavy metal ions has been demonstrated till date. Moreover, most of the reported systems are restricted to one or specific logic operations. Thus, we present a unique system performing multiple logic functions some of which are not very common. X-ray structure analyses of **APDPA** and its Zn^{2+} complex reveal that the solid-state conformation is in correlation with the results observed in solution.

4. 2. Synthesis

4. 2. 1. APDPA

The di-(2-picolyl)amine (DPA) derivative of **AP** was prepared by following a two-step synthetic procedure (Scheme 4.1).

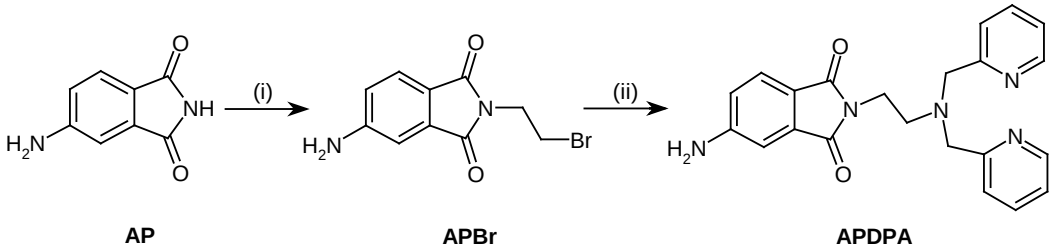

AP **APBr** **APDPA**

Scheme 4.1 Synthetic routes for the fluorescent sensor **APDPA**. Conditions: (i) NaH, dry DMF, 1,2-dibromoethane, room temperature, 24 h; (ii) DPA, MeCN, reflux, 24 h.

The first step consisted of the preparation of **APBr**, which was then reacted with DPA to obtain the sensor system, **APDPA**.

Step 1: N-Bromoethyl-4-aminophthalimide (APBr). As described in chapter 3, section 3.2.1., *Step 4*.

Step 2: 4-Amino-(N-(di-(2-picolyl)amino)ethyl)phthalimide (APDPA). di-(2-picolyl)amine (0.45 mL, 2.5 mmol) and **APBr** (0.269 g, 1 mmol) were taken in dry acetonitrile (50 mL) and the reaction mixture was allowed to reflux under nitrogen atmosphere for 24 h with constant stirring. Subsequently, the solvent was evaporated under vacuum and the residue was purified by column chromatography (neutral alumina, hexane/ethylacetate). Yield 70%. The desired product was characterized by the following analytical results.

CHN Analysis calculated for $C_{22}H_{21}N_5O_2$: C, 68.22; H, 5.43; N, 18.09. Found: C, 67.19; H, 5.31; N, 17.82.

IR (KBr pellet, cm^{-1}): 3431, 3327 (NH_2), 1695 (imide CO).

^1H NMR ($CDCl_3$, 400 MHz): δ (ppm) 2.83 (t, 2H), 3.81 (t, 2H), 3.87 (s, 4H), 4.37 (s, 2H), 6.87 (dd, 1H), 7.03 (d, 1H), 7.10 (m, 2H), 7.39 (m, 2H), 7.46 (m, 2H), 7.59 (d, 1H), 8.47 (d, 2H).

4. 2. 2. APDPA – Zn(II) complex

To a solution of **APDPA** (0.5 g, 1.3 mmol) in methanol (50 mL), $Zn(ClO_4)_2 \cdot 6H_2O$ (0.22 g, 0.6 mmol) dissolved in methanol (20 mL) were added drop-wise and the resulting solution was stirred for 24 h at room temperature and filtered.§ The filtrate was evaporated to dryness under vacuum to obtain a solid residue, which was recrystallized from acetonitrile to afford shiny yellow crystals. Yield 80%. Single crystals suitable for X-ray diffraction studies were grown by slow evaporation of the acetonitrile solution of the complex.

IR (KBr pellet, cm^{-1}): 3452, 3355 (NH_2), 1691 (imide CO), 1085 (ClO).

§ Caution! Care should be taken while treating organic compounds with metal perchlorates as potentially explosive mixtures may be formed.

4. 3. Cation-induced changes in the absorption spectra

The 4-aminophthalimide moiety in this system gives rise to an intramolecular charge transfer (ICT) transition in the UV-vis region due to the push-pull effect of the electron-donating amino and the electron-withdrawing carbonyl groups as an intrinsic part of the fluorophore. Addition of the metal salts to a solution of **APDPA** leads to a bathochromic shift of the absorption maximum. Typical changes in the absorption spectrum of **APDPA** upon subsequent addition of metal ions in THF are depicted in Figure 4.1.

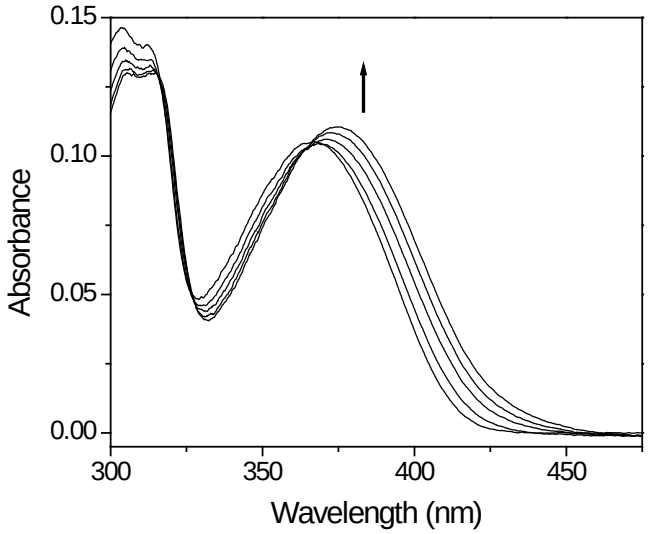

Figure 4.1 Effect of Zn^{2+} ions on the absorption spectrum of **APDPA** (2×10^{-5} M) in THF. The various concentrations of Zn^{2+} in increasing order of absorbance at 400 nm are 0, 3×10^{-6}, 6×10^{-6}, 9×10^{-6} and 1.2×10^{-5} M.

An isosbestic point was observed upon progressive addition of Zn^{2+}, Cd^{2+} or Pb^{2+} salts, indicating the presence of only two species at equilibrium. Thus, the complexation constants (*K*) can be evaluated from the absorption spectral data by the method described in chapter 2, section 2. 7. 1. The binding constant values (*K*) for some of the metal ions with **APDPA**, which could be evaluated accurately from the absorption data, are listed in Table 4.1. The data suggest that these metal ions form tight complexes with **APDPA** in

THF and thus can be detected in trace quantities. A typical plot from which the binding constants have been evaluated is shown in Figure 4.2.

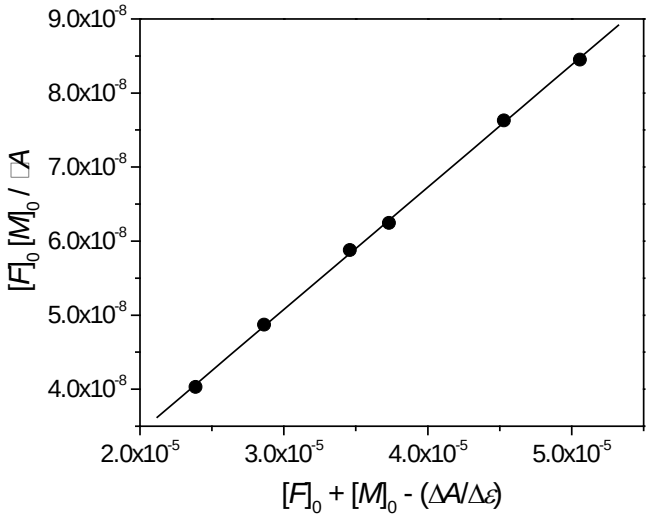

Figure 4.2 A typical plot from which the binding constant was estimated. The data shown in the plot are for Zn^{2+} ions in THF. The change in absorption is monitored at 380 nm. $[F]_o$ and $[M]_o$ are the initial concentrations of **APDPA** and the metal salt respectively. ΔA is the change in absorbance due to the addition of metal salt, and $\Delta\varepsilon$ is the difference between the molar extinction coefficient values of the complex and **APDPA**.

Table 4.1 Binding constant (K) of some metal ions with **APDPA** in THF estimated from absorption spectral data.

metal ion[a]	λ_{max}^{abs} /nm	K
none	367	-
Zn^{2+}	375	1.7×10^6
Cd^{2+}	375	1.5×10^6
Pb^{2+}	374	2.2×10^5
Ni^{2+}	370	-[i]
Cu^{2+}	372	-[i]

[a] Hydrated metal perchlorate salts were used. [i] Binding constant could not be measured accurately.

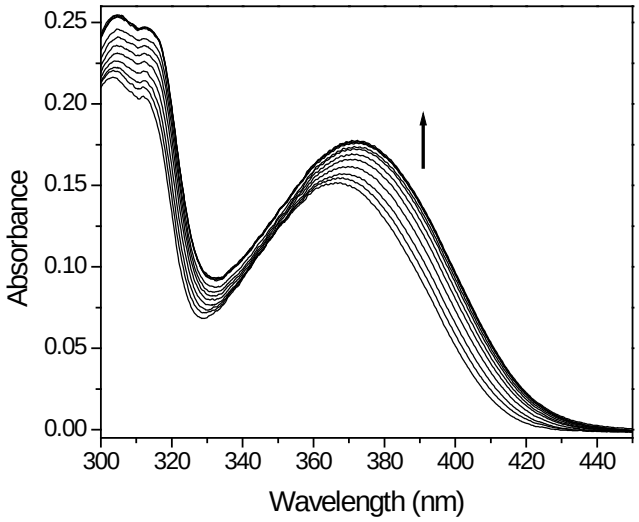

Figure 4.3 Effect of Cu^{2+} ions on the absorption spectrum of **APDPA** (3×10^{-5} M) in THF. The various concentrations of Cu^{2+} in increasing order of absorbance at 400 nm are $0 – 2.2 \times 10^{-5}$ M with increments of 2×10^{-6} M.

However, as seen from Figure 4.3, in the case of metal ions such as Cu^{2+}, the changes were not very uniform and no clear isosbestic point was observed in the concentration range employed for the measurement. Therefore, binding constant values for these metal ions could not be evaluated accurately. The different effect for different metal ions is expected considering the varied coordination chemistry of these metal ions and the difference in the stability of the complexes formed.[11]

4. 4. Cation-induced changes in the fluorescence spectra

4. 4. 1. Metal ion signaling

The fluorescence spectrum of **APDPA** is also characterized by broad structure-less band, centered at 454 nm, typical of the transition to the intramolecular charge-transfer state of the fluorophore moiety. However, although **AP** is highly fluorescent ($\phi_f = 0.70$ in THF),[12] the fluorescence quantum yield of **APDPA** in THF is measured to be only 0.08. A lower fluorescence quantum yield of **APDPA** as compared to that of the parent

fluorophore, **AP**, is attributable to intramolecular PET between the receptor and the fluorophore moieties. Since the magnitude of reduction of the fluorescence quantum yield of a given multi-component system compared to the parent fluorophore is an indication of the maximum fluorescence enhancement (FE) expected in the presence of the guest (assuming complete recovery of fluorescence), **APDPA** is expected to show good signaling efficiency.

In the presence of cationic guest such as Zn^{2+}, Cd^{2+} or Pb^{2+} ions, an enhancement of the fluorescence intensity of the system is observed and is associated with a Stokes shift of the fluorescence maximum (Table 4.2). Typical changes in the fluorescence spectra of **APDPA** upon subsequent addition of these metal ions in THF are depicted in Figure 4.4. The fluorescence enhancement (FE) is attributed to the suppression of the PET due to the guest – receptor interaction.

Table 4.2 Fluorescence properties of **APDPA**[a] in the absence and in the presence of protons and different metal ions[b] in THF.

Input[c]	λ_{max}^{flu} /nm	ϕ_f (FE)[d]
none	454	0.08 (1)
H^+	517	0.70[e], 0.18[f], 0.02[g]
Zn^{2+}	487	0.61 (7.6)
Cd^{2+}	484	0.70 (8.7)
Pb^{2+}	468	0.62 (7.8)
Fe^{3+}	489	0.17 (2.1)
Mn^{2+}	477	0.051 (0.64)
Co^{2+}	482	0.032 (0.40)
Ni^{2+}	467	0.027 (0.34)
Cu^{2+}	482	0.028 (0.35)

[a] 2×10^{-5} M. [b] Alkali and alkaline earth metal ions do not result into any response from **APDPA**. [c] Perchloric acid and hydrated perchlorate salt of the metals were used; metal ion concentrations are in the units of 10^{-5} M. [d] For metal ion input, samples were excited at the isosbestic point and at 365 nm for H^+. [e] $[H^+] = 10^{-5}$ M. [f] $[H^+] = 10^{-3}$ M. [g] $[H^+] = 10^{-1}$ M.

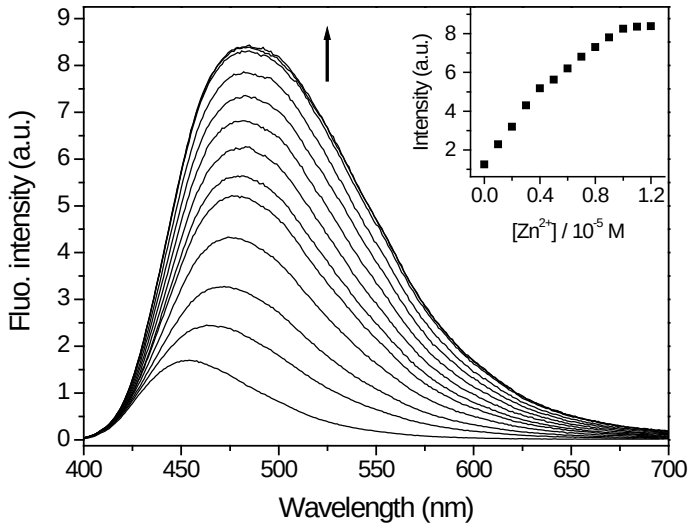

Figure 4.4 Fluorescence spectra of **APDPA** in THF upon progressive addition of Zn^{2+} ions. [**APDPA**] = 2×10^{-5} M, [Zn^{2+}] = 0 – 1.2×10^{-5} M with increments of 1×10^{-6} M. Inset: fluorescence intensity at 480 nm vs. concentration of Zn^{2+} ions. $\lambda_{exc.}$ = 365 nm.

Interestingly, a complete revival of fluorescence is observed even in the presence of Pb^{2+} ions, an intrinsic quencher because of the 'heavy atom' effect. The fluorescence enhancement was observed immediately after the addition of metal salts indicating strong complexation in solution, which was also evident from the binding constant values evaluated from the absorption data (vide Table 4.1). This makes **APDPA** potentially useful for analytical studies.

While alkali and alkaline earth metal ions such as Na^{+}, K^{+}, Mg^{2+} and Ca^{2+} do not result into any significant response from **APDPA**, transition metal ions such as Cu^{2+} and Ni^{2+} quench the fluorescence of the system. Typical changes in the fluorescence spectra of **APDPA** upon subsequent addition of these metal ions in THF are depicted in Figure 4.5. Obviously, this is not due to the quenching nature of these metal ions as in that case Fe^{3+}, one of the most efficient fluorescent quenchers among the transition metal ions, would also have shown the similar behavior. We believe that the resulting quenching is due to the different coordination properties of **APDPA** with these metal ions.

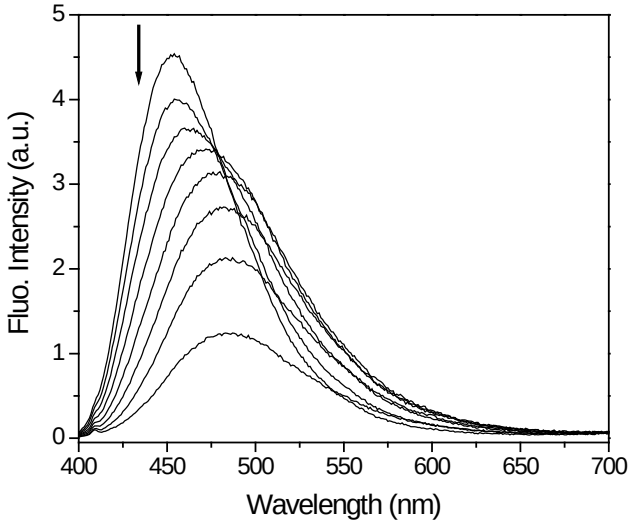

Figure 4.5 Fluorescence spectra of **APDPA** in THF upon progressive addition of Cu^{2+} ions. [**APDPA**] = 3×10^{-5} M, [Cu^{2+}] = 0 – 1.4×10^{-5} M with increments of 2×10^{-6} M. $\lambda_{exc.}$ = 365 nm.

Absorption spectral studies also indicated that the complexation behavior of **APDPA** with these metal ions is quite complicated (vide section 4.3.). Most likely, the imide oxygen atom of the fluorophore is also involved in the coordination, resulting into the unexpected quenching of the fluorescence.

Thus, **APDPA** is an efficient fluorescent sensor able to discriminate post-transition metal ions from other 3d, alkali and alkaline earth metal ions. Further discrimination among Pb^{2+} and Zn^{2+} or Cd^{2+} can be made on the basis of Stokes shift of the emission maximum of **APDPA** in the presence of these metal ions. While Zn^{2+} and Cd^{2+} show 33 nm and 30 nm shift of the emission maximum respectively, only 14 nm shift of the emission maximum is observed in the presence of Pb^{2+}. Therefore, even if the FE value obtained for Pb^{2+} is comparable to that of Zn^{2+} or Cd^{2+}, the selectivity of the present system towards Pb^{2+} can be drawn from the shift in the emission maximum (Table 4.2). It should be noted that the color of the fluorescence output signal is green. Thus, the input ions “switch on” the fluorescence with a color change from blue to green (a Stokes shift as high as 33 nm is observed).

4. 4. 2. Proton signaling

APDPA behaves as a typical "Off-On" switch upto a certain input level of $[H^+]$ (10^{-5} M). However, at high $[H^+]$ (10^{-3} M), quenching of the fluorescence of **APDPA** occurs leading back to the "Off" mode. Thus, **APDPA** acts as an "Off-On-Off" switch driven by protons. Interestingly, when we chose a very high $[H^+]$ (10^{-1} M), **APDPA** becomes a H^+ - driven NOT switch. When we look across the whole range of H^+ concentrations (Table 4.2), **APDPA** clearly shows a maximum fluorescence emission at $[H^+] = 10^{-5}$ M. The fluorescence retreat to the original at $[H^+] = 10^{-3}$ M and falls further at $[H^+] = 10^{-1}$ M. What causes the fall of fluorescence of **APDPA** at high H^+ concentration? At very high proton concentration, the 4-amino group of the fluorophore gets protonated thereby inhibiting the ICT transition and the system acts as a non-fluorescent molecule. The fluorescence spectra of **APDPA** at different concentration of protons representing the different modes are shown in Figure 4.6.

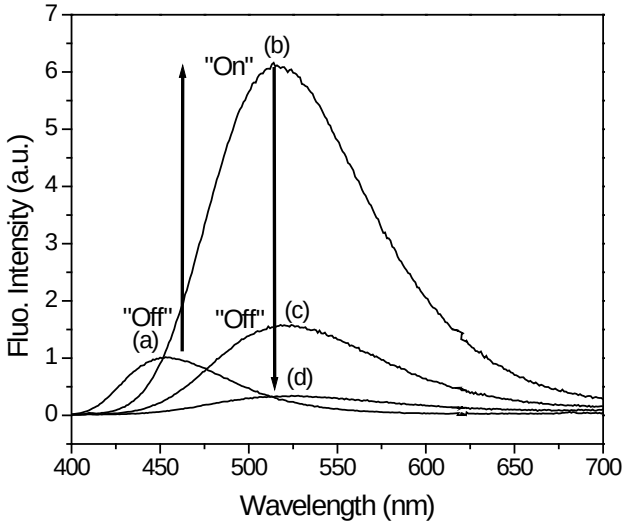

Figure 4.6 Fluorescence spectra of **APDPA** (10^{-5} M) in THF at different input concentration of protons: (a) 0, (b) 10^{-5}, (c) 10^{-3} and (d) 10^{-1} M. $\lambda_{exc.}$ = 365 nm.

4. 4. 3. Photonic logic gate behavior

We have seen that **APDPA** behaves as YES logic with metal ions such as Zn^{2+}, Cd^{2+} or Pb^{2+} as input and the fluorescence as an output (*vide* section 4.4.1). The fluorescence enhancement (FE) caused by Zn^{2+}, Cd^{2+} or Pb^{2+} ions are very similar with a maximum difference by a factor of 1.1 (Table 4.2). The metal ion concentrations required for the maximum FE are also not very different. Indeed, equal amounts of Zn^{2+} and Cd^{2+} are needed. The near-identical response for similar input levels has important implications for the use of the present system as a two-input photonic OR logic system (Figure 4.7) as this constitutes a good quality truth table.[4] Due to the ICT nature of the fluorophore, this system requires lesser excitation energy and provides output in the visible region.

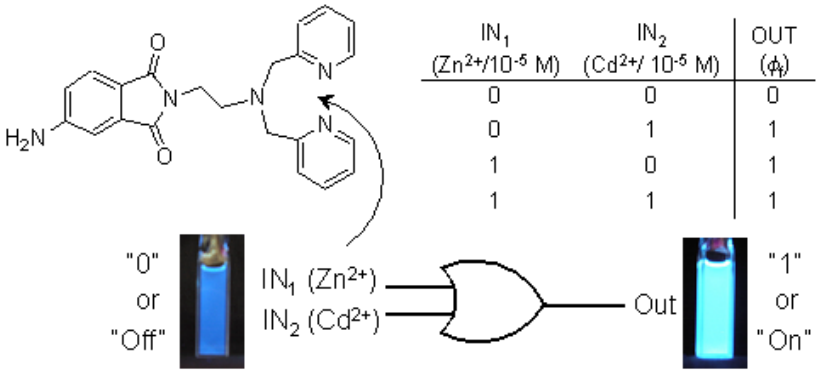

Figure 4.7 Structure of the molecule and preferred site of interaction with the metal ions. Truth table for the input–output relationship with Zn^{2+} and Cd^{2+} ions as inputs and fluorescence as an output. Equivalent logic circuit for the two-input OR gate with the visual fluorescence effect.

APDPA also behaves as H^+-driven "off-on-off" fluorescent switch by using different input levels of protons (*vide* section 4.4.2.). At very high proton concentration, the amino group of the fluorophore gets protonated and the system crosses over the YES and PASS 0 logic to behave as a NOT logic. This, when integrated with the metal ion-induced YES logic results into an Inhibit (INH) logic gate. An INH logic gate can be interpreted as a particular integration of an AND and a NOT logic gates, where the output signal is

inhibited by one of the active inputs.¶ The fluorescence of **APDPA** is "switched on" *only* in the presence of Zn^{2+}, Cd^{2+} or Pb^{2+} ions and absence of excess protons. Under other circumstances, such as the absence of metal ions, the presence of H^+ (>10^{-3} M), no fluorescence is observed. This behavior can be ascribed to an INH logic function. The corresponding truth table and the logic gate for the INH function are illustrated in Figure 4.8. Thus, a fundamental two-input INH action can be seen for **APDPA** with Zn^{2+}, Cd^{2+} or Pb^{2+} as input$_1$ (10^{-5} M) and H^+ as input$_2$ (>10^{-3} M) and fluorescence as the output. This can be comprehended into a more complex multi-input INH logic gate in which the AND logic provides the output by integrating an OR gate and a NOT gate (Figure 4.8).

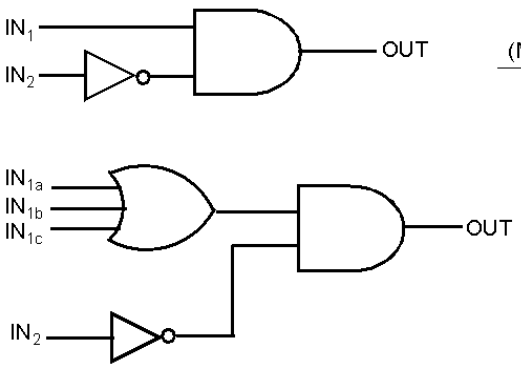

IN_1 ($M^{2+}/10^{-5}$ M)	IN_2 ($H^+/10^{-3}$ M)	OUT (ϕ_f)
0	0	0
0	1	0
1	0	1
1	1	0

Figure 4.8 Logic circuit for a fundamental two-input, one-output INH gate. Corresponding truth table. Equivalent four-input, one-output molecular switch: IN_{1a}, IN_{1b} and IN_{1c} correspond to Zn^{2+}, Cd^{2+} and Pb^{2+} and IN_2 corresponds to H^+.

4. 4. 4. Studies in aqueous medium

Photophysical experiments were carried out in water to explore the possible utility of the present system under physiological pH range. In the presence of metal ions, both the absorption and fluorescence spectra of **APDPA** are red-shifted, however, the observed FE values are very low as compared to those obtained in non-aqueous media. For example the maximum FE observed in the presence of Zn^{2+} ions is as low as 1.3 (ϕ_f =

¶ The INH function, A ^ B', should not be confused with the NAND function, (A ^ B)'.[13]

0.01). The low FE values in the aqueous environment are found to be due to inefficient PET in aqueous solution. Figure 4.9 depicts the fluorescence spectra of optically matched solutions of **AP** and **APDPA** in buffered water (pH 7). It can be seen that the fluorescence quantum yield of **APDPA** is lower than that of **AP** only by a factor of 1.4 in aqueous solution. The inefficient PET in aqueous environment can be accounted for when taken into consideration the fact that the imide oxygen atom of the fluorophore moiety has the possibility to form hydrogen bond with water molecules thereby dropping the quantum yield of the fluorophore (ϕ_f, **AP** = 0.01 in water).[14] This results into an inefficient PET process when water is chosen as a medium (ϕ_f, **APDPA** = 0.007 in water). Furthermore, similar to that observed with systems described in chapter 3, at higher pH values the compound dissociates and becomes non-fluorescent.

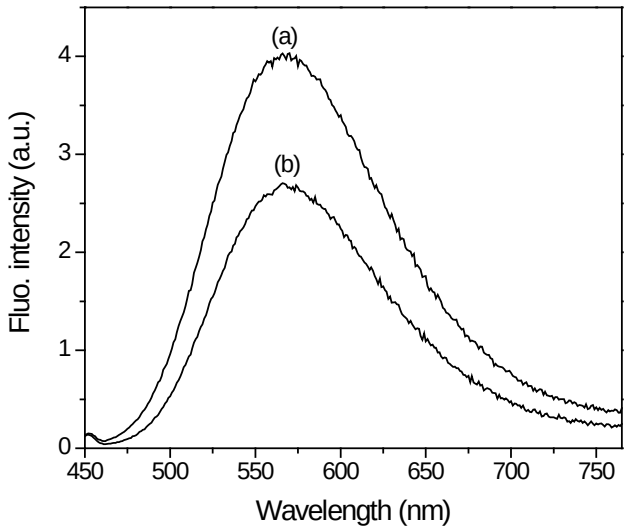

Figure 4.9 Fluorescence spectra of (a) **AP** and (b) **APDPA** in buffered water (pH = 7). $\lambda_{exc.}$ = 365 nm.

4. 5. X-ray crystallographic measurements

4. 5. 1. Structure of APDPA

Single crystal X-ray structure of **APDPA** has been determined to understand the geometry of the molecule in the solid state and with a view to gaining insight on the efficiency of the PET process. Although the PET driving force is estimated from the redox potentials of the receptor and the fluorophore moieties (see section 1.2.6. for details), large spatial separation between the two can make a system unfavorable for PET. A single crystal obtained by slow evaporation of ethylacetate/hexane solution crystallizes in the monoclinic space group $P2_1/n$. The molecular structure is shown in Figure 4.10 and the relevant crystallographic data are presented in Table 4.3.

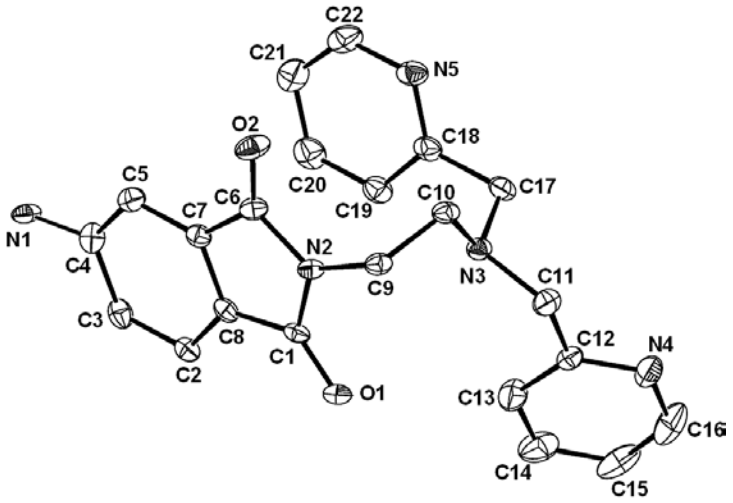

Figure 4.10 Ortep view of the X-ray structure of **APDPA** with atoms represented by thermal ellipsoid at the 30% probability level. Hydrogen atoms are not shown for clarity and only one occupancy site for the disordered NH_2 group is displayed.†

† During the refinement process, a disorder of position was observed for NH_2 group, which was split over two distinct sites, C3 and C4, with occupancy factor of 0.5 each. One hydrogen atom was therefore could not be introduced at the C3 site. The atomic coordinates and details of other parameters are tabulated in Appendix II.

Table 4.3 Crystallographic parameters for **APDPA**

Formula	$C_{22}H_{21}N_5O_2$
Formula wt	387.44
Crystal system	Monoclinic
Space group	$P2_1/n$
a (Å)	7.433(3)
b (Å)	23.390(10)
c (Å)	11.264(5)
β (°)	96.226(7)
V (Å^3)	1946.7(14)
Z	4
F(000)	816
ρ_{calcd} (g cm^{-3})	1.322
Radiation (Å) (Mo-Kα)	0.71073
No. of reflections for measd	3751
θ_{range} □(°)	2.52 – 28.14
μ (mm^{-1})	0.088
Temperature (K)	100
Crystal size	0.48 × 0.25 × 0.10
Color	yellow
Diffractometer	CCD area detector diffractometer
Data collection method	Φ and ω scans
Absorption correction	Multi-scan (SADABS)
T_{min}, T_{max}	0.886, 0.991
Total no. of reflections	21715
No. of unique reflections	4619
No. of observed reflections [I > 2σ(I)]	2851
θ_{max} □(°)	28.35
hkl range	-9 → 9; -30 → 30; -14 → 14
No. of parameters	283
R1 [$F^2 > 2\sigma(F^2)$], wR1 (F^2)	0.0801, 0.1754
GOF	1.125
$\Delta\rho_{max}$, $\Delta\rho_{min}$ (e/Å^3)	0.262, -0.234

While the plane of one of the pyridyl rings is bent relative to the phthalimido ring (35.85°), the other is almost planar (9.18°). The spatial separation between the fluorophore and the nitrogen atoms of the receptor moiety are listed in Table 4.4. While N3 is only 2.9 Å away, the pyridyl nitrogen atoms are much more separated from the fluorophore. Moreover, aliphatic amines are thermodynamically more favorable for the PET process. Thus, the aliphatic amine nitrogen atom of the DPA receptor is solely responsible for the PET quenching in this system.

Table 4.4 Non-bonded distances between the imide nitrogen atom of the fluorophore and the nitrogen atoms of the receptor moiety in **APDPA** and **Zn(APDPA)$_2$**.

	APDPA / Å	**Zn(APDPA)$_2$** / Å
N2–N3	2.925	3.777
N2–N4	6.098	5.787
N2–N5	4.182	6.361
N7–N8	-	3.771
N7–N9	-	5.743
N7–N10	-	6.411

4. 5. 2. Structure of APDPA – Zn(II) complex

Since the hydrated perchlorate salts of the metals were used, the possibility that the observed enhancement of the fluorescence is due to the transfer of proton to the amine moiety next to the fluorophore has to be taken into account. Moreover, there are still important and practical issues that need to be addressed before the realization of a pragmatic molecular device. The independence of the fluorescence output on the nature of the input ions requires that the fluorescence switching is due to ion-induced conformational changes of flexible systems rather than due to mere proximity of the ions, which has been the sole design basis in most of the systems.[15] Furthermore, more advanced practical integration of such molecular level logic gates into circuits is still desired. In order to prove that there is no ambiguity in the fluorescence data presented and to establish the potential of the present molecule for performing logic operations

even when incorporated into a more advanced system, we have carried out single crystal X-ray structure analyses for **APDPA – Zn^{2+}** complex. A single crystal obtained by slow evaporation of acetonitrile solution of the complex crystallizes in the triclinic space group *P*-1. The molecular structure is shown in Figure 4.11 and the relevant crystallographic data are presented in Table 4.5.

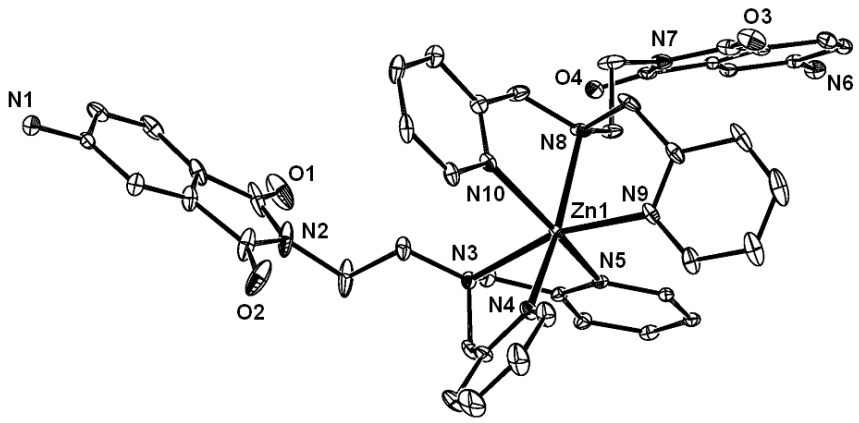

Figure 4.11 Ortep view of the X-ray structure of $[Zn(APDPA)_2](ClO_4)_2$ with atoms represented by thermal ellipsoid at the 10% probability level. Hydrogen atoms, counter ions and the solvent of crystallization have been omitted for clarity.‡

Upon coordination with the metal ions, the molecular arrangement of the system changes considerably. The crystal structure of $[Zn(APDPA)_2](ClO_4)_2$ showed a mononuclear complex in which Zn^{2+} is coordinated to all the three nitrogen atoms of the DPA fragment of each ligand unit. The geometry of the cationic portion is octahedral with each **APDPA** acting as a tridentate ligand. The planes of the pyridyl rings are now highly deviated from planarity relative to their respective phthalimido rings (77.87°, 50.33°, 78.80° and 78.54°).

‡ During the refinement process, a disorder of position was observed for one perchlorate group, two of the terminal oxygen atoms were split over two distinct sites with occupancy factor of 0.5 each. The atomic coordinates and details of other parameters are tabulated in Appendix II.

Table 4.5 Crystallographic parameters for **APDPA – Zn(II)** complex

Formula	$C_{44}H_{42}N_{10}O_4Zn.2(ClO_4).CH_3CN$
Formula wt	1080.20
Crystal system, Space group	Triclinic, *P*-1
a (Å)	10.4430(7)
b (Å)	12.1265(9)
c (Å)	21.2097(15)
α (°)	75.385(1)
β (°)	99.02(2)
γ (°)	65.995(1)
V (Å^3)	2370.0(3)
Z	2
F(000)	1116
ρ_{calcd} (g cm^{-3})	1.514
Radiation (Å) (Mo-Kα)	0.71073
No. of reflections for measd	6704
μ (mm^{-1})	0.707
Temperature (K)	100
Crystal size	0.29 × 0.12 × 0.04
Color	Yellow
Diffractometer	CCD area detector diffractometer
Data collection method	Φ and ω scans
Absorption correction	Multi-scan (SADABS)
T_{min}, T_{max}	0.820, 0.972
Total no. of reflections	27920
No. of unique reflections	11107
No. of observed reflections [I > 2σ(I)]	5729
θ_{max} (°)	28.29
hkl range	-13 → 13; -15 → 15; -28 → 28
No. of parameters	680
R1 [$F^2 > 2\sigma(F^2)$], wR1 (F^2)	0.0909, 0.2450
GOF	1.030
$\Delta\rho_{max}$, $\Delta\rho_{min}$ (e/Å^3)	0.912, -0.848

Interestingly, but not surprisingly, coordination of Zn^{2+} with **APDPA** results in an increased separation of the receptor and fluorophore moieties (Table 4.4; from N2–N3 = 2.93 Å in the unbound state to 3.77 Å in the bound state) along with a twisting of the amine lone electron pair *ca*. 75° away from the π electrons of the fluorophore. These structural modulations suggest that complexation of **APDPA** with the metal ion makes the lone pair of the nitrogen atom unavailable for PET quenching pathway. This also provides direct evidence that PET between the receptor and fluorophore moieties is mediated through space. An important aspect to be noted is that the fluorescence quantum yield of the structurally characterized Zn^{2+}-complex of **APDPA** in THF is measured to be equal to that observed upon addition of Zn^{2+} salt to the solution of **APDPA** in THF. Thus, non-interference of residual protons from the hydration shell of the metal salts is also firmly assured.

4. 6. Conclusions

In summary, we have developed a simple molecular system that shows enhancement of fluorescence in the presence of post-transition metal ions such as Zn^{2+}, Cd^{2+} or Pb^{2+}. Metal ion-induced enhancement of fluorescence is attributed to the inhibition of PET quenching pathway. Access to multiple logic functions makes this system unique in terms of its performance flexibility. Nevertheless, this is a first demonstrated example of an INH logic gate employing HTM ions and H^+ as logic inputs. Furthermore, direct X-ray structure evidence suggests the potential of this system in molecular-scale logic operations and also rules out the possibility of proton interference.

References

1 Gruenwedel, D. W. *Inorg. Chem.* **1968**, *7*, 495.
2 de Silva, S. A.; Zaveleta, A.; Baron, D. E.; Allam, O.; Isidor, E. V.; Kashimura, N.; Percarpio, J. M. *Tetrahedron Lett.* **1997**, *38*, 2237.
3 Walkup, G. K.; Burdette, S. C.; Lippard, S. J.; Tsien, R. Y. *J. Am. Chem. Soc.* **2000**, *122*, 5644.
4 de Silva, A. P.; Gunaratne, H. Q. N.; Maguire, G. E. M. *Chem. Commun.* **1994**, 1213.
5 Ghosh, P.; Bharadwaj, P. K.; Roy, J.; Ghosh, S. *J. Am. Chem. Soc.* **1997**, *119*, 11903.
6 de Silva, A. P.; Gunaratne, H. Q. N.; McCoy, C. P. *Chem. Commun.* **1996**, 2399.
7 Fabbrizzi, L.; Licchelli, M.; Poggi, A.; Taglietti, A. *Eur. J. Inorg. Chem.* **1999**, 35.

8 de Silva, A. P.; Dixon, I. M.; Gunaratne, H. Q. N.; Gunnlaugsson, T.; Maxwell, P. R. S.; Rice, T. E. *J. Am. Chem. Soc*. **1999**, *121*, 1393.
9 Gunnlaugsson, T.; Mac Donail, D. A.; Parker, D. *Chem. Commun.* **2000**, 93.
10 Montenegro, J.-M.; Perez-Inestrosa, E.; Collado, D.; Vida, Y.; Suau, R. *Org. Lett.* **2004**, *6*, 2353.
11 Cotton, F. A.; Wilkinson, G. *Advanced Inorganic Chemistry*; Third ed.; Wiley Eastern Limited: New Delhi, 1976.
12 Soujanya, T.; Fessenden, R. W.; Samanta, A. *J. Phys. Chem.* **1996**, *100*, 3507.
13 Burger, P. *Digital Design: A Practical Course*; Wiley: New York, 1988.
14 Soujanya, T.; Krishna, T. S. R.; Samanta, A. *J. Phys. Chem.* **1992**, *96*, 8544.
15 de Silva, A. P.; Gunaratne, H. Q. N.; Gunnlaugsson, T.; Huxley, A. J. M.; McCoy, C. P.; Rademacher, J. T.; Rice, T. E. *Chem. Rev.* **1997**, *97*, 1515.

Chapter 5

Fluorescent ligands, 2-(4´-aminophthalimidomethyl)pyridine and 2-(4´-aminophthalimidoethyl)pyridine, for the stabilization of copper(I) complexes

This chapter describes the synthesis, structure and photophysical properties of pyridine-derivatized 4-aminophthalimide systems that form two-coordinated linear complexes of copper(I). The unusual stability of the copper(I) complexes, which have been characterized by X-ray crystallography, is attributed to the electronic factors provided by the 4-aminophthalimide of the ligand framework and the perchlorate counter-anion moieties.

5. 1. Introduction

Photoinduced electron transfer (PET) often arises from a tertiary amine whose sensitivity towards the acidity of the medium often obscures/interferes the response to metal ions. The observed photophysical changes of the multi-component systems in the presence of hydrated metal salts in non-aqueous media need to be interpreted cautiously as the changes can be due to the contaminated protons rather than due to metal ion complexation. However, proton sensitivity around neutral pH can be avoided by employing substituted anilines or pyridines (whose p*K* is *ca.* 5.5)[1] instead of aliphatic amines as a receptor moiety. With this idea, pyridine derivatives of 4-aminophthalimide (**AP**) with a *fluorophore-spacer-receptor* architecture, **APMPY** and **APEPY**, have been synthesized. Unexpectedly, the fluorescence quantum yield of these simple molecular systems is very similar to that of the parent fluorophore, **AP**, suggesting the absence of PET in these systems. Thus, these systems turned out to be ineffective for sensing applications. However, the changes in the electronic absorption spectra of **APMPY** and **APEPY** upon subsequent addition of metal ions indicated that they do form complexes with transition metal ions in solution.

Several multi-component systems based on **AP** fluorophore have been developed in recent years.[2,3] However, the coordination properties of the metal ions with these systems are still unexplored primarily because of lack of definite structural information on these systems. Secondly, very few two-coordinate copper(I) complexes,† especially utilizing simple unidentate ligands without steric bulk, are represented in the literature and structurally characterized ones are even rarer.[7-10] This is mainly due to the instability of the copper(I) compounds. Sorrell et al. observed that two-coordinate copper(I) complexes with sterically hindered heterocyclic ligands and having increased orbital overlap between the ligating atoms and copper(I) are inert toward reaction with CO and less reactive with O_2 in aprotic solvents.[7] However, in protic solvents, these complexes react rapidly and irreversibly with dioxygen to form Cu^{2+}. Sanyal et al. also observed a similar phenomenon in a two-coordinate linear complex of copper(I) with imidazole ligand.[8] On the other hand, Le Clainche et al. emphasized on the importance of preorganization of the metal binding site provided by the calix[4]arene platform and an increased orbital overlap between the imidazole-nitrogen atom and copper(I) as the key features for the inertness of copper(I) ions toward dioxygen in the solid state as well as in coordinating or protic solvents.[9] However, the analogous pyridine-based complex is extremely sensitive to air and undergo auto-oxidation within seconds.[9]

Taking these into account, copper(I) complexes of **APMPY** and **APEPY** were synthesized via in-situ reduction of the copper(II) salt. Single crystal X-ray structure reveals that the packing in both the ligands as well as in their complexes is governed by intermolecular hydrogen bonding between the 4-amino nitrogen atom and one of the imide oxygen atoms of the neighboring molecule. X-ray structure of the complexes also reveals a close contact between the oxygen atom of the perchlorate anion and the metal center leading to a linear polymeric network. The copper(I) complexes are highly air-

† Coordinatively unsaturated copper(I) complexes are essential for the understanding of the metal reactivity in various biological processes such as biochemical oxido-reduction and electron transfer processes as well as the reversible binding of small gaseous molecules such as CO, O_2 (Hemocyanin) or the plant hormone ethylene.[4,5] Due to the lack of useful spectroscopic probes for the copper(I) centers in native proteins, it becomes necessary to study its coordination chemistry with small artificial ligands. Furthermore, the study of the interaction of small gaseous molecules like CO, O_2 with copper(I) complexes might provide a reverse way to assess the structure of copper(I) centers in proteins or in solution.[6]

stable and unusually inert towards oxidation in the solid state as well as in potentially coordinating or protic solvents. The electronic factors provided by an electron-deficient **AP** moiety of the ligand framework and the perchlorate counter-anion are the key features for the extraordinary stabilization of cuprous ions.

5. 2. Synthesis

5. 2. 1. APMPY and APEPY

Access to the pyridine-derivatized **AP** was achieved through a single step reaction between **AP** and neat 2-aminomethylpyridine/2-aminoethylpyridine at 65°C/80°C to afford **APMPY** and **APEPY** respectively (Scheme 5.1).

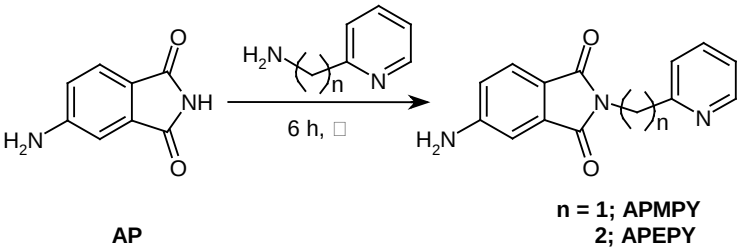

Scheme 5.1 Synthetic route for **APMPY** and **APEPY**.

2-(4´-Aminophthalimidomethyl)pyridine (APMPY). **AP** (0.5 g, 3.09 mmol) and 2-aminomethylpyridine (0.38 mL, 3.7 mmol) were placed in a 25 mL pear-shaped flask fitted with a water condenser and potassium hydroxide guard tube. The reaction mixture was heated at 65°C with constant stirring for 6 h. The sticky material thus formed was purified by column chromatography (neutral alumina, $CHCl_3$) to obtain the desired product that was further recrystallized from $CHCl_3$/hexane to yield yellow crystalline solid, yield 90%. Single crystals suitable for X-ray crystallography were grown by slow evaporation of a chloroform solution over a period of several days. The purified product was characterized by the following analytical results.

CHN analysis calculated for $C_{14}H_{11}N_3O_2$: C, 66.4; H, 4.35; N, 16.6. Found: C, 65.8; H, 4.24; N, 16.4.

IR (KBr, cm^{-1}): 3422, 3312, 1769, 1696, 1618.

^{1}H NMR ($CDCl_3$): δ (ppm) 4.45 (s, 2H), 4.96 (s, 2H), 6.79 (dd, 1H), 6.99 (d, 1H), 7.14 (m, 2H), 7.56-7.60 (m, 2H), 8.51 (d, 1H).

^{13}C NMR ($CDCl_3$): δ (ppm) 168.84, 168.51, 155.72, 153.46, 148.96, 137.20, 134.68, 125.33, 122.57, 121.46, 119.14, 117.71, 108.38, 42.43.

2-(4´-Aminophthalimidoethyl)pyridine (APEPY). **AP** (0.5 g, 3.09 mmol) and 2-aminoethylpyridine (0.44 mL, 3.7 mmol) were placed in a 25 mL pear-shaped flask fitted with a water condenser and potassium hydroxide guard tube. The reaction mixture was heated at 80°C with constant stirring for 6 h. Initially, it formed a clear solution and then solidified into a thick mass, which was triturated and washed with hexane. Recrystallization from $CHCl_3$/hexane yielded the desired product as a yellow crystalline solid, yield 92%. Single crystals suitable for X-ray crystallography were grown by slow evaporation of a $CHCl_3$ solution over a period of several days. The pure compound was characterized by the following analytical results.

CHN analysis calculated for $C_{15}H_{13}N_3O_2$: C, 67.42; H, 4.87; N, 15.73. Found: C, 67.1; H, 4.78; N, 15.55.

IR (KBr, cm^{-1}): 3401, 3350, 1755, 1696, 1615.

^{1}H NMR ($CDCl_3$): δ 3.15 (t, 2H), 4.04 (t, 2H), 4.33 (s, 2H), 6.79 (dd, 1H), 6.99 (d, 1H), 7.14-7.18 (m, 2H), 7.56-7.60 (m, 2H), 8.51 (d, 1H).

^{13}C NMR ($CDCl_3$): δ (ppm) 168.89, 168.63, 158.0, 153.44, 148.77, 137.07, 134.51, 125.0, 123.58, 121.89, 119.0, 117.46, 108.11, 37.43, 36.48.

5. 2. 2. Copper(I) complexes: CuAPMPY and CuAPEPY

The copper(I) complexes, **CuAPMPY** and **CuAPEPY**, were prepared by reacting **APMPY** and **APEPY** with $Cu(ClO_4)_2 \cdot 6H_2O$. Neither the use of any external reducing agents nor that of relatively unstable copper(I) salts were needed. The relative stability of copper(I) and copper(II) in solution depend very strongly on the nature of the anions and the ligands present and vary considerably with the solvent or nature of the neighboring atoms. Therefore, the in-situ reduction of Cu(II) to Cu(I) is attributed to the easily reducible property of $Cu^{II}(ClO_4)_2$ and the greater stability of $Cu^{I}ClO_4$ with these ligands in acetonitrile. The electron-deficient **AP** moiety of the ligand framework reduces the electron density over the metal ions, thus stabilizing the lower oxidation state. When the

reaction was carried out with excess of ligand, the yield of the desired complex had increased substantially suggesting that the ligand system itself acts as a reducing agent. In recent years, hydrothermal/solvothermal reactions under pressure have been used as a synthetic strategy to reduce various metal ions, including copper.[11] Thus, the simultaneous reduction of copper(II) and formation of two-coordinate copper(I) complex have significant implication with a synthetic viewpoint. The detailed synthetic procedure is as follows.

Bis-(2-(4´-Aminophthalimidomethyl)pyridine)copper(I)perchlorate (CuAPMPY). To a solution of **APMPY** (1.01 g, 4 mmol) in methanol (50 mL), $Cu(ClO_4)_2 \cdot 6H_2O$ (0.74 g, 2 mmol) dissolved in methanol (25 mL) were added drop-wise and the resulting solution was stirred for 48 h at room temperature.§ Subsequently the reaction mixture was stored for slow evaporation to afford brown colored tiny crystals, suitable for X-ray diffraction, of **CuAPMPY** in 25% yield. The complex was characterized by the following analytical results.

IR (KBr, cm^{-1}): 3458, 3362, 1757, 1689, 1612, 1090.

^1H NMR (CD_3CN): δ (ppm) 4.43 (s, 2H), 5.12 (bs, 2H), 6.84 (dd, 1H), 6.94 (d, 1H), 7.35-7.82 (m, 4H), 8.48 (b, 1H).

Conductivity measurements revealed the 1:1 cation:anion ratio. The complex was EPR silent.

The yield improved substantially to 55% when the reaction was carried out with excess **APMPY** in methanol-acetonitrile mixed solvent according to the procedure described below, for the synthesis of **CuAPEPY**.

Bis-(2-(4´-Aminophthalimidoethyl)pyridine)copper(I)perchlorate [CuAPEPY]. To a solution of **APEPY** (1.01 g, 4 mmol) in 1:1 methanol-acetonitrile (50 mL), $Cu(ClO_4)_2 \cdot 6H_2O$ (0.37 g, 1 mmol) dissolved in methanol (20 mL) were added drop-wise and the resulting solution was stirred for 24 h at room temperature. Subsequently the reaction mixture was filtered and the filtrate was stored for slow evaporation to afford the desired complex as brown colored crystals suitable for X-ray crystallography. Yield 65%. The complex was characterized by the following analytical results.

§ Caution! Care should be taken while treating organic compounds with metal perchlorates as potentially explosive mixtures may be formed.

IR (KBr, cm^{-1}): 3437, 3360, 1752, 1689, 1609, 1076.

^1H NMR (CD_3CN): δ (ppm) δ 3.12 (t, 2H), 3.92 (t, 2H), 5.12 (bs, 2H), 6.85 (dd, 1H), 6.94 (d, 1H), 7.34-7.39 (m, 2H), 7.48 (d, 1H), 7.82 (m, 1H), 8.48 (b, 1H).

Conductivity measurements revealed the 1:1 cation:anion ratio. The complex was EPR silent.

5. 3. Photophysical properties

The electronic absorption and fluorescence behavior of **APMPY** and **APEPY** has been studied in dioxane, tetrahydrofuran (THF) and acetonitrile (AN). The spectral data of these systems in various solvents are listed in Table 5.1 and representative absorption and fluorescence spectra in different solvents are shown in Figure 5.1. Both the absorption and fluorescence spectra are characterized by broad bands, typical of the transition to the intramolecular charge-transfer state of the fluorophore moiety.[12] Contrary to the absorption spectra, the location of the fluorescence maximum is determined by the polarity of the media (Table 5.1). This behavior is consistent with a higher dipole moment of the excited state of the fluorophore.[12] Both the absorption and the fluorescence spectra are red-shifted (8-9 nm in the absorbance and 5-16 nm in the fluorescence spectra) relative to the parent fluorophore. Apart from the spectral shift the photophysical behavior of these systems is quite similar to that of the parent fluorophore.

Table 5.1 Absorption and fluorescence properties of **AP**, **APMPY**, **APEPY**, **CuAPMPY** and **CuAPEPY** in dioxane, tetrahydrofuran (THF) and acetonitrile (AN).[a]

	Dioxane			**THF**			**AN**		
Compound	λ_{max}^{abs}	λ_{max}^{flu}	Φ_f	λ_{max}^{abs}	λ_{max}^{flu}	Φ_f	λ_{max}^{abs}	λ_{max}^{flu}	Φ_f
AP[b]	352	435	0.73	357	445	0.70	357	458	0.63
APMPY	361	440	0.80	365	453	0.75	366	472	0.78
APEPY	361	440	0.78	365	455	0.75	366	474	0.75
CuAPMPY	-[c]	-[c]	-[c]	-[c]	-[c]	-[c]	367	480	0.53
CuAPEPY	-[c]	-[c]	-[c]	-[c]	-[c]	-[c]	367	477	0.58

[a] Wavelength maximum values are in nm. [b] These data have been collected from ref. 12.
[c] Copper(I) complexes are insoluble in this medium.

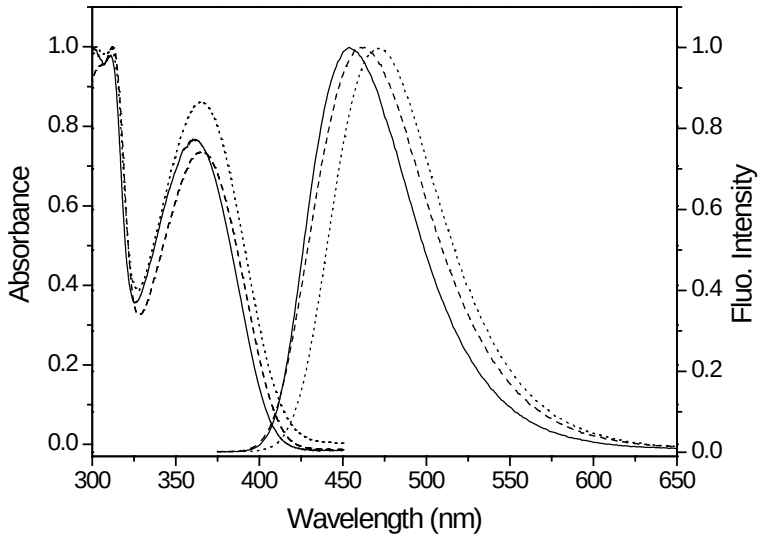

Figure 5.1 Absorption and fluorescence spectra of **APMPY** in dioxane (——), tetrahydrofuran (----) and acetonitrile (····). All spectra are normalized at their respective peak position. $\lambda_{exc.}$ = 360 nm.

These systems exhibit high fluorescence quantum yield (Φ_f = 0.75 in THF) comparable to that of the parent fluorophore, **AP** (Φ_f = 0.70 in THF).[12] This suggests that PET quenching pathway is not present in these systems. Addition of the metal salts leads to a bathochromic shift of the absorption maximum. The fluorescence maximum is also Stokes-shifted and is associated with a drop of the fluorescence intensity of the system. The changes in the absorption and fluorescence spectra of **APMPY** in the presence of Cu^{2+} ions are depicted in Figure 5.2. This indicates that these systems do not act as fluorescent "Off-On" sensors for metal ions. However, they do form complexes with metal ions.

The electronic absorption and fluorescence behavior of the copper(I) complexes, **CuAPMPY** and **CuAPEPY**, is very similar to that of their respective ligand systems (Table 5.1). However, the fluorescence quantum yield of the complexes is found to be slightly lower than that of their respective ligand systems. This could be due to the interaction of the fluorophore with the metal center.

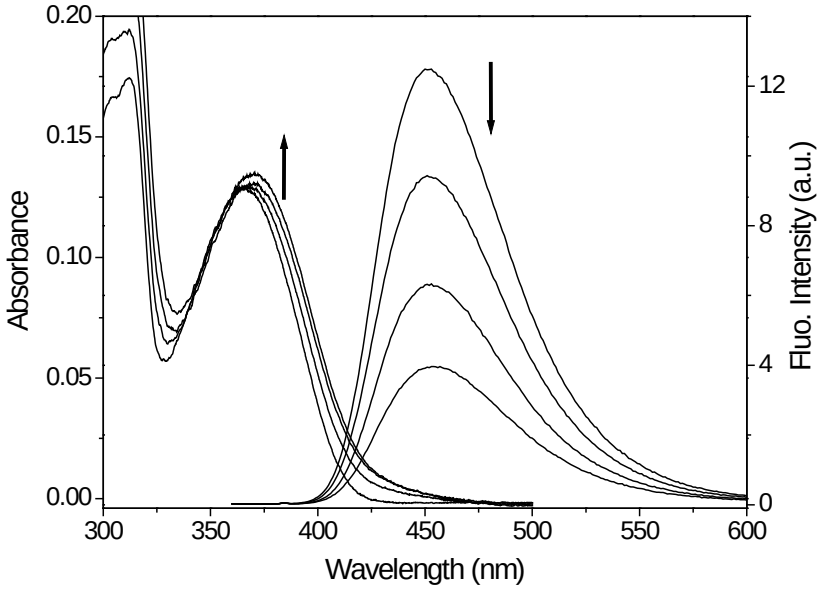

Figure 5.2 Effect of Cu^{2+} ions on the absorption and fluorescence spectrum of **APMPY** (3.3×10^{-5} M) in THF. The various concentrations of Cu^{2+} ions in increasing order of absorbance at 400 nm and decreasing order of fluorescence intensity are 0, 6.0×10^{-5}, 2.9×10^{-4} and 1.1×10^{-3} M. $\lambda_{exc.}$ = 345 nm.

5. 4. X-ray crystallographic measurements

5. 4. 1. Structure of APMPY and APEPY

Slow evaporation of the chloroform solutions of **APMPY** and **APEPY** yielded yellow crystals, suitable for X-ray diffraction studies. An ORTEP view with atom numbering scheme is shown in Figure 5.3 and the relevant crystallographic data are presented in Table 5.2. Atomic coordinates and details of other parameters are tabulated in Appendix III. Compounds **APMPY** and **APEPY**, constructed of *fluorophore-spacer-receptor* architecture, differ only in one methylene unit that separates the **AP** and pyridine moieties. However, large difference exists in their crystallization space groups. While **APMPY** crystallizes in the least common non-centrosymmetric orthorhombic space group Fdd2, **APEPY** crystallizes in relatively more common monoclinic space group *C*2/c.

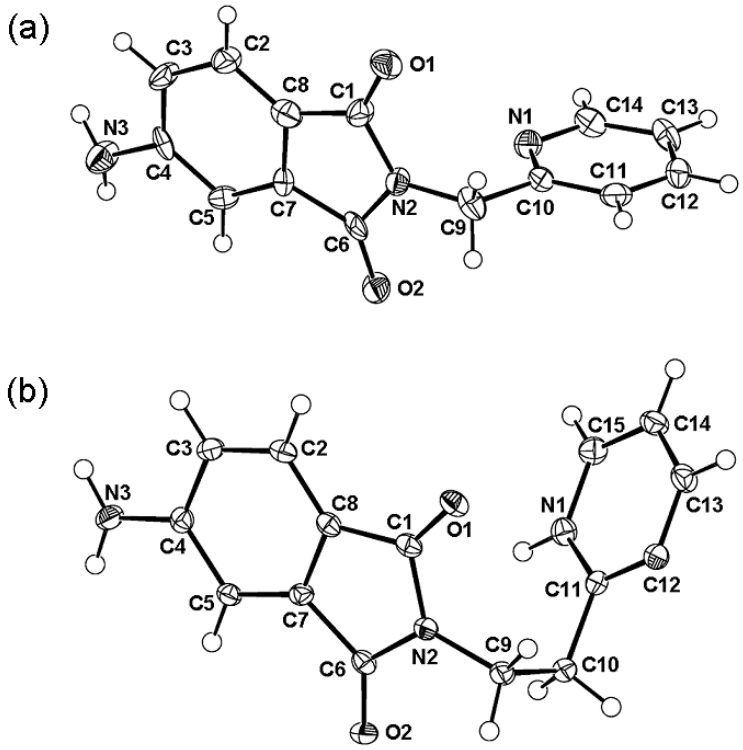

Figure 5.3 Ortep view of the X-ray structure of (a) **APMPY** and (a) **APEPY** with atoms represented by thermal ellipsoid at the 50% probability level.

In both the compounds, the packing is determined by the intermolecular N–H···O and N–H···N hydrogen bonds involving the amino nitrogen atom, the carbonyl oxygen atom and the pyridine nitrogen atom. However, the network of the packed molecules in these systems is largely different (Figure 5.4). The molecules are more closely packed in **APMPY** as compared to **APEPY**. This difference in the packing of the molecule is also reflected by the bending of the plane of the pyridine ring with respect to that of the phthalimide ring in these compounds. The dihedral angle between the planes defined by phthalimido and pyridyl rings in **APMPY** and **APEPY** is 85.79(23)° and 39.33(6)° respectively.

Table 5.2 Crystallographic parameters for **APMPY** and **APEPY**

	APMPY	**APEPY**
Formula	$C_{14}H_{11}N_3O_2$	$C_{15}H_{13}N_3O_2$
Formula wt	253.26	267.28
Crystal system, Space group	Orthorhombic, *F*dd2	Monoclinic, *C*2/c
a (Å)	48.067 (16)	26.312 (4)
b (Å)	7.504 (3)	5.2500 (8)
c (Å)	13.292 (4)	21.028 (3)
α (°)	90	90
β (°)	90	116.08 (2)
γ (°)	90	90
V (Å^3)	4795 (3)	2609.0 (7)
Z	16	8
F(000)	2112	1120
ρ_{calcd} (g cm^{-3})	1.403	1.361
Radiation (Å) (Mo-Kα)	0.71073	0.71073
No. of reflections for measd.	1945	2850
μ (mm^{-1})	0.097	0.093
Temperature (K)	100	100
Crystal size	0.48 × 0.05 × 0.02	0.48 × 0.29 × 0.15
Color, habit	Yellow, block	Yellow, thin plates
Diffractometer	CCD area detector	CCD area detector
Absorption correction	Multi-scan	Multi-scan
T_{min}, T_{max}	0.798, 0.998	0.862, 0.986
Total no. of reflections	12726	14482
No. of unique reflections	1492	3130
No. of obs. reflections [I > 2σ(I)]	1245	2510
θ_{max} (°)	28.17	28.25
hkl range	-63→63; -9→9; -17→17	-34→33; -6→6; -27→27
No. of parameters	178	189
R1 [$F^2 > 2\sigma(F^2)$], wR1 (F^2)	0.0970, 0.2279	0.0544, 0.1237
GOF	1.288	1.075
$\Delta\rho_{max}$, $\Delta\rho_{min}$ (e/Å^3)	0.616, -0.318	0.425, -0.217

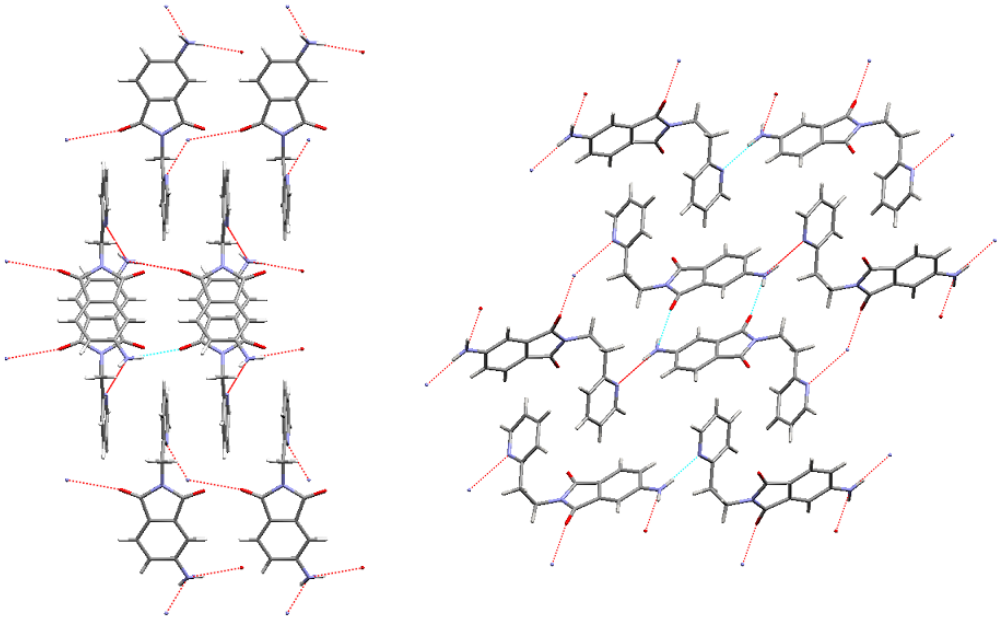

Figure 5.4 Packing diagram along the y-axis illustrating the intermolecular hydrogen bonding shown as dashed lines for (a) **APMPY**: d(N3 – H3A····N1[-x, -y, z]) = 3.034 Å, ∠N3 – H3A····N1[-x, -y, z] = 158.95°; d(N3 – H3B····O1[-x, -y+1/2, z+1/2]) = 3.026 Å, ∠N3 – H3B····O1[-x, -y+1/2, z+1/2] = 152.45° and (b) **APEPY**: d(N3 – H3A····N1[x, -y+1, z-1/2]) = 3.020 Å, ∠N3 – H3A····N1[x, -y+1, z-1/2] = 167.89°; d(N3 – H3B····O2[-x, -y, -z]) = 3.044 Å, ∠N3 – H3B····O2[-x, -y, -z] = 155.71°.

5. 4. 2. Structure of CuAPMPY and CuAPEPY

The crystal structures of **CuAPMPY** and **CuAPEPY** show a mononuclear complex in which copper is coordinated to the pyridine nitrogen atom of each ligand unit. The X-ray structures are shown in Figure 5.5 and the relevant crystallographic data are presented in Table 5.3. Atomic coordinates and details of other parameters are tabulated in Appendix III.

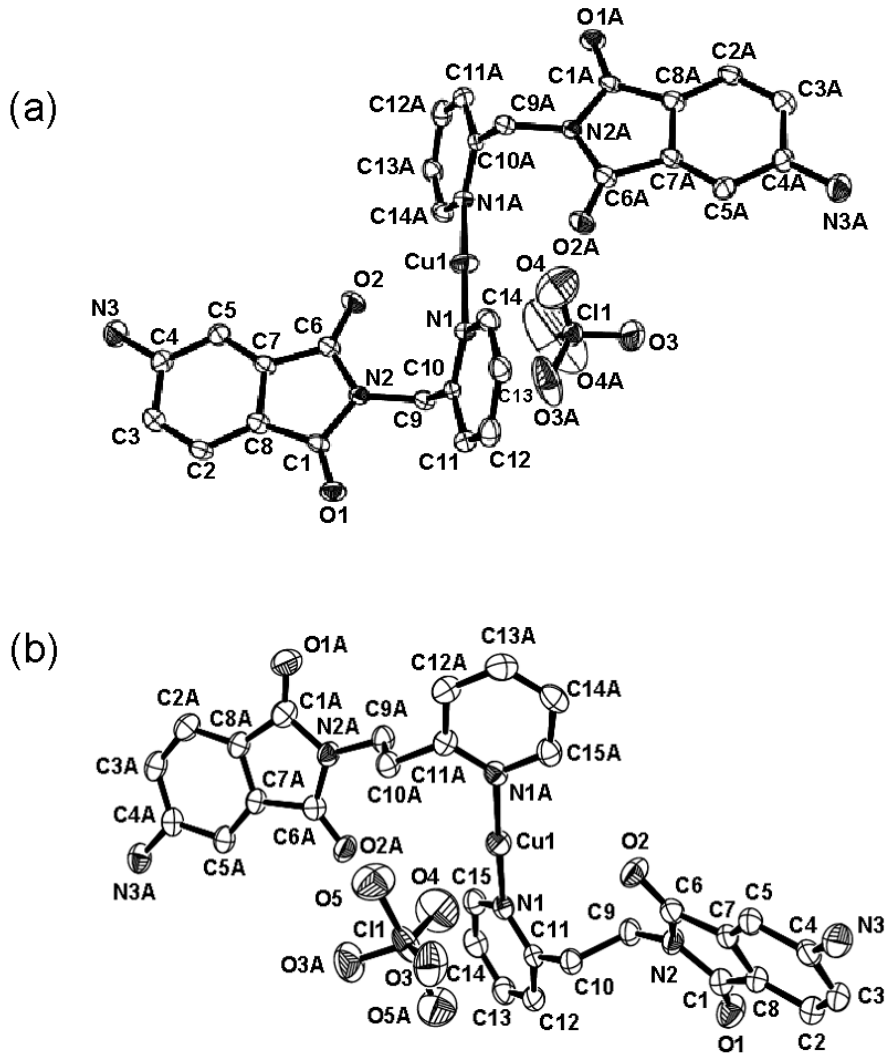

Figure 5.5 Ortep view of the X-ray structure of (a) **CuAPMPY** and (b) **CuAPEPY** with atoms represented by thermal ellipsoid at the 30% and 20% probability level, respectively. Hydrogen atoms have been omitted for clarity.

Table 5.3 Crystallographic parameters for **CuAPMPY** and **CuAPEPY**

	CuAPMPY	**CuAPEPY**
Formula	$C_{28}H_{22}ClCuN_6O_8$	$C_{30}H_{26}ClCuN_6O_8$
Formula wt	669.52	697.56
Crystal system, Space group	Monoclinic, *C*2/c	Monoclinic, *C*2/c
a (Å)	21.536 (8)	24.761 (2)
b (Å)	8.172 (3)	7.5815 (7)
c (Å)	15.408 (3)	16.3684 (15)
α (°)	90	90
β (°)	99.02 (2)	102.915 (2)
γ (°)	90	90
V (Å^3)	2678.3 (14)	2995.0 (5)
Z	4	4
F(000)	1368	1432
ρ_{calcd} (g cm^{-3})	1.66	1.547
Radiation (Å) (Mo-Kα)	0.71073	0.71073
No. of reflections for measd.	25	1933
μ (mm^{-1})	0.981	0.881
Temperature (K)	293	293
Crystal size	0.60 × 0.36 × 0.21	0.24 × 0.15 × 0.05
Color, habit	Brown, thin rods	Brown, thin plates
Diffractometer	Mach-3 four circle (CAD-4)	CCD area detector
Absorption correction	psi-scan	Multi-scan
T_{min}, T_{max}	0.728, 0.821	0.792, 0.957
Total no. of reflections	2418	18730
No. of unique reflections	2361	3616
No. of obs. reflections [I > 2σ(I)]	1407	1430
θ_{max} (°)	24.97	28.27
hkl range	0→25; 0→9; -18→18	-31→28; -10→10; -21→21
No. of parameters	207	220
R1 [F^2 > 2σ(F^2)], wR1 (F^2)	0.0744, 0.2022	0.0854, 0.1947
GOF	1.033	1.027
$\Delta\rho_{max}$, $\Delta\rho_{min}$ (e/Å^3)	0.876, -0.611	0.407, -0.189

The structural features of both the complexes are quite similar. The copper atom and the chlorine atom of ClO_4^- anion are on a crystallographic inversion center. The geometry of the cationic portion is linear L – Cu^I – L moiety with Cu1 – N1 = Cu1 – N1A = 1.89 Å in both **CuAPMPY** and **CuAPEPY**. The Cu – N bond length is quite similar to that previously reported for two-coordinate copper(I) complexes with nitrogen donor ligands.[7-9] Strong intermolecular N–H···O hydrogen bonds between the amino nitrogen atom and the imide oxygen atom of the neighboring molecule forming a two-dimensional network are observable in both the complexes (Figure 5.6 and Figure 5.7). Quite similar to the structures of their respective ligands, the plane of pyridyl ring is bent relative to the phthalimido ring. The dihedral angle between the planes defined by pyridyl and phthalimido ring is 61.8(16)° in **CuAPMPY** and 22.49(15)° in **CuAPEPY**. Interestingly, comparison with that observed for **APMPY** and **APEPY** indicate that the twisting of the pyridyl ring with respect to the phthalimide ring is significantly reduced upon coordination. The relatively large bending in **CuAPMPY** brings O2 and O2A in close contact with the copper ion (Cu1···O2 = Cu1···O2A = 3.03 Å and <O2···Cu1···O2A = 180°) reflecting a weak electronic interaction between Cu^I and one of the imide oxygen atom of the ligand unit. On the other hand, **CuAPEPY** experiences very weak interaction from the imide oxygen atom (Cu1···O2 = Cu1···O2A = 4.0 Å).

Upon careful inspection, a weak Cu^I···O interactions between Cu^I and oxygen atoms of the ClO_4^- anion was also observed (Cu1···O4 = Cu1···O4B = 3.116 Å in **CuAPMPY** and <O4···Cu1···O4B = 180°, by symmetry) that extends to form a zigzagged, weakly bound coordination polymer (Figure 5.8). Such Cu^I···O interaction is found to be much stronger in **CuAPEPY** (Cu1···O4 = 2.707 Å). Very interestingly, the interacting oxygen atom of the ClO_4^- anion in **CuAPEPY** is on a crystallographic inversion center. This leads to a T-shaped structure. The T-shaped molecular units are stacked over one another to form a linear network (Figure 5.9). Weak Cu···O interactions of about 3 Å are found in copper-containing enzymes.[13] Although such additional or multiple weak interactions[14] with an oxygen atom of the ClO_4^- anion are known for linear L – M – L complexes,[15] the resulting polymeric network structure illustrates the novelty of these complexes.

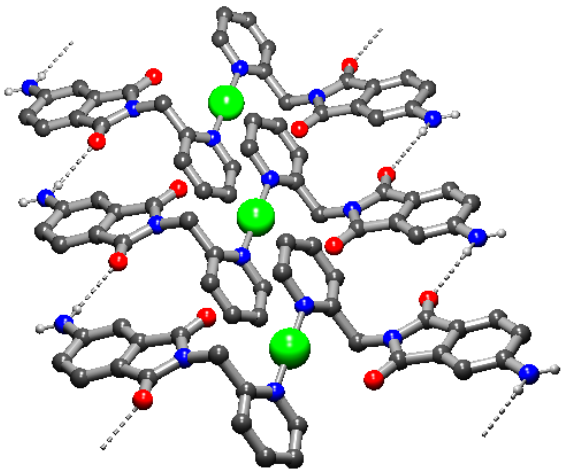

Figure 5.6 View of the 2-D network illustrating the intermolecular hydrogen bonding in **CuAPMPY**, shown as dashed lines: d(N3 – H3B⋯O1[x, y-1, z]) = 3.133 Å and ∠N3 – H3B⋯O1[x, y-1, z] = 159.96°. The anionic portion and the hydrogen atoms, except those that are involved in H-bonding, are omitted for clarity.

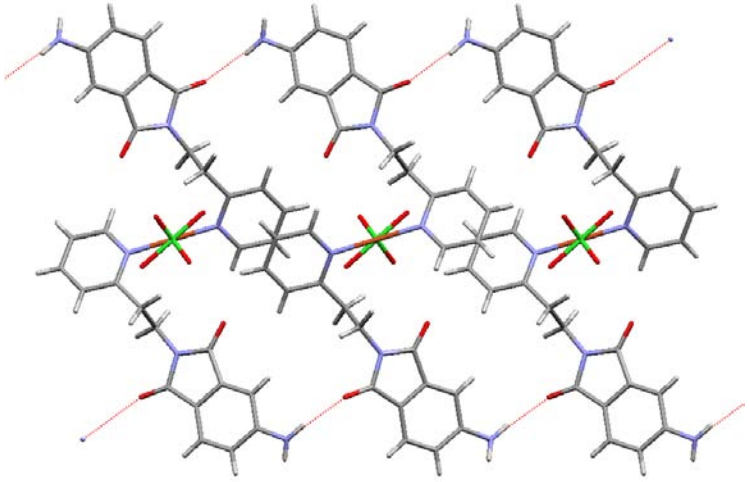

Figure 5.7 View of **CuAPEPY** along y-axis illustrating the intermolecular hydrogen bonding, shown as dashed lines, leading to a 2-D network: d(N3 – H3A⋯O1[x, -y+1, z+1/2]) = 2.965 Å and ∠N3 – H3A⋯O1[x, -y+1, z+1/2] = 172.75°.

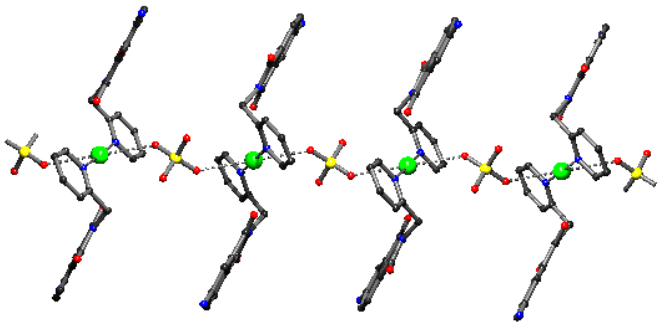

Figure 5.8 View of **CuAPMPY** along y-axis showing the close contact of copper with oxygen atoms of the ClO_4^- counteranion leading to a linear polymeric chain: Cu1····O4 = Cu1····O4B = 3.116(17) Å and ∠O4····Cu1····O4B = 180.0°, by symmetry.

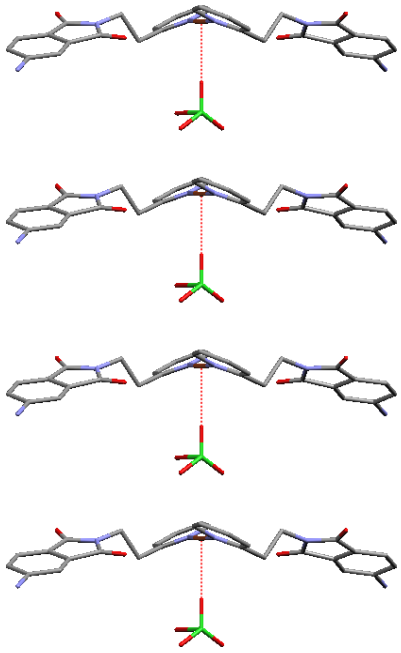

Figure 5.9 View of **CuAPEPY** along z-axis showing the close contact of copper with one of the oxygen atom of the ClO_4^- counter-anion forming a T-shaped molecule and leading to a linear network: Cu1····O4 = 2.707(8) Å, ∠O4····Cu1····N1 = ∠O4····Cu1····N1A = 91.58(12)°

5. 5. Stability and redox properties

Although the linear geometry is known to disfavor O_2 and CO interaction under certain conditions, the two-coordinate copper(I) complexes with sterically unhindered monodentate ligands undergo rapid auto-oxidation in air, especially in protic solvents.[7-9] However, both the complexes, **CuAPMPY** and **CuAPEPY** exhibit indefinite stability in the solid state. Oxidation of Cu^{+} to Cu^{2+} in polar or coordinating solvents such as acetonitrile or even in protic solvents such as methanol was not observed even if they are kept in an open air for several months. Thus, the stability of both the complexes toward oxidation is remarkable and quite interesting.

Cyclic voltammetry studies of the ligands **APMPY**, **APEPY** and their copper(I) complexes, **CuAPMPY** and **CuAPEPY** in acetonitrile reveal an irreversible oxidation with a very high current, which is associated with the oxidation of the **AP** moiety of the ligand framework (Figure 5.10).

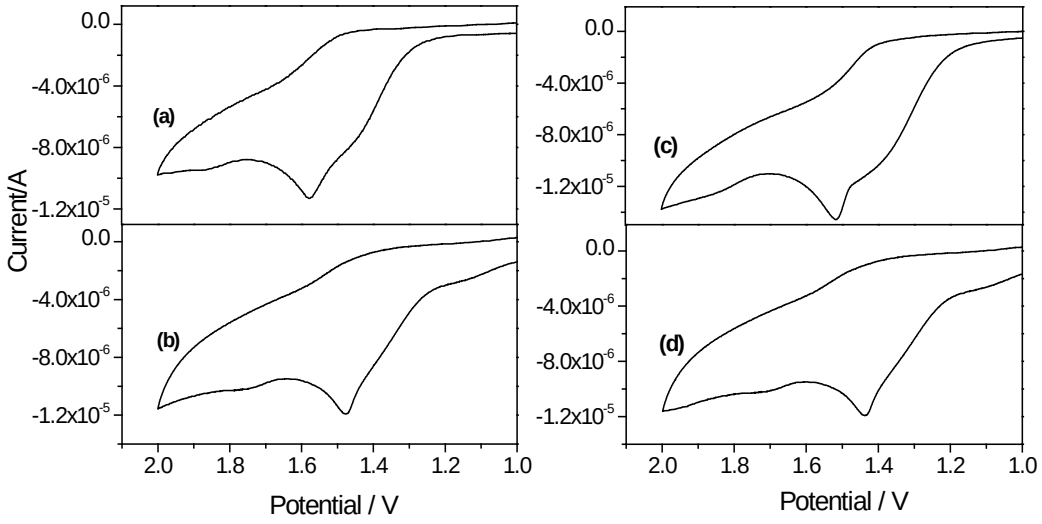

Figure 5.10 Cyclovoltammogram for **APMPY** (a), **CuAPMPY** (b), **APEPY** (c) and **CuAPEPY** (d) in acetonitrile with 0.1 M $[Bu_4N]ClO_4$ as supporting electrolyte (potential plotted against Fc/Fc^{+} couple).

The measured potentials range between 1.58 and 1.44 V (vs Fc/Fc^+ in CH_3CN/0.1 M $[Bu_4N]ClO_4$). No significant oxidation wave for the Cu(I)/Cu(II) couple was observed indicating significant stabilization of the monovalent oxidation state. The extraordinary stabilization to the Cu(I) state is provided by the weak interactions with the imide and perchlorate oxygen atoms which puts the Cu^+ ion in an octahedral hole. This is further supported by the fact that **CuAPEPY**, in which the metal center is more separated from the **AP** moieties, exhibits lesser stability than **CuAPMPY**. Copper(II) complexes have a tendency to form four-coordinate and in some cases five-coordinate complexes in solution, typically via coordination with a solvent molecule as the fifth ligand. Steric and/or electronic shielding by the **AP** moiety perhaps destabilizes the Cu(II) oxidation state. Therefore, this exceptional inertness is attributable to the highly favorable electronic factors provided by the 4-aminophthalimide and the perchlorate moieties.

5. 6. Conclusions

In conclusion, we have synthesized new fluorescent ligands **APMPY** and **APEPY** and their two-coordinate copper(I) complexes, **CuAPMPY** and **CuAPEPY**, having a linear geometry. The single crystal structures of all the four have been described. We have shown that stable two-coordinate linear complexes of copper(I) with monodentate ligands can be accessed easily if the ligand system and the counter-anion are chosen judiciously. These complexes are unusually inert towards oxidation even in a protic aerated medium. The copper(I) complex **CuAPEPY**, in which the metal center is more separated from the **AP** moiety, exhibits lesser stability than the copper(I) complex of **APMPY**, **CuAPMPY**. Thus, the electronic environment near the metal binding site is the key feature for the control of Cu^I-oxidation reactivity.

References

1 Brown, H. C. e. a. In *Determination of Organic Structures by Physical Methods*; Braude, E. A., Nachod, F. C., Eds.; Academic Press: New York, 1955.
2 Ramachandram, B. Ph.D. Thesis, University of Hyderabad, Hyderabad, India, 2000.
3 Sankaran, N. B. Ph.D. Thesis, University of Hyderabad, Hyderabad, India, 2003.
4 Holm, R. H.; Kennepohl, P.; Solomon, E. I. *Chem. Rev.* **1996**, *96*, 2239.
5 Kaim, W.; Rall, J. *Angew. Chem. Int. Ed. Engl.* **1996**, *35*, 43.
6 Sorell, T. N.; Malachowski, M. R. *Inorg. Chem.* **1983**, *22*, 1883.

7 Sorell, T. N.; Jameson, D. L. *J. Am. Chem. Soc.* **1983**, *105*, 6013.
8 Sanyal, I.; Karlin, K. D.; Strange, R. W.; Blackburn, N. J. *J. Am. Chem. Soc.* **1993**, *115*, 11259.
9 Le Clainche, L.; Giorgi, M.; Reinaud, O. *Eur. J. Inorg. Chem.* **2000**, 1931.
10 Liang, H.-C.; Kim, E.; Incarvito, C. D.; Rheingold, A. L.; Karlin, K. D. *Inorg. Chem.* **2002**, *41*, 2209.
11 Lu, J. Y.; Babb, A. M. *Inorg. Chem.* **2002**, *41*, 1339 and references therein.
12 Soujanya, T.; Fessenden, R. W.; Samanta, A. *J. Phys. Chem.* **1996**, *100*, 3507.
13 Kaim, W.; Schwederski, B. *Bioinorganic Chemistry*; Wiley: Chichester, U.K., 1994.
14 Albrecht, M.; Hubler, K.; Zalis, S.; Kaim, W. *Inorg. Chem.* **2000**, *39*, 4731.
15 Munukata, M.; Kitagawa, S.; Shimono, H.; Masuda, H. *Inorg. Chim. Acta* **1989**, *168*, 217.

Chapter 6

4-(Di-(2-picolyl)amino)-7-nitrobenzoxa[1,3]diazole

This chapter deals with the synthesis, photophysical properties and metal ion signaling behavior of the title compound. This simple molecular system, which is based on 4-amino-7-nitrobenzoxa[1,3]diazole chromophore, shows simultaneous blue shift and intensity loss of the absorption maximum as well as quenching of fluorescence ("On-Off"), selectively, in the presence of Cu^{2+} ions at physiological pH.

6. 1. Introduction

As stated previously, development of practical fluorescence "Off-On" sensors for transition metal ions such as Cu^{2+} still remains a challenge because of the inherent fluorescence quenching nature of the paramagnetic species. In most cases, to suppress the quenching interaction between these metal ions and the fluorophore, considerable synthetic effort had to be put in to obtain sensor systems, usually employing a structurally well-developed receptor unit in the fluoroionophore system.[1-3] Moreover, most of the fluorescent sensors, based on photo-induced electron transfer (PET) mechanism, employ tertiary amines as a receptor unit whose pH sensitivity is a major drawback for their applications under physiological conditions. As an alternative to fluorescent chemosensors, chromogenic or colorimetric sensors are emerging as an attractive approach for the recognition of hazardous trace metals and will have applications in environmental and biomedical fields.[4-6]

Usually, an electron donor-acceptor (EDA) system is employed which displays intense color because of the absorption due to the internal charge-transfer (ICT) transition. The modulation of the charge density near the donor or acceptor group would result into hypsochromic or bathochromic shift of the absorption maximum. Therefore, in our design for a chromogenic sensor, we have chosen a polarity sensitive 4-amino-7-nitrobenzoxa[1,3]diazole (**ANBD**) chromophore moiety, which has been integrated with

di-(2-picolyl)amine receptor to develop 4-(di-(2-picolyl)amino)-7-nitrobenzoxa[1,3]diazole (**NBDDPA**).

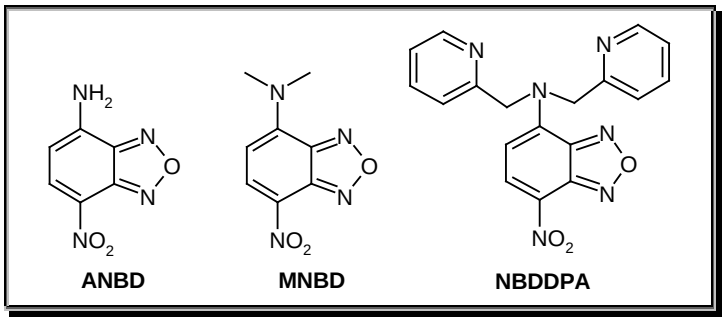

In the presence of Cu^{2+} ions, **NBDDPA** shows two-dimensional changes in the absorption spectra (blue shift of 42 nm and loss of absorption intensity in water) as well as quenching of fluorescence. This is a first example of a molecular sensor that shows such a large hypsochromic shift selectively in the presence of Cu^{2+} ions at physiological pH.

6. 2. Synthesis

NBDDPA was synthesized through a single step reaction of 4-chloro-7-nitrobenzoxa[1,3]diazole and di-(2-picolyl)amine (DPA) in ethylacetate according to the following procedure (Scheme 6.1).

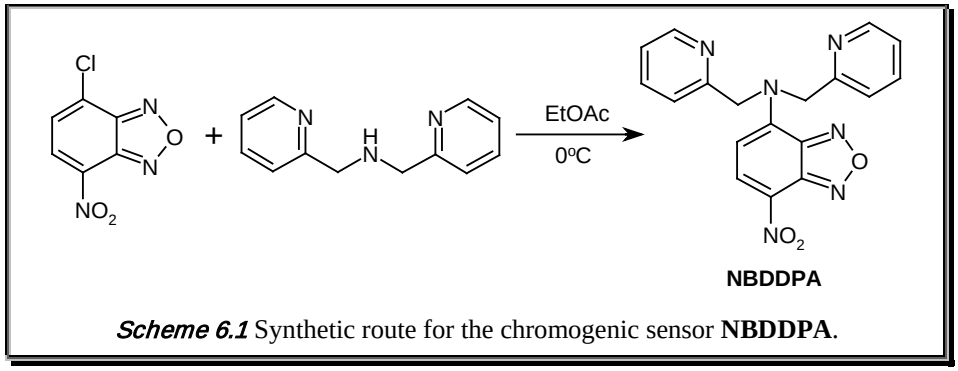

Scheme 6.1 Synthetic route for the chromogenic sensor **NBDDPA**.

4-(Di-(2-picolyl)amino)-7-nitrobenzoxa[1,3]diazole (NBDDPA). DPA (0.45 mL, 2.5 mmol) in ethylacetate (30 mL) were taken in a 100-mL two-necked round-bottomed flask and cooled to 0°C. 4-chloro-7-nitrobenzoxa[1,3]diazole (0.2 g, 1 mmol) dissolved in ethylacetate (20 mL) were added drop-wise. The reaction mixture was stirred for 1 h at 0°C. The reaction was further carried out at room temperature for another 2 h to ensure the completion. Subsequently, the solvent was evaporated under vacuum and the residue was purified by column chromatography (neutral alumina, hexane/ethylacetate). Yield 82%. The desired product was characterized by the following analytical results.

CHN analysis calculated for $C_{18}H_{14}N_6O_3$: C, 59.67; H, 3.87; N, 23.20. Found: C, 59.39; H, 3.61; N, 22.92.

^{1}H NMR ($CDCl_3$, 400MHz): δ 5.42 (bs, 4H), 6.33 (d, 1H), 7.23 (m, 4H), 7.67 (m, 2H), 8.37 (d, 1H), 8.56 (s, 2H).

6. 3. Spectral features

6. 3. 1. Absorption and fluorescence behavior

The electronic absorption and fluorescence spectra of **NBDDPA** are characterized by intense band ($\varepsilon = 3.5 \times 10^4$ $mol^{-1}Lcm^{-1}$), which can be assigned to the internal charge-transfer (ICT) transition because of the push-pull effect of the electron-donating amine and the electron-withdrawing nitro group of the fluorophore moiety (Figure 6.1). The absorption and fluorescence spectral data are listed in Table 6.1.

Table 6.1 Absorption and fluorescence properties of **ANBD**, **MNBD** and **NBDDPA** in tetrahydrofuran (THF) and water.

	THF			Water		
Compound	λ_{max}^{abs} /nm	λ_{max}^{flu} /nm	Φ_f	λ_{max}^{abs} /nm	λ_{max}^{flu} /nm	Φ_f
ANBD[a]	445	517	0.79	-	-	-
MNBD[a]	468	527	0.14	497	558	0.01
NBDDPA	468	537	0.74	483	551	0.05

[a] These data have been collected from ref. 7.

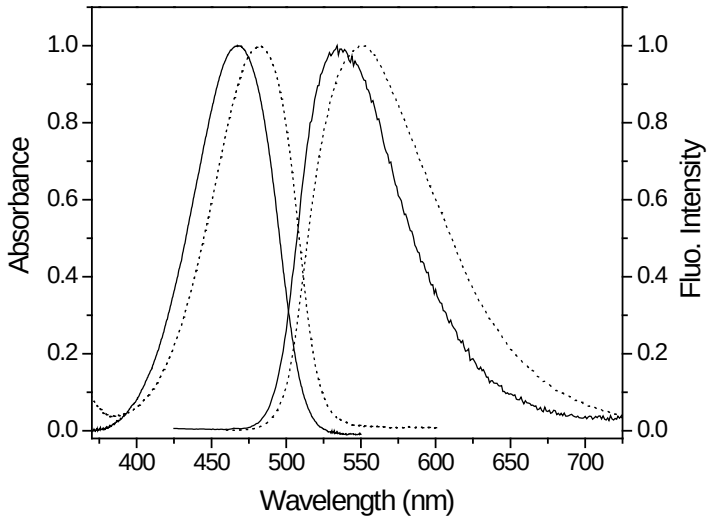

Figure 6.1 Absorption and fluorescence spectra of **NBDDPA** in THF (——) and water (····). All spectra were normalized at their respective peak position.

The location of the ICT band maxima is highly sensitive to the polarity of the media. Both the absorption and fluorescence maxima are Stokes-shifted with increase in the polarity of the medium. This behavior is consistent with that observed in **ANBD** and its derivatives.[7] This system exhibits high fluorescence quantum yield, which is significantly higher in THF compared to that in water. This is most likely due to the specific hydrogen bonding interactions in protic solvents.

6. 3. 2. pH sensitivity

The spectral properties of **NBDDPA** are dependent on pH between pH 1 and pH 5. Figure 6.2 shows the changes in the absorption spectra upon titration of an alkaline solution of **NBDDPA** (pH 13.5) with diluted HCl solution. The spectrum remains unaffected above pH 5. From pH 5 to pH 3, a gradual decrease in the intensity with a blue shift (17 nm) and an isosbestic point at 460 nm was observed, corresponding to the protonation of the pyridyl moiety. Upon lowering of pH the spectrum is further blue-shifted (22 nm) with a new isosbestic point at 445 nm.

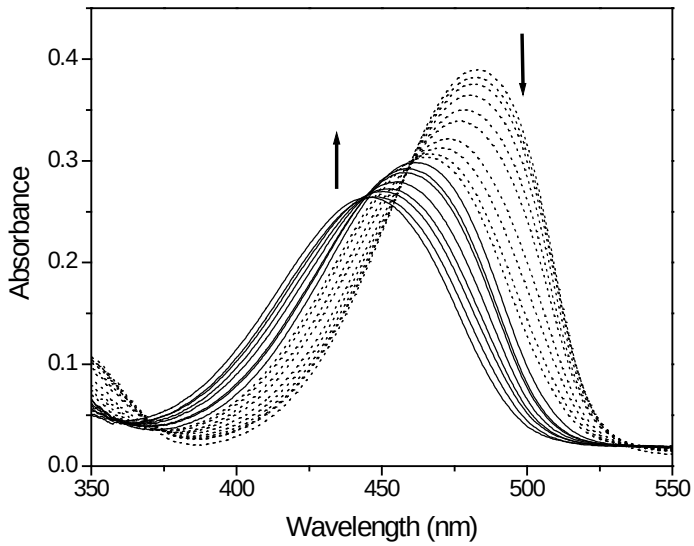

Figure 6.2 Changes in the absorption spectra of an alkaline solution of **NBDDPA** upon pH titration with HCl acid; from pH 13.5 to pH 5.0 (no change); from pH 5.0 to pH 3.0 (dotted line); from pH 3.0 to pH 1.2 (solid line).

Interestingly, the absorption spectra of both **ANBD** and **MNBD** are independent of pH indicating that the amino nitrogen atom in these chromophores has no affinity for protons. This is not surprising because of strong electron withdrawing nitro group in conjugation. Thus, the observed blue shift and the intensity loss of the absorption maximum of **NBDDPA** in the presence of protons is attributed primarily to the redistribution of electron density due to the interaction between the protonated pyridyl moieties and the nitrogen atom connected to the chromophore.

By plotting the absorption changes at 445 nm and 460 nm as a function of pH, sigmoidal curves were obtained where the major changes occurred over two pH windows (Figure 6.3). These changes were fully reversible, as the addition of strong base to this acidic solution reversed these effects. From these changes, pK_a values of 3.6 and 2.7 for the protonation of pyridyl moieties were evaluated. The lower pK_a values than those reported for pyridine (4.38 in 50% ethanol)[8] are due to the electron-withdrawing tendency of the chromophore unit, which lessens the electron density at the pyridyl

nitrogen atom thereby reducing its affinity for protonation. No changes in the absorption spectrum of **NBDDPA** above pH 5 clearly demonstrate the utility of the sensor system in the physiological environment where pH > 5.

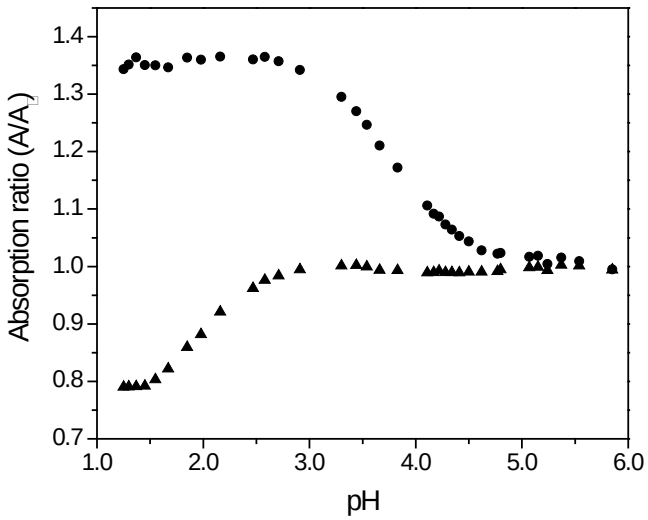

Figure 6.3 Changes in the UV-vis spectra of an alkaline solution of **NBDDPA** at 445 nm (●) and 460 nm (▲) upon titration with diluted HCl acid.

6. 3. 3. Metal ion signaling behavior

The effect of metal ions on the absorption spectrum of **NBDDPA** was examined in an aqueous solution of 10 mM HEPES buffer (pH 7.4). In the presence of alkali and alkaline earth metal ions such as Na^+, K^+, Mg^{2+} and Ca^{2+}, **NBDDPA** does not show any obvious spectral change. This is not unexpected considering the available binding sites for complexation. Among transition metal ions, Cu^{2+} induces a drastic change in the UV-vis spectrum. As can be seen in Figure 6.4, upon progressive addition of Cu^{2+}, the absorption gradually loses in intensity with a blue shift from 483 nm to 441 nm. The observation of an isosbestic point at 450 nm indicates that this optical response arises from the presence of two species in equilibrium, **NBDDPA** and **NBDDPA-Cu^{2+}**.

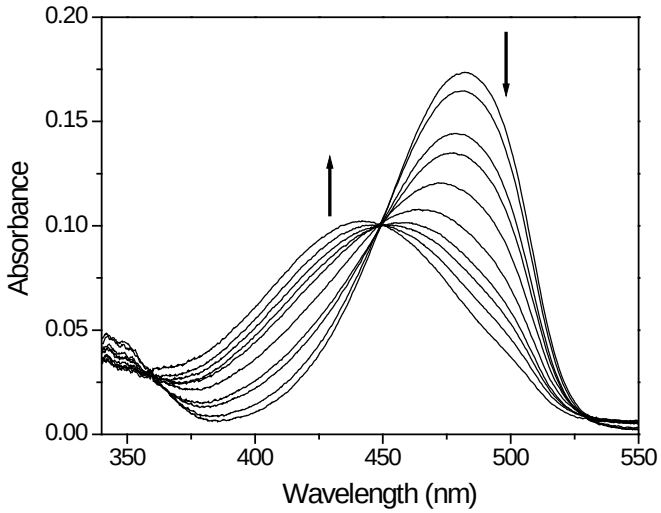

Figure 6.4 Absorption spectra of **NBDDPA** (5×10^{-6} M) in water (pH 7.4, 10 mM HEPES) after the addition of 0, 0.05, 0.2, 0.25, 0.5, 0.75, 1, 1.25, 1.5, 2 mM Cu^{2+} ions.

It is expected that the electron density at the 4-N atom to be reduced by the electron-withdrawing effect of coordinated metal ions thereby decreasing the charge separation in the electron donor-acceptor chromophore and that remarkable changes in the absorption spectra should be caused when complexed to a metal ion. As stated earlier, due to the unavailability of lone-pair of electrons for complexation, the 4-amino nitrogen atom could not be involved in coordination with the metal ions. Therefore, the binding sites for complexation with the metal ions are only the nitrogen atoms of the pyridyl moieties. However, as commonly believed, if only the pyridyl nitrogen atoms were involved in coordination with the Cu^{2+} ions, the energy states of the chromophore are not expected to be much affected as the pyridyl moieties are connected to the chromophore by a non-conjugating spacer and there is no evidence of through-bond transfer of charge. Of course, a small hypsochromic shift due to the electrostatic interaction between the metal ion and the nitrogen atom associated with the chromophore moiety is known.[9] This suggests that upon complexation the electron density of the system is considerably redistributed giving rise to such a large blue shift, nevertheless, steric crowding upon coordination with the Cu^{2+} ions could also possibly cause the twisting of the 4-N-

aromatic C bond leading to the blue shift. Thus, we show that while direct coordination of the metal ions with the nitrogen atom involved in the ICT process leads to the disappearance of the ICT band,[10] non-bonded interaction as in the present case results into the recognition of the guest by an hypsochromic shift of the absorption maximum.[9]

The effect of metal ions on the fluorescence spectrum of **NBDDPA** was also examined in an aqueous solution of 10 mM HEPES buffer (pH 7.4). The fluorescence spectrum of **NBDDPA** in buffered water (pH = 7.4) is centered at 551 nm. Addition of Cu^{2+} ions leads to a loss of fluorescence intensity with a very small hypsochromic shift (Figure 6.5). Quenching of fluorescence is attributed to the electron or energy transfer between Cu^{2+} and the excited fluorophore.

Addition of transition metal ions other than Cu^{2+}, such as Ni^{2+} and Zn^{2+} does not result into any significant change in either absorption or fluorescence spectrum of **NBDDPA**. Figure 6.6 highlights the selectivity and sensitivity of the present sensor system. At very high concentration of these metal ions, however, a gradual reduction in the intensity of the absorption maximum of **NBDDPA** with a small hypsochromic shift (8-12 nm) is observed (Figure 6.7). Thus, **NBDDPA** has poor affinity for metal ions other than Cu^{2+}. Binding constant for Cu^{2+} is determined[11] as Log β = 3.5 suggesting that the interaction of Cu^{2+} itself is not very strong. This is not surprising because the effect of removing the interaction with the 4-amino donor will reduce the binding constant significantly. Hence, metal ions such as Ni^{2+} and Zn^{2+}, placed below Cu^{2+} in the Irving-Williams series, are expected to have negligible interaction. Comparatively, a very large blue shift of 42 nm only in the presence of Cu^{2+} ions makes the present system essentially selective for Cu^{2+} ions.

Thus, while selective detection of Cu^{2+} ions based solely on the change in the absorbance parameter (A/A_o) could be masked by increased concentrations of the weaker binding metal ions, an additional dimensional change with a shift parameter ($\Delta\lambda$) allows discrimination of Cu^{2+} ions from rest of the transition metal ions. A three-dimensional plot shown in Figure 6.8 represents the two-dimensional operation of **NBDDPA**. More interestingly, the linearity in the absorption maximum of **NBDDPA** vs Cu^{2+} concentration profile (Figure 6.6) over a certain range of concentration makes the present system appropriate for the analytical detection of Cu^{2+} in solution.

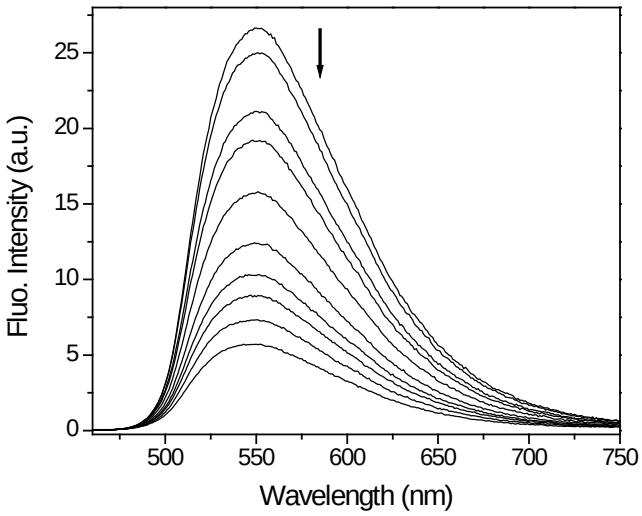

Figure 6.5 Fluorescence spectra of **NBDDPA** (5×10^{-6} M) in water (pH 7.4, 10 mM HEPES) after the addition of 0, 0.05, 0.2, 0.25, 0.5, 0.75, 1, 1.25, 1.5, 2 mM Cu^{2+} ions. $\lambda_{exc.}$ = 450 nm.

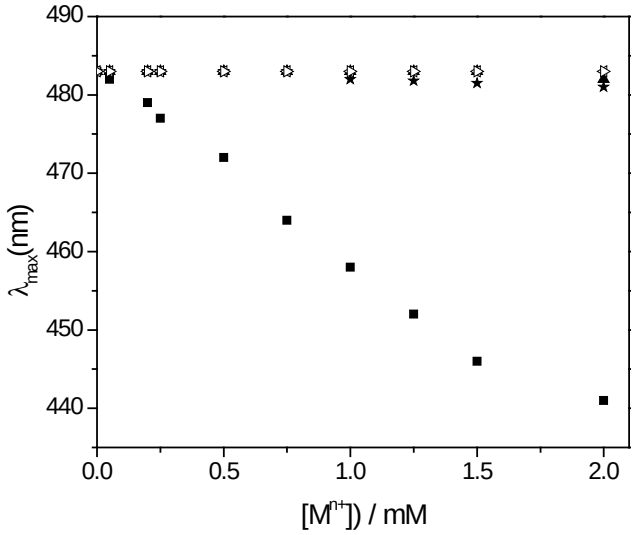

Figure 6.6 Hypsochromic shift of the ICT absorption maximum of **NBDDPA** (5×10^{-6} M) induced by various metal cations; (■) Cu^{2+}, (◖) Ni^{2+}, (▲) Zn^{2+}, (◁) Na^{+}, (▷) Mg^{2+}.

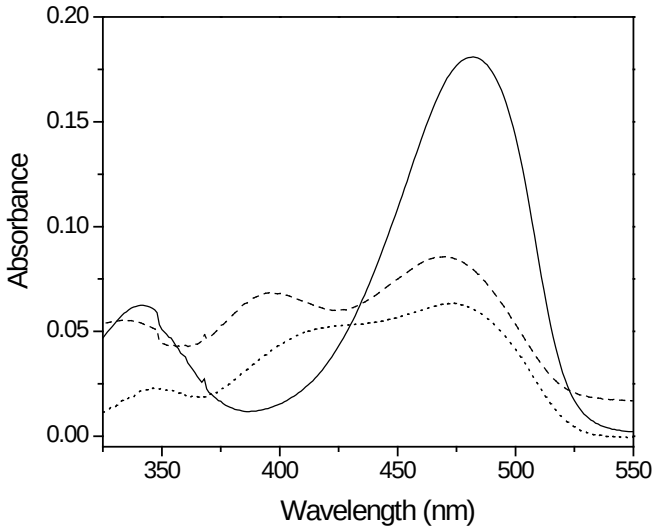

Figure 6.7 Absorption spectra of **NBDDPA** (5×10^{-6} M) in water (pH 7.4, 10 mM HEPES) in the presence of metal cations. (—) Mg^{2+}, Ca^{2+} in excess, (····) Zn^{2+} (2×10^{-2} M) and (----) Ni^{2+} (1×10^{-2} M).

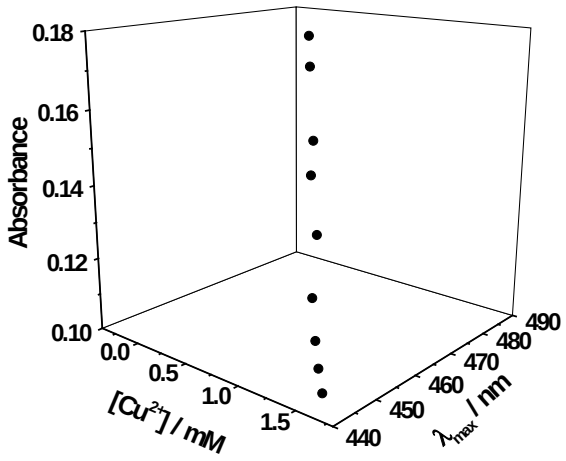

Figure 6.8 A three-dimensional plot representing the two-dimensional operation of **NBDDPA**.

6. 3. 4. Sensor or dosimeter?

Systems in which the recognition events are not reversible are termed as chemodosimeter[12] rather than chemosensor. A dosimeter is thus an irreversible device, which progressively accumulates the dose, each time adding up the signal, and which after extended use, has to be discarded. This limits the practical application of the device.

The recognition of Cu^{2+} ions by **NBDDPA** is found to be reversible as the addition of EDTA reversed the absorption spectra (Figure 6.9). Thus, **NBDDPA** can be termed as a molecular *sensor*, a feature that requires reversibility and potential re-utilization. A similar system with a cyclam receptor at 4-position, for the detection of Cu^{2+}, that acts as a molecular *dosimeter* was reported recently.[13]

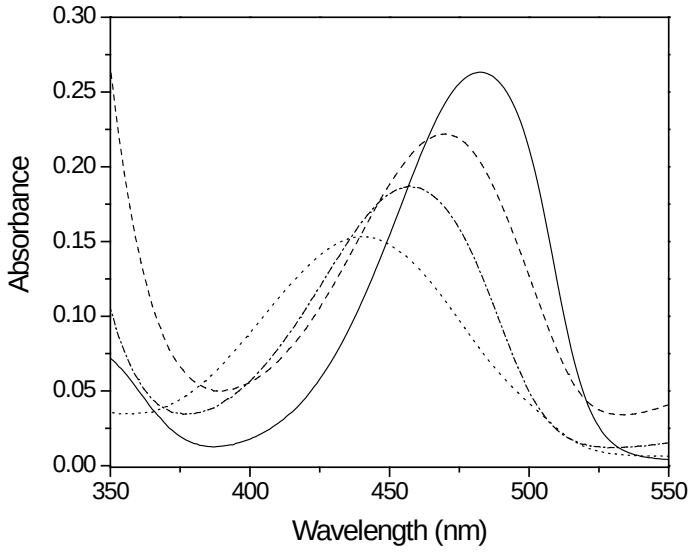

Figure 6.9 Absorption spectra of **NBDDPA** before and after the addition of Cu^{2+} ions and reversed changes upon addition of EDTA. (——) **NBDDPA** (5×10^{-6} M), (····) **NBDDPA** + Cu^{2+} (2×10^{-3} M), (– · – ·) **NBDDPA** + Cu^{2+} + EDTA (2×10^{-3} M) and (– – –) **NBDDPA** + Cu^{2+} + EDTA (excess).

6. 4. Theoretical calculations

The rational explanation for the observed blue shift of the absorption maximum of **NBDDPA** in the presence of protons or Cu^{2+} ions may be obtained from molecular modeling and semi-emperical calculations. Semi-emperical (PM3) calculations of **NBDDPA** in the free, singly and doubly protonated forms gave results that indicate that upon protonation of the pyridyl moieties, the ICT character of the system gets significantly altered (Table 6.1). The results also explain the lower than usual pK_a values obtained for the protonation of the pyridyl moieties.

Table 6.1 PM3 calculated geometrical parameters for **NBDDPA**, **NBDDPA–H$^+$**, **NBDDPA–2H$^+$**.[a]

Geometrical parameters	**NBDDPA**	**NBDDPA–H$^+$**	**NBDDPA–2H$^+$**
4-N–C (Å)	1.395	1.452	1.455
Angles around 4-N (º)	123.44	117.06	114.53
	118.88	115.18	120.30
	115.19	114.19	115.04
Formal charge on 4-N	+0.148	-0.007	-0.008
Formal charge on pyridyl N atoms	-0.094	+0.57	+0.54
	-0.069	-0.104	+0.55
Formal charge on nitro O atoms	-0.632	-0.568	-0.547
	-0.582	-0.555	-0.531

[a] Molecular geometry was optimized by PM3 method using commercially available HyperChem software.

6. 5. Conclusions

The necessity of detecting hazardous trace metal ions in environmental and biological systems lead us to develop a simple chromogenic sensor **NBDDPA** for selective detection of Cu^{2+} ions under physiological conditions (pH > 5). This system also behaves as a fluorescence inverter. The exclusive two-parameter optical signaling based on (i) a linear 483 nm-to-441 nm blue shift and (ii) the loss of absorbance intensity allows quantitative as well as qualitative discrimination of Cu^{2+} ions from rest of the transition metal ions.

References

1 Ghosh, P.; Bharadwaj, P. K.; Roy, J.; Ghosh, S. *J. Am. Chem. Soc.* **1997**, *119*, 11903.
2 Rurack, K.; Kollmannsberger, M.; Resch-Genger, U.; Daub, J. *J. Am. Chem. Soc.* **2000**, *122*, 968.
3 Talanova, G. G.; Elkarim, N. S. A.; Talanov, V. S.; Bartsch, R. A. *Anal. Chem.* **1999**, *71*, 3106.
4 Gostkowski, M. L.; McDoniel, J. B.; Wei, J.; Curey, T. E.; Shear, J. B. *J. Am. Chem. Soc.* **1998**, *120*, 18.
5 Fodor, S. P. A.; Rava, R. P.; Huang, X. C.; Pease, A. C.; Holmes, C. P.; Adams, C. L. *Nature* **1993**, *364*, 555.
6 Malmqvist, M. *Nature* **1993**, *361*, 186.
7 Saha, S.; Samanta, A. *J. Phys. Chem. A* **1998**, *102*, 7903.
8 Brown, H. C. e. a. In *Determination of Organic Structures by Physical Methods*; Braude, E. A., Nachod, F. C., Eds.; Academic Press: New York, 1955.
9 Sakamoto, H.; Ishikawa, J.; Nakao, S.; Wada, H. *Chem. Commun.* **2000**, 2395.
10 Gunnlaugsson, T.; Leonard, J. P.; Murray, N. S. *Org. Lett.* **2004**, *6*, 1557.
11 Connors, K. A. *Binding Constants*; Wiley: New York, 1987.
12 Chae, M.-Y.; Czarnik, A. W. *J. Am. Chem. Soc.* **1992**, *114*, 9704.
13 Boiocchi, M.; Fabbrizzi, L.; Licchelli, M.; Sacchi, D.; Vasquez, M.; Zampa, C. *Chem. Commun.* **2003**, 1812.

Chapter 7

N-Anthracen-9-ylmethyl-N-7-nitrobenzoxa[1,3]diazol-4-yl-N´,N´-dimethylethylenediamine

This chapter describes the synthesis, photophysical properties and transition metal ion signaling behavior of the title compound. This dual-fluorophore system consisting of anthracene and 4-amino-7-nitrobenzoxa[1,3]diazole chromophores, allows ratiometric fluorescence detection of the transition metal ions. In the presence of metal ions, the fluorescence due to the anthracene moiety is enhanced, while the fluorescence due to the 4-amino-7-nitrobenzoxa[1,3]diazole moiety is quenched. These changes have been attributed to the guest-induced suppression of the energy transfer process between the two fluorophore moieties and inhibition of the photoinduced electron transfer communication between the terminal nitrogen atom and the anthracene moiety of the multi-component system.

7. 1. Introduction

Although intensity-based fluorescence signaling is simple and accurate in the laboratory, this can be inadequate in real-world situations. As stated previously, a major disadvantage of intensity-based sensing is the problem of referencing the intensity measurements. The efficiency of light transmission and collection can vary from one instrument to another, and a constant intensity reference is often unavailable. The fluorescence intensity can also vary due to light scattering and/or absorption characteristics of the sample. Moreover, most fluorophores photobleach rapidly, which further complicates the ability to quantitatively use the intensity measurements. These effects require frequent recalibration and other corrections. In fact, in the case of fluorescence microscopy, it is often impossible to know the probe concentration at each point in the image because the intensity changes continually due to photobleaching, phototransformation etc.[1,2]

In principle, these problems can be avoided using wavelength-ratiometric probes, fluorophores that display changes in the location of their emission maximum on binding or interaction with the analytes.[3-5] Fluorescent sensors that display changes in the monomer-excimer emission intensity ratio, in the presence of guest, are also frequently encountered for signaling various metal ions.[6-12] However, quantitative detection may become difficult considering the dependence of excimer emission on the initial probe concentration.

Most of the multi-component fluorescent sensor systems are based on simple *fluorophore-spacer-receptor* format. Interaction of the guest at the receptor site is signaled by the changes in the fluorescence properties of the system primarily due to the disruption of the communication between the two terminal moieties. As stated earlier, PET is the most commonly employed mode of communication between the receptor and the fluorophore moieties in such design format. Systems based on *fluorophore$_1$-spacer-fluorophore$_2$* format with properly chosen components may show resonance energy transfer (RET) from the donor fluorophore to the acceptor fluorophore.[13] It would be profitable to combine these two design principles within a single sensor system. Conceptually, this would lead to a *fluorophore$_1$-spacer$_1$-fluorophore$_2$-spacer$_2$-receptor* format. Importantly, systems with this design format can give rise to photochemical molecular devices displaying two distinct emitting states and thus can lead to fluorescent ratiometric probes. Therefore, we have designed a multi-component system, **AMNEA**, with a *fluorophore$_1$-spacer$_1$-fluorophore$_2$-spacer$_2$-receptor* architecture. This system comprising two different fluorophore moieties is targeted as an alternative to the simple intensity-based systems for signaling transition metal ions, in particular. As a starting case, we have chosen a simple amine as a receptor component. Anthracene and 4-amino-7-nitrobenzoxa[1,3]diazole (**ANBD**) are chosen as the fluorophore components because of their distinct absorption and emission features. Moreover, fluorophores based on **ANBD** absorb at the wavelength region where fluorophores based on anthracene emits. This feature is essential for RET between these fluorophore moieties.

PET between the terminal nitrogen atom and the anthracene chromophore (PET between the terminal nitrogen atom and the **ANBD** moiety is found to be not very efficient) and at the same time, energy transfer between the anthracene and **ANBD**

fluorophore moieties give rise to dual emission with large intensity ratio. In the presence of the transition metal ions, the fluorescence due to the anthracene moiety is enhanced, while the fluorescence due to the **ANBD** moiety is quenched.

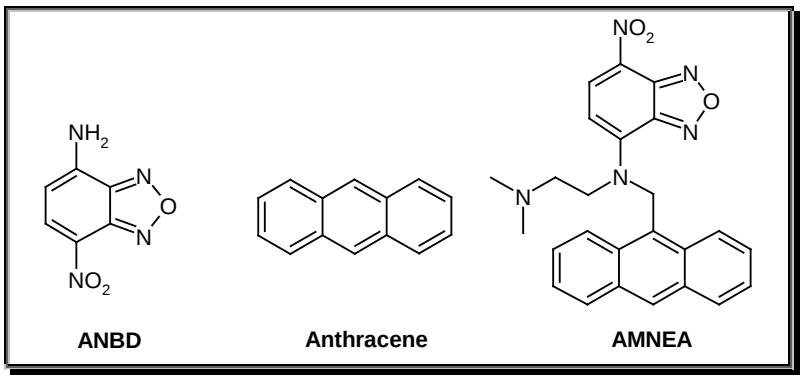

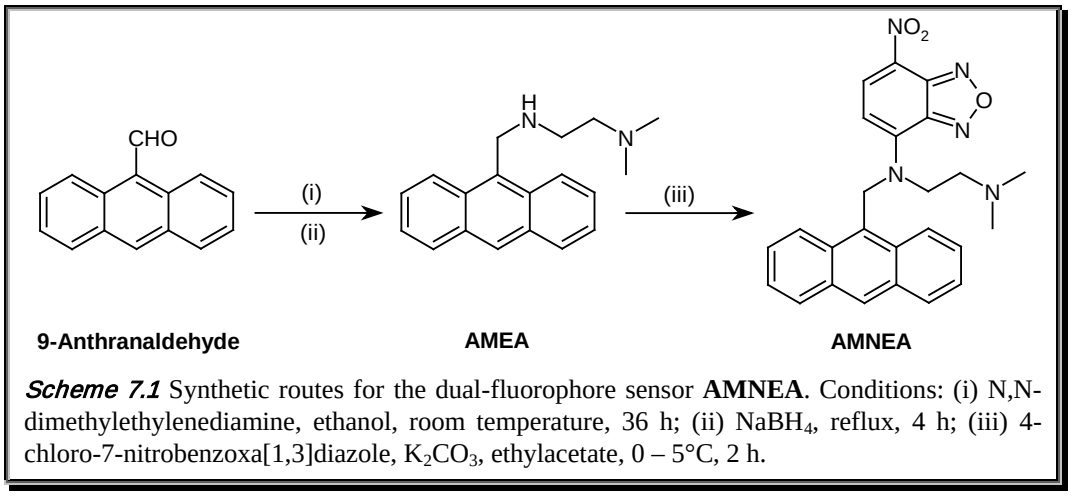

Scheme 7.1 Synthetic routes for the dual-fluorophore sensor **AMNEA**. Conditions: (i) N,N-dimethylethylenediamine, ethanol, room temperature, 36 h; (ii) $NaBH_4$, reflux, 4 h; (iii) 4-chloro-7-nitrobenzoxa[1,3]diazole, K_2CO_3, ethylacetate, 0 – 5°C, 2 h.

7. 2. Synthesis

AMNEA was prepared by following a two-step synthetic procedure (Scheme 7.1). The first step consisted of in-situ preparation of N,N-dimethyl-N´-anthracen-9-ylmethylethylenediamine (**AMEA**) by simultaneous condensation of 9-anthranaldehyde with N,N-dimethylethylenediamine and reduction of the Schiff base formed with sodium

borohydride. **AMEA** was then reacted with 4-chloro-7-nitrobenzoxa[1,3]diazole to obtain the desired dual-fluorophore system, **AMNEA**.

Step 1: N,N-dimethyl-N'-anthracen-9-ylmethylethylenediamine (AMEA). 9-anthranaldehyde (1 g, 5 mmol) and N,N-dimethylethylenediamine (0.6 mL, 5.5 mmol) were taken in ethanol (50 mL) and the reaction mixture was stirred for 36 h at room temperature. The Schiff base formed was not isolated but immediately treated with an excess of solid $NaBH_4$ and the mixture was heated to reflux for 4 h. The pale yellow solid remained after complete removal of the solvent under reduced pressure was shaken with water (100 mL) and the desired product was extracted with $CHCl_3$ (3 × 50 mL). The organic layer, after drying over anhydrous Na_2SO_4, was filtered and completely evaporated to obtain **AMEA** as a brown semisolid. Yield 92%. The product was characterized by the following analytical results.

CHN analysis calculated for $C_{19}H_{22}N_2$: C, 82.01; H, 7.91; N, 10.07. Found: C, 81.73; H, 8.07; N 9.91.

^{1}H NMR ($CDCl_3$, 400 MHz): δ (ppm) 2.17 (s, 6H), 2.47 (t, 2H), 2.93 (t, 2H), 4.73 (s, 2H), 5.23 (s, 1H), 7.44(t, 2H), 7.52 (t, 2H), 7.88 (d, 2H), 8.3 (m, 3H).

Step 2: N-Anthracen-9-ylmethyl-N-7-nitrobenzoxa[1,3]diazol-4-yl-N´,N´-dimethylethylenediamine (AMNEA). **AMEA** (0.1 g, 0.36 mmol) and K_2CO_3 (0.55 g, 0.4 mmol) were taken in ethylacetate (25 mL) and the mixture was stirred for 30 min. The solution was then cooled to 0°C and subsequently a solution of 4-chloro-7-nitrobenzoxa[1,3]diazole (0.07 g, 0.35 mmol) dissolved in ethylacetate (20 mL) was added drop-wise with continued stirring for 2 h maintaining the temperature at 0 – 5°C. The reaction mixture was then brought to room temperature and stirred for another 2 h to ensure the completion of the reaction. Subsequently, the solvent was evaporated under vacuum and the residue was purified by column chromatography (neutral alumina, hexane/ethylacetate). Yield 70%. The desired product isolated as an orange colored solid was characterized by the following analytical results.

CHN analysis calculated for $C_{25}H_{23}N_5O_3$: C, 68.03; H, 5.22; N, 15.87. Found: C, 67.72; H, 4.97; N, 16.05.

^{1}H NMR ($CDCl_3$, 400MHz): δ (ppm) 2.03 (s, 6H), 2.55 (t, 2H), 3.33 (t, 2H), 4.45 (s, 2H), 7.12(m, 3H), 7.79-7.81 (m, 6H), 8.24 (d, 1H), 8.56 (d, 1H).

7. 3. Spectral features

7. 3. 1. Electronic absorption

The absorption behavior of **AMNEA** has been studied in tetrahydrofuran (THF) and acetonitrile (AN). The absorption spectrum of the system is characterized by structureless broad band between 400 – 525 nm and a structured progression between 310 – 400 nm. The former is assigned to the intramolecular charge transfer (ICT) transition, which is typical of the 4-amino-7-nitrobenzoxa[1,3]diazole (**ANBD**) fluorophore.[14] The structured absorption is characteristic of the anthracene chromophore. The absorption peaks due to the anthracene and **ANBD** moieties of the multi-component system are well separated. Representative absorption spectra of **AMNEA** and the parent fluorophores, anthracene and **ANBD**, are shown in Figure 7.1, and the spectral data are listed in Table 7.1. While the structured band is found to be insensitive to the solvent polarity, the long wavelength band maximum exhibits Stokes shift with increase in the polarity of the medium. This also confirms the charge-transfer nature of the absorption in the long wavelength region and the observed behavior is consistent with that observed in other **ANBD** derivatives.[14]

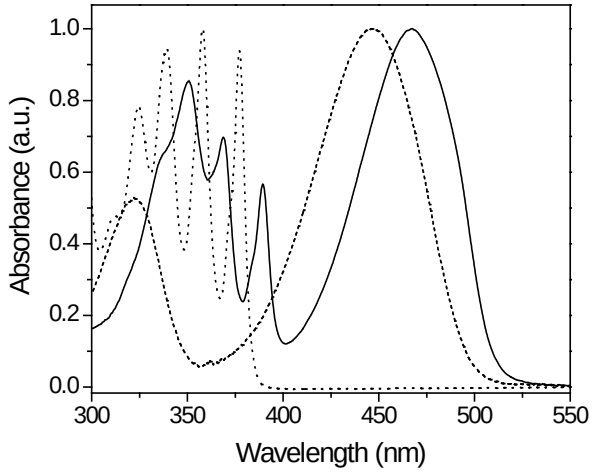

Figure 7.1 Absorption spectra (normalized) of **AMNEA** (——), **ANBD** (----) and **Anthracene** (····) in THF.

Table 7.1 Absorption and fluorescence properties of **AMNEA, ANBD,** and **anthracene** in tetrahydrofuran (THF) and acetonitrile (AN).

	THF			AN		
Compound	λ (abs.)/nm	λ (flu.)/nm	Φ_f	λ (abs.)/nm	λ (flu.)/nm	Φ_f
AMNEA	351,369,389	397,420,444	0.0023[a]	350,366,386	393,416,440	0.0019[a]
	468	528	0.46[b]	473	548	0.35[b]
ANBD[c]	445	527	0.79	445	531	0.57
Anthracene	339,358,377	382,403,427	0.297[d]	338,357,376	378,399,423	0.29

[a] Measured for the short wavelength anthracene-like emission; $\lambda_{exc.}$ = 350 nm. [b] Measured for the long wavelength **ANBD**-like emission; $\lambda_{exc.}$ = 440 nm. [c] From ref. 13. [d] From ref. 14.

7. 3. 2. Fluorescence

7. 3. 2. 1. Steady-state behavior

The fluorescence behavior of **AMNEA** has also been studied in THF and AN. Similar to what has been observed in absorption, the fluorescence spectrum of **AMNEA** is characterized by high energy structured progression and a low energy broad band. The well-separated absorption of **AMNEA** allows selective excitation of each fluorophore. When the low energy **ANBD** fluorophore moiety is excited, only the long wavelength emission has been observed. Even when the system is excited at 350 nm, where the absorption is predominantly due to the anthracene moiety (*vide* Figure 7.1), the fluorescence spectrum consists of mostly the long wavelength band due to the **ANBD** moiety. The observation clearly suggests very efficient RET from anthracene to **ANBD** moiety. Representative spectra are shown in Figure 7.2 and the spectral data are listed in Table 7.1. The structured band typical of the anthracene chromophore emits between 380 – 460 nm in THF, while the polarity sensitive ICT band associated with the **ANBD** moiety is centered at 528 nm in THF and 548 nm in AN. Thus, the spectral feature of this system can be understood in terms of the spectral features of the constituting chromophores.

The fluorescence quantum yield of the emission due to the **ANBD** moiety is measured to be 0.46 in THF, which is slightly lower than that of the parent fluorophore devoid of any other components (Φ_f, **ANBD** = 0.79 in THF).[14] This suggests that the possible PET between the receptor and the **ANBD** moieties of the system is not very efficient. On the other hand, the fluorescence quantum yield of the short-wavelength emission is measured to be only 0.0023 in THF. The lower quantum yield as compared to the bare fluorophore (Φ_f, anthracene = 0.297 in THF)[15] could be attributed to the combined effect of PET between the receptor and the anthracene moieties and RET from the anthracene moiety to the **ANBD** moiety of the system. For RET to occur from an initially excited donor (anthracene moiety) to an acceptor (**ANBD** moiety), the acceptor must absorb light at the donor emission wavelengths. This condition is fulfilled in **AMNEA**. The other factors such as the relative orientation of the donor and the acceptor transition dipoles and the distance between the donor and the acceptor molecules that determine the rate and efficiency of the energy transfer processes also must be favorable in the present system.

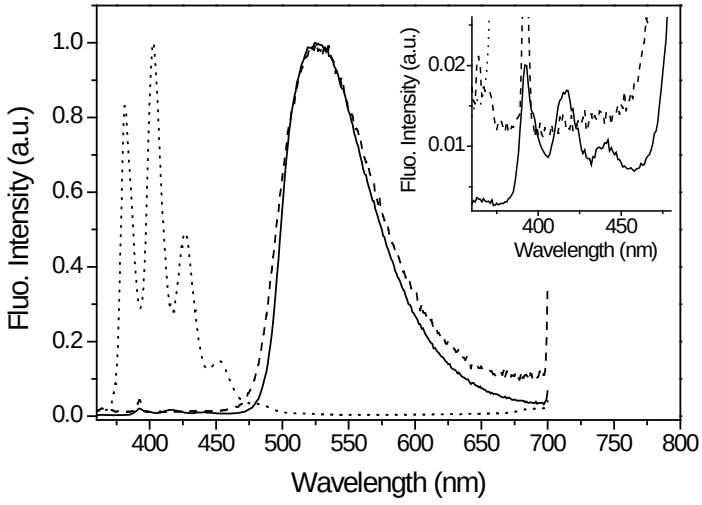

Figure 7.2 Fluorescence spectra of **AMNEA** (——), **ANBD** (----) and **anthracene** (····) in THF, normalized at their respective peak positions. Inset: spectra depicting the short wavelength structured emission of **AMNEA** in an expanded scale. $\lambda_{exc.}$ = 350 nm.

7. 3. 2. 2. Time-resolved behavior

The fluorescence decay behavior of **AMNEA** has been studied in THF monitoring the individual emission bands. The decay curves of **AMNEA** in THF at short and long wavelength region with the excitation wavelength set at 374 nm are shown in Figure 7.3. The time-profile of the fluorescence of **AMNEA**, when monitored at the short wavelength region where only the anthracene moiety emits, is characterized by a tri-exponential decay with the lifetime of the major component of the decay is measured to be in the sub-nanosecond range. The time-profile of the fluorescence in the long wavelength region is also best fitted to a tri-exponential decay function. However, the lifetime of the major component of the decay is measured to be 8.1 ns in THF, which is comparable to that of **ANBD** (τ_f, **ANBD** = 11.5 ns in THF). The decay parameters are listed in Table 7.2.

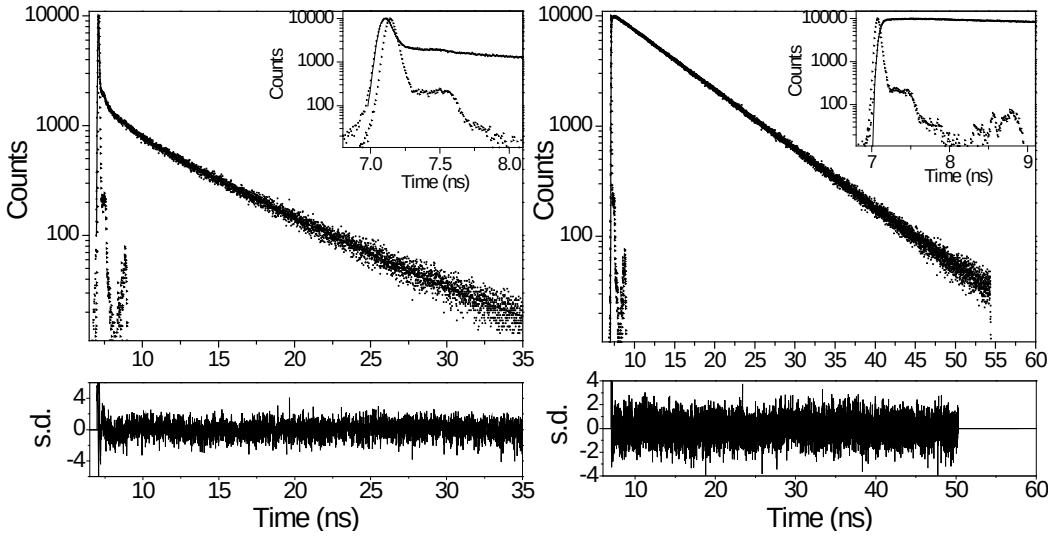

Figure 7.3 Fluorescence decay behavior of **AMNEA** in THF. The solutions were excited at 374 nm and monitored at 425 nm (left) and 550 nm (right). The insets show the short-time behavior of the decay profiles more clearly.

Table 7.2 Fluorescence decay parameters[a] for **AMNEA**, **ANBD** and **anthracene** in THF at 425 nm[b] and 550 nm[c] emission wavelengths.

	Emission Wavelength					
	425 nm			550 nm		
Compound	τ_1 (α_2)	τ_2 (α_2)	τ_3 (α_3)	τ_1 (α_1)	τ_2 (α_2)	τ_3 (α_3)
AMNEA[d]	0.031 (95)	6.1 (2.8)	1.0 (2.2)	8.1 (100)	0.035 (-89)	0.35 (-11)
AMNEA[e]	-	-	-	8.1	-	-
ANBD	-	-	-	11.5	-	-
Anthracene	3.8	-	-	-	-	-

[a] τ values are in ns and α represents relative % of each component. [b] **Anthracene** moiety. [c] **ANBD** moiety. [d] $\lambda_{exc.}$ = 374 nm. [e] $\lambda_{exc.}$ = 439 nm.

The decay parameters associated with the anthracene-like emission, monitored at 425 nm, suggest that the major lifetime component (95%) is significantly shorter than the lifetime of anthracene. Clearly this is a reflection of RET and PET in the system. The presence of multiple decay components is suggestive of more than one dominant conformer of the system and is consistent with the flexibility of the system. On the other hand, the presence of a negative pre-exponential factor at 550 nm with lifetime almost identical with that associated with the anthracene moiety unambiguously establishes RET between the anthracene and **ANBD** moieties. The presence of a second negative component at 550 nm implies that there are multiple conformers of the molecules from which the energy transfer process occurs. When the sample is excited at 439 nm, where the anthracene moiety does not absorb, the time-profile of the fluorescence at the long wavelength region is best fitted to a single exponential decay with a lifetime of 8.1 ns with no negative pre-exponential factor due to RET (as expected). The fact that the lifetime is slightly shorter than that of **ANBD** (11.5 ns in THF) confirms that PET between the terminal nitrogen atom and **ANBD** moiety is not very efficient. The fluorescence decay curve is shown in Figure 7.4.

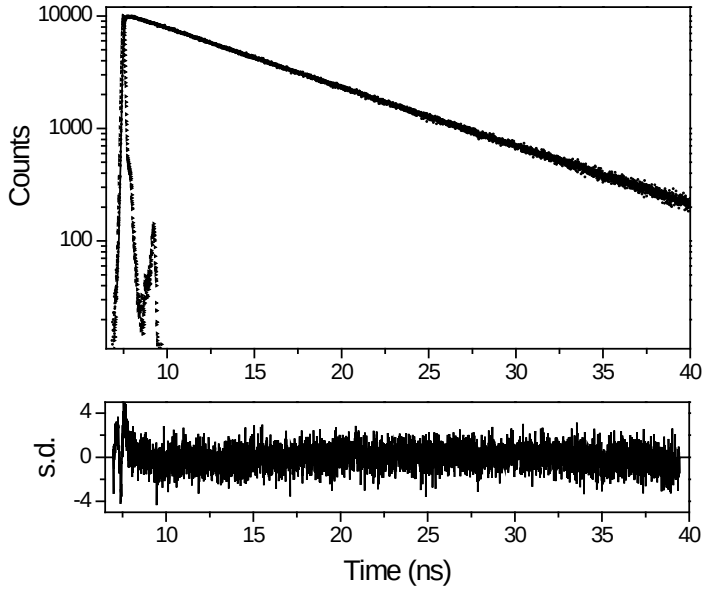

Figure 7.4 Fluorescence decay behavior of **AMNEA** in THF. The solution was excited at 439 nm and the decay profile monitored at 550 nm.

7. 4. Metal ion signaling behavior

7. 4. 1. Changes in the absorption spectra

The effect of metal ions on the absorption spectrum of **AMNEA** was examined in THF and AN. In the presence of alkali and alkaline earth metal ions, **AMNEA** does not show any spectral change. Upon addition of the transition metal salts, both the long-wavelength ICT absorption and the structured absorption in the short-wavelength region gradually lose in intensity. Visual detection could also be possible as the bright yellow color of **AMNEA** solution fades out to a colorless solution in the presence of the transition metal ions. Typical changes in the absorption spectrum of **AMNEA** in the presence of the transition metal ions are depicted in Figure 7.5. Isosbestic points could be observed over a certain concentration range of the metal ions, suggesting the presence of two species at equilibrium. However, as can be seen from Figure 7.5 (b), in the presence of Cu^{2+} ions, the loss of the long-wavelength ICT absorption is associated with a

hypsochromic shift from 468 nm to 448 nm in THF. A different behavior of Cu^{2+} ions on the ICT band of **ANBD** chromophore is consistent with that observed for the **ANBD** based system described in the preceding chapter.

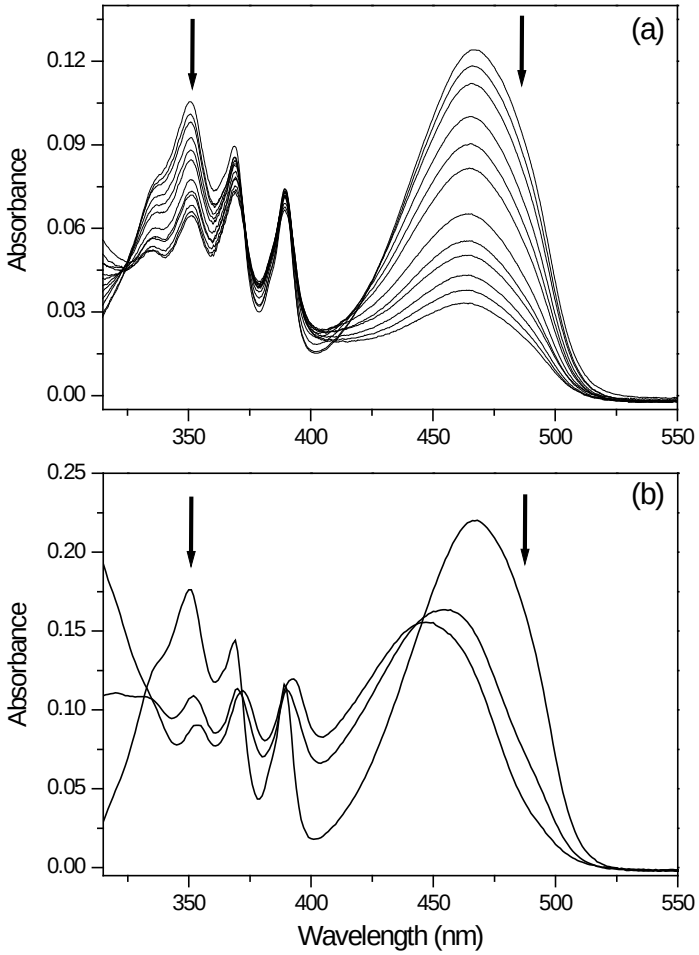

Figure 7.5 Effect of (a) Zn^{2+} and (b) Cu^{2+} ions on the absorption spectrum of **AMNEA** (10^{-5} M) in THF. The various amounts of Zn^{2+} ions in decreasing order of absorbance at 475 nm are 0 – 1.1 equivalents with increments of 0.1 equivalent. The amounts of Cu^{2+} ions are 0, 0.8 and 1.1 equivalents.

7. 4. 2. Changes in the fluorescence spectra

The effect of metal ions on the fluorescence spectrum of **AMNEA** was also examined in THF and AN. Addition of transition metal salts leads to an enhancement of the short-wavelength emission intensity and simultaneous loss of the long-wavelength emission intensity thereby allowing ratiometric detection of the transition metal ions. Typical changes in the fluorescence spectrum of **AMNEA** in the presence of transition metal ions are depicted in Figure 7.6, and plots of the fluorescence intensity ratio in the presence of Zn^{2+} ions are shown in Figure 7.7. Interestingly, even at higher excitation wavelength, the long wavelength emission associated with the **ANBD** moiety is quenched upon progressive addition of the transition metal ions (Figure 7.8). Thus, in the presence of transition metal ions, the energy transfer process between the fluorophore moieties and the PET communication between the terminal nitrogen atom and the anthracene fluorophore are inhibited.

As can be seen from Figure 7.6 (b), in the presence of transition metal ions such as Cu^{2+}, that although the quenching of the long-wavelength emission is similar to that observed in the presence of Zn^{2+} ions, the enhancement of the short-wavelength emission is rather small. This is obviously due to the internal quenching of the fluorophore moiety upon interaction with the paramagnetic metal ions that are notorious quenchers of fluorescence.

7. 4. 3. Effect on the fluorescence decay behavior

The effect of the transition metal salts on the fluorescence decay behavior of **AMNEA** has also been examined monitoring the short wavelength region. The amplitude associated with the sub-nanosecond component of the fluorescence decay disappears completely and a significant increase in the amplitude of the long component is observed on progressive addition of the transition metal salts. For instance, the decay parameters for **AMNEA** observed at 425 nm in the presence of one equivalent of Zn^{2+} are 8.2 ns (96%) and 1.1 ns (4%) in THF. The average lifetime of the decay that is observed in the presence of the metal ions is, as expected, very similar to that of the bare fluorophores, anthracene (3.8 ns in THF) and **ANBD** (11.5 ns in THF).

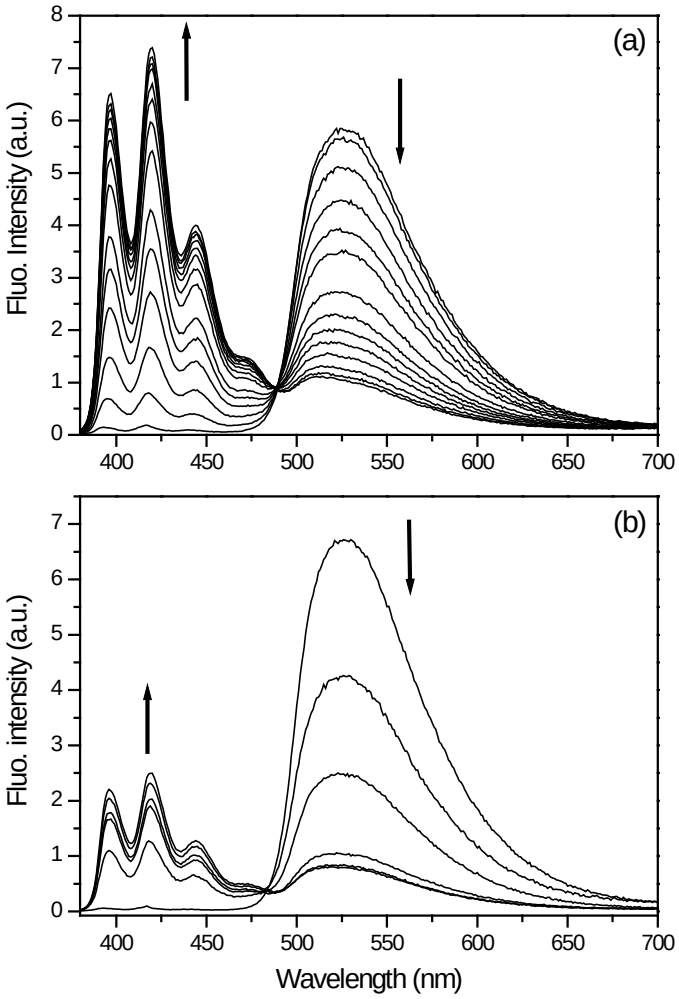

Figure 7.6 Fluorescence spectra of **AMNEA** (10^{-5} M) in THF in the presence of Zn^{2+} ions (a) and Cu^{2+} ions (b). The various amounts of Zn^{2+} ions in increasing order of the fluorescence intensity at 425 nm and decreasing order of fluorescence intensity at 550 nm are 0 – 1.3 equivalents with increments of 0.1 equivalent. The amounts of Cu^{2+} ions are 0, 0.4, 0.8, 1.1, 1.2 and 1.3 equivalents. $\lambda_{exc.}$ = 370 nm.

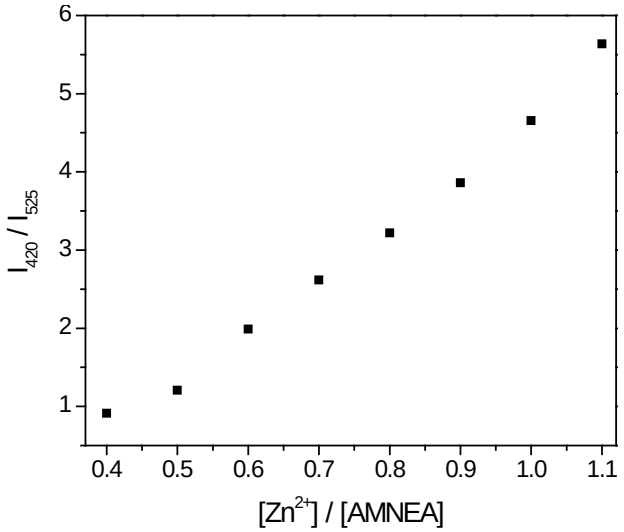

Figure 7.7 Plots of the fluorescence intensity ratio of **AMNEA** in THF between 420 and 525 nm in the presence of Zn^{2+} ions. $\lambda_{exc.}$ = 370 nm.

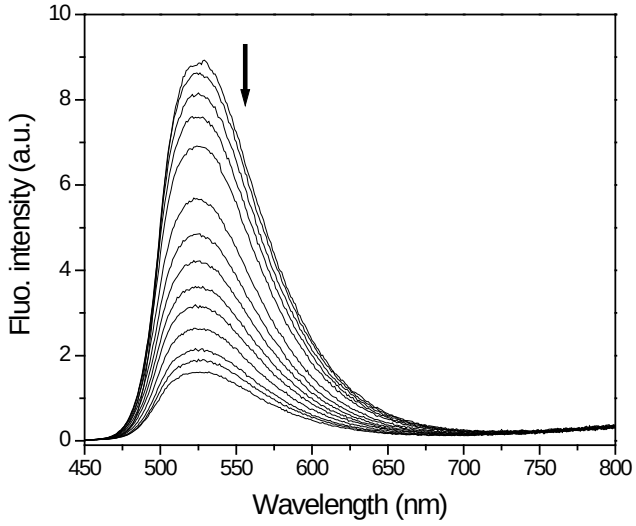

Figure 7.8 Fluorescence spectra of **AMNEA** (10^{-5} M) in THF in the presence of Zn^{2+} ions. The various amounts of Zn^{2+} ions in decreasing order of fluorescence intensity at 550 nm are 0 – 1.3 equivalents with increments of 0.1 equivalent. $\lambda_{exc.}$ = 440 nm.

Figure 7.9 depicts the typical change in the fluorescence behavior of **AMNEA** on addition of the transition metal ions. An increase in the lifetime of **AMNEA** in the presence of the metal ions is due to the metal ion-induced suppression of energy transfer between the fluorophore moieties of the multi-component system.

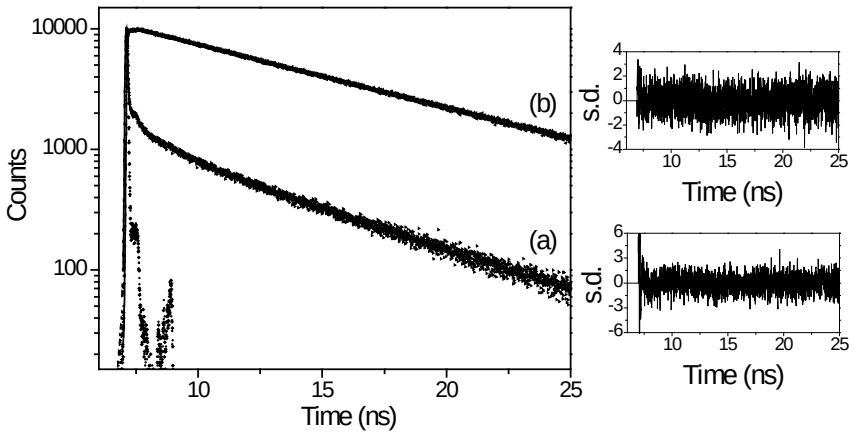

Figure 7.9 Fluorescence decay curves of **AMNEA** (10^{-5} M) in THF as measured at 425 nm (a) in the absence and (b) in the presence of one equivalent of Zn^{2+} ions. The excitation wavelength was 374 nm. The excitation prompt profiles, best exponential fit to the measured decay curves and the corresponding weighted residuals are also shown.

7. 5. Conclusions

In summary, we have synthesized a simple molecular system for the ratiometric detection of transition metal ions. This multi-component system with the *fluorophore$_1$-spacer$_1$-fluorophore$_2$-spacer$_2$-receptor* format gives insight into the overlapping of the PET and RET mechanisms. The metal ions can be detected by monitoring several parameters such as visual effects, fluorescence intensity ratio and the fluorescence lifetime values. The results obtained here are very promising and suggest an excellent example for the potential applications of combining two complimentary signaling mechanisms within a single sensor molecule.

References

1 Lakowicz, J. R. In *Topics in Fluorescence Spectroscopy*; Lakowicz, J. R., Ed.; Plenum Press: New York, 1994; Vol. 4.
2 White, R. A.; Kutz, K. J.; Wampler, J. E. In *Topics in Fluorescence Spectroscopy*; Lakowicz, J. R., Ed.; Plenum Press: New York, 1991; Vol. 1.
3 Grynkiewicz, G.; Poenie, M.; Tsien, R. Y. *J. Biol. Chem.* **1985**, *260*, 3440.
4 Whitaker, J. E.; Haugland, R. P.; Prendergast, F. G. *Anal. Biochem.* **1991**, *194*, 330.
5 Akkaya, E. U.; Lakowicz, J. R. *Anal. Biochem.* **1993**, *213*, 285.
6 Fages, F.; Desvergne, J.-P.; Kampke, K.; Bouas-Laurent, H.; Lehn, J.-M.; Meyer, M.; Albrecht-Gary, A.-M. *J. Am. Chem. Soc.* **1993**, *115*, 3658.
7 Marquis, D.; Desvergne, J.-P.; Bouas-Laurent, H. *J. Org. Chem.* **1995**, *60*, 1784.
8 Kubo, K.; Sakurai, T. *Chem. Lett.* **1996**, 959.
9 Scalfani, J. A.; Maranto, M. T.; Sisk, T. M.; Van Arman, S. A. *Tetrahedron Lett.* **1996**, *37*, 2193.
10 Kubo, K.; Kato, N.; Sakurai, T. *Bull. Chem. Soc. Jpn.* **1997**, *70*, 3041.
11 Nishizawa, N.; Watanabe, M.; Uchida, T.; Terame, N. *J. Chem. Soc. Perkin Trans. 2* **1999**, 141.
12 Strauss, J.; Daub, J. *Org. Lett.* **2002**, *4*, 683.
13 Valeur, B.; Bourson, J.; Pouget, J. In *Fluorescent Chemosensors for Ion and Molecule Recognition*; Czarnik, A. W., Ed.; ACS Symposium Series: Washington, D. C., 1993; Vol. 538.
14 Saha, S.; Samanta, A. *J. Phys. Chem. A* **1998**, *102*, 7903.
15 Ghosh, P.; Bharadwaj, P. K.; Mandal, S.; Ghosh, S. *J. Am. Chem. Soc.* **1996**, *118*, 1553.

Chapter 8

Concluding Remarks

This chapter summarizes the various projects undertaken, the achievements and their implications on transition metal ion signaling and molecular photonic devices. The future prospects based on the present findings and the upcoming challenges conclude this chapter as well as the thesis.

8. 1. Overview

The work embodied in the thesis has been undertaken with a view to obtaining new design strategies and approaches for the development of devices capable of sensing heavy and transition metal (HTM) ions. In this context several simple as well complex photoactive multi-component systems have been designed and subsequently developed. Thus, synthesis and characterization of the supermolecules constitute an important part of the thesis. Once developed, these systems have been studied thoroughly to investigate their potential in signaling transition metal ions. For these purposes several instrumental techniques and methodologies such as CHN analysis, IR, UV-vis absorption, steady-state and time-resolved fluorescence spectroscopy, NMR and Mass spectroscopy, X-ray crystallography and theoretical calculations have been employed. The objective of the various projects undertaken and the results obtained from the investigation are outlined below.

Due to the fluorescence quenching nature of the transition metal ions, an efficient fluorosensor for their detection could be designed after considering several factors. Whatever be the case, the net result should nullify the quenching interaction between these metal ions and the fluorophore. This can be achieved by employing an electron-deficient fluorophore within the architecture of the supermolecule. Alternatively, the quenching interaction can be made unimportant by employing a structurally well-developed macrocyclic receptor unit, which would result into strong complexation with the metal ions. This might as well lead to selective detection of specific metal ions due to

their restricted conformations and cavity sizes allowing only site-selective metal ions to form strong complexes. Putting these ideas together, two related projects have been undertaken to develop photoactive multi-component systems based on *fluorophore-spacer-receptor* design format. Electron deficient 4-aminophthalimide (AP) and dimethylene moieties are chosen as the fluorophore and spacer components, respectively, in both the systems while the receptor components are chosen to be macrocyclic cryptand and calix[4]azacrown.

The electronic absorption, steady-state and time resolved fluorescence properties of the systems have been studied in the absence and presence of transition metal ions. The fluorescence quantum yield and lifetime of the systems are measured to be significantly lower than that of the parent fluorophore due to the intramolecular photo-induced electron transfer (PET) between the receptor and the fluorophore moieties. Addition of metal salts leads to "switching on" of the fluorescence of the system and is associated with a Stokes shift. While the fluorescence response of the cryptand derivative towards the transition metal ions is non-selective, the calix[4]azacrown derivative responds selectively towards Fe^{3+} and Cu^{2+} ions. Absorption and fluorescence measurements reveal that these systems exhibit strong complexation with transition metal ions. However, X-ray crystallography studies reveal that calix[4]azacrown receptor devoid of a fluorophore exhibits poor affinity towards metal ions. This implies that a slight modification of the calix[4]azacrown framework may result into potential hosts for the selective recognition of transition of transition metal ions. The poor complexation properties could be attributed to the highly ordered hydrogen-bonding pattern found in the solid state leading to a supramolecular dimeric structure.

The results also indicate that even though strong binding properties of the sensor systems employing macrocyclic cryptand and calix[4]azacrown enable the detection of metal ions in trace quantities, the maximum fluorescence enhancement (FE) of these systems need not be higher than that of a similar system comprising a much simple and flexible amine moiety as the receptor. Thus, an important lesson that we have learnt from this study is that the molecular components of a sensor system have to be chosen such that optimized conditions for PET and guest binding are attained.

Based on the above finding we focused our attention to develop a structurally similar multi-component system employing di-(2-picolyl)amine (DPA) as the receptor component. The tridentate DPA ligand is known for strong binding with the transition metal ions and moreover, unlike the macrocyclic cryptand and calix[4]azacrown ligands, DPA is very much flexible.

The electronic absorption behavior of this simple system in the presence of metal ions enables us to evaluate its metal ion-binding properties. The data suggest that metal ions such as Zn^{2+}, Cd^{2+} and Pb^{2+} form strong complexes with this system. The absorbance changes in the presence of metal ions such as Cu^{2+} are not uniform and hence complexation properties of the system with these metal ions could not be determined accurately. The fluorescence quantum yield of the system in non-aqueous medium is measured to be significantly lower than that of the parent fluorophore, AP, due to intramolecular PET between the receptor and the fluorophore moieties. In the presence of Zn^{2+}, Cd^{2+} and Pb^{2+}, the fluorescence of the system “switches on” with a color change from blue to green. This is due to the metal ion-induced suppression of PET communication between the receptor and the fluorophore moieties. However, the practical utility of a sensor system depends on whether the guest molecule can be detected in aqueous environment under physiological pH range. Therefore, to explore the possible utility of the system in aqueous environment, photophysical and metal ion signaling experiments have been carried out in water. The results suggest that PET is inefficient in aqueous environment leading to the low FE values in the presence of metal ions. The imide oxygen atoms of the AP moiety have the possibility to form hydrogen bond with water molecules, which would result into an inefficient PET process in aqueous environment. This implies that although it has been established that AP serves well as a fluorophore component for the design of fluorescent “off-on” sensor systems for transition metal ions in aprotic media, sensor systems comprising AP may not be effective in aqueous environment.

The fluorescence enhancement (FE) of this system caused by these metal ions is very similar. The metal ion concentrations required for the maximum FE are also not very different. The almost identical response for similar input levels has important implications for the use of this system as a photonic OR logic system as this would

constitute a good quality truth table. X-ray structural analysis of the system and its Zn^{2+} complex indicates that on binding with the metal ion, the lone pair of electrons on the nitrogen atom becomes unavailable for PET due to the structural modulation of the sensor system as well as its engagement with metal ion. The experimental measurements carried out on the complex provide direct evidence for the non-interference of residual protons from the hydration shell of the metal salts used.

This system also behaves as H^+-driven "off-on-off" fluorescence switch. At very high proton concentration the amino group of the AP fluorophore gets protonated and the system behaves as NOT logic. Integration of the metal ion-induced OR logic gate and H^+-induced NOT gate would result into the INH logic system in which the AND logic provides the output. Both our brains and modern silicon-based electronics technology are heavily dependent on integration. Thus, we have demonstrated that functional integration of molecular logic is also feasible. Moreover, this system is a first example of an INH logic gate employing HTM ions and H^+ as logic inputs. Thus, this simple multi-component system acts as an efficient fluorescence "off-on" sensor for metal ions such as Zn^{2+}, Cd^{2+} and Pb^{2+} and has access to several logic functions.

To avoid proton sensitivity around neutral pH, multi-component systems with *fluorophore-spacer-receptor* format have been synthesized employing AP and pyridine as the fluorophore and receptor components, respectively. The effects of metal ions on the electronic absorption spectra of the systems indicate that they form complexes with transition metal ions. However, the fluorescence quantum yield of these simple molecular systems is measured to be very similar to that of the parent fluorophore. At first sight these systems appear to be worthless since they cannot be used for sensing applications. However, these systems turn out to be judicious candidate for the stabilization of copper(I).

Although several multi-component systems based on AP have been developed in recent years, the coordination properties of the metal ions with the systems are still unexplored. Secondly, very few two-coordinate copper(I) complexes are reported in the literature primarily due to the instability of the copper(I) compounds. Taking these into account copper(I) complexes of these systems are synthesized. The electronic absorption and fluorescence behavior of the copper(I) complexes are very similar to that of their

respective ligands. X-ray structure reveals that the packing in the ligand systems as well as in the complexes is governed by intermolecular hydrogen bonding between the 4-amino nitrogen atom and one of the imide oxygen atoms of the neighboring molecule.

X-ray structure of the complexes reveals a weak electronic interaction between copper(I) and one of the imide oxygen atoms of the ligand unit. A close contact between the oxygen atom of the perchlorate anion and the metal center is also inspected that leads to linear polymer network. The complexes are highly air-stable and unusually inert towards oxidation in the solid state as well as in potentially coordinating or protic solvents. Cyclic voltammetry studies reveal no noticeable oxidation wave for Cu(I)/Cu(II) couple indicating significant stabilization of the monovalent oxidation state. The key features for the extraordinary stabilization of cuprous ions are the electronic factors provided by an electron deficient AP moiety of the ligand framework and the perchlorate counter-anions. Thus, we have shown that stable two-coordinate linear complexes of copper(I) with monodentate ligands can be accessed easily if the ligand systems and the counter-anion are chosen judiciously.

As an alternative to the fluorescent ("off-on") chemosensors, we have designed a chromogenic sensor comprising a polarity sensitive 4-amino-7-nitrobenzoxa[1,3]diazole (ANBD) chromophore moiety integrated with a DPA receptor. The electronic absorption and fluorescence behavior of this system is found to be consistent with that of the parent fluorophore. In the presence of protons, the system displays large blue shift and intensity loss of the absorption maximum. This is attributed to the redistribution of the electronic density due to the interaction between the protonated pyridyl moieties of the receptor unit and the nitrogen atom connected to the chromophore. Results from the molecular modeling and semi-empirical calculations also indicate that the dipole of the system gets significantly altered in the presence of cationic guest and large blue shift can be expected. However, the system is found to be insensitive above pH 5 demonstrating its metal ion signaling utility in physiological environment where pH > 5.

Thus, the system is tested for metal ion signaling in the aqueous solution with pH 7.4. This system shows a blue shift of 42 nm and gradual loss of the absorption intensity selectively in the presence of Cu^{2+} ions. The plot of absorption maximum of the system *vs.* concentration of Cu^{2+} ions gives a linear profile suggesting the potential utility of the

system for the analytical detection of Cu^{2+} ions. Addition of transition metal ions other than Cu^{2+}, such as Ni^{2+} and Zn^{2+} does not result into any significant change within the concentration range employed for the measurements. Selective detection of Cu^{2+} ions based solely on the change in the absorbance parameter could be masked by increased concentration of the weaker binding metal ions. However, an additional shift parameter allows discrimination of Cu^{2+} ions from the rest of the metal ions. Furthermore, Cu^{2+} ions can be removed by the addition of excess EDTA. Thus, the system is equipped with a reset function. The fluorescence of the system is also quenched and is associated with a hypsochromic shift, although the shift is not as large as that observed in the absorption spectrum.

To avoid the disadvantage associated with the intensity-based sensing, alternative approaches, such as use of ratiometric fluorescent probes, are highly sought. In this context, we have designed a sensor system with a *fluorophore$_1$-spacer$_1$-fluorophore$_2$-spacer$_2$-receptor* format such that PET between the receptor and the fluorophore as well as energy transfer between the two different fluorophores, anthracene and ANBD in the present case, are simultaneously feasible. The electronic absorption and fluorescence spectral features of the system are characteristic of both the parent fluorophores. However, the emission due to the ANBD moiety is much more prominent than that due to the anthracene moiety. This gives rise to a large intensity ratio of the two bands. In the presence of metal ions, the PET communication between the receptor and the fluorophore moieties and the energy transfer process between the fluorophore moieties are inhibited. This results into an enhancement of the anthracene emission and simultaneous quenching of the ANBD emission. Thus, addition of metal ions reverses the initial situation allowing ratiometric detection of the metal ions. This provides a new design strategy for the quantitative detection of metal ions.

8. 2. Future scope

While we have reconfirmed in the present investigation that efficient fluorescent signaling systems for transition metal ions can be developed by employing an electron-deficient fluorophore such as AP in the *fluorophore-spacer-receptor* design format, it has been found that this fluorophore is not particularly suitable in aqueous environment.

Therefore we need to develop systems employing other fluorophores that can be applied in aqueous environment and will be useful for real-world applications. Disadvantages, such as pH sensitivity, are associated with the sensor systems based PET signaling mechanism and to overcome this, other possible signaling strategies need to be explored.

Colorimetric signaling systems need to be explored more vigorously. A convenient procedure involves the incorporation of a push-pull chromophore into a multi-dentate ligand such that coordinative interaction with a given metal alters the dipole of the chromophore, thus modifying the energy of the charge transfer transition and hence, the color. With an enormous number of receptors available for specific binding and recognition of metal ions, one just needs to integrate them to obtain colorimetric sensors for a given ion of interest.

We have shown for the first time by employing both energy transfer and PET in a single sensor system that ratiometric detection of the transition metal ions is indeed possible. Ratiometric fluorescent sensors are superior to the conventional intensity-based sensors because the quantitative detection of an analyte is much more accurate with the former systems. Based on this new design strategy, several systems can be developed for signaling specific analytes by just varying the nature of the receptor components. Furthermore, different combination of fluorophores may also be employed to improve the signaling efficiency.

The realization of stable copper(I) complexes, and understanding of the key feature for their stabilization (electronic factors provided by the electron-deficient AP moiety) have opened up a wide scope for the development of copper(I) chemistry as several ligand systems based on electron-deficient systems are available on hand.

Despite a lot of effort and expectations, molecular-scale electronics/photonics is undergoing gradual evolution via wires, switches, and diodes. Although it has been possible to mimic some of the logic functions at the molecular level by combining chemical and photonic signals, molecular-scale logic gates for real-world applications are quite far from the reality. We have demonstrated the INH logic gate, which is basically an integration of an AND and a NOT logic functions. Integration of simple molecular logic systems into higher-level devices remains an important goal. One needs to design

molecules capable of functioning as multiple logic functions independently of each other for this purpose.

Appendix I

Table AI.1 Atomic coordinates ($\times 10^4$), equivalent isotropic and anisotropic displacement parameters ($Å^2 \times 10^3$) for **L2·CH$_3$OH**. U(eq) is defined as one third of the trace of the orthogonalized U_{ij} tensor. The anisotropic displacement factor exponent takes the form: $-2\pi^2[h^2a^{*2}U_{11} + ... + 2hka^*b^*U_{12}]$.

atom	x	y	z	U(eq)	U_{11}	U_{22}	U_{33}	U_{23}	U_{13}	U_{12}
O(1)	7787(3)	2123(2)	1246(2)	38(1)	44(2)	37(2)	33(2)	-1(2)	5(2)	12(2)
O(2)	5950(3)	2205(2)	-8(2)	46(1)	34(2)	74(3)	30(2)	15(2)	6(2)	6(2)
O(3)	6541(3)	3160(2)	-1315(2)	37(1)	41(2)	38(2)	33(2)	4(2)	9(2)	10(2)
O(4)	8020(3)	3444(2)	118(2)	48(1)	62(3)	39(3)	36(2)	2(2)	-12(2)	-3(2)
O(5)	6755(3)	1772(2)	-2959(2)	68(1)	98(4)	70(3)	42(3)	-16(2)	30(3)	1(3)
O(6)	9813(3)	575(3)	1175(2)	84(2)	106(4)	86(4)	69(3)	32(3)	40(3)	74(3)
N(1)	6496(3)	1512(3)	-1689(3)	41(1)	48(3)	38(3)	37(3)	-2(3)	7(2)	8(3)
N(2)	8396(4)	536(3)	-913(3)	48(1)	51(4)	42(3)	48(3)	6(3)	3(3)	14(3)
N(3)	9272(3)	1722(3)	400(3)	44(1)	55(3)	38(3)	41(3)	4(3)	10(3)	19(3)
C(1)	8988(4)	3680(3)	1698(3)	45(2)	46(4)	52(4)	35(3)	-8(3)	0(3)	6(3)
C(2)	8862(4)	4405(4)	1087(3)	36(1)	28(3)	39(4)	40(4)	-8(3)	1(3)	2(3)
C(3)	9266(4)	5205(4)	1294(3)	47(2)	38(4)	45(4)	54(4)	-8(4)	-4(3)	0(3)
C(4)	9183(5)	5865(4)	739(4)	55(2)	55(4)	34(4)	74(5)	1(4)	-1(4)	-7(3)
C(5)	8646(4)	5729(4)	-26(4)	48(2)	36(4)	43(4)	63(5)	5(4)	4(3)	0(3)
C(6)	8204(4)	4929(4)	-253(3)	40(2)	42(4)	40(4)	40(4)	-3(3)	11(3)	-6(3)
C(7)	7604(4)	4804(3)	-1090(3)	42(2)	58(4)	31(4)	39(4)	9(3)	14(3)	3(3)
C(8)	6383(4)	4677(4)	-1102(3)	39(2)	40(4)	39(4)	37(4)	7(3)	6(3)	4(3)
C(9)	5736(5)	5381(4)	-1000(3)	47(2)	55(4)	39(4)	45(4)	4(3)	-2(3)	-7(4)
C(10)	4636(5)	5275(4)	-977(3)	51(2)	61(5)	40(4)	49(4)	-2(3)	3(4)	18(4)
C(11)	4183(4)	4461(4)	-1041(3)	45(2)	34(4)	53(4)	46(4)	2(3)	1(3)	14(4)
C(12)	4811(4)	3741(4)	-1132(3)	35(1)	39(4)	40(4)	25(3)	4(3)	-2(3)	4(3)
C(13)	4302(4)	2853(3)	-1151(3)	39(2)	33(4)	47(4)	36(3)	-4(3)	-1(3)	0(3)
C(14)	4099(4)	2545(3)	-334(3)	35(1)	35(4)	31(4)	39(3)	-9(3)	7(3)	-2(3)
C(15)	3075(4)	2546(3)	-127(3)	45(2)	33(4)	48(4)	54(4)	-4(3)	5(3)	-1(3)
C(16)	2875(5)	2288(4)	626(4)	54(2)	36(4)	59(5)	70(5)	-1(4)	19(4)	-6(3)
C(17)	3729(5)	2029(3)	1169(3)	47(2)	51(4)	45(4)	48(4)	-5(3)	23(4)	-6(3)
C(18)	4795(5)	1998(3)	1003(3)	38(1)	47(4)	31(4)	37(4)	3(3)	12(3)	-5(3)
C(19)	5715(4)	1738(3)	1639(3)	44(2)	52(4)	46(4)	37(4)	3(3)	13(3)	1(3)
C(20)	6365(4)	2511(3)	1976(3)	38(2)	43(4)	39(4)	30(3)	3(3)	4(3)	5(3)
C(21)	5955(5)	3072(4)	2489(3)	53(2)	51(4)	64(5)	46(4)	-8(4)	18(3)	0(4)
C(22)	6518(5)	3807(4)	2759(3)	58(2)	76(5)	55(5)	49(4)	-24(4)	28(4)	2(4)

Table AI.1 Continued

atom	x	y	z	U(eq)	U_{11}	U_{22}	U_{33}	U_{23}	U_{13}	U_{12}
C(23)	7493(5)	3986(4)	2502(3)	51(2)	58(4)	51(4)	43(4)	-15(3)	7(3)	-9(4)
C(24)	7940(4)	3433(4)	1998(3)	37(2)	41(4)	45(4)	25(3)	6(3)	2(3)	10(3)
C(25)	7370(5)	2690(3)	1765(3)	36(1)	45(4)	37(4)	24(3)	0(3)	-2(3)	12(3)
C(26)	4943(4)	2249(3)	229(3)	34(1)	27(3)	29(3)	48(4)	-2(3)	12(3)	3(3)
C(27)	5892(5)	3874(4)	-1195(3)	36(1)	41(4)	34(4)	32(4)	-1(3)	3(3)	12(3)
C(28)	8347(4)	4270(4)	314(3)	38(2)	40(4)	33(4)	42(4)	-8(3)	8(3)	-3(3)
C(29)	8539(4)	1504(3)	1620(3)	46(2)	56(4)	40(4)	41(4)	5(3)	6(3)	15(3)
C(30)	9273(5)	1213(4)	1040(4)	47(2)	38(4)	54(5)	46(4)	1(4)	0(3)	16(4)
C(31)	9833(4)	1510(4)	-267(3)	49(2)	37(4)	57(4)	55(4)	-3(4)	15(3)	-1(3)
C(32)	9036(4)	1311(4)	-1014(3)	49(2)	46(4)	58(4)	46(4)	1(3)	14(3)	9(4)
C(33)	7736(4)	257(3)	-1665(3)	55(2)	60(4)	45(4)	58(4)	-11(4)	3(4)	11(4)
C(34)	6575(4)	583(3)	-1751(3)	49(2)	57(4)	36(4)	51(4)	-4(3)	2(3)	6(3)
C(35)	6614(4)	2033(4)	-2305(4)	44(2)	39(4)	49(4)	42(4)	-1(4)	6(3)	4(3)
C(36)	6589(4)	2983(3)	-2146(3)	48(2)	62(4)	54(4)	33(4)	2(3)	20(3)	11(3)
O(7)	7022(4)	561(3)	274(3)	83(2)	95(4)	61(3)	101(4)	-29(3)	43(3)	-14(3)
C(37)	6608(6)	-239(4)	377(4)	110(3)	202(10)	70(6)	68(5)	-3(5)	54(6)	-21(6)

Table AI.2 Bond lengths (Å) for **L2·CH_3OH**.

O(1)-C(25)	1.396(5)	C(2)-C(28)	1.379(6)	C(15)-C(16)	1.391(6)
O(1)-C(29)	1.423(5)	C(3)-C(4)	1.381(6)	C(16)-C(17)	1.357(7)
O(2)-C(26)	1.376(5)	C(4)-C(5)	1.379(6)	C(17)-C(18)	1.399(6)
O(3)-C(27)	1.405(5)	C(5)-C(6)	1.391(7)	C(18)-C(26)	1.401(6)
O(3)-C(36)	1.438(5)	C(6)-C(28)	1.395(7)	C(18)-C(19)	1.504(6)
O(4)-C(28)	1.372(5)	C(6)-C(7)	1.507(6)	C(19)-C(20)	1.512(6)
O(5)-C(35)	1.213(6)	C(7)-C(8)	1.532(6)	C(20)-C(21)	1.379(6)
O(6)-C(30)	1.202(6)	C(8)-C(9)	1.386(6)	C(20)-C(25)	1.382(6)
N(1)-C(35)	1.342(6)	C(8)-C(27)	1.389(6)	C(21)-C(22)	1.383(7)
N(1)-C(34)	1.453(5)	C(9)-C(10)	1.388(7)	C(22)-C(23)	1.378(7)
N(2)-C(32)	1.470(6)	C(10)-C(11)	1.384(6)	C(23)-C(24)	1.384(6)
N(2)-C(33)	1.470(6)	C(11)-C(12)	1.388(6)	C(24)-C(25)	1.382(7)
N(3)-C(30)	1.338(6)	C(12)-C(27)	1.384(6)	C(29)-C(30)	1.506(6)
N(3)-C(31)	1.449(5)	C(12)-C(13)	1.518(6)	C(31)-C(32)	1.514(6)
C(1)-C(24)	1.520(6)	C(13)-C(14)	1.515(6)	C(33)-C(34)	1.521(6)
C(1)-C(2)	1.521(6)	C(14)-C(15)	1.372(6)	C(35)-C(36)	1.503(6)
C(2)-C(3)	1.368(6)	C(14)-C(26)	1.386(6)	O(7)-C(37)	1.367(6)

Table AI.3 Bond angles (°) for **L2·CH_3OH**.

C(25)-O(1)-C(29)	115.6(4)	C(18)-C(19)-C(20)	111.2(4)
C(27)-O(3)-C(36)	113.6(4)	C(21)-C(20)-C(25)	118.0(5)
C(35)-N(1)-C(34)	121.9(5)	C(21)-C(20)-C(19)	120.7(5)
C(32)-N(2)-C(33)	112.6(4)	C(25)-C(20)-C(19)	121.2(5)
C(30)-N(3)-C(31)	123.3(5)	C(20)-C(21)-C(22)	120.8(5)
C(24)-C(1)-C(2)	113.9(4)	C(23)-C(22)-C(21)	119.5(6)
C(3)-C(2)-C(28)	118.8(6)	C(22)-C(23)-C(24)	121.5(6)
C(3)-C(2)-C(1)	120.3(5)	C(25)-C(24)-C(23)	117.2(5)
C(28)-C(2)-C(1)	120.9(5)	C(25)-C(24)-C(1)	123.2(5)
C(2)-C(3)-C(4)	121.0(5)	C(23)-C(24)-C(1)	119.5(6)
C(5)-C(4)-C(3)	119.7(6)	C(20)-C(25)-C(24)	122.8(5)
C(4)-C(5)-C(6)	120.8(6)	C(20)-C(25)-O(1)	118.1(5)
C(5)-C(6)-C(28)	117.6(5)	C(24)-C(25)-O(1)	118.9(5)
C(5)-C(6)-C(7)	119.6(5)	O(2)-C(26)-C(14)	116.7(5)
C(28)-C(6)-C(7)	122.8(5)	O(2)-C(26)-C(18)	120.7(5)
C(6)-C(7)-C(8)	112.5(4)	C(14)-C(26)-C(18)	122.6(5)
C(9)-C(8)-C(27)	118.0(5)	C(12)-C(27)-C(8)	122.9(5)
C(9)-C(8)-C(7)	119.4(5)	C(12)-C(27)-O(3)	118.8(5)
C(27)-C(8)-C(7)	122.5(5)	C(8)-C(27)-O(3)	118.2(5)
C(8)-C(9)-C(10)	120.4(6)	O(4)-C(28)-C(2)	116.8(5)
C(11)-C(10)-C(9)	120.0(6)	O(4)-C(28)-C(6)	121.2(5)
C(10)-C(11)-C(12)	121.1(5)	C(2)-C(28)-C(6)	121.9(5)
C(27)-C(12)-C(11)	117.4(5)	O(1)-C(29)-C(30)	109.9(4)
C(27)-C(12)-C(13)	122.9(5)	O(6)-C(30)-N(3)	125.1(6)
C(11)-C(12)-C(13)	119.6(5)	O(6)-C(30)-C(29)	120.2(6)
C(14)-C(13)-C(12)	113.2(4)	N(3)-C(30)-C(29)	114.8(5)
C(15)-C(14)-C(26)	117.7(5)	N(3)-C(31)-C(32)	111.0(4)
C(15)-C(14)-C(13)	121.3(5)	N(2)-C(32)-C(31)	111.8(5)
C(26)-C(14)-C(13)	121.0(5)	N(2)-C(33)-C(34)	112.6(4)
C(14)-C(15)-C(16)	122.2(5)	N(1)-C(34)-C(33)	113.4(4)
C(17)-C(16)-C(15)	118.1(5)	O(5)-C(35)-N(1)	123.3(6)
C(16)-C(17)-C(18)	123.3(5)	O(5)-C(35)-C(36)	120.1(5)
C(17)-C(18)-C(26)	115.9(5)	N(1)-C(35)-C(36)	116.6(5)
C(17)-C(18)-C(19)	120.9(5)	O(3)-C(36)-C(35)	111.5(4)
C(26)-C(18)-C(19)	123.2(5)		

Table AI.4 Atomic coordinates ($\times 10^4$), equivalent isotropic and anisotropic displacement parameters ($Å^2 \times 10^3$) for **2L2-$HClO_4 \cdot 5H_2O$**. U(eq) is defined as one third of the trace of the orthogonalized U_{ij} tensor. The anisotropic displacement factor exponent takes the form: $-2\pi^2[h^2a^{*2}U_{11} + ... + 2hka^*b^*U_{12}]$.

atom	x	y	z	U(eq)	U_{11}	U_{22}	U_{33}	U_{23}	U_{13}	U_{12}
C(1)	6324(4)	7946(3)	11308(2)	63(1)	62(3)	69(3)	51(2)	-19(2)	-13(2)	-5(2)
C(2)	7513(4)	8009(3)	10888(2)	61(1)	64(3)	59(2)	58(2)	-8(2)	-22(2)	-9(2)
C(3)	8219(4)	8189(3)	11204(3)	74(1)	78(3)	78(3)	64(3)	-17(2)	-33(3)	-4(3)
C(4)	9301(5)	8251(3)	10822(3)	82(1)	75(3)	82(3)	102(4)	-17(3)	-50(3)	-15(3)
C(5)	9707(4)	8084(3)	10135(3)	75(1)	60(3)	88(3)	82(3)	-16(3)	-24(2)	-22(2)
C(6)	9038(4)	7888(3)	9793(2)	64(1)	62(3)	64(3)	68(3)	-6(2)	-18(2)	-20(2)
C(7)	9550(4)	7639(3)	9045(2)	69(1)	61(3)	85(3)	63(3)	-3(2)	-14(2)	-31(2)
C(8)	9786(3)	6647(3)	9005(2)	59(1)	45(2)	84(3)	46(2)	-10(2)	-2(2)	-26(2)
C(9)	10737(4)	5996(4)	9215(2)	68(1)	42(2)	100(4)	64(3)	-17(2)	-11(2)	-23(2)
C(10)	10921(4)	5095(4)	9212(2)	67(1)	42(2)	92(4)	65(3)	-15(2)	-15(2)	-12(2)
C(11)	10175(4)	4815(3)	9009(2)	65(1)	50(2)	81(3)	62(3)	-16(2)	-14(2)	-13(2)
C(12)	9238(3)	5414(3)	8799(2)	57(1)	44(2)	78(3)	45(2)	-12(2)	-7(2)	-17(2)
C(13)	8408(4)	5079(3)	8615(2)	62(1)	54(2)	81(3)	53(2)	-22(2)	-16(2)	-12(2)
C(14)	7684(3)	4646(3)	9241(2)	57(1)	49(2)	67(3)	62(2)	-12(2)	-26(2)	-15(2)
C(15)	7943(4)	3720(3)	9378(3)	68(1)	56(3)	75(3)	85(3)	-23(3)	-31(2)	-16(2)
C(16)	7355(4)	3311(3)	9981(3)	72(1)	64(3)	62(3)	97(4)	-2(3)	-40(3)	-15(2)
C(17)	6488(4)	3853(3)	10461(3)	72(1)	70(3)	77(3)	80(3)	10(3)	-34(3)	-34(3)
C(18)	6165(3)	4781(3)	10352(2)	59(1)	49(2)	65(3)	67(3)	-2(2)	-21(2)	-19(2)
C(19)	5234(4)	5338(3)	10903(2)	62(1)	51(2)	71(3)	61(2)	0(2)	-13(2)	-22(2)
C(20)	5728(3)	5743(3)	11307(2)	55(1)	45(2)	69(3)	45(2)	1(2)	-8(2)	-18(2)
C(21)	6283(4)	5194(3)	11807(2)	66(1)	56(3)	73(3)	56(2)	7(2)	-10(2)	-16(2)
C(22)	6819(4)	5530(3)	12139(2)	68(1)	60(3)	84(3)	46(2)	3(2)	-17(2)	-11(2)
C(23)	6836(4)	6404(3)	11975(2)	64(1)	52(2)	86(3)	45(2)	-10(2)	-12(2)	-11(2)
C(24)	6286(3)	6992(3)	11483(2)	58(1)	46(2)	72(3)	42(2)	-12(2)	-5(2)	-5(2)
C(25)	5725(3)	6634(3)	11169(2)	56(1)	44(2)	70(3)	42(2)	-3(2)	-10(2)	-5(2)
C(26)	7929(4)	7872(3)	10183(2)	57(1)	57(2)	61(2)	54(2)	-10(2)	-21(2)	-12(2)
C(27)	9070(3)	6326(3)	8794(2)	55(1)	40(2)	80(3)	37(2)	-7(2)	-5(2)	-15(2)
C(28)	6754(3)	5186(3)	9731(2)	54(1)	42(2)	72(3)	51(2)	-7(2)	-17(2)	-19(2)
C(29)	3965(4)	7616(3)	10930(2)	67(1)	50(2)	75(3)	70(3)	-6(2)	-17(2)	-11(2)
C(30)	3565(4)	8419(3)	10417(3)	70(1)	63(3)	65(3)	80(3)	-19(2)	-31(3)	-1(2)
C(31)	4089(5)	9615(3)	9539(3)	86(2)	107(4)	72(3)	75(3)	-10(3)	-32(3)	-13(3)
C(32)	3637(6)	9614(3)	8944(3)	95(2)	119(5)	65(3)	86(4)	-3(3)	-46(3)	4(3)
C(33)	4277(4)	8128(3)	8492(3)	68(1)	63(3)	62(3)	79(3)	4(2)	-23(2)	-21(2)
C(34)	5231(4)	7506(3)	7969(3)	72(1)	62(3)	87(3)	72(3)	-11(2)	-23(2)	-25(2)

Table AI.4 Continued

atom	x	y	z	U(eq)	U_{11}	U_{22}	U_{33}	U_{23}	U_{13}	U_{12}
C(35)	7239(4)	7518(3)	7629(2)	65(1)	65(3)	79(3)	44(2)	-6(2)	-12(2)	-15(2)
C(36)	8333(4)	7248(3)	7853(2)	64(1)	53(2)	88(3)	43(2)	-5(2)	-8(2)	-18(2)
C(37)	1759(4)	7654(3)	2784(2)	67(1)	85(3)	82(3)	42(2)	3(2)	-22(2)	-38(3)
C(38)	508(4)	7722(3)	3172(2)	57(1)	68(3)	53(2)	53(2)	3(2)	-25(2)	-17(2)
C(39)	-274(5)	7769(3)	2813(3)	78(1)	99(4)	94(3)	60(3)	8(2)	-41(3)	-44(3)
C(40)	-1399(5)	7783(4)	3165(3)	86(2)	102(4)	107(4)	80(3)	17(3)	-60(3)	-53(3)
C(41)	-1745(4)	7746(3)	3882(3)	67(1)	65(3)	61(3)	89(3)	10(2)	-40(2)	-28(2)
C(42)	-996(3)	7683(2)	4268(2)	52(1)	54(2)	39(2)	65(2)	3(2)	-26(2)	-12(2)
C(43)	-1411(3)	7622(3)	5056(2)	58(1)	40(2)	60(2)	72(3)	-9(2)	-18(2)	-9(2)
C(44)	-935(3)	6689(3)	5427(2)	54(1)	45(2)	58(2)	53(2)	-2(2)	-10(2)	-15(2)
C(45)	-1413(4)	6005(3)	5496(2)	62(1)	49(2)	76(3)	68(3)	-1(2)	-19(2)	-27(2)
C(46)	-958(4)	5160(3)	5814(2)	67(1)	60(3)	73(3)	80(3)	4(2)	-22(2)	-37(2)
C(47)	-3(4)	4974(3)	6059(2)	63(1)	62(3)	58(2)	68(3)	5(2)	-15(2)	-25(2)
C(48)	517(3)	5646(3)	6004(2)	53(1)	51(2)	62(2)	46(2)	-1(2)	-15(2)	-18(2)
C(49)	1613(4)	5409(3)	6237(2)	58(1)	64(3)	65(2)	49(2)	8(2)	-25(2)	-24(2)
C(50)	2652(3)	4850(3)	5739(2)	51(1)	51(2)	54(2)	60(2)	1(2)	-30(2)	-21(2)
C(51)	3078(4)	3924(3)	5889(2)	64(1)	63(3)	62(3)	77(3)	13(2)	-40(2)	-25(2)
C(52)	4007(4)	3411(3)	5410(3)	73(1)	67(3)	46(2)	116(4)	-3(3)	-53(3)	-8(2)
C(53)	4501(4)	3814(3)	4780(3)	64(1)	49(2)	57(3)	92(3)	-13(2)	-32(2)	-8(2)
C(54)	4111(3)	4741(3)	4612(2)	54(1)	43(2)	55(2)	74(3)	-9(2)	-28(2)	-14(2)
C(55)	4685(3)	5187(3)	3922(2)	62(1)	44(2)	73(3)	68(3)	-17(2)	-11(2)	-14(2)
C(56)	3914(3)	5513(3)	3412(2)	56(1)	46(2)	71(3)	51(2)	-15(2)	-6(2)	-20(2)
C(57)	3791(4)	4871(3)	3077(2)	69(1)	62(3)	74(3)	73(3)	-22(2)	-12(2)	-20(2)
C(58)	3077(4)	5141(4)	2643(2)	77(1)	84(3)	91(4)	69(3)	-31(3)	-14(3)	-36(3)
C(59)	2446(4)	6036(4)	2540(2)	71(1)	82(3)	90(4)	56(3)	-14(2)	-28(2)	-32(3)
C(60)	2526(4)	6697(3)	2868(2)	59(1)	66(3)	71(3)	43(2)	-6(2)	-13(2)	-26(2)
C(61)	3309(3)	6409(3)	3278(2)	54(1)	55(2)	72(3)	41(2)	-15(2)	-4(2)	-29(2)
C(62)	131(3)	7695(2)	3898(2)	50(1)	56(2)	41(2)	58(2)	-1(2)	-27(2)	-12(2)
C(63)	4(3)	6492(3)	5702(2)	49(1)	43(2)	58(2)	47(2)	-2(2)	-11(2)	-19(2)
C(64)	3189(3)	5249(2)	5099(2)	48(1)	48(2)	49(2)	58(2)	-2(2)	-25(2)	-19(2)
C(65)	4420(4)	7368(3)	3220(2)	59(1)	55(2)	73(3)	51(2)	-14(2)	-2(2)	-28(2)
C(66)	4324(4)	8249(3)	3431(2)	60(1)	60(3)	61(3)	58(2)	-5(2)	-20(2)	-15(2)
C(67)	3034(5)	9671(4)	3850(3)	90(2)	83(4)	73(3)	94(4)	-22(3)	5(3)	-18(3)
C(68)	2968(5)	9802(4)	4584(3)	94(2)	72(3)	74(3)	135(5)	-37(3)	-6(3)	-27(3)
C(69)	1706(4)	9913(3)	5823(3)	73(1)	85(3)	45(2)	100(4)	-16(2)	-44(3)	-13(2)
C(70)	517(5)	9906(3)	6256(2)	72(1)	93(4)	54(3)	71(3)	-16(2)	-35(3)	-6(2)
C(71)	81(3)	8645(3)	5983(2)	52(1)	47(2)	55(2)	47(2)	-10(2)	-13(2)	-4(2)
C(72)	-33(3)	7723(3)	6231(2)	54(1)	51(2)	70(3)	40(2)	-6(2)	-10(2)	-20(2)

Table AI.4 Continued

atom	x	y	z	U(eq)	U_{11}	U_{22}	U_{33}	U_{23}	U_{13}	U_{12}
N(1)	4386(4)	8738(3)	9951(2)	73(1)	73(3)	67(2)	74(2)	-2(2)	-28(2)	-10(2)
N(2)	4460(4)	9007(3)	8402(2)	80(1)	92(3)	68(3)	82(3)	1(2)	-37(3)	-18(2)
N(3)	6336(3)	7311(2)	8102(2)	65(1)	54(2)	82(2)	56(2)	-1(2)	-20(2)	-16(2)
N(4)	3279(3)	8728(3)	3755(2)	74(1)	67(2)	73(3)	76(2)	-22(2)	-4(2)	-21(2)
N(5)	1941(3)	9642(3)	5101(2)	71(1)	66(2)	62(2)	87(3)	-16(2)	-26(2)	-11(2)
N(6)	387(3)	9001(2)	6405(2)	63(1)	75(2)	59(2)	56(2)	-15(2)	-25(2)	-10(2)
O(1)	5176(2)	7183(2)	10661(1)	59(1)	46(2)	75(2)	46(1)	-2(1)	-13(1)	-8(1)
O(2)	7181(2)	7729(2)	9887(2)	68(1)	57(2)	100(2)	52(2)	-14(2)	-11(1)	-29(2)
O(3)	8122(2)	6961(2)	8589(1)	61(1)	48(2)	86(2)	41(1)	-2(1)	-12(1)	-16(1)
O(4)	6482(2)	6091(2)	9556(1)	62(1)	57(2)	62(2)	54(2)	-5(1)	-6(1)	-14(1)
O(5)	2532(3)	8745(2)	10463(2)	98(1)	66(2)	92(3)	129(3)	-20(2)	-43(2)	3(2)
O(6)	7214(3)	7887(3)	7039(2)	90(1)	73(2)	135(3)	53(2)	10(2)	-22(2)	-28(2)
O(7)	3439(2)	7059(2)	3606(1)	56(1)	50(2)	75(2)	46(1)	-16(1)	-3(1)	-27(1)
O(8)	925(2)	7701(2)	4220(1)	59(1)	49(2)	87(2)	47(1)	-10(1)	-16(1)	-22(1)
O(9)	476(2)	7199(2)	5639(1)	48(1)	45(1)	54(2)	44(1)	-8(1)	-8(1)	-17(1)
O(10)	2770(2)	6167(2)	4970(1)	55(1)	59(2)	45(2)	53(2)	-4(1)	-9(1)	-14(1)
O(11)	5188(3)	8486(2)	3260(2)	80(1)	66(2)	68(2)	111(3)	-7(2)	-17(2)	-33(2)
O(12)	-125(3)	9056(2)	5430(2)	64(1)	76(2)	62(2)	61(2)	0(1)	-35(2)	-19(2)
Cl(1)	2995(2)	147(1)	1872(1)	95(1)	101(1)	87(1)	94(1)	-14(1)	-24(1)	-23(1)
O(13)	1922(5)	315(4)	2331(3)	166(2)	102(4)	182(5)	163(5)	-35(4)	28(4)	-27(3)
O(14)	3908(7)	-260(8)	2158(4)	288(6)	148(6)	413(14)	162(6)	100(8)	-39(5)	10(7)
O(15)	3236(5)	972(4)	1538(4)	168(2)	133(4)	124(4)	229(7)	8(4)	-46(4)	-35(3)
O(16)	3091(10)	-315(10)	1402(7)	357(9)	274(11)	488(18)	393(15)	-339(15)	93(11)	-214(12)
Cl(2)	7409(2)	2563(1)	2697(1)	102(1)	114(1)	82(1)	120(1)	4(1)	-72(1)	-15(1)
O(17)	7056(6)	2875(4)	2078(3)	169(3)	240(6)	127(4)	213(6)	43(4)	-183(6)	-67(4)
O(18)	6905(11)	1972(8)	3140(6)	294(6)	345(13)	319(12)	310(11)	167(10)	-190(11)	-234(11)
O(19)	8482(7)	2078(7)	2542(3)	279(6)	173(6)	400(13)	117(5)	-5(6)	-71(5)	108(8)
O(20)	7393(12)	3203(6)	3039(5)	278(6)	489(17)	177(7)	265(10)	-43(6)	-233(11)	-91(8)
O(21)	8189(6)	233(6)	2164(5)	219(3)	122(5)	224(7)	321(10)	-107(7)	-26(5)	-47(5)
O(22)	6026(4)	9987(3)	2828(3)	118(2)	121(4)	103(3)	139(4)	29(3)	-56(3)	-50(3)
O(23)	546(5)	9692(5)	1483(4)	194(3)	127(4)	230(7)	222(7)	-63(6)	13(4)	-83(5)
O(24)	2682(4)	7777(2)	5421(2)	96(1)	95(3)	69(2)	126(3)	-29(2)	-38(2)	-10(2)
O(25)	4603(16)	1361(16)	3953(8)	458(13)	450(20)	690(30)	283(14)	-170(17)	133(14)	-370(20)

Table AI.5 Bond lengths (Å) for **2L2-$HClO_4 \cdot 5H_2O$**.

C(1)-C(24)	1.495(6)	C(29)-O(1)	1.432(5)	C(53)-C(54)	1.386(6)
C(1)-C(2)	1.514(6)	C(29)-C(30)	1.514(6)	C(54)-C(64)	1.393(6)
C(2)-C(3)	1.383(6)	C(30)-O(5)	1.220(5)	C(54)-C(55)	1.509(6)
C(2)-C(26)	1.385(6)	C(30)-N(1)	1.337(6)	C(55)-C(56)	1.536(6)
C(3)-C(4)	1.380(7)	C(31)-N(1)	1.458(6)	C(56)-C(61)	1.380(6)
C(4)-C(5)	1.363(7)	C(31)-C(32)	1.487(7)	C(56)-C(57)	1.406(6)
C(5)-C(6)	1.394(6)	C(32)-N(2)	1.494(7)	C(57)-C(58)	1.362(6)
C(6)-C(26)	1.393(6)	C(33)-N(2)	1.458(6)	C(58)-C(59)	1.379(7)
C(6)-C(7)	1.515(6)	C(33)-C(34)	1.536(7)	C(59)-C(60)	1.395(6)
C(7)-C(8)	1.512(6)	C(34)-N(3)	1.436(5)	C(60)-C(61)	1.393(5)
C(8)-C(27)	1.389(6)	C(35)-O(6)	1.217(5)	C(61)-O(7)	1.414(5)
C(8)-C(9)	1.414(6)	C(35)-N(3)	1.335(5)	C(62)-O(8)	1.368(4)
C(9)-C(10)	1.368(7)	C(35)-C(36)	1.498(6)	C(63)-O(9)	1.414(4)
C(10)-C(11)	1.374(6)	C(36)-O(3)	1.426(4)	C(64)-O(10)	1.367(4)
C(11)-C(12)	1.372(6)	C(37)-C(60)	1.506(6)	C(65)-O(7)	1.438(4)
C(12)-C(27)	1.386(6)	C(37)-C(38)	1.518(6)	C(65)-C(66)	1.498(6)
C(12)-C(13)	1.504(6)	C(38)-C(39)	1.380(6)	C(66)-O(11)	1.213(5)
C(13)-C(14)	1.505(6)	C(38)-C(62)	1.385(5)	C(66)-N(4)	1.319(5)
C(14)-C(15)	1.378(6)	C(39)-C(40)	1.382(7)	C(67)-N(4)	1.460(6)
C(14)-C(28)	1.423(6)	C(40)-C(41)	1.366(7)	C(67)-C(68)	1.506(8)
C(15)-C(16)	1.378(7)	C(41)-C(42)	1.376(5)	C(68)-N(5)	1.459(7)
C(16)-C(17)	1.382(7)	C(42)-C(62)	1.402(6)	C(69)-C(70)	1.497(7)
C(17)-C(18)	1.375(6)	C(42)-C(43)	1.501(6)	C(69)-N(5)	1.511(6)
C(18)-C(28)	1.398(6)	C(43)-C(44)	1.526(5)	C(70)-N(6)	1.461(6)
C(18)-C(19)	1.507(6)	C(44)-C(45)	1.383(6)	C(71)-O(12)	1.225(4)
C(19)-C(20)	1.514(6)	C(44)-C(63)	1.389(5)	C(71)-N(6)	1.325(5)
C(20)-C(25)	1.382(6)	C(45)-C(46)	1.375(6)	C(71)-C(72)	1.486(6)
C(20)-C(21)	1.392(6)	C(46)-C(47)	1.375(6)	C(72)-O(9)	1.442(4)
C(21)-C(22)	1.374(6)	C(47)-C(48)	1.408(6)	Cl(1)-O(16)	1.266(8)
C(22)-C(23)	1.363(6)	C(48)-C(63)	1.382(5)	Cl(1)-O(13)	1.362(5)
C(23)-C(24)	1.397(6)	C(48)-C(49)	1.516(5)	Cl(1)-O(14)	1.363(8)
C(24)-C(25)	1.397(6)	C(49)-C(50)	1.506(6)	Cl(1)-O(15)	1.429(6)
C(25)-O(1)	1.399(4)	C(50)-C(51)	1.385(6)	Cl(2)-O(19)	1.292(7)
C(26)-O(2)	1.373(5)	C(50)-C(64)	1.392(5)	Cl(2)-O(20)	1.331(7)
C(27)-O(3)	1.398(5)	C(51)-C(52)	1.392(7)	Cl(2)-O(18)	1.341(8)
C(28)-O(4)	1.354(5)	C(52)-C(53)	1.363(7)	Cl(2)-O(17)	1.396(5)

Table AI.6 Bond angles (°) for **2L2-$HClO_4 \cdot 5H_2O$**.

C(24)-C(1)-C(2)	112.5(3)	C(23)-C(24)-C(1)	120.5(4)	C(46)-C(45)-C(44)	120.8(4)
C(3)-C(2)-C(26)	118.4(4)	C(20)-C(25)-C(24)	123.3(4)	C(47)-C(46)-C(45)	120.6(4)
C(3)-C(2)-C(1)	120.7(4)	C(20)-C(25)-O(1)	117.5(4)	C(46)-C(47)-C(48)	120.9(4)
C(26)-C(2)-C(1)	120.9(4)	C(24)-C(25)-O(1)	119.1(4)	C(63)-C(48)-C(47)	116.3(4)
C(4)-C(3)-C(2)	120.9(4)	O(2)-C(26)-C(2)	116.2(4)	C(63)-C(48)-C(49)	123.7(4)
C(5)-C(4)-C(3)	119.7(4)	O(2)-C(26)-C(6)	121.8(4)	C(47)-C(48)-C(49)	119.9(4)
C(4)-C(5)-C(6)	121.8(5)	C(2)-C(26)-C(6)	122.0(4)	C(50)-C(49)-C(48)	112.3(3)
C(26)-C(6)-C(5)	117.1(4)	C(12)-C(27)-C(8)	123.0(4)	C(51)-C(50)-C(64)	117.9(4)
C(26)-C(6)-C(7)	122.5(4)	C(12)-C(27)-O(3)	119.3(3)	C(51)-C(50)-C(49)	121.4(4)
C(5)-C(6)-C(7)	120.2(4)	C(8)-C(27)-O(3)	117.7(4)	C(64)-C(50)-C(49)	120.7(3)
C(8)-C(7)-C(6)	112.5(4)	O(4)-C(28)-C(18)	123.2(4)	C(50)-C(51)-C(52)	120.7(4)
C(27)-C(8)-C(9)	117.0(4)	O(4)-C(28)-C(14)	116.4(3)	C(53)-C(52)-C(51)	120.3(4)
C(27)-C(8)-C(7)	122.6(4)	C(18)-C(28)-C(14)	120.4(4)	C(52)-C(53)-C(54)	120.9(4)
C(9)-C(8)-C(7)	120.3(4)	O(1)-C(29)-C(30)	109.4(4)	C(53)-C(54)-C(64)	118.3(4)
C(10)-C(9)-C(8)	120.5(4)	O(5)-C(30)-N(1)	124.4(5)	C(53)-C(54)-C(55)	120.6(4)
C(9)-C(10)-C(11)	120.0(4)	O(5)-C(30)-C(29)	119.0(5)	C(64)-C(54)-C(55)	121.1(4)
C(12)-C(11)-C(10)	122.1(5)	N(1)-C(30)-C(29)	116.6(4)	C(54)-C(55)-C(56)	111.8(3)
C(11)-C(12)-C(27)	117.3(4)	N(1)-C(31)-C(32)	114.1(4)	C(61)-C(56)-C(57)	118.0(4)
C(11)-C(12)-C(13)	120.5(4)	C(31)-C(32)-N(2)	114.9(5)	C(61)-C(56)-C(55)	123.1(4)
C(27)-C(12)-C(13)	122.2(4)	N(2)-C(33)-C(34)	111.0(4)	C(57)-C(56)-C(55)	118.8(4)
C(12)-C(13)-C(14)	113.4(3)	N(3)-C(34)-C(33)	110.7(4)	C(58)-C(57)-C(56)	119.9(5)
C(15)-C(14)-C(28)	118.3(4)	O(6)-C(35)-N(3)	123.6(4)	C(57)-C(58)-C(59)	121.0(4)
C(15)-C(14)-C(13)	121.1(4)	O(6)-C(35)-C(36)	120.0(4)	C(58)-C(59)-C(60)	121.4(4)
C(28)-C(14)-C(13)	120.5(4)	N(3)-C(35)-C(36)	116.4(4)	C(61)-C(60)-C(59)	116.4(4)
C(14)-C(15)-C(16)	122.0(5)	O(3)-C(36)-C(35)	110.5(3)	C(61)-C(60)-C(37)	123.9(4)
C(15)-C(16)-C(17)	118.4(4)	C(60)-C(37)-C(38)	110.7(3)	C(59)-C(60)-C(37)	119.7(4)
C(18)-C(17)-C(16)	122.9(5)	C(39)-C(38)-C(62)	118.0(4)	C(56)-C(61)-C(60)	123.2(4)
C(17)-C(18)-C(28)	118.0(4)	C(39)-C(38)-C(37)	120.9(4)	C(56)-C(61)-O(7)	118.4(3)
C(17)-C(18)-C(19)	120.6(4)	C(62)-C(38)-C(37)	121.0(3)	C(60)-C(61)-O(7)	118.3(4)
C(28)-C(18)-C(19)	121.4(4)	C(38)-C(39)-C(40)	121.4(4)	O(8)-C(62)-C(38)	115.3(4)
C(18)-C(19)-C(20)	112.1(3)	C(41)-C(40)-C(39)	119.4(4)	O(8)-C(62)-C(42)	123.1(3)
C(25)-C(20)-C(21)	117.5(4)	C(40)-C(41)-C(42)	121.7(4)	C(38)-C(62)-C(42)	121.6(4)
C(25)-C(20)-C(19)	122.6(4)	C(41)-C(42)-C(62)	117.8(4)	C(48)-C(63)-C(44)	123.7(4)
C(21)-C(20)-C(19)	119.7(4)	C(41)-C(42)-C(43)	119.6(4)	C(48)-C(63)-O(9)	119.0(3)
C(22)-C(21)-C(20)	120.7(4)	C(62)-C(42)-C(43)	122.6(3)	C(44)-C(63)-O(9)	117.2(3)
C(23)-C(22)-C(21)	120.5(4)	C(42)-C(43)-C(44)	114.2(3)	O(10)-C(64)-C(50)	116.8(3)
C(22)-C(23)-C(24)	121.6(4)	C(45)-C(44)-C(63)	117.5(4)	O(10)-C(64)-C(54)	121.3(3)
C(25)-C(24)-C(23)	116.3(4)	C(45)-C(44)-C(43)	121.3(4)	C(50)-C(64)-C(54)	121.9(4)
C(25)-C(24)-C(1)	123.2(4)	C(63)-C(44)-C(43)	121.2(4)	O(7)-C(65)-C(66)	111.8(3)

Table AI.6 Continued

O(11)-C(66)-N(4)	125.4(4)	C(30)-N(1)-C(31)	121.0(4)	O(16)-Cl(1)-O(14)	108.2(8)
O(11)-C(66)-C(65)	118.1(4)	C(33)-N(2)-C(32)	114.1(4)	O(13)-Cl(1)-O(14)	116.4(4)
N(4)-C(66)-C(65)	116.4(4)	C(35)-N(3)-C(34)	123.5(4)	O(16)-Cl(1)-O(15)	108.6(8)
N(4)-C(67)-C(68)	113.2(5)	C(66)-N(4)-C(67)	121.1(4)	O(13)-Cl(1)-O(15)	110.9(4)
N(5)-C(68)-C(67)	112.5(4)	C(68)-N(5)-C(69)	115.4(4)	O(14)-Cl(1)-O(15)	100.7(6)
C(70)-C(69)-N(5)	110.5(4)	C(71)-N(6)-C(70)	123.5(4)	O(19)-Cl(2)-O(20)	103.8(8)
N(6)-C(70)-C(69)	112.5(4)	C(25)-O(1)-C(29)	114.5(3)	O(19)-Cl(2)-O(18)	101.5(7)
O(12)-C(71)-N(6)	122.3(4)	C(27)-O(3)-C(36)	114.7(3)	O(20)-Cl(2)-O(18)	110.9(8)
O(12)-C(71)-C(72)	121.9(4)	C(61)-O(7)-C(65)	113.0(3)	O(19)-Cl(2)-O(17)	108.9(4)
N(6)-C(71)-C(72)	115.8(3)	C(63)-O(9)-C(72)	113.6(3)	O(20)-Cl(2)-O(17)	115.1(4)
O(9)-C(72)-C(71)	108.2(3)	O(16)-Cl(1)-O(13)	111.3(5)	O(18)-Cl(2)-O(17)	115.1(5)

Appendix II

Table AII.1 Atomic coordinates ($\times 10^4$), equivalent isotropic and anisotropic displacement parameters ($Å^2 \times 10^3$) for **APDPA**. U(eq) is defined as one third of the trace of the orthogonalized U_{ij} tensor. The anisotropic displacement factor exponent takes the form: $-2\pi^2[h^2a^{*2}U_{11} + ... + 2hka^*b^*U_{12}]$.

atom	x	y	z	U(eq)	U_{11}	U_{22}	U_{33}	U_{23}	U_{13}	U_{12}
O(1)	-697(2)	1470(1)	2742(2)	33(1)	27(1)	39(1)	31(1)	1(1)	-8(1)	3(1)
O(2)	2124(3)	1502(1)	6539(2)	42(1)	53(1)	39(1)	30(1)	8(1)	-11(1)	-12(1)
N(1)	1906(6)	3780(2)	5487(4)	31(1)	35(3)	26(3)	28(3)	5(2)	-13(2)	-5(2)
N(1A)	825(7)	3779(2)	3282(4)	34(1)	42(3)	26(3)	30(3)	-4(2)	-12(2)	0(2)
N(2)	717(3)	1341(1)	4650(2)	26(1)	21(1)	30(1)	25(1)	3(1)	-2(1)	-4(1)
N(3)	2925(3)	610(1)	3279(2)	27(1)	29(1)	25(1)	26(1)	2(1)	-2(1)	0(1)
N(4)	2653(4)	-56(1)	398(2)	44(1)	45(2)	44(2)	42(2)	-14(1)	7(1)	-6(1)
N(5)	6362(3)	1220(1)	4950(2)	37(1)	24(1)	52(2)	35(2)	1(1)	2(1)	-3(1)
C(1)	77(3)	1667(1)	3657(2)	26(1)	16(1)	34(2)	27(2)	4(1)	1(1)	3(1)
C(2)	237(3)	2761(1)	3315(3)	29(1)	25(1)	32(2)	31(2)	3(1)	4(1)	5(1)
C(3)	791(4)	3275(1)	3846(3)	34(1)	39(2)	29(2)	36(2)	5(1)	10(1)	7(1)
C(4)	1611(4)	3289(1)	5039(3)	34(1)	41(2)	29(2)	33(2)	1(1)	11(1)	-1(1)
C(5)	1864(4)	2783(1)	5692(3)	33(1)	33(2)	37(2)	29(2)	-1(1)	0(1)	-1(1)
C(6)	1480(4)	1684(1)	5576(2)	29(1)	26(1)	34(2)	27(2)	3(1)	0(1)	-5(1)
C(7)	1327(3)	2277(1)	5140(2)	26(1)	21(1)	31(2)	28(2)	2(1)	4(1)	0(1)
C(8)	514(3)	2264(1)	3972(2)	27(1)	18(1)	32(2)	33(2)	3(1)	8(1)	4(1)
C(9)	679(3)	726(1)	4699(2)	28(1)	26(1)	27(2)	29(2)	3(1)	-2(1)	-7(1)
C(10)	2497(4)	476(1)	4480(2)	29(1)	31(1)	24(2)	29(2)	6(1)	-6(1)	-2(1)
C(11)	2248(4)	166(1)	2433(3)	36(1)	49(2)	24(2)	33(2)	3(1)	-5(1)	-2(1)
C(12)	2202(4)	343(1)	1146(3)	32(1)	32(2)	33(2)	31(2)	-5(1)	-3(1)	-3(1)
C(13)	1671(5)	882(1)	760(3)	47(1)	73(2)	38(2)	29(2)	3(1)	1(2)	9(2)
C(14)	1606(5)	1006(2)	-432(3)	58(1)	76(3)	53(2)	40(2)	14(2)	-12(2)	-11(2)
C(15)	2062(5)	603(2)	-1211(3)	60(1)	75(3)	76(3)	29(2)	-2(2)	2(2)	-39(2)
C(16)	2547(6)	87(2)	-765(3)	64(1)	80(3)	70(3)	47(2)	-25(2)	26(2)	-23(2)
C(17)	4863(4)	714(1)	3241(3)	34(1)	29(2)	38(2)	34(2)	3(1)	-1(1)	10(1)
C(18)	5412(3)	1264(1)	3873(3)	32(1)	19(1)	44(2)	35(2)	1(1)	6(1)	1(1)
C(19)	4903(4)	1782(1)	3364(3)	37(1)	27(1)	40(2)	44(2)	2(2)	3(1)	0(1)
C(20)	5393(4)	2277(2)	3949(3)	46(1)	30(2)	45(2)	62(2)	1(2)	9(2)	-4(1)
C(21)	6383(4)	2241(2)	5063(3)	47(1)	31(2)	55(2)	56(2)	-13(2)	13(2)	-15(2)
C(22)	6812(4)	1711(2)	5515(3)	45(1)	25(2)	71(3)	41(2)	-8(2)	6(1)	-14(2)

Table AII.2 Bond lengths (Å) and angles (°) for **APDPA**.

O(1)-C(1)	1.215(3)	C(6)-N(2)-C(1)	111.3(2)	C(13)-C(12)-C(11)	122.1(3)
O(2)-C(6)	1.215(3)	C(6)-N(2)-C(9)	123.8(2)	C(14)-C(13)-C(12)	118.8(3)
N(1)-C(4)	1.264(5)	C(1)-N(2)-C(9)	124.8(2)	C(15)-C(14)-C(13)	120.2(4)
N(1A)-C(3)	1.342(6)	C(10)-N(3)-C(11)	111.1(2)	C(16)-C(15)-C(14)	117.3(3)
N(2)-C(6)	1.388(3)	C(10)-N(3)-C(17)	112.2(2)	C(15)-C(16)-N(4)	124.9(4)
N(2)-C(1)	1.394(3)	C(11)-N(3)-C(17)	111.6(2)	N(3)-C(17)-C(18)	110.2(2)
N(2)-C(9)	1.442(3)	C(12)-N(4)-C(16)	116.9(3)	N(5)-C(18)-C(19)	122.5(3)
N(3)-C(10)	1.457(3)	C(22)-N(5)-C(18)	116.5(3)	N(5)-C(18)-C(17)	117.0(3)
N(3)-C(11)	1.461(3)	O(1)-C(1)-N(2)	124.2(3)	C(19)-C(18)-C(17)	120.5(3)
N(3)-C(17)	1.466(3)	O(1)-C(1)-C(8)	129.7(2)	C(20)-C(19)-C(18)	120.0(3)
N(4)-C(12)	1.324(4)	N(2)-C(1)-C(8)	106.2(2)	C(19)-C(20)-C(21)	118.2(3)
N(4)-C(16)	1.346(5)	C(8)-C(2)-C(3)	118.7(3)	C(22)-C(21)-C(20)	118.2(3)
N(5)-C(22)	1.336(4)	N(1A)-C(3)-C(2)	125.3(3)	N(5)-C(22)-C(21)	124.5(3)
N(5)-C(18)	1.340(4)	N(1A)-C(3)-C(4)	113.6(3)		
C(1)-C(8)	1.467(4)	C(2)-C(3)-C(4)	120.5(3)		
C(2)-C(8)	1.383(4)	N(1)-C(4)-C(5)	123.6(3)		
C(2)-C(3)	1.385(4)	N(1)-C(4)-C(3)	116.0(3)		
C(3)-C(4)	1.415(4)	C(5)-C(4)-C(3)	120.0(3)		
C(4)-C(5)	1.395(4)	C(7)-C(5)-C(4)	118.4(3)		
C(5)-C(7)	1.377(4)	O(2)-C(6)-N(2)	123.9(3)		
C(6)-C(7)	1.471(4)	O(2)-C(6)-C(7)	129.6(3)		
C(7)-C(8)	1.388(4)	N(2)-C(6)-C(7)	106.4(2)		
C(9)-C(10)	1.516(4)	C(5)-C(7)-C(8)	121.5(3)		
C(11)-C(12)	1.504(4)	C(5)-C(7)-C(6)	130.7(3)		
C(12)-C(13)	1.378(4)	C(8)-C(7)-C(6)	107.8(2)		
C(13)-C(14)	1.369(5)	C(2)-C(8)-C(7)	120.8(3)		
C(14)-C(15)	1.355(5)	C(2)-C(8)-C(1)	130.9(3)		
C(15)-C(16)	1.343(6)	C(7)-C(8)-C(1)	108.2(2)		
C(17)-C(18)	1.504(4)	N(2)-C(9)-C(10)	110.9(2)		
C(18)-C(19)	1.377(4)	N(3)-C(10)-C(9)	110.9(2)		
C(19)-C(20)	1.362(4)	N(3)-C(11)-C(12)	113.8(2)		
C(20)-C(21)	1.387(5)	N(4)-C(12)-C(13)	121.8(3)		
C(21)-C(22)	1.365(5)	N(4)-C(12)-C(11)	116.0(3)		

Table AII.3 Atomic coordinates ($\times 10^4$) and equivalent isotropic displacement parameters ($Å^2 \times 10^3$) for **APDPA – Zn(II)**. U(eq) is defined as one third of the trace of the orthogonalized U_{ij} tensor.

atom	x	y	z	U(eq)	atom	x	y	z	U(eq)
Zn(1)	11138(1)	8775(1)	2603(1)	36(1)	C(23)	12523(9)	5823(6)	364(3)	63(2)
O(1)	5100(7)	8034(8)	3562(3)	146(3)	C(24)	12860(6)	5915(6)	-880(3)	53(2)
O(2)	6922(7)	9275(7)	4938(3)	130(3)	C(25)	12160(6)	6149(5)	-1426(3)	49(2)
O(3)	13650(6)	5614(5)	552(3)	85(2)	C(26)	10703(6)	6449(5)	-1393(3)	43(1)
O(4)	8905(6)	6626(4)	660(2)	65(1)	C(27)	9939(6)	6516(5)	-792(3)	42(1)
N(1)	4713(7)	6268(6)	6718(3)	64(2)	C(28)	10099(8)	6342(5)	437(3)	49(2)
N(2)	6205(6)	8757(8)	4120(3)	108(3)	C(29)	10650(6)	6270(5)	-253(3)	42(1)
N(3)	8744(4)	9660(4)	2836(2)	44(1)	C(30)	12086(6)	5973(5)	-288(3)	45(1)
N(4)	10980(5)	10086(5)	3119(3)	53(1)	C(31)	11275(10)	5926(6)	1467(3)	82(3)
N(5)	10222(5)	9858(4)	1681(2)	36(1)	C(32)	11229(8)	7136(5)	1617(3)	58(2)
N(6)	10058(7)	6722(5)	-1961(3)	59(2)	C(33)	13276(8)	6441(6)	2260(3)	73(2)
N(7)	11288(7)	6041(5)	770(3)	59(2)	C(34)	13913(7)	7375(7)	2041(3)	58(2)
N(8)	11693(6)	6986(4)	2267(2)	51(1)	C(35)	15254(8)	7125(10)	1702(4)	90(3)
N(9)	13208(5)	8458(5)	2202(2)	53(1)	C(36)	15802(8)	8029(13)	1554(4)	112(4)
N(10)	11377(5)	7341(5)	3508(2)	45(1)	C(37)	15052(8)	9132(11)	1707(4)	99(3)
C(1)	5458(8)	8070(11)	4073(4)	112(4)	C(38)	13785(7)	9317(8)	2027(3)	70(2)
C(2)	4604(7)	6630(8)	4969(4)	76(2)	C(39)	11080(9)	6244(6)	2772(3)	66(2)
C(3)	4462(7)	6233(7)	5629(4)	64(2)	C(40)	11290(6)	6313(6)	3448(3)	51(2)
C(4)	4927(6)	6653(6)	6069(3)	47(2)	C(41)	11330(7)	5355(7)	3977(3)	65(2)
C(5)	5616(7)	7469(7)	5823(3)	57(2)	C(42)	11444(7)	5464(9)	4589(3)	73(2)
C(6)	6373(7)	8726(10)	4765(4)	94(3)	C(43)	11547(7)	6515(9)	4653(3)	70(2)
C(7)	5756(6)	7842(7)	5161(3)	61(2)	C(44)	11497(6)	7438(7)	4109(3)	57(2)
C(8)	5235(6)	7457(8)	4732(3)	69(2)	Cl(1)	6001(2)	7502(2)	7867(1)	63(1)
C(9)	6619(7)	9541(11)	3566(4)	143(5)	O(5)	6954(6)	7266(5)	8322(3)	82(2)
C(10)	8207(6)	8992(7)	3428(3)	62(2)	O(6)	5689(7)	8587(6)	7410(3)	106(2)
C(11)	8530(7)	10902(6)	2888(3)	61(2)	O(7)	6784(13)	6642(8)	7459(5)	236(7)
C(12)	9673(8)	10881(6)	3251(3)	61(2)	O(8)	4887(9)	7243(11)	8105(5)	214(6)
C(13)	9425(12)	11653(8)	3672(4)	101(3)	Cl(2)	7974(4)	5419(3)	3175(1)	111(1)
C(14)	10550(15)	11610(11)	3952(6)	130(4)	O(9)	7911(6)	6529(6)	2785(3)	107(2)
C(15)	11874(12)	10814(12)	3810(5)	117(4)	O(10)	7837(7)	5420(8)	3816(3)	132(3)
C(16)	12057(9)	10075(8)	3393(4)	79(2)	O(11)	9670(10)	4494(7)	3069(4)	84(3)
C(17)	8083(6)	9722(6)	2256(3)	52(2)	O(11A)	8180(30)	4400(20)	3212(15)	170(13)
C(18)	8852(6)	10123(5)	1646(3)	40(1)	O(12)	7316(16)	4917(12)	2892(5)	66(4)
C(19)	8187(7)	10731(5)	1068(3)	48(2)	O(12A)	6053(16)	5834(15)	3263(9)	137(6)
C(20)	8941(7)	11024(5)	512(3)	47(2)	C(45)	5784(9)	7390(9)	-92(4)	100(3)
C(21)	10343(7)	10745(5)	545(3)	46(1)	C(46)	4625(8)	8433(9)	24(4)	73(2)
C(22)	10950(6)	10171(5)	1129(3)	38(1)	N(11)	3687(8)	9323(9)	108(4)	110(3)

Table AII.4 Anisotropic displacement parameters ($Å^2 \times 10^3$) for **APDPA – Zn(II)**. The anisotropic displacement factor exponent takes the form: $-2\pi^2[h^2a^{*2}U_{11}+...+2hka^*b^*U_{12}]$.

atom	U_{11}	U_{22}	U_{33}	U_{23}	U_{13}	U_{12}
Zn(1)	28(1)	40(1)	39(1)	-17(1)	-4(1)	-5(1)
O(1)	108(5)	211(8)	50(4)	-47(4)	-23(3)	27(5)
O(2)	105(5)	194(7)	107(5)	66(5)	-52(4)	-116(5)
O(3)	84(4)	74(3)	82(4)	-24(3)	-49(3)	4(3)
O(4)	83(4)	53(3)	58(3)	-22(2)	14(3)	-27(3)
N(1)	62(4)	65(4)	62(4)	-10(3)	7(3)	-27(3)
N(2)	30(3)	194(9)	54(4)	42(5)	-7(3)	-35(4)
N(3)	31(2)	49(3)	40(3)	0(2)	-2(2)	-9(2)
N(4)	53(3)	61(3)	56(3)	-34(3)	6(3)	-23(3)
N(5)	39(2)	27(2)	42(3)	-5(2)	-5(2)	-12(2)
N(6)	71(4)	56(4)	55(3)	-14(3)	-16(3)	-24(3)
N(7)	99(5)	36(3)	41(3)	-11(2)	-15(3)	-18(3)
N(8)	78(4)	29(3)	32(3)	-3(2)	-18(2)	-3(2)
N(9)	31(3)	75(4)	45(3)	-31(3)	-3(2)	-3(3)
N(10)	35(3)	56(3)	39(3)	-16(2)	-6(2)	-7(2)
C(1)	37(4)	195(11)	35(4)	-21(5)	1(3)	23(5)
C(2)	48(4)	104(6)	87(6)	-64(5)	-11(4)	-12(4)
C(3)	49(4)	68(5)	84(5)	-45(4)	-3(4)	-15(3)
C(4)	42(3)	47(4)	48(4)	-18(3)	6(3)	-9(3)
C(5)	56(4)	83(5)	42(4)	-10(3)	-7(3)	-39(4)
C(6)	43(4)	167(9)	56(5)	37(5)	-21(3)	-52(5)
C(7)	36(3)	106(6)	42(4)	-5(4)	-6(3)	-31(4)
C(8)	29(3)	118(7)	51(4)	-36(4)	-3(3)	-8(4)
C(9)	31(4)	217(12)	78(6)	72(7)	4(4)	-8(5)
C(10)	23(3)	87(5)	50(4)	7(4)	-3(3)	-8(3)
C(11)	47(4)	59(4)	48(4)	-18(3)	5(3)	9(3)
C(12)	75(5)	43(4)	57(4)	-23(3)	13(4)	-14(3)
C(13)	126(8)	84(6)	92(7)	-67(6)	29(6)	-23(6)
C(14)	170(12)	146(10)	129(9)	-113(8)	35(8)	-82(9)
C(15)	125(9)	191(11)	102(7)	-103(8)	36(6)	-102(9)
C(16)	86(6)	113(7)	72(5)	-57(5)	15(4)	-58(5)
C(17)	33(3)	64(4)	49(4)	6(3)	-12(3)	-14(3)
C(18)	40(3)	33(3)	45(3)	-1(3)	-8(3)	-14(2)
C(19)	50(3)	43(3)	45(4)	1(3)	-11(3)	-14(3)
C(20)	64(4)	37(3)	44(3)	-4(3)	-16(3)	-20(3)
C(21)	66(4)	31(3)	40(3)	-9(3)	1(3)	-18(3)
C(22)	42(3)	32(3)	43(3)	-13(2)	3(3)	-17(2)

Table AII.4 Continued

atom	U_{11}	U_{22}	U_{33}	U_{23}	U_{13}	U_{12}
C(23)	83(5)	40(4)	58(4)	-13(3)	-26(4)	-7(4)
C(24)	42(3)	46(4)	65(4)	-16(3)	-11(3)	-6(3)
C(25)	55(4)	37(3)	47(4)	-8(3)	-5(3)	-10(3)
C(26)	55(4)	30(3)	45(3)	-8(3)	-11(3)	-15(3)
C(27)	51(3)	30(3)	46(3)	-11(3)	-5(3)	-15(3)
C(28)	76(5)	24(3)	46(4)	-13(3)	-2(3)	-15(3)
C(29)	55(4)	25(3)	41(3)	-7(2)	-3(3)	-12(3)
C(30)	52(4)	31(3)	47(3)	-7(3)	-16(3)	-7(3)
C(31)	159(8)	34(4)	51(4)	-3(3)	-37(5)	-28(4)
C(32)	102(5)	31(3)	37(3)	-6(3)	-20(3)	-17(3)
C(33)	85(5)	48(4)	35(3)	-12(3)	-15(3)	32(4)
C(34)	47(4)	71(5)	33(3)	-20(3)	-10(3)	9(3)
C(35)	45(4)	137(8)	52(4)	-53(5)	-8(3)	22(5)
C(36)	38(4)	241(14)	78(6)	-80(8)	7(4)	-49(7)
C(37)	54(5)	200(11)	81(6)	-88(7)	14(4)	-59(6)
C(38)	40(4)	123(7)	68(5)	-47(5)	5(3)	-40(4)
C(39)	108(6)	40(4)	47(4)	-1(3)	-19(4)	-26(4)
C(40)	46(3)	58(4)	38(3)	-5(3)	-11(3)	-10(3)
C(41)	57(4)	81(5)	47(4)	5(4)	-15(3)	-23(4)
C(42)	52(4)	128(7)	37(4)	8(4)	-7(3)	-46(5)
C(43)	47(4)	140(8)	37(4)	-28(4)	8(3)	-48(5)
C(44)	40(3)	92(5)	40(4)	-24(4)	1(3)	-21(3)
Cl(1)	59(1)	40(1)	87(1)	1(1)	-34(1)	-13(1)
O(5)	78(4)	98(4)	76(4)	-34(3)	-25(3)	-24(3)
O(6)	99(4)	94(4)	118(5)	25(4)	-38(4)	-46(4)
O(7)	295(13)	139(7)	212(10)	-104(7)	-182(10)	77(8)
O(8)	132(7)	300(12)	197(9)	152(9)	-81(7)	-164(8)
Cl(2)	238(4)	113(2)	44(1)	-2(1)	-10(2)	-137(2)
O(9)	92(4)	107(5)	103(5)	12(4)	13(4)	-46(4)
O(10)	107(5)	242(9)	48(3)	-55(4)	1(3)	-56(5)
O(11)	105(7)	41(5)	97(7)	-38(5)	47(6)	-25(5)
O(11A)	160(20)	82(16)	230(30)	-55(18)	120(20)	-47(15)
O(12)	129(12)	77(9)	28(5)	-18(5)	9(6)	-77(9)
O(12A)	107(11)	149(13)	177(15)	12(12)	-40(11)	-88(11)
C(45)	87(6)	105(7)	64(5)	-31(5)	-9(4)	14(5)
C(46)	43(4)	120(7)	61(5)	-38(5)	-2(3)	-26(5)
N(11)	64(5)	156(8)	97(6)	-64(6)	-16(4)	-2(5)

Table AII.5 Bond lengths (Å) angles (°) for **APDPA – Zn(II)**.

Zn(1)-N(4)	2.089(5)	C(13)-C(14)	1.374(14)	N(4)-Zn(1)-N(9)	97.0(2)
Zn(1)-N(9)	2.112(5)	C(14)-C(15)	1.365(15)	N(4)-Zn(1)-N(5)	104.46(19)
Zn(1)-N(5)	2.173(4)	C(15)-C(16)	1.354(10)	N(9)-Zn(1)-N(5)	92.85(18)
Zn(1)-N(10)	2.209(5)	C(17)-C(18)	1.494(8)	N(4)-Zn(1)-N(10)	91.8(2)
Zn(1)-N(8)	2.274(5)	C(18)-C(19)	1.386(7)	N(9)-Zn(1)-N(10)	104.81(19)
Zn(1)-N(3)	2.313(4)	C(19)-C(20)	1.365(8)	N(5)-Zn(1)-N(10)	154.46(17)
O(1)-C(1)	1.217(10)	C(20)-C(21)	1.372(8)	N(4)-Zn(1)-N(8)	164.14(19)
O(2)-C(6)	1.185(11)	C(21)-C(22)	1.367(8)	N(9)-Zn(1)-N(8)	79.1(2)
O(3)-C(23)	1.208(8)	C(23)-C(30)	1.470(8)	N(5)-Zn(1)-N(8)	91.13(16)
O(4)-C(28)	1.202(8)	C(24)-C(25)	1.373(8)	N(10)-Zn(1)-N(8)	74.69(17)
N(1)-C(4)	1.353(8)	C(24)-C(30)	1.385(9)	N(4)-Zn(1)-N(3)	77.69(19)
N(2)-C(1)	1.380(14)	C(25)-C(26)	1.407(8)	N(9)-Zn(1)-N(3)	163.55(19)
N(2)-C(6)	1.396(11)	C(26)-C(27)	1.396(8)	N(5)-Zn(1)-N(3)	73.81(16)
N(2)-C(9)	1.444(10)	C(27)-C(29)	1.364(7)	N(10)-Zn(1)-N(3)	90.99(16)
N(3)-C(11)	1.461(8)	C(28)-C(29)	1.497(8)	N(8)-Zn(1)-N(3)	110.15(19)
N(3)-C(17)	1.474(7)	C(29)-C(30)	1.387(8)	C(1)-N(2)-C(6)	112.8(7)
N(3)-C(10)	1.479(7)	C(31)-C(32)	1.557(8)	C(1)-N(2)-C(9)	123.6(8)
N(4)-C(16)	1.338(9)	C(33)-C(34)	1.480(11)	C(6)-N(2)-C(9)	123.3(10)
N(4)-C(12)	1.348(8)	C(34)-C(35)	1.422(10)	C(11)-N(3)-C(17)	109.9(5)
N(5)-C(18)	1.343(7)	C(35)-C(36)	1.380(14)	C(11)-N(3)-C(10)	112.5(5)
N(5)-C(22)	1.352(7)	C(36)-C(37)	1.341(14)	C(17)-N(3)-C(10)	110.4(5)
N(6)-C(26)	1.373(7)	C(37)-C(38)	1.348(10)	C(11)-N(3)-Zn(1)	103.0(3)
N(7)-C(28)	1.396(8)	C(39)-C(40)	1.511(8)	C(17)-N(3)-Zn(1)	105.7(3)
N(7)-C(23)	1.403(9)	C(40)-C(41)	1.388(9)	C(10)-N(3)-Zn(1)	114.9(3)
N(7)-C(31)	1.447(8)	C(41)-C(42)	1.367(9)	C(16)-N(4)-C(12)	118.9(6)
N(8)-C(39)	1.461(8)	C(42)-C(43)	1.362(11)	C(16)-N(4)-Zn(1)	124.0(5)
N(8)-C(32)	1.477(7)	C(43)-C(44)	1.381(10)	C(12)-N(4)-Zn(1)	116.5(4)
N(8)-C(33)	1.509(9)	Cl(1)-O(8)	1.319(7)	C(18)-N(5)-C(22)	117.9(5)
N(9)-C(34)	1.321(8)	Cl(1)-O(6)	1.372(6)	C(18)-N(5)-Zn(1)	116.7(4)
N(9)-C(38)	1.354(9)	Cl(1)-O(5)	1.390(5)	C(22)-N(5)-Zn(1)	125.1(4)
N(10)-C(40)	1.325(8)	Cl(1)-O(7)	1.429(9)	C(28)-N(7)-C(23)	113.2(5)
N(10)-C(44)	1.339(7)	Cl(2)-O(11A)	1.15(2)	C(28)-N(7)-C(31)	124.1(7)
C(1)-C(8)	1.440(11)	Cl(2)-O(10)	1.345(5)	C(23)-N(7)-C(31)	122.6(6)
C(2)-C(3)	1.367(11)	Cl(2)-O(12)	1.363(10)	C(39)-N(8)-C(32)	111.2(5)
C(2)-C(8)	1.368(11)	Cl(2)-O(9)	1.373(6)	C(39)-N(8)-C(33)	111.6(5)
C(3)-C(4)	1.395(9)	Cl(2)-O(11)	1.683(9)	C(32)-N(8)-C(33)	110.2(5)
C(4)-C(5)	1.404(9)	Cl(2)-O(12A)	1.850(14)	C(39)-N(8)-Zn(1)	106.0(4)
C(5)-C(7)	1.366(8)	O(11)-O(11A)	1.59(3)	C(32)-N(8)-Zn(1)	115.2(3)
C(6)-C(7)	1.487(11)	O(11A)-O(12)	1.09(3)	C(33)-N(8)-Zn(1)	102.3(4)
C(7)-C(8)	1.384(9)	O(12)-O(12A)	1.59(2)	C(34)-N(9)-C(38)	118.4(6)
C(9)-C(10)	1.526(9)	C(45)-C(46)	1.394(11)	C(34)-N(9)-Zn(1)	115.9(5)
C(11)-C(12)	1.506(10)	C(46)-N(11)	1.157(10)	C(38)-N(9)-Zn(1)	125.2(4)
C(12)-C(13)	1.376(10)			C(40)-N(10)-C(44)	117.3(6)

Table AII.5 Continued

C(40)-N(10)-Zn(1)	115.5(4)	C(19)-C(20)-C(21)	118.8(6)	C(42)-C(41)-C(40)	119.7(8)
C(44)-N(10)-Zn(1)	127.1(5)	C(22)-C(21)-C(20)	119.3(6)	C(43)-C(42)-C(41)	117.9(7)
O(1)-C(1)-N(2)	124.2(10)	N(5)-C(22)-C(21)	122.6(5)	C(42)-C(43)-C(44)	119.7(6)
O(1)-C(1)-C(8)	130.2(13)	O(3)-C(23)-N(7)	123.5(7)	N(10)-C(44)-C(43)	122.7(7)
N(2)-C(1)-C(8)	105.7(7)	O(3)-C(23)-C(30)	131.4(8)	O(8)-Cl(1)-O(6)	113.1(5)
C(3)-C(2)-C(8)	118.9(6)	N(7)-C(23)-C(30)	105.1(6)	O(8)-Cl(1)-O(5)	115.2(5)
C(2)-C(3)-C(4)	122.1(7)	C(25)-C(24)-C(30)	117.8(6)	O(6)-Cl(1)-O(5)	117.3(4)
N(1)-C(4)-C(3)	119.8(6)	C(24)-C(25)-C(26)	121.7(6)	O(8)-Cl(1)-O(7)	105.9(8)
N(1)-C(4)-C(5)	121.5(6)	N(6)-C(26)-C(27)	121.5(6)	O(6)-Cl(1)-O(7)	99.9(6)
C(3)-C(4)-C(5)	118.7(6)	N(6)-C(26)-C(25)	118.7(6)	O(5)-Cl(1)-O(7)	102.8(4)
C(7)-C(5)-C(4)	117.9(6)	C(27)-C(26)-C(25)	119.7(5)	O(11A)-Cl(2)-O(10)	98.8(16)
O(2)-C(6)-N(2)	126.1(8)	C(29)-C(27)-C(26)	118.1(5)	O(11A)-Cl(2)-O(12)	50.3(16)
O(2)-C(6)-C(7)	129.5(7)	O(4)-C(28)-N(7)	126.9(6)	O(10)-Cl(2)-O(12)	124.1(6)
N(2)-C(6)-C(7)	104.4(8)	O(4)-C(28)-C(29)	128.7(6)	O(11A)-Cl(2)-O(9)	147.9(15)
C(5)-C(7)-C(8)	122.7(7)	N(7)-C(28)-C(29)	104.4(6)	O(10)-Cl(2)-O(9)	113.1(5)
C(5)-C(7)-C(6)	129.9(7)	C(27)-C(29)-C(30)	122.0(5)	O(12)-Cl(2)-O(9)	109.3(6)
C(8)-C(7)-C(6)	107.4(7)	C(27)-C(29)-C(28)	129.5(6)	O(11A)-Cl(2)-O(11)	65.0(14)
C(2)-C(8)-C(7)	119.6(7)	C(30)-C(29)-C(28)	108.3(5)	O(10)-Cl(2)-O(11)	102.8(5)
C(2)-C(8)-C(1)	130.8(8)	C(24)-C(30)-C(29)	120.8(5)	O(12)-Cl(2)-O(11)	101.6(7)
C(7)-C(8)-C(1)	109.6(9)	C(24)-C(30)-C(23)	130.1(6)	O(9)-Cl(2)-O(11)	102.7(4)
N(2)-C(9)-C(10)	110.1(6)	C(29)-C(30)-C(23)	109.0(6)	O(11A)-Cl(2)-O(12A)	91.2(14)
N(3)-C(10)-C(9)	115.0(5)	N(7)-C(31)-C(32)	110.3(5)	O(10)-Cl(2)-O(12A)	84.1(7)
N(3)-C(11)-C(12)	111.3(5)	N(8)-C(32)-C(31)	114.4(5)	O(12)-Cl(2)-O(12A)	56.8(8)
N(4)-C(12)-C(13)	121.4(8)	C(34)-C(33)-N(8)	113.6(5)	O(9)-Cl(2)-O(12A)	95.5(6)
N(4)-C(12)-C(11)	115.7(5)	N(9)-C(34)-C(35)	120.1(8)	O(11)-Cl(2)-O(12A)	155.9(6)
C(13)-C(12)-C(11)	122.8(7)	N(9)-C(34)-C(33)	117.0(6)	O(11A)-O(11)-Cl(2)	41.1(8)
C(14)-C(13)-C(12)	118.4(9)	C(35)-C(34)-C(33)	122.8(7)	O(12)-O(11A)-Cl(2)	74.9(17)
C(15)-C(14)-C(13)	120.0(8)	C(36)-C(35)-C(34)	118.7(8)	O(12)-O(11A)-O(11)	124(2)
C(16)-C(15)-C(14)	119.2(9)	C(37)-C(36)-C(35)	120.1(8)	Cl(2)-O(11A)-O(11)	73.8(16)
N(4)-C(16)-C(15)	122.1(8)	C(36)-C(37)-C(38)	118.5(10)	O(11A)-O(12)-Cl(2)	54.8(15)
N(3)-C(17)-C(18)	110.5(5)	C(37)-C(38)-N(9)	124.1(8)	O(11A)-O(12)-O(12A)	109.3(17)
N(5)-C(18)-C(19)	121.4(5)	N(8)-C(39)-C(40)	111.5(6)	Cl(2)-O(12)-O(12A)	77.2(7)
N(5)-C(18)-C(17)	117.0(5)	N(10)-C(40)-C(41)	122.6(6)	O(12)-O(12A)-Cl(2)	45.9(5)
C(19)-C(18)-C(17)	121.6(5)	N(10)-C(40)-C(39)	116.7(5)	N(11)-C(46)-C(45)	177.7(11)
C(20)-C(19)-C(18)	119.9(6)	C(41)-C(40)-C(39)	120.7(6)		

Appendix III

Table AIII.1 Atomic coordinates ($\times 10^4$), equivalent isotropic and anisotropic displacement parameters ($Å^2 \times 10^3$) for **APMPY**. U(eq) is defined as one third of the trace of the orthogonalized U_{ij} tensor. The anisotropic displacement factor exponent takes the form: $-2\pi^2[h^2a^{*2}U_{11} + ... + 2hka^*b^*U_{12}]$.

atom	x	y	z	U(eq)	U_{11}	U_{22}	U_{33}	U_{23}	U_{13}	U_{12}
O(2)	430(1)	4031(7)	10676(3)	28(1)	23(3)	40(3)	20(3)	4(2)	-4(2)	5(2)
O(1)	447(1)	3904(7)	7240(4)	30(1)	31(3)	38(3)	22(3)	1(2)	4(2)	1(2)
C(6)	352(1)	3732(10)	9833(5)	22(2)	17(3)	24(4)	26(4)	0(3)	2(3)	13(3)
C(3)	-345(2)	1329(11)	8452(5)	27(2)	27(4)	28(4)	27(4)	-4(3)	-4(3)	-14(3)
C(1)	358(2)	3690(10)	8080(5)	25(2)	24(4)	27(4)	23(4)	-1(3)	1(3)	-9(3)
C(10)	1013(1)	3806(9)	9024(6)	24(1)	20(3)	34(3)	18(3)	-4(3)	3(3)	-1(2)
C(5)	-122(1)	2128(9)	10028(5)	22(2)	28(4)	24(4)	13(3)	0(3)	-2(3)	-1(3)
C(4)	-341(1)	1327(10)	9499(5)	24(2)	14(3)	22(4)	34(4)	3(3)	4(3)	14(3)
C(7)	90(1)	2875(9)	9484(5)	20(1)	13(3)	21(3)	24(3)	2(3)	-1(2)	2(3)
C(2)	-124(2)	2082(10)	7900(6)	28(2)	28(4)	34(5)	23(4)	-5(3)	-6(3)	3(3)
C(8)	96(2)	2851(11)	8429(5)	28(2)	31(4)	30(4)	22(4)	0(3)	1(3)	8(3)
N(1)	967(1)	2083(7)	9128(5)	25(1)	24(3)	27(3)	26(3)	-2(2)	3(2)	-7(2)
C(9)	764(1)	5065(9)	8950(6)	28(1)	25(3)	32(3)	26(3)	6(3)	7(3)	6(3)
C(13)	1463(1)	1592(9)	9137(6)	30(2)	24(3)	33(4)	34(4)	0(3)	7(3)	11(3)
C(11)	1282(1)	4533(9)	8978(6)	28(1)	32(3)	29(3)	22(3)	-8(3)	6(3)	-9(3)
N(3)	-557(1)	558(10)	10019(5)	33(2)	33(4)	38(4)	29(3)	2(3)	-3(3)	-12(3)
N(2)	499(1)	4187(7)	8957(5)	22(1)	18(2)	27(3)	20(2)	2(3)	-1(2)	-3(2)
C(12)	1507(1)	3409(8)	9043(6)	28(2)	20(3)	32(4)	32(4)	-4(3)	8(3)	-8(3)
C(14)	1190(1)	988(10)	9182(5)	29(2)	31(3)	31(4)	25(4)	0(3)	6(3)	2(3)

Table AIII.2 Bond lengths (Å) for **APMPY**.

O(2)-C(6)	1.204(9)	C(1)-C(8)	1.483(10)	C(7)-C(8)	1.403(8)
O(1)-C(1)	1.207(9)	C(10)-N(1)	1.319(8)	C(2)-C(8)	1.393(10)
C(6)-N(2)	1.402(9)	C(10)-C(11)	1.403(8)	N(1)-C(14)	1.355(9)
C(6)-C(7)	1.487(10)	C(10)-C(9)	1.527(9)	C(9)-N(2)	1.437(8)
C(3)-C(4)	1.391(9)	C(5)-C(7)	1.372(9)	C(13)-C(12)	1.386(10)
C(3)-C(2)	1.409(11)	C(5)-C(4)	1.401(10)	C(13)-C(14)	1.386(10)
C(1)-N(2)	1.399(9)	C(4)-N(3)	1.374(9)	C(11)-C(12)	1.374(10)

Table AIII.3 Bond angles (°) for **APMPY**.

O(2)-C(6)-N(2)	124.8(7)	C(7)-C(5)-C(4)	118.0(6)	C(7)-C(8)-C(1)	108.9(7)
O(2)-C(6)-C(7)	129.4(6)	N(3)-C(4)-C(3)	119.7(7)	C(10)-N(1)-C(14)	117.8(5)
N(2)-C(6)-C(7)	105.8(6)	N(3)-C(4)-C(5)	119.6(6)	N(2)-C(9)-C(10)	114.3(5)
C(4)-C(3)-C(2)	120.9(7)	C(3)-C(4)-C(5)	120.7(7)	C(12)-C(13)-C(14)	118.0(6)
O(1)-C(1)-N(2)	124.4(7)	C(5)-C(7)-C(8)	122.4(7)	C(12)-C(11)-C(10)	118.9(6)
O(1)-C(1)-C(8)	130.4(7)	C(5)-C(7)-C(6)	130.0(6)	C(1)-N(2)-C(6)	112.6(5)
N(2)-C(1)-C(8)	105.2(6)	C(8)-C(7)-C(6)	107.5(6)	C(1)-N(2)-C(9)	123.1(6)
N(1)-C(10)-C(11)	122.7(6)	C(8)-C(2)-C(3)	118.3(7)	C(6)-N(2)-C(9)	124.3(6)
N(1)-C(10)-C(9)	118.7(5)	C(2)-C(8)-C(7)	119.7(8)	C(11)-C(12)-C(13)	119.3(6)
C(11)-C(10)-C(9)	118.5(6)	C(2)-C(8)-C(1)	131.4(7)	N(1)-C(14)-C(13)	123.2(7)

Table AIII.4 Atomic coordinates ($\times 10^4$), equivalent isotropic and anisotropic displacement parameters ($Å^2 \times 10^3$) for **APEPY**. U(eq) is defined as one third of the trace of the orthogonalized U_{ij} tensor. The anisotropic displacement factor exponent takes the form: $-2\pi^2[h^2a^{*2}U_{11} + ... + 2hka^*b^*U_{12}]$.

atom	x	y	z	U(eq)	U_{11}	U_{22}	U_{33}	U_{23}	U_{13}	U_{12}
O(1)	1260(1)	9175(2)	1677(1)	20(1)	17(1)	19(1)	23(1)	-5(1)	6(1)	-3(1)
O(2)	91(1)	2232(2)	1088(1)	19(1)	16(1)	22(1)	21(1)	-2(1)	10(1)	-5(1)
N(1)	1684(1)	7199(3)	3471(1)	19(1)	18(1)	21(1)	18(1)	-3(1)	9(1)	-2(1)
N(2)	644(1)	5821(3)	1516(1)	16(1)	14(1)	20(1)	16(1)	-3(1)	7(1)	-2(1)
N(3)	867(1)	1343(3)	-936(1)	21(1)	25(1)	21(1)	22(1)	-4(1)	15(1)	-7(1)
C(1)	1017(1)	7292(3)	1351(1)	16(1)	11(1)	17(1)	18(1)	2(1)	3(1)	2(1)
C(2)	1340(1)	6610(3)	355(1)	17(1)	14(1)	16(1)	20(1)	1(1)	6(1)	-2(1)
C(3)	1284(1)	5014(3)	-197(1)	18(1)	15(1)	21(1)	19(1)	4(1)	9(1)	0(1)
C(4)	924(1)	2870(3)	-386(1)	16(1)	15(1)	18(1)	14(1)	3(1)	5(1)	3(1)
C(5)	613(1)	2342(3)	3(1)	15(1)	14(1)	15(1)	16(1)	0(1)	5(1)	-2(1)
C(6)	423(1)	3780(3)	1057(1)	16(1)	12(1)	17(1)	16(1)	0(1)	4(1)	1(1)
C(7)	680(1)	3933(3)	550(1)	15(1)	12(1)	17(1)	16(1)	3(1)	6(1)	1(1)
C(8)	1035(1)	6048(3)	732(1)	16(1)	13(1)	15(1)	16(1)	1(1)	3(1)	1(1)
C(9)	534(1)	6220(3)	2129(1)	18(1)	14(1)	24(1)	18(1)	-5(1)	8(1)	-1(1)
C(10)	902(1)	4473(3)	2744(1)	18(1)	16(1)	23(1)	17(1)	-3(1)	9(1)	-3(1)
C(11)	1519(1)	5173(3)	3036(1)	16(1)	17(1)	19(1)	13(1)	2(1)	7(1)	-1(1)
C(12)	1887(1)	3860(3)	2843(1)	19(1)	20(1)	18(1)	18(1)	-2(1)	8(1)	0(1)
C(13)	2443(1)	4655(3)	3102(1)	21(1)	18(1)	23(1)	22(1)	0(1)	10(1)	4(1)
C(14)	2618(1)	6739(3)	3549(1)	21(1)	14(1)	24(1)	21(1)	2(1)	5(1)	-2(1)
C(15)	2226(1)	7929(3)	3720(1)	21(1)	21(1)	20(1)	19(1)	-5(1)	7(1)	-4(1)

Table AIII.5 Bond lengths (Å) for **APEPY**.

O(1)-C(1)	1.213(2)	C(1)-C(8)	1.476(2)	C(7)-C(8)	1.392(2)
O(2)-C(6)	1.216(2)	C(2)-C(8)	1.385(2)	C(9)-C(10)	1.532(2)
N(1)-C(15)	1.341(2)	C(2)-C(3)	1.386(2)	C(10)-C(11)	1.508(2)
N(1)-C(11)	1.344(2)	C(3)-C(4)	1.412(2)	C(11)-C(12)	1.387(2)
N(2)-C(6)	1.387(2)	C(4)-C(5)	1.416(2)	C(12)-C(13)	1.382(2)
N(2)-C(1)	1.407(2)	C(5)-C(7)	1.368(2)	C(13)-C(14)	1.383(3)
N(2)-C(9)	1.455(2)	C(6)-C(7)	1.494(2)	C(14)-C(15)	1.382(2)
N(3)-C(4)	1.362(2)				

Table AIII.6 Bond angles (°) for **APEPY**.

C(15)-N(1)-C(11)	117.52(15)	C(3)-C(4)-C(5)	118.79(15)	C(7)-C(8)-C(1)	108.49(15)
C(6)-N(2)-C(1)	112.08(14)	C(7)-C(5)-C(4)	118.16(15)	N(2)-C(9)-C(10)	111.35(14)
C(6)-N(2)-C(9)	122.90(14)	O(2)-C(6)-N(2)	124.70(16)	C(11)-C(10)-C(9)	111.43(14)
C(1)-N(2)-C(9)	124.81(14)	O(2)-C(6)-C(7)	129.45(15)	N(1)-C(11)-C(12)	122.29(15)
O(1)-C(1)-N(2)	123.96(16)	N(2)-C(6)-C(7)	105.85(14)	N(1)-C(11)-C(10)	115.98(15)
O(1)-C(1)-C(8)	130.30(16)	C(5)-C(7)-C(8)	122.75(15)	C(12)-C(11)-C(10)	121.68(15)
N(2)-C(1)-C(8)	105.74(14)	C(5)-C(7)-C(6)	129.39(15)	C(13)-C(12)-C(11)	119.24(16)
C(8)-C(2)-C(3)	118.44(16)	C(8)-C(7)-C(6)	107.84(15)	C(12)-C(13)-C(14)	119.04(16)
C(2)-C(3)-C(4)	121.84(16)	C(2)-C(8)-C(7)	120.02(16)	C(15)-C(14)-C(13)	118.10(16)
N(3)-C(4)-C(3)	121.11(16)	C(2)-C(8)-C(1)	131.47(15)	N(1)-C(15)-C(14)	123.81(16)
N(3)-C(4)-C(5)	120.09(16)				

Table AIII.7 Atomic coordinates ($\times 10^4$), equivalent isotropic and anisotropic displacement parameters ($Å^2 \times 10^3$) for **CuAPMPY**. U(eq) is defined as one third of the trace of the orthogonalized U_{ij} tensor. The anisotropic displacement factor exponent takes the form: $-2\pi^2[h^2a^{*2}U_{11} + ... + 2hka^*b^*U_{12}]$.

atom	x	y	z	U(eq)	U_{11}	U_{22}	U_{33}	U_{23}	U_{13}	U_{12}
Cu(1)	0	0	0	47(1)	50(1)	32(1)	62(1)	8(1)	16(1)	9(1)
N(1)	-307(3)	2013(7)	-497(4)	33(1)	30(3)	30(3)	38(3)	-3(3)	3(2)	5(3)
N(2)	-1728(3)	830(7)	-478(4)	34(1)	25(3)	30(3)	47(4)	-3(3)	5(3)	1(3)
N(3)	-3321(4)	-4598(9)	-2092(5)	60(2)	56(5)	44(5)	75(5)	-2(4)	-1(4)	-8(4)
O(1)	-2423(2)	2860(6)	-1011(3)	44(1)	43(3)	29(3)	61(3)	7(3)	8(3)	7(2)
O(2)	-1269(3)	-1681(7)	-185(4)	62(2)	43(3)	47(3)	86(4)	-2(3)	-16(3)	15(3)
C(1)	-2288(3)	1441(9)	-959(5)	34(2)	23(4)		46(4)	6(3)	12(3)	3(3)
C(2)	-3228(3)	-163(10)	-1852(5)	42(2)	33(4)	40(4)	53(4)	6(4)	5(3)	11(4)
C(3)	-3449(4)	-1689(10)	-2087(5)	44(2)	35(4)	50(5)	45(4)	5(4)	2(3)	1(4)
C(4)	-3093(3)	-3104(9)	-1836(5)	38(2)	36(4)	35(4)	46(4)	2(3)	14(3)	-11(3)
C(5)	-2499(4)	-2923(9)	-1318(5)	43(2)	44(5)	32(4)	53(5)	0(4)	2(4)	0(4)
C(6)	-1699(3)	-873(10)	-536(5)	40(2)	32(4)	43(5)	44(4)	3(4)	2(3)	5(4)
C(7)	-2294(3)	-1395(9)	-1078(5)	35(2)	26(4)	35(4)	45(4)	6(3)	7(3)	2(3)
C(8)	-2646(3)	16(10)	-1333(4)	37(2)	33(4)	38(4)	42(4)	7(4)	7(3)	2(4)
C(9)	-1283(3)	1793(9)	110(5)	39(2)	29(4)	45(4)	42(4)	-6(3)	5(3)	5(3)
C(10)	-830(3)	2757(8)	-353(4)	31(2)	22(3)	34(4)	34(4)	-9(3)	0(3)	-1(3)
C(11)	-960(4)	4366(9)	-603(5)	48(2)	43(4)	37(4)	59(5)	-10(4)	-5(4)	6(4)
C(12)	-569(4)	5189(10)	-1048(5)	49(2)	57(5)	38(4)	46(4)	7(4)	-8(4)	-10(4)
C(13)	-45(4)	4413(9)	-1247(5)	44(2)	39(4)	40(4)	50(4)	8(3)	-1(4)	-6(3)
C(14)	79(3)	2857(10)	-961(4)	41(2)	33(4)	54(5)	37(4)	-3(4)	7(3)	4(4)
Cl(1)	0	1237(4)	2500	48(1)	54(2)	42(2)	43(2)	0	-3(1)	0
O(3)	454(4)	2177(12)	2980(7)	154(5)	119(7)	117(7)	189(10)	-84(7)	-91(7)	45(6)
O(4)	271(8)	380(20)	2037(12)	337(13)	213(17)	440(30)	340(20)	-330(20)	-12(13)	80(16)

Table AIII.8 Bond lengths (Å) and angles (°) for **CuAPMPY**.

Cu(1)-N(1)#1	1.889(6)	N(1)#1-Cu(1)-N(1)	180.0(5)	O(2)-C(6)-C(7)	129.6(7)
Cu(1)-N(1)	1.889(6)	N(1)#1-Cu(1)-O(2)	84.1(2)	N(2)-C(6)-C(7)	106.3(6)
Cu(1)-O(2)	3.032(6)	N(1)-Cu(1)-O(2)	95.9(2)	C(5)-C(7)-C(8)	122.9(7)
Cu(1)-O(4)	3.116(17)	N(1)#1-Cu(1)-O(4)	71.3(4)	C(5)-C(7)-C(6)	129.5(7)
N(1)-C(10)	1.328(8)	N(1)-Cu(1)-O(4)	108.7(4)	C(8)-C(7)-C(6)	107.6(6)
N(1)-C(14)	1.365(9)	O(2)-Cu(1)-O(4)	99.4(4)	C(2)-C(8)-C(7)	118.4(7)
N(2)-C(6)	1.396(9)	C(10)-N(1)-C(14)	117.2(6)	C(2)-C(8)-C(1)	133.2(7)
N(2)-C(1)	1.405(8)	C(10)-N(1)-Cu(1)	125.7(5)	C(7)-C(8)-C(1)	108.4(6)
N(2)-C(9)	1.444(8)	C(14)-N(1)-Cu(1)	116.7(5)	N(2)-C(9)-C(10)	113.6(6)
N(3)-C(4)	1.352(10)	C(6)-N(2)-C(1)	111.3(6)	N(1)-C(10)-C(11)	121.9(7)
O(1)-C(1)	1.196(8)	C(6)-N(2)-C(9)	123.5(6)	N(1)-C(10)-C(9)	117.7(6)
O(2)-C(6)	1.196(8)	C(1)-N(2)-C(9)	124.6(6)	C(11)-C(10)-C(9)	120.4(7)
C(1)-C(8)	1.464(10)	C(6)-O(2)-Cu(1)	114.5(5)	C(12)-C(11)-C(10)	120.0(8)
C(2)-C(3)	1.363(11)	O(1)-C(1)-N(2)	124.1(7)	C(11)-C(12)-C(13)	119.0(8)
C(2)-C(8)	1.385(10)	O(1)-C(1)-C(8)	129.6(7)	C(14)-C(13)-C(12)	119.2(8)
C(3)-C(4)	1.408(10)	N(2)-C(1)-C(8)	106.3(6)	C(13)-C(14)-N(1)	122.6(7)
C(4)-C(5)	1.404(10)	C(3)-C(2)-C(8)	119.8(7)	O(4)#2-Cl(1)-O(4)	109(2)
C(5)-C(7)	1.356(10)	C(2)-C(3)-C(4)	121.7(7)	O(4)#2-Cl(1)-O(3)	112.1(11)
C(6)-C(7)	1.478(10)	N(3)-C(4)-C(5)	121.2(7)	O(4)-Cl(1)-O(3)	105.9(9)
C(7)-C(8)	1.402(10)	N(3)-C(4)-C(3)	120.2(7)	O(4)#2-Cl(1)-O(3)#2	105.9(9)
C(9)-C(10)	1.517(10)	C(5)-C(4)-C(3)	118.5(7)	O(4)-Cl(1)-O(3)#2	112.1(11)
C(10)-C(11)	1.386(10)	C(7)-C(5)-C(4)	118.7(7)	O(3)-Cl(1)-O(3)#2	111.6(8)
C(11)-C(12)	1.347(11)	O(2)-C(6)-N(2)	124.1(7)	Cl(1)-O(4)-Cu(1)	128.2(12)
C(12)-C(13)	1.372(11)				
C(13)-C(14)	1.358(10)				
Cl(1)-O(4)#2	1.214(12)				
Cl(1)-O(4)	1.214(12)				
Cl(1)-O(3)	1.366(8)				
Cl(1)-O(3)#2	1.366(8)				

Symmetry transformations used to generate equivalent atoms: #1 -x,-y,-z; #2 -x,y,-z+1/2.

Table AIII.9 Atomic coordinates ($\times 10^4$), equivalent isotropic and anisotropic displacement parameters ($Å^2 \times 10^3$) for **CuAPEPY**. U(eq) is defined as one third of the trace of the orthogonalized U_{ij} tensor. The anisotropic displacement factor exponent takes the form: $-2\pi^2[h^2a^{*2}U_{11} + ... + 2hka^*b^*U_{12}]$.

atom	x	y	z	U(eq)	U_{11}	U_{22}	U_{33}	U_{23}	U_{13}	U_{12}
Cu(1)	5000	6561(1)	7500	80(1)	79(1)	94(1)	66(1)	0	12(1)	0
N(2)	6901(2)	6432(6)	8258(3)	73(1)	52(3)	86(3)	75(3)	-2(3)	3(2)	-3(2)
N(3)	8329(2)	3788(9)	11423(4)	103(2)	80(4)	122(5)	96(4)	0(4)	-3(3)	15(4)
C(11)	5721(2)	6080(6)	6363(3)	66(1)	60(4)	66(3)	69(4)	-16(3)	6(3)	-10(3)
N(1)	5228(2)	6630(5)	6472(3)	66(1)	68(3)	66(3)	59(3)	-1(2)	3(2)	-5(2)
C(1)	7456(3)	6486(8)	8215(4)	85(2)	72(5)	96(4)	84(4)	-16(4)	10(4)	-10(4)
C(12)	5849(2)	6153(8)	5591(4)	83(2)	75(4)	105(5)	70(4)	-17(4)	15(3)	-14(4)
O(2)	6397(2)	5639(6)	9215(2)	94(1)	57(2)	135(4)	90(3)	11(2)	14(2)	11(2)
C(4)	8138(3)	4478(7)	10632(4)	76(2)	71(4)	73(4)	74(4)	-20(3)	-5(4)	6(3)
O(1)	7621(2)	7027(7)	7615(3)	118(2)	89(3)	172(5)	96(3)	16(3)	24(3)	-13(3)
C(7)	7403(2)	5368(7)	9514(3)	66(1)	55(3)	70(3)	65(4)	-14(3)	1(3)	2(3)
C(14)	4981(3)	7413(8)	5026(4)	89(2)	107(6)	82(4)	66(4)	11(3)	-3(4)	-9(4)
C(13)	5475(3)	6820(9)	4920(4)	93(2)	98(5)	114(5)	64(4)	-8(4)	15(4)	-27(4)
C(9)	6455(2)	7002(7)	7571(3)	78(2)	63(3)	80(4)	82(4)	-4(3)	-5(3)	-2(3)
C(8)	7773(2)	5811(7)	9021(4)	75(2)	57(4)	83(4)	79(4)	-13(3)	5(3)	-1(3)
C(10)	6137(2)	5456(7)	7117(3)	73(2)	67(4)	73(3)	72(3)	-3(3)	4(3)	-3(3)
C(5)	7569(2)	4714(7)	10305(4)	77(2)	62(4)	76(4)	86(4)	-15(3)	2(3)	2(3)
C(15)	4862(2)	7288(7)	5806(4)	82(2)	78(4)	78(4)	82(4)	0(3)	2(3)	-1(3)
C(3)	8506(2)	4949(8)	10131(5)	89(2)	56(4)	96(5)	106(5)	-23(4)	-1(4)	1(3)
C(6)	6834(3)	5788(7)	9023(4)	71(2)	71(4)	73(4)	66(4)	-7(3)	7(3)	-2(3)
C(2)	8336(2)	5588(8)	9334(4)	90(2)	68(4)	108(5)	92(5)	-18(4)	14(4)	-9(4)
Cl(1)	5000	1302(3)	7500	103(1)	134(2)	70(2)	76(2)	0	-41(2)	0
O(3)	5375(2)	382(8)	8035(3)	154(2)	115(4)	167(5)	149(4)	31(4)	-34(3)	6(4)
O(4)	5000	2990(10)	7500	234(5)	247(11)	70(5)	398(16)	0	102(11)	0
O(5)	4552(5)	1256(18)	8092(7)	171(5)	171(11)	243(15)	108(8)	2(8)	47(8)	15(10)

Table AIII.10 Bond lengths (Å) and angles (°) for **CuAPEPY**.

Cu(1)-N(1)	1.891(4)	N(1)-Cu(1)-N(1)#1	176.8(2)	N(2)-C(9)-C(10)	111.8(4)
Cu(1)-N(1)#1	1.891(4)	C(6)-N(2)-C(1)	112.0(5)	C(2)-C(8)-C(7)	119.7(6)
N(2)-C(6)	1.387(7)	C(6)-N(2)-C(9)	125.4(5)	C(2)-C(8)-C(1)	131.8(6)
N(2)-C(1)	1.394(7)	C(1)-N(2)-C(9)	122.6(5)	C(7)-C(8)-C(1)	108.5(5)
N(2)-C(9)	1.454(6)	N(1)-C(11)-C(12)	121.1(5)	C(11)-C(10)-C(9)	110.3(4)
N(3)-C(4)	1.378(8)	N(1)-C(11)-C(10)	117.9(5)	C(7)-C(5)-C(4)	118.3(6)
C(11)-N(1)	1.339(6)	C(12)-C(11)-C(10)	120.9(5)	N(1)-C(15)-C(14)	122.0(6)
C(11)-C(12)	1.371(7)	C(11)-N(1)-C(15)	118.4(5)	C(2)-C(3)-C(4)	123.2(6)
C(11)-C(10)	1.497(7)	C(11)-N(1)-Cu(1)	124.9(4)	O(2)-C(6)-N(2)	124.5(5)
N(1)-C(15)	1.348(6)	C(15)-N(1)-Cu(1)	116.7(4)	O(2)-C(6)-C(7)	129.6(6)
C(1)-O(1)	1.215(7)	O(1)-C(1)-N(2)	124.3(6)	N(2)-C(6)-C(7)	105.9(5)
C(1)-C(8)	1.469(8)	O(1)-C(1)-C(8)	129.5(6)	C(3)-C(2)-C(8)	117.8(6)
C(12)-C(13)	1.366(8)	N(2)-C(1)-C(8)	106.2(6)	O(4)-Cl(1)-O(3)#1	121.8(3)
O(2)-C(6)	1.199(6)	C(13)-C(12)-C(11)	120.1(6)	O(4)-Cl(1)-O(3)	121.8(3)
C(4)-C(3)	1.401(8)	N(3)-C(4)-C(3)	121.0(6)	O(3)#1-Cl(1)-O(3)	116.4(5)
C(4)-C(5)	1.402(7)	N(3)-C(4)-C(5)	120.8(6)	O(4)-Cl(1)-O(5)	91.2(5)
C(7)-C(5)	1.361(7)	C(3)-C(4)-C(5)	118.2(6)	O(3)#1-Cl(1)-O(5)	85.0(5)
C(7)-C(8)	1.391(7)	C(5)-C(7)-C(8)	122.8(5)	O(3)-Cl(1)-O(5)	93.7(5)
C(7)-C(6)	1.491(7)	C(5)-C(7)-C(6)	129.7(6)	O(4)-Cl(1)-O(5)#1	91.2(5)
C(14)-C(13)	1.350(8)	C(8)-C(7)-C(6)	107.5(5)	O(3)#1-Cl(1)-O(5)#1	93.7(5)
C(14)-C(15)	1.376(7)	C(13)-C(14)-C(15)	119.0(6)	O(3)-Cl(1)-O(5)#1	85.0(5)
C(9)-C(10)	1.512(6)	C(14)-C(13)-C(12)	119.4(6)	O(5)-Cl(1)-O(5)#1	177.5(10)
C(8)-C(2)	1.383(7)				
C(3)-C(2)	1.367(8)				
Cl(1)-O(4)	1.279(8)				
Cl(1)-O(3)#1	1.324(5)				
Cl(1)-O(3)	1.324(5)				
Cl(1)-O(5)	1.627(12)				
Cl(1)-O(5)#1	1.627(12)				

Symmetry transformations used to generate equivalent atoms: #1 -x+1,y,-z+3/2.